TITLE:
FUNDAMENTAL STUDIES ON THE FABRIC OF SOIL-CEMENT MIXTURE AND ITS MECHANICAL PROPERTIES(Dissertation_全文)

AUTHOR(S):
Kawamura, Mitsunori

CITATION:
Kawamura, Mitsunori. FUNDAMENTAL STUDIES ON THE FABRIC OF SOIL-CEMENT MIXTURE AND ITS MECHANICAL PROPERTIES. 京都大学, 1971, 工学博士

ISSUE DATE:
1971-07-23

URL:
https://doi.org/10.14989/doctor.r1829

RIGHT:

京都大学学術情報リポジトリ
KURENAI 紅
Kyoto University Research Information Repository

FUNDAMENTAL STUDIES ON THE FABRIC OF SOIL-CEMENT MIXTURE AND ITS MECHANICAL PROPERTIES

Mitsunori KAWAMURA

October, 1970

FUNDAMENTAL STUDIES ON THE FABRIC OF SOIL-CEMENT MIXTURE AND ITS MECHANICAL PROPERTIES

by

Mitsunori KAWAMURA

October, 1970

ACKNOWLEDGMENTS

The author is deeply grateful to Prof. Kiyoshi Okada for his continuous guidance and encouragement throughout the periods of the author's graduate study, and to Prof. Shigemasa Hasaba for his assistance, advice and encouragement, especially in the use of clay lumps for soil-cement mixtures.

The author also wishes to express his gratitude to Prof. Seiji Sugiura for his advice concerning clay mineralogy.

Most of the research was conducted in the laboratories of Kanazawa University and Kyoto University. It is a pleasure to acknowledge the author's indebtedness to a number of his associates at Kanazawa University and Kyoto University, both staff members and graduate students, for their assistance in the experiments.

FUNDAMENTAL STUDIES ON THE FABRIC OF SOIL-CEMENT MIXTUPE AND ITS MECHANICAL PROPERTIES

TABLE OF CONTENTS

	PAGE
CHAPTER I PREFACE	1
CHAPTER II INTERACTION BETWEEN CEMENT AND CLAY MINERALS	5
1. INTRODUCTION	5
2. HYDRATION OF CEMENT	6
3. PHYSICOCHEMICAL PROPERTIES OF CLAYS	9
4. REVIEW OF THE LITERATURES	14
5. MATERIALS AND OUTLINE OF EXPERIMENTS	17
6. RESULTS AND DISCUSSIONS	20
7. SUMMARY AND CONCLUSIONS	67
REFERENCES	67
CHAPTER III VISCOELASTIC PROPERTIES OF SOIL-CEMENT MIXTURES	72
1. INTRODUCTION	72
2. REVIEW OF THE LITERATURES	72
3. INFLUENCE OF ''CLAY POCKETS'' ON THE VISCOELASTIC PROPERTIES OF CLAY-CEMENT MIXTURE	73
4. VISCOELASTIC PROPERTIES OF SOIL-CEMENT USING GRANULAR SOILS	87
5. SUMMARY AND CONCLUSIONS	102
REFERENCES	102
CHAPTER IV SHRINKAGE CHARACTERISTICS AND SHRINKAGE STRESSES IN SOIL-CEMENT	104
1. INTRODUCTION	104
2. REVIEW OF THE LITERATURES	104
3. INFLUENCE OF ''CLAY POCKETS'' ON SHRINKAGE CHARACTERISTICS OF SOIL-CEMENT MIXTURES	105
4. SHRINKAGE STRESSES IN SOIL-CEMENT MIXTURES	110
5. A CONSIDERATION ON SHRINKAGE CRACKING IN SOIL-CEMENT AS A VISCOELASTIC MATERIAL	120
6. SUMMARY AND CONCLUSIONS	131
REFERENCES	132
CHAPTER V SUMMARY AND CONCLUSIONS	134

CHAPTER I PREFACE

It is said that the first use of soil-cement as a road pavement material in United State was in 1917 (Catton, 1959). Since 1930's, a great number of fundamental and practical researches have been carried out to improve its engineering properties.

Soil-cement is regarded as a construction material not only for low-cost paving but also for hydraulic structures, such as the lining for canals, reservoirs, highway drainage ditches, facing for levees and slope protection for earth dams. Recently, interest has been expressed in the use of building complete dams of soil-cement in U.S.A. (Shideler, 1969). Therefore, research should be developed to aim not only at improvement of engineering properties but also at design of rational mix proportion as a low-cost material.

The past researches almost belong to either of the following two groups:

(]) Researches concerning function as a part of pavement structure for roads,

(2) Researches for the purpose of designing a rational mix proportion.

Several subjects belonging to the latter are as follows:

Generally speaking, the factors to be controlled in this material for the successful achievement of the compacted soil-cement pavement are:]. Moisture content, 2. Density, 3. Cement content. The factors required for soil material are the physical properties associated with the first two, such as grading, consistency, pulverization and moisture. Furthermore, in both research and practice, it may be much more important to understand the inter-relations between soils and portland cement. Therefore, the better understanding of both the physicochemical properties of soil and chemistry of portland cement should be essential to the investigation of the physicochemical properties of soil-cement mixtures.

Each subject mentioned above has been studied, and many of these studies have been completed. However , in order positively to improve the engineering properties of soil-cement as a new construction material , we must proceed with our study in a way of so-called ''the design of material'', of which term is often used in material science. Such conception has been adopted in the study of other engineering materials, for example high polymer, steel, concrete, etc..

When researches of soil-cement mixtures are carried out from the viewpoint, the relationship between the structure and mechanical properties may be considered as a principal subject. The complete understanding of such a extensive problem may be almost impossible due to the complexity of chemistry of cement and of the physicochemical properties of soil. In this paper, the problem may now be considered from three viewpoints, as described below.

Bofinger (1964) proposed a following hypothesis on the structure of soil-cement. His theory says that if a soil is composed of sand and clay, the structure of soil-cement can be represented by the cross-section shown in Fig. 2.1. It demonstrates that soil-cement consists of relatively coarse sand, silt grains and clay pockets which are surrounded by a continuous cementitious skeleton. The skeleton is largely composed of cementing compounds and clay particles (see Fig. 2.2). Furthermore, Bofinger experimentally proved that the continuous skeleton was always formed even for low cement contents, though the lower the cement contents, the greater the fraction of clay pockets. As to the structure of skeleton, the author has a little different concept from Bofinger's, which will be described in the following chapter. However, as far as soil-cement is produced using a soil including sand, silt, clay and colloid particles, the structure of soil-cement indicated by Fig. 2.1 and Fig. 2.2 seems almost reasonable.

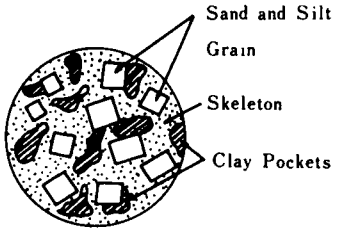

Fig. 2.1 Suggested cross-section of soil-cement (Bofinger(1964))

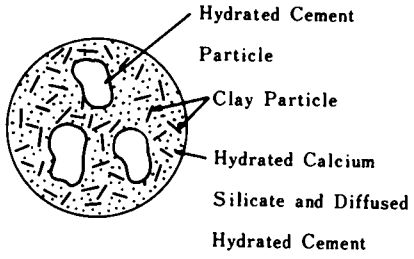

Fig. 2.2 Suggested cross-section of skeleton (Bofinger (1964))

Provided the general structure of soil-cement is allowed to be regarded as such one that sand, silt and clay pockets are embedded in the continuous phase consisting of clay, colloid particles and cementing compounds (the most part of these is calcium silicate hydrate or calcium aluminate hydrate), the subject concerning the relationship between the structure and mechanical properties can be considered to involve the following three problems.

(1) The relationship between the fabric of continuous phase and its mechanical properties, which vary with the physicochemical properties of the phase (so-called, clay-cement mixtures) before, during and after cement hydration.

(2) The effect of the volume fraction and the physical, mechanical properties of clay pockets on the mechanical properties of soil-cement

(3) Some problems relating to bonds between comparatively coarse grains (sand and silt) and continuous phase.

The first problem must be approached from both chemistry of cement and physical chemistry of clay. Even if the mineralogical properties of clay or colloid particles are not taken into consideration, these microscopic particles of a few micron size (especially, anisometric clay mineral particles shaped either as flat plates or as needles or laths, have a dimension of ten and a few angstrom in the minimum) are chemically very reactive. Therefore, it may be unquestionable that the interaction of these clay or colloid particles with cement hydration products has a significant effect on the fabric of clay-cement mixtures in the equilibrium state attained after a certain curing time.

The principal subjects to be noticed within a few hours after the addition of water are the mechanical properties of clay-cement-water system and the interparticle forces in the system (between clay or colloid particles themselves, hydrating cement particles and clay or colloid particles of soil, hydrating cement particles themselves). As far as this subject is concerned, an approach from clay colloid chemistry is important. In this respect, considerable progress can be found in the researches of clay-lime system (Diamond and Kinter, 1966). However, there seem to exist few studies concerning the fabric of clay-cement mixtures formed after complete cement hydration. As to the former, this paper a little refers to lime retention of clay-cement-water system. As mentioned above, in the latter, the interaction between clay and cement greatly influences the final fabric of clay-cement mixtures. In CHAPTER II, several new findings as to this problem in clay-cement mixtures compacted at optimum moisture content will be presented. A hypothesis of clay-cement structure is also proposed in CHAPTER II., which will be estimated from these experimental results obtained by the mineralogical and mechanical tests. The problem to be discussed is the relationship between the physical structure and mechanical properties of skeleton phase, i.e. clay minerals

-cement mixtures. This should be far more microscopically approached compared with the following problem. This phase in soil-cement is considered to be equivalent to cement paste phase in concrete. The effect of this phase on the mechanical properties of soil-cement is extremely significant. For the better understanding of the formation process of the fabric in this phase, the physicochemical interaction between cement and clay minerals is the primary problem to be revealed. In CHAPTER II, such physicochemical process in the clay minerals-cement interaction is revealed by X-ray diffraction, thermal analysis (D.T.A., T.G., D. T.G.), pH tests and an examination with optical microscope. It is found that the interaction between clay minerals and cement plays a significant role in the formation of microscopic structure of clay minerals-cement mixtures and their strength development. The characteristics of the interaction and the substances from which the strength originates are varied with the species of clay minerals used. After all, it may be concluded that cementitious reaction products primarily and secondarily resulting from the cement hydration and subsequent pozzolanic reaction are complicatedly entangled with clay and unhydrated cement particles to form rigid structure. The physical structure of clay minerals-cement mixtures may be similar to that of cement paste in nature. However, water- and air- filled voids in compacted clay minerals-cement mixtures are extremely greater than those in cement paste, and the lime-silica ratio of CSH(gel) produced in the mixtures varies with curing time and properties of clay mineral samples used. Several particular strength development characteristics of clay minerals-cement mixtures may be related to these facts.

The second problem with respect to the effect of clay pockets on the mechanical properties of soil-cement can be treated as a two phase composite material in relatively macroscopic sence. If the dynamic phase alteration is taken into account, the diffusion of Ca^{++} ions must play an important role in this problem. However, since detailed discussions on the influence of the diffusion of Ca^{++} ions make it far more complex to understand the effect of clay pockets, in this paper, only an attempt is made to estimate the effect of such diffusion from creep tests. The effect of clay pockets on viscoelastic properties of soil-cement will be stated in CHAPTER III; on shrinkage characteristics in CHAPTER IV. Furthermore, the effect of the amount of silt in the original granular soils on the viscoelastic properties of soil-cement is also discussed. The relationship between the properties of clay pockets and creep deformation characteristics of soil-cement is analyzed by the use of the concept of distribution function of retardation time and Burgers model. In consequence, the constituent phases (clay pockets and skeleton parts) distribution in the clay lumps samples-cement mixtures varies during the cure, depending upon moisture content and lumps size of the sample. This also indicates that the diffusion of Ca^{++} ions plays a very important role in the formation of the macroscopic structure of the soil-cement. Naturally, such properties of clay pockets also affect the shrinkage characteristics of soil-cement. Shrinkage of clay lumps-cement mixtures greatly depends upon the shrinkage characteristics and volume fraction of clay pockets. In practice, the use of the clayey soil completely dried up or with considerably high moisture (about 30 percent) appears to reduce ultimate shrinkage, even if clay lumps included in the soil are to only a little degree disintegrated.

The third problem could not be revealed without understanding the nature of chemical bonds between hydrating cement and coarse grains of quartz or feldspar. In this respect, there exists Handy's interesting hypothesis (Handy, 1958). This subject also appears to be related to the origin of strength of cement paste. This paper presents only an interpretive review including the author's suggestion in CHAPTER II.

The relationship between the structure and mechanical properties in soil-cement should substantially be discussed from three aspects stated above, not separately, but as a whole. But, discussions in this paper are restricted to two points, that is to say, to the effect of clay pockets and to the interaction of

clay minerals with cement, as described above at each article.

In general, shrinkage cracking has been considered as a serious fault in soil-cement pavement. As demonstrated in CHAPTER IV, this subject is discussed from a point of view of ''deigning a material'' so as to minimize the shrinkage stress on the exposed surface of pavement, because it may be assumed that cracking occurs when such shrinkage stresses exceed the tensile strength of the material. Since shrinkage stresses in soil-cement are controlled by its shrinkage characteristics and viscoelastic properties, some informations on the structure in which shrinkage stresses are as small as possible should be obtained. Among a number of factors affecting shrinkage cracking, silt fraction in sandy soil and volume fraction and physical properties of clay pockets are discussed. In this paper, an experimental stresses determination and stress analysis in a viscoelastic body (Burgers body) are proposed. These stresses calculation results show that grain size of soil has a significant effect on shrinkage stresses and that the presence of clay pockets is a deleterious element for reducing shrinkage cracking of soil-cement.

REFERENCES

Bofinger,H.E. (1964) :''The Structure of Soil-Cement'', Journal of Australian Road Research Vol. 2, No. 1, pp. 46 - 49.

Catton,M.D. (1959) :''Early Soil-Cement Research and Development'', Portland Cement Association Development Bulletin D 42, p. 3, Jan..

Diamond,S. and Kinter,E.B. (1966) :''Mechanisms of Soil-Lime Stabilization - An Interpretive Review'', Highway Research Record No. 92, pp. 83 - 92.

Handy,R.L. (1958) :''Cementation of Soil Minerals with Portland Cement or Alkalis'', Highway Research Board Bull 198, pp. 55 - 64.

Shideler,J.J. (1969) :''Soil-Cement Innovations'', A.C.I. Journal Proceedings Vol. 66 No. 11, Nov., pp. N1 - N2.

CHAPTER II INTERACTION BETWEEN CEMENT AND CLAY MINERALS

1. INTRODUCTION

Cement and soil constituting soil-cement mixtures have many complex physicochemical phenomena on which no scientific interpretation has yet been given. Furthermore, soil-cement produced by mixing such cement, soil and water yields far more complex system. On account of a great number of factors affecting its engineering properties, great difficulties are accompanied in the research of soil-cement.

As described in the previous chapter, the objective of this chapter is to obtain several informations on the fabric of clay-cement mixtures simultaneously revealing the alteration in its physicochemical properties with curing time. Hitherto, it has been confirmed that the surface chemical property of soil is an important factor for soil-cement (Winterkorn, 1942). It is since 1950's that, in the study of soil-cement , physicochemical properties of soil were taken into account. Comparatively small number of reports are found on the physicochemical study of soil-cement.

Judging from such a few reports on this subject published in the past, the following points should be kept in mind when doing the actual experiments.

Easy derivation of conclusions only from scanty experiments may lead to misunderstanding of phenomena, because test conditions such as curing temperature and moisture content of soil-cement samples are very variable and a clay mineral sample usually available includes more or less other non-clay mineral components. Furthermore, it is also a possible cause for misunderstanding experimental results that the grain size distribution and the degree of crystallinity of clay minerals samples are different for different investigations. In fact, different conclusions are drawn between several reports on this subject, as reviewed in the following paragraph. Therefore, in the study of the interaction between cement and clay minerals, many experiments from various aspects should be carried out under a similar condition to the one under which the soil-cement in an actual pavement is placed.

It is generally revealed that the calcium hydroxide produced by cement hydration plays a significant role in the interaction between cement and clay minerals. In this respect, soil-lime can be regarded as a further simplified soil-cement system. In a part of this chapter, it will be indicated that the nature of interaction of cement with clay minerals is still more definitely elucidated by comparing test results for clay-cement with those for clay-$Ca(OH)_2$ mixtures. A great number of studies on soil-lime in the past should also be utilized as a back ground for the research of soil-cement.

The purpose of this work is to reveal the physicochemical process in the interaction between clay minerals and cement, and the subsequent alteration in the fabric of clay-cement mixtures with curing time by X-ray diffraction, thermal analysis (D.T.A., T.G. and D.T.G.), pH tests and an examination with optical microscope. Unconfined compression tests as well as the above mineralogical experiments are also carried out to discuss the effect of such changes in physicochemical properties of clay-cement mixtures on their strength. Furthermore, additional tests on consistency of clay-cement mixtures within a few hours after the addition of water are carried out.

Discussions in this chapter include the following four subjects.

(1) Characteristic of the various species of clay minerals-cement interaction. Clay minerals selected here are montmorillonite, kaolinite, sericite, chrolite-vermiculite mixed layer and allophane.

(2) A role of calcium hydroxide resulting from cement hydration in the formation of clay-cement structure and in its progressive strength development. Simultaneously, the substantial dissimilarity and the similarity between soil-cement and soil-lime are also discussed from the results obtained.

(3) The influence of exchangeable cations held on a clay mineral on the strength of clay-cement mixtures, hydration of cement and reaction products.

(4) The hydration rate of C_3S and βC_2S in bentonite- and kaolinite-cement. This is an interesting subject, because the surrounding conditions under which these constituents of cement in soil-cement hydrate, are considerably different from those in cement paste usually used in concrete.

2. HYDRATION OF CEMENT

Some publications concerning the cement chemistry such as the one by Bogue (1955) and the one edited by Taylor (1964) involving the results discussed in the 4th International Symposium of Chemistry of Cement (1962) are available. Recently, the proceedings of the 5th International Symposium of Chemistry of Cement has been published (1968).

In this paragraph, several informations on the chemistry of cement, especially relating to the research of soil-cement are described, mainly involving the hydration mechanism of cement and physical structure of cement paste.

It is well known that the four main compounds of portland cement are C_3S, C_2S, C_3A and C_4AF*. Of these, C_3S is the most important since it is usually the main constituent in portland cement. The C_3S paste has largely reacted in 28 days, and almost completely in a year. On the contrary, reaction of the βC_2S is considerably slower than with C_3S, and much βC_2S remains even after a year. Reaction products of C_3S are $Ca(OH)_2$, and the calcium silicate hydrate; the latter shows X-ray powder diagrams with the three broad peaks at 3.07 Å, 2.82 Å and 1.81 Å and is variously known as CSH, CSH gel or tobermorite gel. The main product formed in βC_2S paste, a calcium silicate hydrate, is also closely similar to that formed from C_3S. Much less $Ca(OH)_2$ is formed because of the lower Ca/Si ratio of the starting material. Thus, calcium hydroxide and calcium silicate hydrate constitute the almost portion of products formed in the hydration of portland cement. Especially, the complete hydration of cement produces about 30 percent calcium hydroxide by weight of cement. The hydration of C_3S and βC_2S are given ideally by

$$2(3CaO\ SiO_2) + 6H_2O \longrightarrow 3CaO\ 2SiO_2\ 3H_2O + 3(CaO\ H_2O)$$

$$2(2CaO\ SiO_2) + 4H_2O \longrightarrow 3CaO\ 2SiO_2\ 3H_2O + CaO\ H_2O$$

In the interaction between cement and clay minerals, attention should be given to three phases of the calcium hydroxide, clay minerals and CSH gel. There was a great controversy between two theories as to the mechanism of cementing action in the early days of cement chemistry. That is to say, Le Chatelier attributed this to interlocking of crystals of hydrated compounds precipitated accompanying with the dissolution of the anhydrous compounds (crystal theory); Michäelis considered that cohesion in cement paste resulted from the formation and subsequent desiccation of a gel (gel theory). At present, it is said that both of these theories have an element of truth. The origin of cohesion in cement paste is generally attributed to a gel consisting of crystalline particles in colloidal size formed by dissolution and precipitation in the initial stages of reaction. These colloidal particles adhere strongly to each other so as to form a dence and continuous network in cement pastes, and to other bodies, because of the combination of their high surface energy (386 ergs/cm^2, according to Brunauer, Kantro and Weise (1959)) and high surface area

---

* In cement chemistry the composition of compounds are often represented as the sums of oxides, the formulas of which are then abreviated: C = CaO, S = SiO_2, A = Al_2O_3, H = H_2O

(260 m^2/g, according to Powers and Brownyard (1947)).

The secondary products formed by pozzolanic reaction in clay-cement mixtures are probably similar to calcium silicate hydrate or to calcium aluminate hydrate resulting from cement hydration. Therefcre, Powers's concept (Powers and Brownyard, 1947) on the physical structure of cement pastes may be of great value for the better understanding of the structure of clay-cement mixtures.

Powers and Brownyard (1947) calculated that 1 cm^3 of cement produces 2.2 cm^3 of hydration products. In a typical portland cement paste, the ratio of water to cement is around 0.5 by weight, or 1.5 by volume. The hydration products must partly be formed in space previously occupied by cement. Complete hydration of cements must require at least 1.2 cm^3 of space filled with water initially. This corresponds to an initial water-cement ratio by weight of 0.38. That is to say, only those with water-cement ratio greater than 0.38 have sufficient space for all the unhydrated cement particles to be converted into gel. Thus, initial water-filled space available for the formation of hydration products has a significant effect on hydration process of cements.

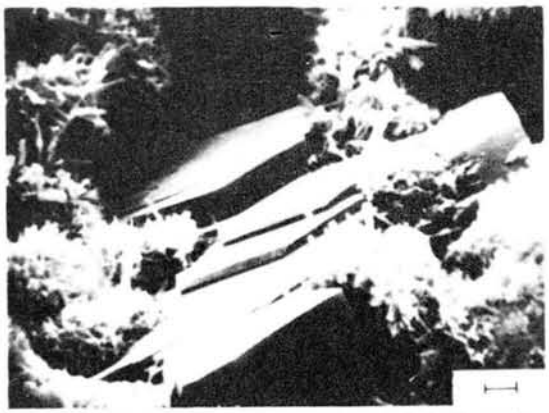

Fig.3.1 Fractured surface of a hydrated cement paste examined using the scanning electron microscope. The large, platey crystals are probably $Ca(OH)_2$ or aluminate hydrates; the fibres could be ettringite or calcium silicate hydrate. All surfaces were coated with a layer of metal 600 Å thick in preparing the specimen for examination. The ruled line represents 1 μ. (Chatterji and Jeffery, 1966).

Volume fraction of space filled with air and water in compacted soil-cement mixtures is very great in comparison with cement pastes; for example, those for kaolinite- and bentonite-cement specimens used in this study are around 33 percent and 50 percent, respectively. The initial ratio of such space to unhydrated cement solid in kaolinite- and bentonite-cement is 251% and 625%, respectively. Thus, cement hydration in compacted soil-cement mixtures is found to take place under a considerably different surrounding condition from that in cement paste, even if the effect of mineralogical properties of soil used and of the amount of water available for cement hydration are now not taken into account.

Many workers have reported the results of studies on cement pastes by electron microscopy; of these, a microphotograph on fractured surface of a hydrated cement paste recently obtained by Chatterji and Jeffery (1966) using a scanning electron microscope (Fig. 3.1) and the one by Sierra (Fig. 3.2)(1968) demonstrate some very interesting results concerning their internal structure. The large, platy crystals in Fig. 3.1 are likely $Ca(OH)_2$ or a hexagonal aluminate; the coarser fibres could be ettringite and the finer ones calcium silicate hydrate. In connection with the problem of the interaction between hydrating cement and clay minerals, it may be very

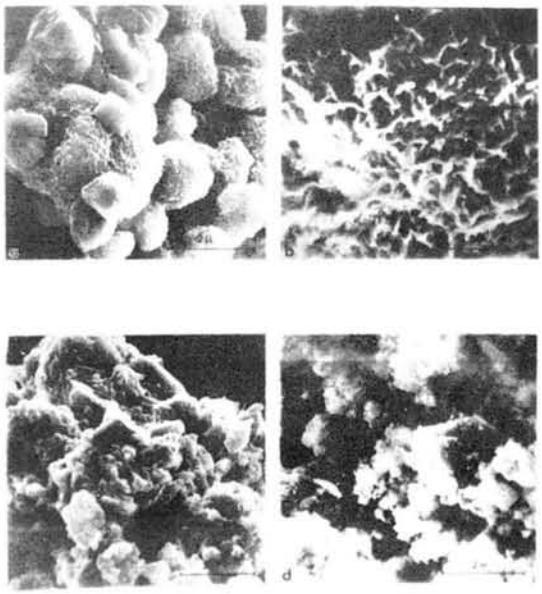

Fig. 3.2 Observation by the scanning electron microscope
a. C_3S hydrate at one month age (x 14000)
b. C_3S hydrate at one month age (x 58000)
c. cement paste after 4 hours hydration (x 10000)
d. cement paste after 5 years hydration x 11000) (from Sierra(1968))

interesting, but seems much complicated how $Ca(OH)_2$ is present in cement pastes. Sierra (1968) states in his report as follows: " Lime could probably be found not as a separate phase, but as a phase which is intimately incorporated into tobermorite gel". It may safely be said that these finer fibres of calcium silicate hydrate responsible for cohesion of cement pastes could also play a significant part in the strengh development of soil-cement mixtures. The chemical composition of this calcium silicate hydrate resembles tobermorite which was found as a naturally occuring mineral with the chemical composition of $3CaO\ 2SiO_2\ 3H_2O$ at Tobermory in Scotland. All of papers concerning various properties of calcium silicate hydrate would not be reviewed in detail. Only two subjects are summarized in the following, which seem interesting in the research of soil-cement.

One is associated with the relationship between the CaO/SiO_2 ratio of calcium silicate hydrate and its morphologic habits; the other concerning its similarity to some clay minerals in the crystal structure.

It may well be confirmed by many workers that various compositions of calcium silicate hydrate yield depending upon CaO contents in solution. Roughly speaking, the poor lime-calcium silicate hydrate shows crinkly foil-like crystal habit and the rich lime one is found as fibers. Taylor distinguished CSH(I) of the former from CSH(II) of the latter. Kalousek (1958) points out that the CaO/SiO_2 ratio at transition from the one to the other is 1.33. This fact is also admitted by another investigation using electron microscopy. Richartz and Locher (1965) mention in their report that the calcium silicate hydrate with the CaO/SiO_2 ratio smaller than 1.3 is plate-like and that the one greater than 1.4 is always fibrous or needle-like. Furthermore, they draw the conclusion that the morphology of calcium silicate hydrate in cement pastes relates to their strength (Richartz and Locher, 1965). The calcium silicate hydrate in cement pastes seems almost fibrous. It may be presumed that a soil with different physico-chemical properties has a different physico-chemical process in cement hydration occuring in the soil-cement, producing calcium silicate hydrates with various CaO/SiO_2 ratio depending especially upon the extent of the cation exchange and subsequent pozzolanic reaction of free lime with clay minerals. Thus, the relationship between the CaO/SiO_2 ratio of calcium silicate hydrate produced as a secondary product and the strength of soil-cement mixtures would be an interesting problem in the research of soil-cement.

The structural similarity between cement hydration products and clay minerals has been pointed out by many workers (Arnould,1967b)(Gard, Howison and Taylor, 1959).

Gard, Howison and Taylor (1959) explain a transition process from the plate-like CSH(I) to the CSH(II) with fibrous crystal habit by comparing the crystal structure of CSH(I) and CSH(II) with that of the comparable two species of clay minerals, respectively, as shown in Fig. 3.3.

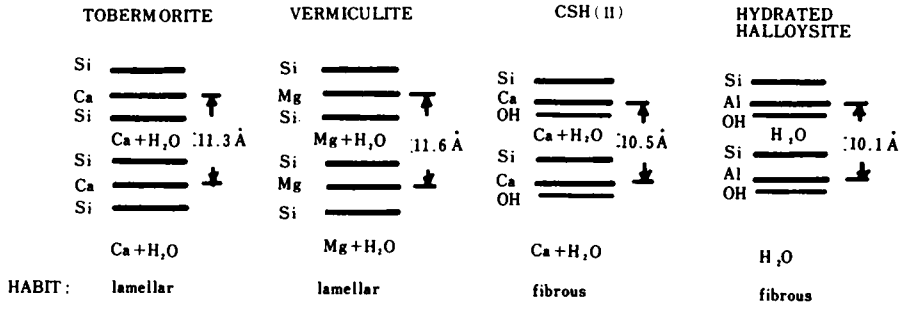

Fig.3.3 Diagrammatic representation of the sequence of layer in tobermorite, vermiculite, and hydrated halloysite, and the suggested sequence for CSH(II)

Arnould (1967a) states that the comparison of tobermorite with clay minerals could be useful for the research of additives in concrete technology. In the research of soil-cement, such similarity may lead to the presumption of "epitaxy"

(Farran, 1956)(Royer, 1954). Although, at present, little substantial evidence would be given on likelihood of epitaxy, it is to be expected that such a process would favour strength development (Herzog and Mitchell, 1963)(Gillot, 1968).

This paragraph summarizes the chemistry of cement in reference to the study of soil-cement. Author believes that well understanding of recent new informations on the chemistry of cement, in which the mechanism of cement hydration is intrinsically being revealed, would be helpful for the research of soil-cement.

3. PHYSICOCHEMICAL PROPERTIES OF CLAYS

Some physicochemical properties of clays associated with soil-cement stabilization are summarized in the follwing.

Silicates are composed of silica tetrahedra in which the silicon ions are surrounded by a tetrahedral group of four oxygen ions. The silicon-oxygen bond is not completely ionic and is probably partly covalent. The linkage of these silica tetrahedra among themselves or with other ions results in various species of silicates. Classification of these silicates is presented in Fig. 3.4. No mutual linkage of silica tetrahedra gives island silicates, such as olivines (Fig. 3.4). When each tetrahedron shares two corners, the structure of "chains" or "rings" is formed (Fig.3.4). Joint of two and a half corners in each tetrahedron on the average results in the structure of the "bands" type (Fig. 3.4). "Layer" structures are formed by sharing three oxygens of each silica tetrahedron. Most clay minerals have the layer silicate structure. Three-dimensional framework structures result, when adjacent silica tetrahedra share all oxygens. Silicic anhydride is the simplest species

COMBINATION OF TETRAHEDRA	DIAGRAMMATIC REPRESENTATION OF STRUCTURE	Si - O Group and Negative Charge	Oxygen to Silicon Ratio	EXAMPLE
INDEPENDENT	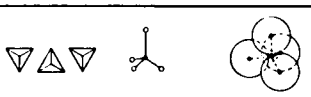	$(SiO_4)^{4-}$	4:1	OLIVINES
DOUBLE	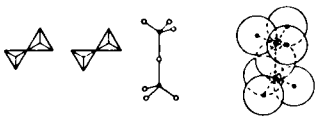	$(Si_2O_7)^{6-}$	7:2	AKERMANITE
RINGS	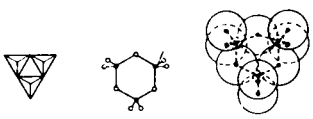	$(Si_3O_9)^{6-}$	3:1	BENITOITE
	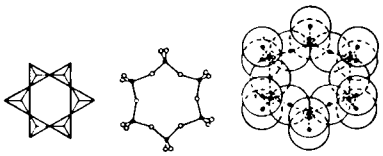	$(Si_6O_{18})^{12-}$		BERYL
CHAINS	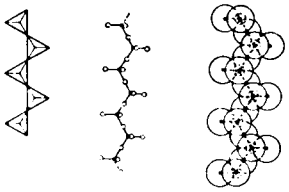	$(SiO_3)_n^{2-}$	3:1	PYROXENES
BANDS	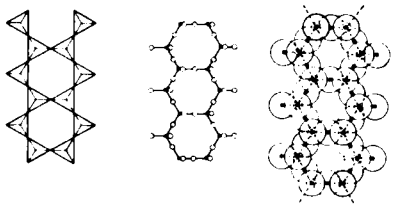	$(Si_4O_{11})_n^{6-}$	11:4	AMPHIBOLES

Fig.3.4

of these. Feldspar also belongs to this type of silicate. As stated above, the minerals which are of most importance in clays have layer structures and are classified as phyllosilicates. All of them have two types of structural unit. These are the silica tetrahedron (SiO_4) and octahedral unit of brucite ($Mg(OH)_2$), or of gibbsite ($Al(OH)_3$) (Fig.3.5) (Grim, 1968). The general structural model of the layer silicate minerals is generated by the combination of each sheet of tetrahedral and octahedral units. All of these minerals are summarized as Table 3.1 (Brindley, 1965).

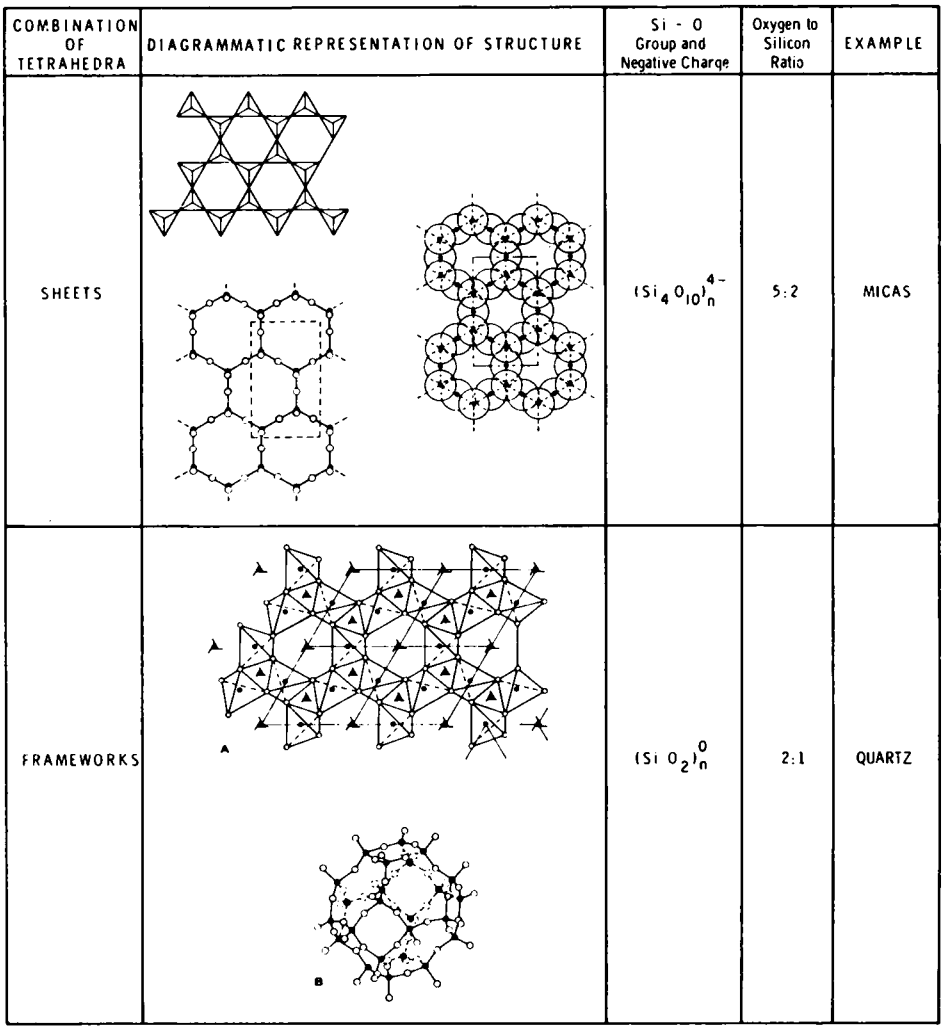

Fig. 3.4 Chief varieties of structural combination in silicates. *A.* After DEER et al. (1963, 4 : 184) *B.* After WINCHELL (1951, p.240).

A combination of one octahedral and tetrahedral layer in the manner indicated in Fig. 3.6 generates a 1:1 type of layer structure. This is the basic structural plane of the kaolinite-serpentine group of minerals. When a second tetrahedral layer is added in a similar manner with replacement of hydroxyls in the sheets on the opposite side of the octahedral cation, a 2:1 type of layer structure results (Fig. 3.7). This arrangement is found in the pyrophyllite-talc group, the smectites, the vermiculites and the mica groups (Table 3.1). In the chlorite minerals there is an additional octahedral layer which is located between successive 2:1 units.

Generally, clays show unusual physicochemical properties, because their specific surface is very high, and crystal structure of many minerals is two dimensional and heterogeneous. Despite of the similarity between the morphology and crystal structure of tobermorite gel particles of the main cement hydration product and those of clay minerals, properties of clay particles in colloidal state are different from those of hydrating cement particles. In most respects, clays behave like hydrophobic, but cement particles do like hydrophilic. This fact seems to give an interesting suggestion on the change in consistency of soils due to the addition of cement.

A concise description on clay colloid chemistry will be given in the following.

Usually, the surfaces of crystalline solid have specific physicochemical properties because atomic bondings are broken at those sites.

Weyle has discussed the atomic structure of surfaces in terms of crystal chemical principles (Weyle, 1953). He describes that the surface energy of a homogeneous solid can be decreased by decreasing its surface area and by four types of structural changes: (i) polarization of surface ions, (ii) increasing the number of anions, (iii) distortion of surface structure, (iv) chemisorption of molecules or ions. According to his concept, important surface phenomena concerning solid surface-liquid interaction in colloid system can be accounted for in terms of screening of cations. The state of polarization of NaCl surfaces is interpreted by showing the schematic diagram (Fig. 3.8).

The following descriptions are concerning several characteristics of clay colloid particles attributed to heterogeneity of crystal plane in clay minerals. Only subjects which seem to be related to the research of clay-cement mixtures are picked up from the publication by Marshall (1964).

The (001) or cleavage planes in clays are very different in surface composition from the (hk0) or edge planes. In kaolinite a facile cleavage separates planes of composition $(OH)_3$ from Si_2O_3 planes. Hence the external flat surfaces should consist on the avarage of equal numbers of these two compositions. The edge planes represent the most active sites in crystal growth. Thus the members of the kaolin groups may be expected to show three superimposed surface chemisties. The platy character with a:c ratios, between 5:1 and 20:1 would insure that the surface area would be predomi-

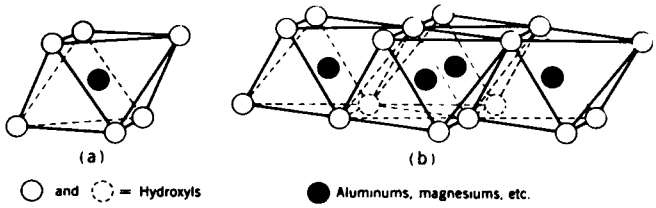

Fig.3.5(a) Diagrammatic sketch showing (a) a single octahedral unit and (b) the sheet structure of the octahedral units.

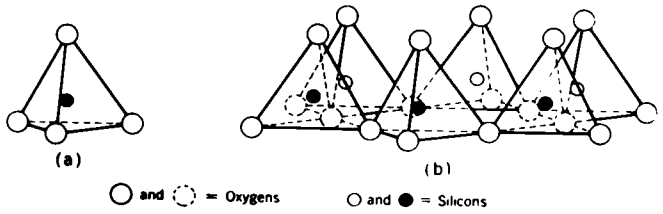

Fig.3.5(b) Diagrammatic sketch showing (a) a single silica tetrahedron and (b) the sheet structure of silica tetrahedrons arranged in a hexagonal network.

Table 3.1

PROPOSED CLASSIFICATION SCHEME FOR THE PHYLLOSILICATES (RELATED TO CLAY MINERALS)
(As submitted by the C.I.P.E.A. nomenclature committee to the International Mineralogical Association, after BRINDLEY, 1966.)

Type	*Group* (x = layer charge)	*Subgroup*	*Species*[1]
2 : 1	Pyrophyllite–talc ($x \sim 0$)	Pyrophyllites	Pyrophyllite
		Talcs	Talc
	Smectite or Montmorillonite–saponite ($x \sim 0.5$–1.0)	Dioctahedral smectites or Montmorillonites	Montmorillonite, beidellite, nontronite
		Trioctahedral smectites or Saponites	Saponite, hectorite, sauconite
	Vermiculite ($x \sim 1.0$–1.5)	Dioctahedral vermiculite	Dioctahedral vermiculite
		Trioctahedral vermiculite	Trioctahedral vermiculite
	Mica[2] ($x \sim 2$)	Dioctahedral micas	Muscovite, paragonite
		Trioctahedral micas	Biotite, phlogopite
	Brittle mica ($x \sim 4$)	Dioctahedral brittle micas	Margarite
		Trioctahedral brittle micas	Seybertite, xanthophyllite, brandisite
2 : 1 : 1	Chlorite (x variable)	Dioctahedral chlorites	
		Trioctahedral chlorites	Pennine, clinochlore, prochlorite
1 : 1	Kaolinites–serpentine ($x \sim 0$)	Kaolinites	Kaolinite, halloysite
		Serpentines	Chrysotile, lizardite, antigorite

[1] Only a few examples given.
[2] The status of illite (or hydromica), sericite, etc., must at present be left open since it is not clear whether or at what level they would enter the table: many materials so designated may be interstratified.

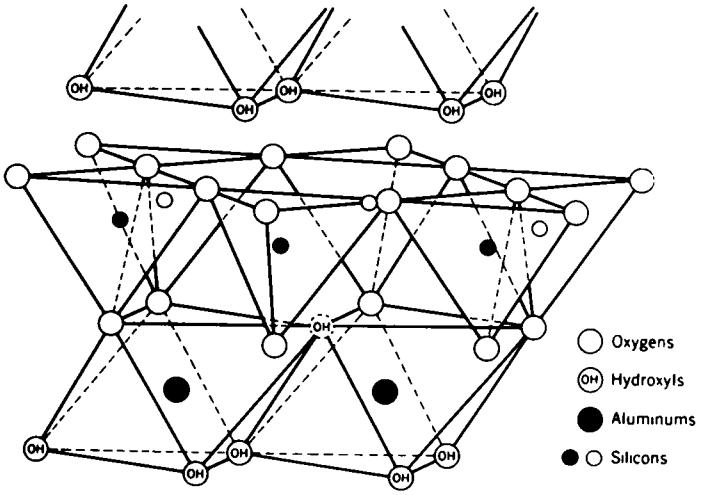

Fig. 3.6 Diagrammatic sketch of the structure of the kaolinite layer. (After Gruner.)

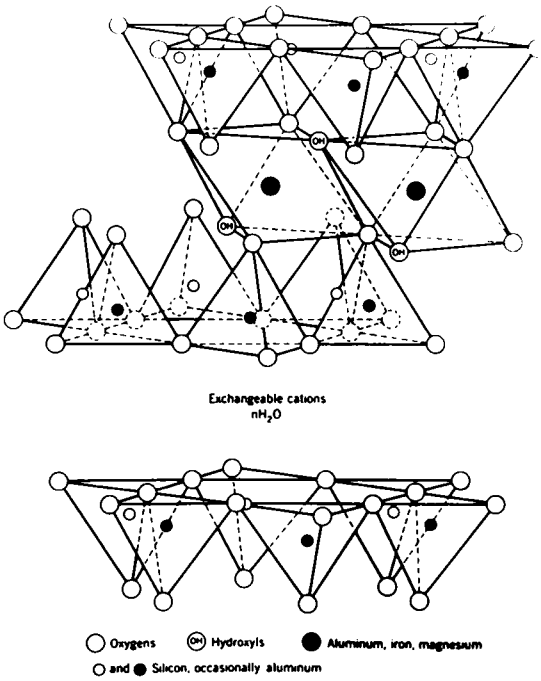

Fig.3.7 Diagrammatic sketch of the structure of smectite according to Hofmann, Endell, and Wilm, Marshall, and Hendricks.

nantly (001). Yet if the exposed Si_2O_3 and $(OH)_3$ planes are relatively inert in respect of adsorption and dissociation of ions, the electrochemical properties of the edges may dominate. The characteristic grouping at kaolinite edges of ideal composition would be

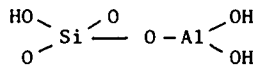

the silicon being tetrahedral and the aluminum octahedral. The electrochemical properties would be those of the OH groups, one set attached to silicon, the other to aluminum. Those belonging to silicon would have the properties of aluminosilicic acids, with an acidic function stronger than that of polysilicic acid and weaker than that of montmorillonite or beidellite. The hydroxyls attached to aluminum would strongly resemble those already present in the $(OH)_3$ surfaces as regards chemical properties, but geometrically they are more accessible, so that the ease of replacement with a larger ions such as chloride would be greater. Such reactions with anions are highly pH dependent. Thus at each edge there would be rows of acidic or negative sites altering with rows of positive sites, the exact balance being a sensitive function of pH. In acidic systems the dissociation of the negative sites would be suppressed, and binding of anions at positive sites would be favored. In clays of the montmorillonite and mica groups it is evident that edge hydroxyls attached to aluminum will be much less in evidence than kaolinite clays. In the montmorillonite and illite clays there is a strong, negative charge on the lattice itself, a function which is not dependent on pH.

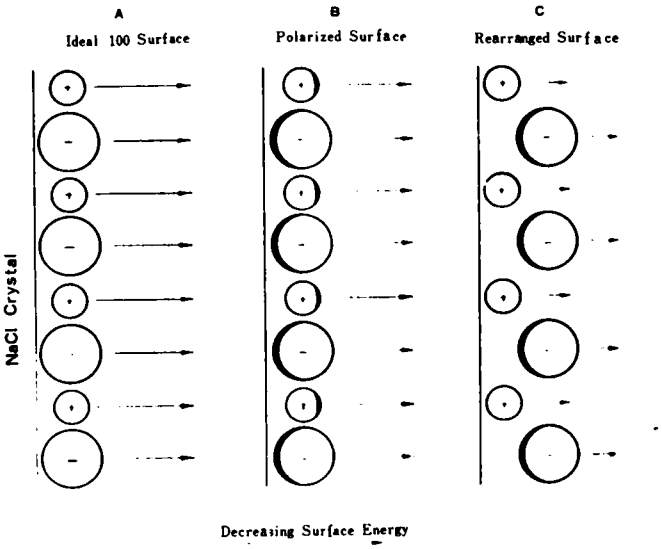

Fig.3.8 —Electronic deformation and ion in rearrangement in a NaCl surface

The stability of colloidal suspensions results from the electric charge associated with the particles. This charge is believed to originate from three principal mechanisms. The charge may result from imperfections such as vacancies or unbalanced ionic substitutions in the crystal structure (Fig. 3.9(a)); from the physical or chemical adsorption of ions at active sites associated with broken bonds (Fig. 3.9(b)); and from the adsorption of ions of the same type as those in the structure of the particle (Fig. 3.9(c)).

A Van Olphen's concept as to a property of clay colloid suspensions will be noted below.

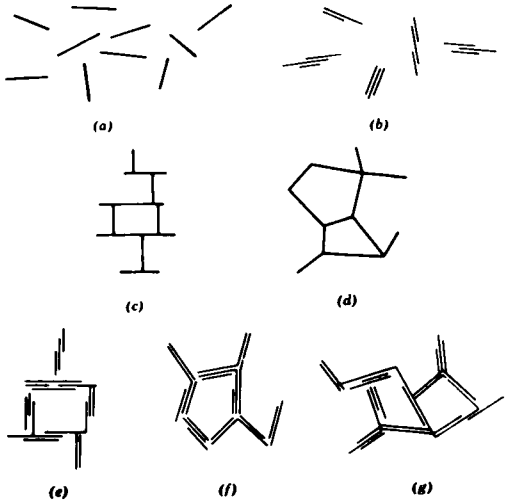

Fig.3.9 Modes of particle association in clay suspensions, and terminology. (*a*) "Dispersed" and "deflocculated." (*b*) "Aggregated" but "deflocculated" (face-to-face association, or parallel or oriented aggregation). (*c*) Edge-to-face flocculated but "dispersed." (*d*) Edge-to-edge flocculated but "dispersed." (*e*) Edge-to-face flocculated and "aggregated." (*f*) Edge-to-edge flocculated and "aggregated." (*g*) Edge-to-face and edge-to-edge flocculated and "aggregated."

When the charge on the colloidal particle results from adsorption, the type of ion adsorbed is dependent on the relative ionic concentrations and the pH of the solution. The charge on the particle is sometimes reversible as in the case of aluminium hydroxide which acquires a positive charge due to adsorption of aluminium ions in acid solution and a negative charge due to adsorption of hydroxyl or aluminate ions in alkaline solution. Van Olphen has proposed that this negative charge is associated with the flat (001) surfaces whereas the edge surfaces may acquire a positive charge (Van Olphen, 1963). He points out that where aluminum is the dominant octahedral cation the broken edge of the octahedral sheet is comparable to the surface of a particle of alumina. As mentioned previously, alumina acquires a positive charge in an acid environment. Van Olphen further suggests that silica sheets may be preferentially broken at the places where aluminum ions have substituted. Hence the exposed edges of the tetrahedral layer may resemble the octahedral layer and may also develop a positive charge (Van Olphen, 1963). The behavior of colloidal suspensions of clay minerals is affected by the fact that the edge surfaces acquire a positive charge while the flat surfaces have the permanent negative charge. On flocculation clay platelets may associate in an edge-to-face, face-to-face, or edge-to-edge manner depending on the complex balance between the attractive and repulsive forces involved. Modes of particle association have been suggested by Van Olphen (Fig. 3.10)(1963).

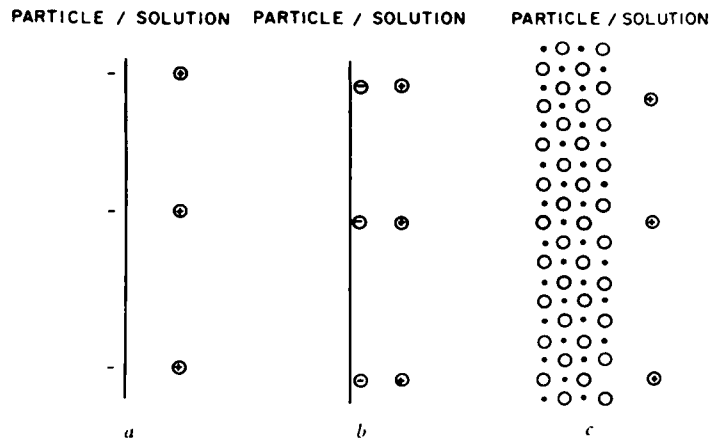

Fig.3.10 Formation of an electric double layer. (*a*) Interior lattice charge. (*b*) Specific ion adsorption. (*c*) Lattice-ion adsorption.

Finally, the cation exchange will briefly be dealt with. This phenomenon may be very important in the strength development of clay-cement.

The counter ions associated with colloidal particles such as clay minerals are in a state of dynamic equilibrium with the ions in the surrounding solution. If the composition of the bulk solution changes,

the ionic content of the diffuse double layers also changes. There are following four principal mechanisms responsible for cation exchange. Thus, the exchange capacities of the different clay minerals cover a considerable range of values.

(1) Cations are held in exchangeable form on or near the surface of clay minerals by electrostatic forces which result from the net negative charge on the structure arising from ionic substitutions This is the chief cause of the cation exchange capacity of the 2:1 layer silicates.

(2) At edges and corners there are ''broken bonds'' or unsatisfied valincies to which exchange ions can become attached. The number of such sites increases as particle size decreases and fine fractions of many minerals show an increase in exchange capacity. This effect is shown by kaolinite.

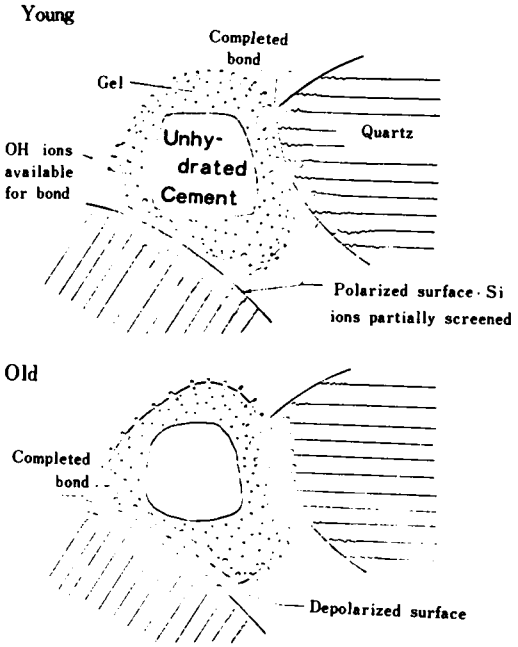

Fig.3.11 Diagrammatic representation of a theory of cementation. Early cementation bonding is weak due to distortion polarization of the quartz surface. However, the early chemical bonding causes distortion to slowly disappear. This in turn allows even greater chemical bonding (Handy, 1956)

(3) The hydrogen of exposed hydroxyls (which are an integral part of the structure rather than due to broken bonds) may be replaced by a cation which might be exchangeable. This cause of exchange capacity would be important for kaolinite and halloysite because of the presence of the sheet of hydroxyls on one side of the basal cleavage plane.

(4) Under certain conditions cations from within the structure may become exchangeable. For example, in an acid environment the aluminium ions move from within the silicate structure of clay minerals into exchange positions.

4. REVIEW OF THE LITERATURE

Handy (1968) emphasized in his paper that chemical bonds developing between the cement and mineral surfaces become more important in finer-grained mixtures such as soil-cement than in coarse-graded mixtures such as concrete. He attempted to explain the long-term development of strength in certain soil-cement mixtures on the basis of the hypothesis which follows Weyl's proposals (1953) of polarization of ions near the surface of the silica (Handy, 1958)(Handy, 1956). Quartz adsorbs OH ions due to insufficient polarization screening, and OH ions are supplied from the surface of particles of hydrated cement gel. Under proper conditions the ions adsorption screening gradually replaces structural polarization screening with time, and bonding becomes stronger (Fig. 3.11). The relatively inert polarized layer in the surface of quartz particles is dissolved in the alkaline environment and converted to silicate gel which bonds directly to active quartz.

As stated in CHAPTER I , Handy's concept should be applicable to the soil-cement mixtures produced by using soils including silt and sand as the major constituents (therefore, predominant minerals in such soils would be quartz and feldspars).

The strength of soil-cement would mainly originate from the secondary chemical bonds such as Van der Waals forces acting between quartz or feltspar and hydrated cement gel particles. It could be said at

this point that Handy's hypothesis lays emphasis in the effect of the surface structure of quartz particles on the strength of soil-cement mixtures. However, colloidal chemical properties of cement gel particles which almost consist of tobermorite gel particles should be taken into account in the discussions of bonds between quartz and cement gel particles. Physicochemical processes progressing in the contact zone between a quartz particle and tobermorite gel and the properties of tobermorite gel particles should be more important factors for development of the strength of soil-cement mixtures.

According to Weyl's theory (1953), clay flakes are so thin (7 - 10 Å) as to prevent satisfactory structural screening, and the electrical effects observed on clay, as descrived in the previous paragraph, are attributed to this cause. Thus, probably more important are long-term chemical changes within the clay minerals brought on as a result of the change in the environment (Weyl, 1953).

The physicochemical changes occuring in clay minerals-cementitious additives mixtures, which correspond to continuous phase in the soil-cement structures (Fig. 2.2), must have been an highly interesting phenomenon to many investigators. Scientific interest has been devoted to the reaction between clay minerals and $Ca(OH)_2$ for a long time. Excellent reviews of the literature of soil-lime interaction were made by Diamond (1966) and Ariizumi (1967). Some notes on the mechanism of the soil-lime reaction will briefly be cited from those reviews in the following.

The effects of lime on plastic soils could be divided into two phenomena. One is short-time effect and the other is the long-time cementitious reaction responsible for the development of strength. The rapid cementation is attributed to immediate formation of tetracalcium aluminate hydrate by reaction of $Al(OH)_x$ groups at the edges of the clay particles with adsorbed calcium hydroxide on the faces of adjacent planar surfaces. Since the long-time cementitious reactions contribute to slow development of strength in soil-lime systems, an interest has been taken in the properties of the reaction products. In general, the products formed are usually tobermorite gel and a calcium hydrate phase; other compounds formed under special circumstances are tricalcium aluminate hexahydrate and calcium silicate hydrate(I). The information on the chemical mechanisms in the lime-clay mineral transformations would tend to suggest a "through solution" mechanism dependent on the rate of dissolution of the clay (or of silica and alumina from the clay), since it is implied that the reaction depends on attainment of a high pH and since addition of sodium hydroxide accelerates strength development. On the other hand, evidence that the reaction proceeds from an initial state of physical adsorption of lime on the surface of the clay would suggest a surface chemical reaction not dependent on prior dissolution of material from the clay.

Willovghby et al. (1968), in their recent investigations by an electron microscope, describe an interesting fact that, despite of the attack along the edge of kaolinite particles on the addition of calcium hydroxide, a reaction product is formed on the (001) planes. They also state that the strength gains in alkali-stabilized clays must considerably be affected by an ionic migration into the lattice of the clay mineral.

A relatively few reports concerning the mineralogical investigations of the interaction between clay minerals and portland cement are found. These investigations will be reviewed briefly here.

Herzog and Mitchell (1963) investigated the reaction of kaolinite and montmorillonite with tricalcium silicate and portland cement. They noted the reduction in the height of peak of basal reflection of these clay minerals with curing time. Furthermore, the disappearance of calcium hydroxide and subsequent formation of the new reaction products were also reported, though these experiments were conducted at the elevated curing temperature, 60° C. The possibility of epitaxial crystal growth was pointed out through

the similarity between the crystal structures of the reaction products and clay minerals.

Moh (1962) noted that the reactive calcium in cement can be utilized in the production of cementitious silica gel and that the quantity of cementitious material available for bonding in soil-cement is greater than in neat cement.

Ingles (1966) drew the conclusion that the strength developed in soil-lime and -cement as well as in ceramics was a logarithmic function of porosity. Naturally, porosity in soil-lime and-cement mixtures depends upon the amount of cementitious gel included. Jambor (1963) elucidated as well that the strength of lime-pozzolana pastes is a power function of the volume fraction of hydration products produced in them; this is in agreement with the discovery of Powers (1960) concerning hardened cement pastes.

In another paper, Moh (1965) reported the investigation of the interaction between quartz, kaolinite and tricalcium silicate, calcium hydroxide. The results obtained in his examination showed the reduction in the X-ray diffraction peak height of quartz and calcium hydroxide. The formation of poorly crystallized CSH was also reported. These results seem to prove that the surface of quartz particles is dissolved in alkaline environment and converted to silicate gel. The quartz sample used in Moh's experiments was obtained by grinding Ottawa sand. Although the ground mineral was allowed to stand in air under room temperature and humidity for at least 3 months before use, it would appear questionable whether quartz particles have screened surfaces.

Mitchell and Jack (1966) observed the alteration in the fabric of clay-cement with curing time by an electron microscope and described the attack along the edge of kaolinite. Recent papers by Croft (1967) and Noble (1967) gave the interesting results regarding the interaction of several clay minerals with portland cement. Noble (1967) explained the mechanism of the reaction of clay minerals with portland cement. He emphasized the restriction of cement hydration due to the very fine-grained clay. Croft (1967) demonstrated that soils characterized by montmorillonite and mixed-layer minerals and degraded weathering products retarded the hydration and hardening of cement. Especially, Noble (1967) attributed the absence of calcium hydroxide in montmorillonite-cement mixture to the suppression of cement hydration by fine particles. On the contrary, several investigations suggest that the disappearance of calcium hydroxide in montmorillonite-cement may be responsible for its adsorption onto montmotillonite clay particles and subsequent pozzolanic reaction with them.

Cement hydration process in compacted clay-cement mixtures still remains uncertain. Based on Shestoperv's theory on cement hydration, Bezruk (1950) mentioned that the hydrolysis and hydration of cement surrounded by reactive substances are retarded in one case, while acceralated in another. For example, experiments by isothermal calorimetry indicate that the hydration of the C_3S is influenced very little by gibbsite; it is influenced by bayrite to a somewhat large extent (Jong, Stein and Stevels, 1968). Therefore, it may be presumed that the degree of the crystallinity of clay minerals used has a delicate effect on cement hydration in clay-cement mixtures. Recently, an attempt is made on the utilization of some clay minerals as an admixture in concrete. In this case, the interaction between clay minerals and hydrating cement should also be important.

Lipowski (1968) proposed that the powdered and dried clays could be mixed with cement to produce a new cementing material desirable for the production of concrete. He obtained several experimental results concerning the physicochemical phenomena in the hardening process of the material. The results obtained are as follows:

The specific surface of powdered clays added highly affects the hydration of the cement. The adsorption

of Ca^{2+} ion to clay minerals occurs on hydration of the mixtures. It accelarates the hydrolysis of alite, so that its setting and hardening behaviors become considerably different from those of the usual additive-free portland cement. The absence of calcium hydroxide in such clay-cement material is also described. It is concluded that the predominant clay mineral in clay used definitely influences the properties of cement-clay products. Furthermore, it would be much interesting to note the fact that the maximum strength of cement mortars using the clay-cement material is attained at 40 to 50 %, 60 to 70 % and about 30% of clay content by weight of cement for kaolinite, illite and bentonite, respectively, followed by the reduction in strength with the further addition of clay.

Ariizumi (1969) reports the investigation regarding the use of hydrated halloysite as an acceralator for concrete.

5. MATERIALS AND OUTLINE OF EXPERIMENTS

Experiments

(a) consistency tests, (b) Unconfined compression test, (c) Thermal analysis, (d) X-ray diffraction, (e) pH test, (f) Examination by the optical microscopy

Materials and Preparation of Samples

a) Cements and Calcium Hydroxide

Cements used are the normal, high early strength and moderate heat commercial portland cement. The chemical compositions of cements used are given in Table 3.2. The $Ca(OH)_2$ used was freshly opened first grade reagent, which was supplied by Katayama pharmaceutical Co. .

b) Clay Mineral Samples

Mg-bentonite(MB) and Ca-bentonite(CB) were supplied by the Kanto Bentonite Co. and the Kunimine Kogyo Co., respectively. Na-bentonite (NB) was obtained by exchanging Mg ions in Mg-bentonite(MB) for Na ions through the process described in the latter of this paragraph. Pyrophylite was supplied by the Kanto Bentonite Co.. Kaolinite (Ka(I), Ka(II) and Ka(III)) from Hiraki, Hyogo Prefecture and sericite(S) from Kanazawa, Ishikawa Prefecture were made under 250 μ (105 μ for Ka(II) and Ka(III)) by grinding the respective rocks. Chlorite-vermiculite mixed-layer mineral

Table 3.2 Chemical Compositions of Cements

Cement	Normal	High-Early-Strength	Moderate-Heat
SiO_2(%)	22.3	20.8	23.2
Al_2O_3(%)	5.4	4.6	4.5
Fe_2O_3(%)	3.2	2.8	3.9
CaO(%)	64.7	66.0	64.3
MgO(%)	1.2	1.4	1.3
SO_3(%)	1.6	2.7	1.6
Ig. Loss (%)	0.5	0.8	0.4
Insol.(%)	0.1	0.2	0.1
Total (%)	99.0	99.3	99.3
C_3S(%)	49	69	45
C_2S(%)	27	8	33
C_3A(%)	9	8	5
C_4AF(%)	10	9	12

(R) and allophane (A(I) and A(II)) were from Noto, Ishikawa Prefecture and Ina, Nagano Prefecture. The natural soil was from Utatsuyama hill in Kanazawa, Ishikawa Prefecture.

The predominant clay and non-clay minerals contained in samples and their physical properties are presented in Table 3.3. The chemical composition and cation exchange capacity of these clay samples are also shown in Table 3.4. The method employed for determination of cation exchange capacity was Yoshida et al.'s method (1953) which is based on Schollenberger's method. That is to say, a clay sample was allowed to be saturated with the ammonium. The ammonium was replaced by sodium cations using 10 percent sodium chloride solution and the amount of ammonium replaced was determined by the colorimeter.

The Na-bentonite sample used was obtained through the following process, which is based on the method of the determination of cation exchange capacity described above.

2ℓ of a 1 N ammonium acetate solution (pH 7) were added to 200g of Mg-bentonite sample and filtered using a funnel over during about 10 hours. The excess ammonium acetate remaining in clay sample, after the filtration, was removed using 1ℓ of 80 percent methyl alcohol (the first grade reagent). Ammonium ions were leached out by filtrating 2ℓ of 10 percent sodium chloride solution through the ammonium-saturated clay for about 10 hours, producing the Na-bentonite sample. Finally, extra salts were leached out using 2ℓ of 80 percent methyl alcohol. The Na-bentonite sample obtained was dried in a constant temperature oven held at 30° C and ground in a ball mill to pass the 74μ sieve. The (001) peak in X-ray pattern of montmorillonite in the Na-bentonite after the application of the treatment stated above was found at 12.6 Å, while that in Mg-bentonite at 15 Å (Fig. 3.12). This fact proves that the predominant component in the bentonite is Na-montmorillonite. The change of Mg-bentonite is proved by the chemical composition as well, as given in Table 3.4.

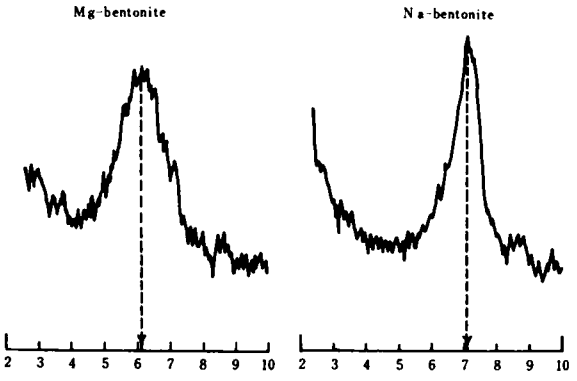

Fig.3.12 (001) peak of montmorillonite in Mg-and Na-bentonite

Water used is distilled water.

The Amount of Additives and the Curing Time of Specimens

The cement contents selected are 10, 20 and 30 percent by weight of dry clay mineral samples. The amounts of the $Ca(OH)_2$ added are 3, 6 and 9 percent by weight of dry clay mineral samples. Each experiment is carried out for specimens cured for 1, 3, 7, 14, 28, 91, 182 or 200 and 364 days.

Procedure

(a) Unconfined compression test

Air-dried minerals and cement are first mixed and followed by the addition of the distilled water and the subsequent mixing by hand until an uniform specimen is obtained. Cylindrical specimens, which are 5 cm in diameter and 10 cm high, are compacted statically by an oil jack so as to equal the optimum moisture content and maximum dry density of each clay-cement combination. Specimens sealed by paraffin wax are cured at 20° C under a 85 % relative humidity. The loading speed at the compression test is 0.2 kg/cm^2/sec.. Each type of specimens were made in triplicate; the compressive strength is their average.

(b) pH test

The pH value for each sample is the abration pH, which was measured by a glass electrode pH meter (manufactured by Toadempakogyo Co.) for filtrate prepared by the following procedure:

Table 3.3 Physical Properties

Properties	Bentonite			Kaolinite			Mixed-Layer	Allophane		Natural Soil	Pyroph-yllite	Sericite (SE)
	MB	CB	NB	Ka(I)	Ka(II)	Ka(III)	(R)	A(I)	A(II)	(NS)	(PR)	
Size Ranges:												
> 74 μ(%)	00	00	00	58	25	17	1	40	44	4	00	26
74 - 5 μ(%)	17	21	22	35	69	73	92	43	30	93	53	42
< 5 μ(%)	83	79	78	7	7	10	7	17	26	3	47	32
L.L. (%)	328	420	443	25.3	33.0	34.2	77.0	137	88.0	63.4	42.0	28.4
P.L. (%)	41	34	48	17.3	20.5	18.6	27.1	106	____	30.9	31.5	20.7
P.I.	277	386	395	8.0	9.5	15.6	49.9	31	N.P.	32.5	10.5	7.7
Maximum Dry Density (g/cm^3)	1.015	1.345	____	1.860	1.770	1.720	1.535	0.920	0.950	1.371	1.570	1.842
Optimum Moisture Content(%)	50.0	35.0	____	13.7	15.1	18.4	23.5	66.5	58.5	31.5	24.5	15.7
Predominant Clay and Non-clay Minerals	montmorillonite, cristobalite, quartz			kaolinite quartz			chlorite-vermiculite mineral, quartz	allophane, hydrated halloysite (only A(II))		quartz, feldspar, kaolinite, illite, montmori-llonite	Pyroph-yllite quartz	sericite, pyrophyllite,

CB : Ca-bentonite, MB : Mg-bentonite, NB : Na-bentonite

Table 3.4 Chemical Compositions and Cation Exchange Capacity

	Mg-bentonite	Ca-bentonite	Na-bentonite	Kaolinite	Mixed-layer	Sericite	Allophane A(II)
SiO_2(%)	70.98	70.93	71.48	50.34	67.00	66.48	52.07
Al_2O_3(%)	16.41	13.01	15.02	34.82	16.96	26.93	28.45
Fe_2O_3(%)	1.92	2.07	1.60	0.64	3.18	2.55	2.23
CaO(%)	0.56	1.90	0.28	0.78	0.84	0.12	2.57
MgO(%)	2.17	0.34	0.06	0.33	1.90	0.64	0.36
Na_2O(%)	0.15	0.15	4.90	0.43	0.32	0.05	0.26
K_2O(%)	0.23	0.24	0.71	0.64	0.24	0.10	0.45
Cation Exchange Capacity (meq./100g)	73	68	____	7.4	8.6	9.6	25

Note : Cation exchange capacity of natural soil (NS) and allophane (A(I)) is 30 and 27 meq./100g, respectively.

Ten grams of the ground specimens passing the 74 μ sieve were mixed with 50 cc distilled water with an electric stirrer for 10 minutes. The suspension was filtered immediately.

(c) X-ray diffraction

The samples ground in a mortar were examined by an X-ray diffractometer, "Geigerflex" of Rigakudenki Co., under the following measuring conditions.

For the purpose of identifying the reaction products: Target: CuKα, Filter: Ni, Voltage: 30 kV, Current: 15 mA, Scale factor: 2, Time constant: 8, Multiplier: 0.8, Scanning speed: 2°/min., Divergency slit: 1°, Scattering slit: 1°, Receiving slit: 0.15 mm, Chart speed: 2 cm/min..

For the purpose of measuring intensity of two alite and belite peaks: Target: CuKα, Filter: Ni, Voltage: 40 kV, Current: 15 mA, Scale factor: 8, Time constant: 4, Multiplier: 1.0, Scanning speed: 0.5°/min., Devergency slit: 2.5°, Scattering slit: 2.5°, Receiving slit: 0.30 mm, Chart speed: 1 cm/min..

(d) Thermal analysis

The same ground samples as those for X-ray diffraction were used for thermal analysis. A "Derivatograph", manufactured in Hungary, equipped with a single-unit platinum block with platinum-rhodium thermocouples was used at the heating rate, 10° C/min., with 1000 mg sample. Calcined aluminum oxide was used as the referecce material. The results obtained by this equipment were D.T.A., T.G. and D.T.G. curves. Some of the D.T.A. curves of bentonite-cement (Fig. 3.37, Fig. 3.38) were obtained at the heating rate, 6.5° C/min., with 300 mg sample.

(e) Preparation of thin sections of clay-cement mixtures

The absorbed water in the compression test specimen was removed in an oven at 30° C for 3 hours. The dry clay-cement lump was impregnated with a urea resin (Oshika resin, No. 105, refractive index: 1.555) in an outgassed desiccator for about 12 hours. The lump was bonded on to the plate glass with lake cement, from which a thin section, 30 microns in thickness, was made.

(f) Consistency test

Plastic limit was determined basing on JIS A 1205. Clay-additives mixtures to which water had been added up to a little smaller moisture content than the plastic limit, were left for about an hour before the test.

6. RESULTS AND DISCUSSIONS

THE INTERACTION BETWEEN VARIOUS CLAY MINERALS AND PORTLAND CEMENT

(1) Relationship between the plastic limit of clay-cement and the amount of additives

Some consistency tests were carried out to investigate the meaning of the lime retention point* in soil-cement mixtures. Fig. 3.13 shows the change in the plastic limit of Mg-bentonite(MB)-cement accompanying with the addition of portland cement. The addition of cement up to 5 percent increases the plastic limit of the mixture and the further increments bring little increase. The plastic limit of Mg-bentonite varies with the addition of calcium hydroxide, as shown in Fig. 3.14.

The point of inflection of the plot of $Ca(OH)_2$ added vs. P.L. occurs at about 4.5 percent. That is to

---

* This term was proposed by workers at Iowa State University and defined as that percentage of lime beyond which additional increments of lime produced no appreciable increase in P.L.. However, Diamond and Kinter prefer "fixation point" to "retention point". There was a controversy between two groups as to whether the adsorption of lime onto clays could be regarded as a molecular or an ionic adsorption (Diamond and Kinter, 1966).

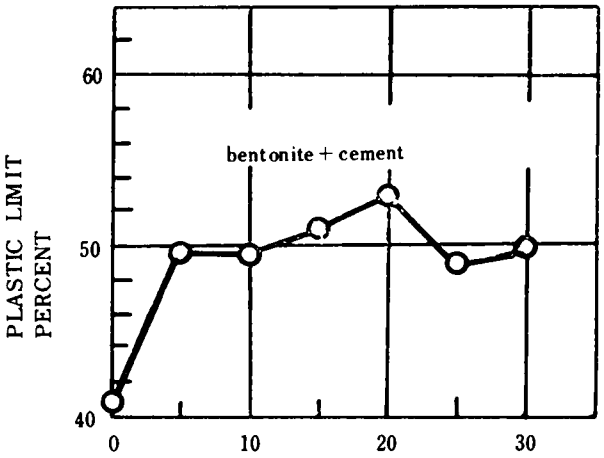

Fig.3.13 Effect of cement on the plastic limit of bentonite

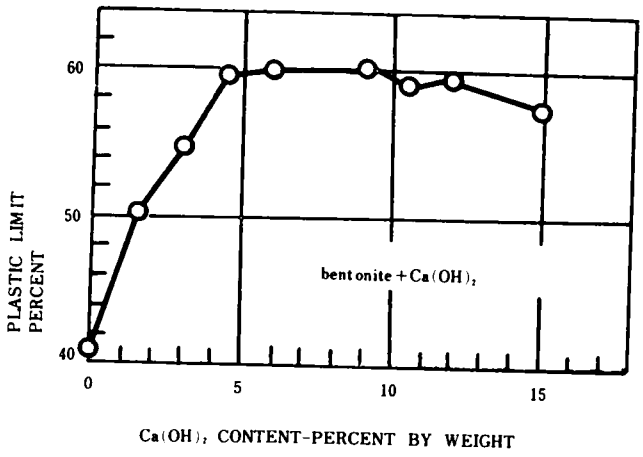

Fig.3.14 Effect of $Ca(OH)_2$ on the plastic limit of bentonite

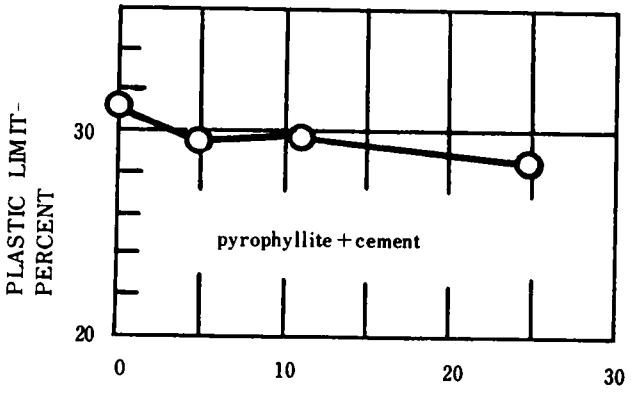

Fig.3.15 Effect of cement on the plastic limit of pyrophyllite

say, Mg-bentonite used in this investigation has a retention point at about 4.5 percent of the $Ca(OH)_2$ content. The amount of cement added vs. P.L. curve also shows an inflection point which seems to correspond to lime retention point.

An experiment concerning the amount of $Ca(OH)_2$ produced accompanying cement hydration demonstrated that the $Ca(OH)_2$ in neat cement paste within one day curing is 1.5 to 3.5 percent by weight of cement (Fujii, 1952). Thus, the percentage of the $Ca(OH)_2$ in Mg-bentonite-cement on testing is found to be far smaller than that at lime retention point of this clay sample. This fact interprets that a point corresponding to the lime retention point in clay-cement (Fig. 3.13) would probably be responsible not only for the $Ca(OH)_2$ resulting from cement hydration but also for other factors described in the following.

Other factors causing the inflection in the plot of the amount of cement added vs. P.L. may be; (a) the effect of anhydrous cement particles and (b) the change in physicochemical properties of the association of montmorillonite clay particles in Mg-bentonite-cement, which is attributed to the calcium aluminate hydrate and ettringite which result from relatively initial cement hydration. Of these factors, the effect of unhydrated cement particles seems to be able to leave out of consideration, because no inflection is found in the amount of cement added vs. P.L. curve of pyrophyllite-cement mixture (Fig. 3.15).

(2) X-ray Diffraction

(a) Mg-bentonite(MB)-cement

Fig. 3.16 shows X-ray diffraction data at the end of 3, 28, 91 and 200 days curing of bentonite (MB)-cement sample. As curing progresses, the height of the peak of alite and belite at 2.76 Å in all samples

decreases, while that of CSH(gel) at 3.07 Å increases (Fig. 3.16, 3.17 and 3.18). This tendency is similar to that of neat cement paste which is molded with a water-cement ratio, 30 percent, and cured under the same condition. This fact indicates that the cement hydration takes place in each bentonite(MB)-cement mixture in the same manner as in the cement paste.

However, none of the bentonite(MB)-cement samples has the peaks identified as calcium hydroxide. This may suggest that, in the bentonite (MB)-cement, a large amount of Ca ions resulting from cement hydration is adsorbed on the cation exchange sites and extensive interaction of montmorillonite or other silicates minerals with $Ca(OH)_2$ takes place. It was also confirmed by X-ray examination that the latter pozzolanic reaction produces C_4AH_{13} as well as CSH(gel). Such a pozzolanic reaction may be evidenced by Fig. 3.18 which represents the change in the height of the peak of CSH(gel) at 3.07 Å with time of curing. The height of the peak of CSH(gel) in all bentonite(MB)-cement mixtures is similar to that in neat cement paste, indicating that the CSH(gel) in the bentonite(MB)-cement is produced not only by cement hydration but also by secondary clays- or other silicates-$Ca(OH)_2$ interaction. However, it should be kept in mind that the height of the peak at 3.07 Å at the initial ages is considerably influenced by the 3.02 Å peak of alite and belite.

As shown in Fig. 3.18, until the curing time of 28 days, the bentonite(MB)-cement mixture of 20 percent cement content has greater height of the peak than that of 30 percent. This may be due to the faster hydration of 20 percent cement specimens than that of 30 percent ones, because the water-cement ratio of 20 percent cement specimens is greater than that of 30 percent ones.

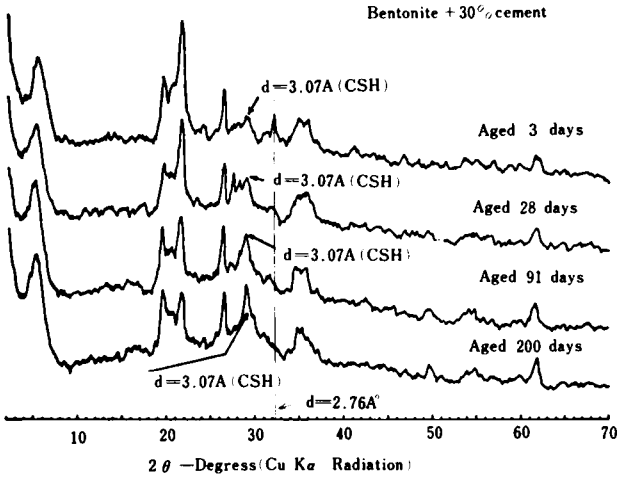

Fig.3.16 X-ray diagrams for bentonite+30% cement samples cured for 3, 28, 91 and 200 days

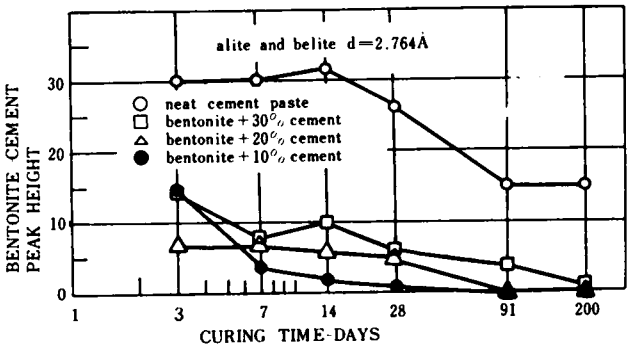

Fig.3.17 X ray diffraction peaks for hydrating bentonite-cement and portland cement

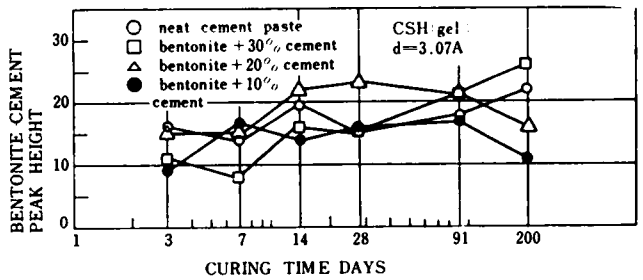

Fig.3.18 X ray diffraction peaks for hydrating bentonite-cement and portland cement

The amount of calcium hydroxide resulting from hydrating cement in the bentonite(MB)-cement would probably be controled not only by cement content but also by water-cement ratio. Since the $Ca(OH)_2$-bentonite(MB) interaction is considered to affect the formation of CSH(gel), the amount of CSH(gel) produced in the

bentonite(MB)-cement depends upon both cement content and water cement ratio.

As regards the rate of formation of $Ca(OH)_2$ in cement hydration, Copeland et al. (1960) and Taplin (1959) reported that the amount of $Ca(OH)_2$ produced in cement hydration increased with increasing water-cement ratio.

Although the water-cement ratio in the bentonite(MB)-cement can not simply be the ratio of added water to the cement by weight because of the adsorption of water between the layers of montmorillonite, it may be permitted to suggest that the water-cement ratio in specimens of 20 percent cement content is greater than that in 30 percent ones.

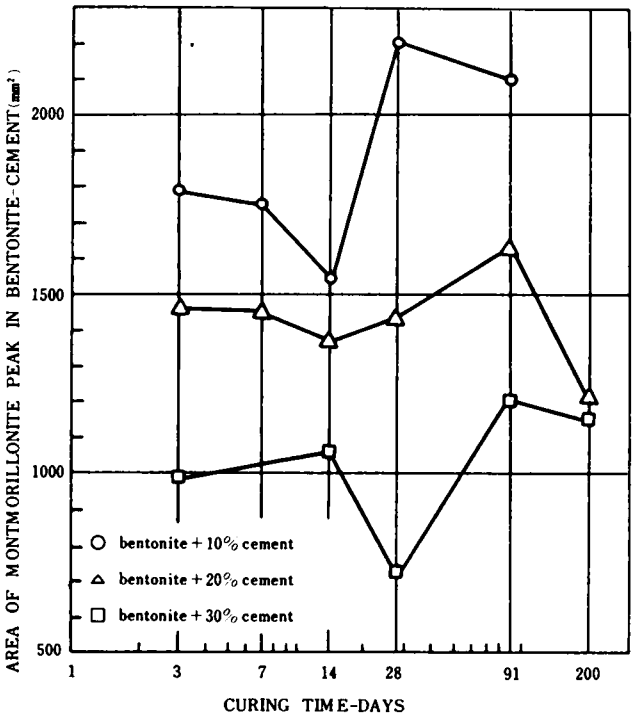

Fig. 3.19 Variation in area of montmorillonite peak for hydrating bentonite-cement

The area of a triangle (A_0) which covers the (001) peak of montmorillonite in the X-ray diffraction pattern can be used as a measure of the intensity of basal reflection. The Fig. 3.19 indicates the change in A_0 of each sample with curing time. For the specimens with 10 and 20 percent cement, a slow decrease in A_0 is observed until 14 days, followed by a rapid increase until 28 days for the former and until 91 days for the latter. On the other hand, A_0 of the specimens with 30 percent cement falls down at 28 days of curing. This may be caused by the encapsulation of a portion of the basal plane surfaces of montmorillonite with CSH(gel) and amorphous calcium hydroxide primarily resulting from initial cement hydration. The relatively rapid increase in A_0 in the former two specimens at 28 and 91 days of curing may probably be due to the adsorption of Ca^{++} ions between the silicate sheets.

As Eades and Grim(1969) reported, a small amount of lime does not affect the structure of montmorillonite and substantially the basal reflections are intensified.

Herzog and Mitchell(1962) also stated that at 15 percent cement content the 14 Å montmorillonite basal reflection increased in height and sharpness during the longer curing periods, but that at a cement content of 30 percent the montmorillonite reflections weakened with increased curing time suggesting major structural breakdown. The clay-cement specimens in their experiments were cured for different periods at 60° C in a 100 percent relative humidity atmosphere (Herzog and Mitchell,1962).

Since $Ca(OH)_2$ resulting from cement hydration affects the structure of montmorillonite, the intensity of the basal reflection depends upon the amount of $Ca(OH)_2$ produced with increasing curing time and the extent of the adsorption of Ca^{++} onto clay particles. Within 91 days curing, the extent of the adsorption of Ca^{++} may be developed with the curing time to give rise to rapid increase in A_0 as stated by Herzog and Mitchell(1962). However, after the maximum A_0 is attained, the calcium hydroxide resulting from further hydration of cement causes the deterioration of montmorillonite. The decrease of A_0 at 91 and 200 days curing may support this explanation.

(b) Kaolinite-cement

The X-ray diffraction data of kaolinite(Ka(I))-cement are given in Fig. 3.20. Fig. 3.21 shows the change in the peak height of alite and belite at 2.76 Å with curing time in kaolinite(Ka(I))-cement. The similar tendency in the change of 2.76 Å peak between the bentonite(MB)- and the kaolinite (Ka(I))-cement (Fig. 3.17 and Fig. 3.21) indicates that the cement hydration and subsequent liberation of $Ca(OH)_2$ progress in the same manner in both of them. It is a remarkable difference between them that, despite of the absence of the peak of $Ca(OH)_2$ in the X-ray diagrams of the bentonite(MB)-cement, those of the kaolinite(Ka(I))-cement with 30 and 20 percent cement content exhibit an apparent peak at 2.63 Å (

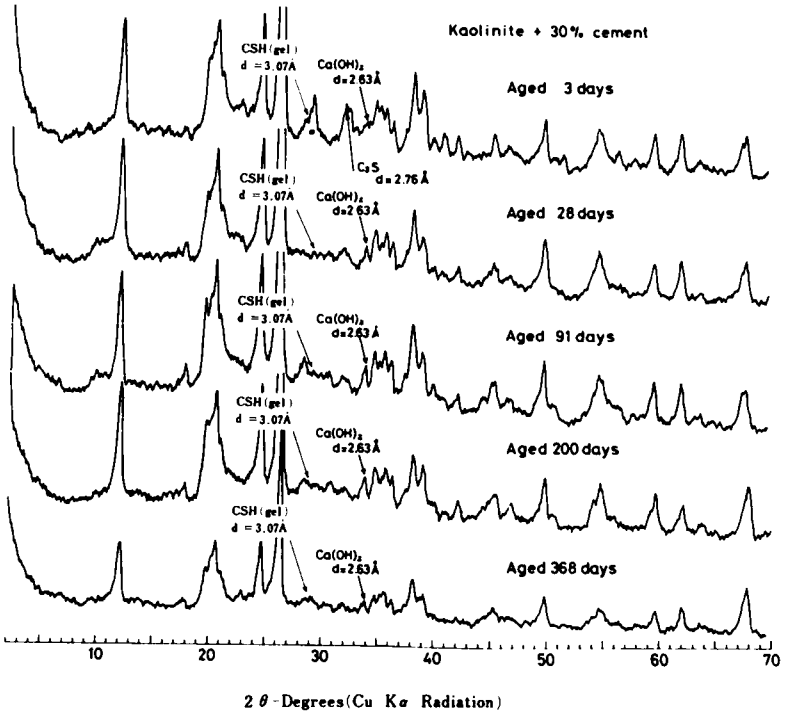

Fig.3.20 X-ray diagrams for kaolinite (Ka(I))+30% cement samples cured for 3, 28, 89, 180 and 364 days

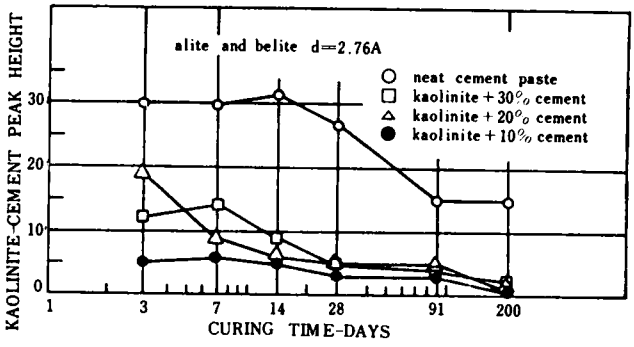

Fig.3.21 X-ray diffraction peaks for hydrating kaolinite-cement and portland cement

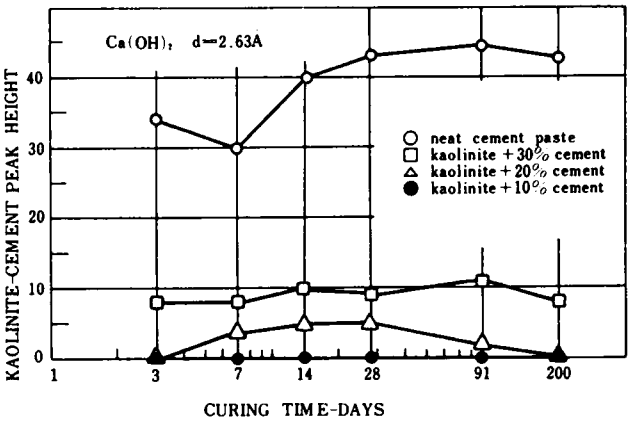

Fig.3.22 X-ray diffraction peaks for hydrating kaolinite-cement and portland cement

Fig. 3.22). The peak height of $Ca(OH)_2$ in neat cement paste increases with curing time until 28 days of curing, followed by little increase (Fig. 3.22). That of the 30 percent cement content kaolinite (Ka(I))-cement shows little change with curing time and that of the 20 percent ones a gradual increase until 28 days of curing followed by a gradual decrease. Comparison in the variation of the peak height of $Ca(OH)_2$ between the kaolinite(Ka(I))-cement and neat cement paste also suggests that a portion of $Ca(OH)_2$ liberated from hydrating cement may be consumed by the interaction of $Ca(OH)_2$ with kaolinite.

The peak height of CSH(gel) at 3.07 Å in the kaolinite(Ka(I))-cement mixture varied with the curing time as indicated in Fig. 3.23. A slow decrease with increasing curing time is observed until 28 days followed by a slow increase until 200 days. This does not seem to agree with the normal hydration be-

havior of alite and belite. It may presumably be due to the overlap of the peak of anhydrous cement compounds or of $Ca(OH)_2$ on that of CSH(gel) at its early stage of formation.

(c) Sericite-cement

The X-ray diffraction data of sericite-cement are represented in Fig. 3.24. A tendency of the reduction in the peak height of alite and belite in sericite-cement is very much the same as other clay-cement mixtures, as stated above (Fig. 3.25). However, the peak height of $Ca(OH)_2$ in sericite-cement tends to increase a little with curing time, and even a 10 percent cement content sample exhibits an apparent peak of $Ca(OH)_2$ after the cure of 91 days (Fig. 3.26). The difference in the variation of the peak height of $Ca(OH)_2$ between kaolinite- and sericite-cement mixtures may be responsible for the difference in the activity of their reaction with $Ca(OH)_2$. That is to say, it may be found that the interaction of kaolinite with $Ca(OH)_2$ is more active than that of sericite with it.

The detection of CSH(gel) peak at 3.07 Å in sericite-cement was impossible because of the overlap of the peak of pyrophylite and quartz included in the sericite sample on it.

(d) Chlorite-Vermiculite mixed-layer mineral-cement

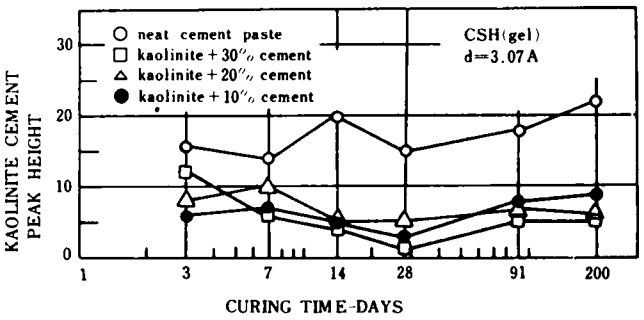

Fig.3.23 X-ray diffraction peaks hydrating kaolinite-cement and portland cement

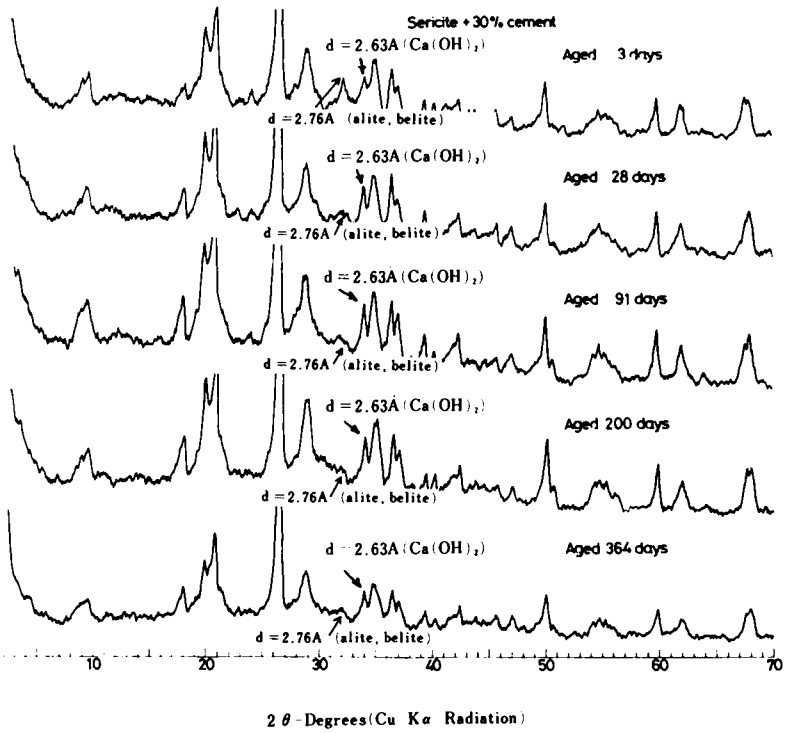

Fig.3.24 X-ray diagrams for sericite + 30% cement samples cured for 3, 28, 91, 200 and 364 days

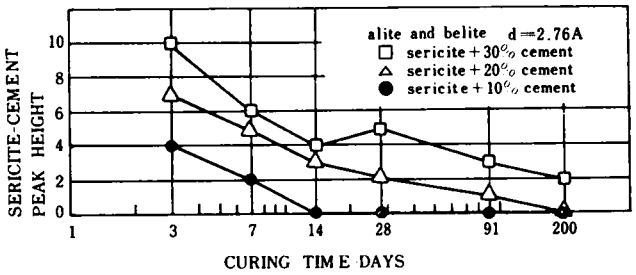

Fig.3.25 X-ray diffraction peaks for hydrating sericite-cement

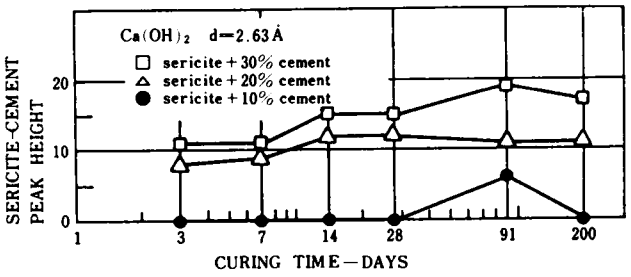

Fig.3.26 X-ray diffraction peaks for hydrating sericite-cement

Fig. 3.27 shows the X-ray diffraction data of mixed-layer mineral-cement mixtures. Fig. 3.28 indicates the reduction of the X-ray diffraction peak height of alite and belite at 2.76 Å with curing time. This tendency is not much different from that in Mg-bentonite(MB)-, kaolinite(Ka(I))- and sericite-cement, as stated above. The very high $Ca(OH)_2$ peak appears in most samples of them; even in 10 percent cement content samples, a sharp peak at 2.63 Å is found at the cure of 7, 14 and 28 days (Fig. 3.29). The long-term curing samples with 30 percent cement content have the broad peak covering the range of 3.20 Å to 3.07 Å. The basal reflection greatly weakens with increasing curing time (Fig. 3.27). A sharp peak at 10 Å exists in the X-ray diffraction diagrams of 182 and 364 days curing samples with 30 and 20 percent cement content. This peak becomes considerably large with curing time. It may be a X-ray diffraction peak of the basic magnesium silicate hydrate, which is given in the ASTM's powder diffraction file (ASTM, 1968)

(e) Allophane-cement

Fig. 3.30, Fig. 3.31 and Fig. 3.32, Fig. 3.33 show the X-ray diffraction diagrams and the change in the peak height of alite and belite at 2.76 Å, respectively. Little change with curing time is found in the peak height of allophane(I)-cement at 2.76 Å, but the slow decrease in that of allophane(II)-cement. This fact indicates that allophane suppresses the cement hydration. However, no suppression of the cement hydration occurs in the clay-cement mixtures using the allophane including the crystalline hydrated halloy-

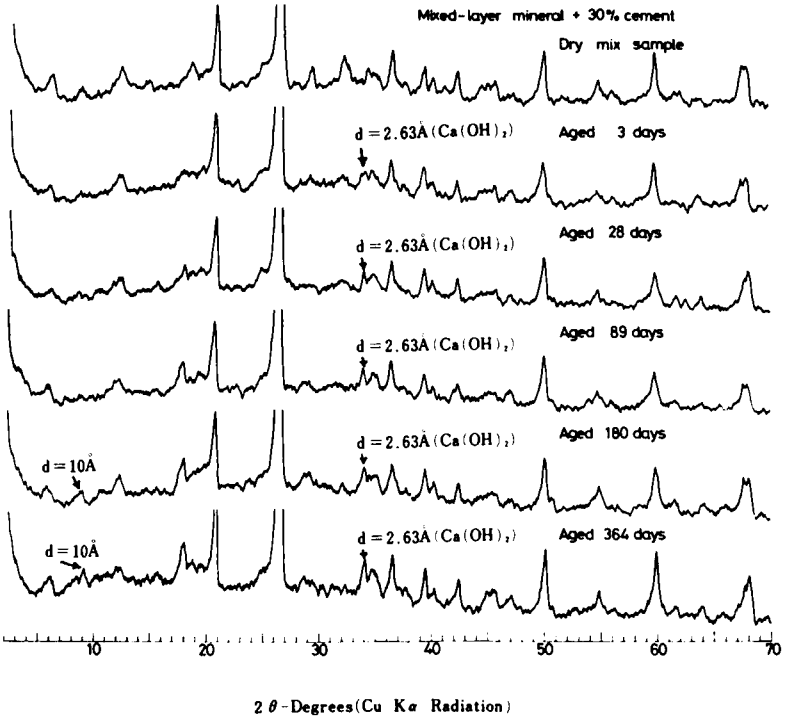

Fig.3.27 X-ray diagrams for mixed-layer mineral + 30% cement samples cured for 3, 28, 89, 180 and 364 days

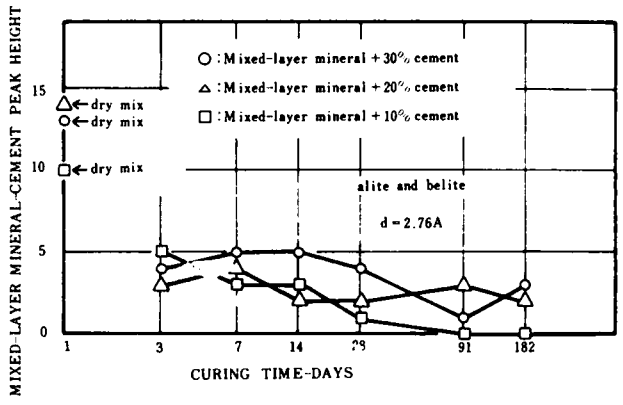

Fig.3.28 X-ray diffraction peaks for hydrating mixed-layer mineral cement mixture

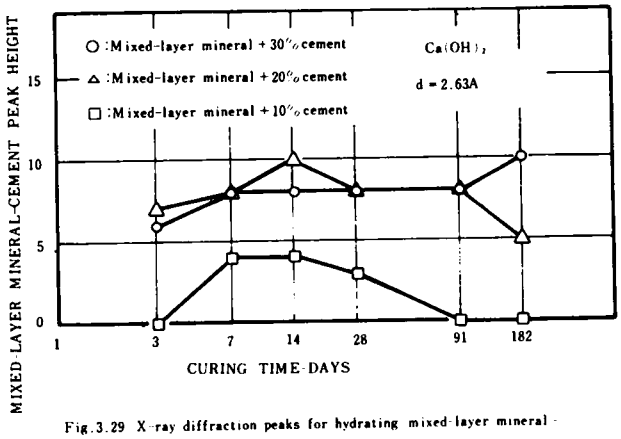

Fig.3.29 X-ray diffraction peaks for hydrating mixed-layer mineral - cement mixture

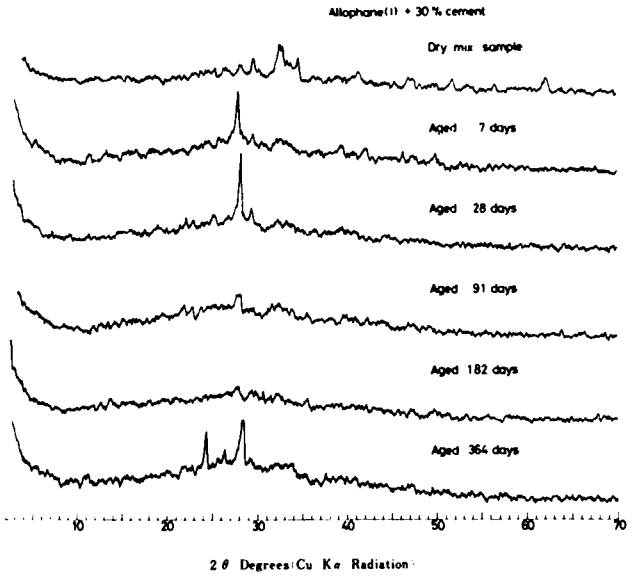

Fig.3.30 X-ray diagrams for allophane(I)+30% cement samples cured for 7,28,91,182 and 364 days

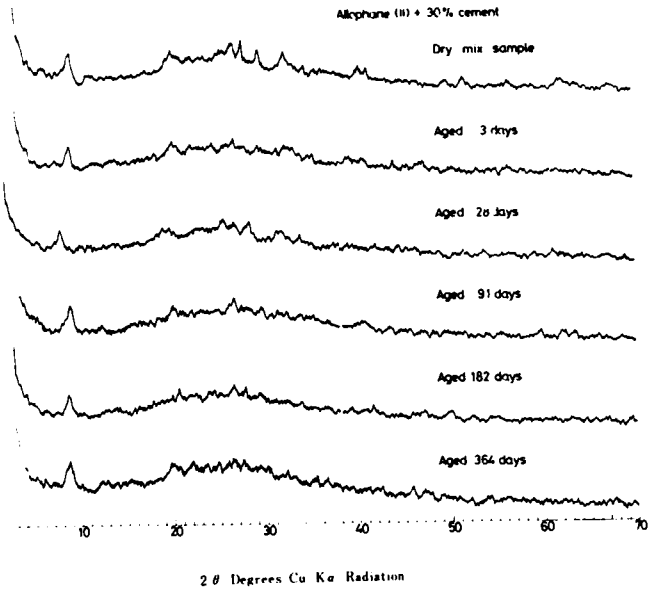

Fig.3.32 X ray diagrams for allophane II + 30 % cement samples cured for 3,28,91,182 and 364 days

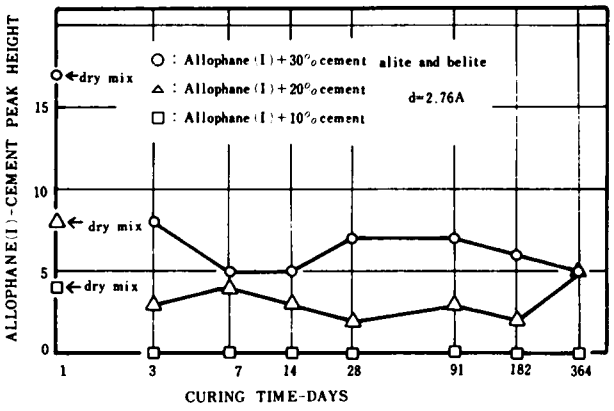

Fig.3.31 X-ray diffraction peaks for hydrating allophane(I)-cement mixture

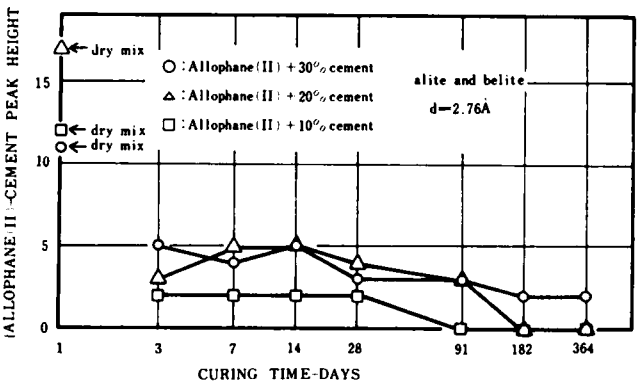

Fig.3.33 X-ray diffraction peaks for hydrating Allophane(II)-cement mixture

site. That is to say, such a small amount of the crystalline inclusion in the amorphous allophane greatly affects the cement hydration in the compacted clay-cement mixture.

No X-ray diffraction peaks of the reaction products such as $Ca(OH)_2$, CSH(gel) and calcium aluminate hydrate are found.

(f) Natural soil-cement

A number of great peaks of quartz and feldspar included in natural soil also make it impossible to examine the detailed behavior of the peak height of CSH(gel), alite and belite (Fig. 3.34). None of the natural soil-cement mixtures indicates the X-ray diffraction peaks of $Ca(OH)_2$.

The amount of clay minerals in the natural soil sample used might be so small that they could be identified only by the X-ray diffraction tests using an oriented section.

The disappearance of $Ca(OH)_2$ in natural soil-cement mixtures may be considered to be due to the sup-

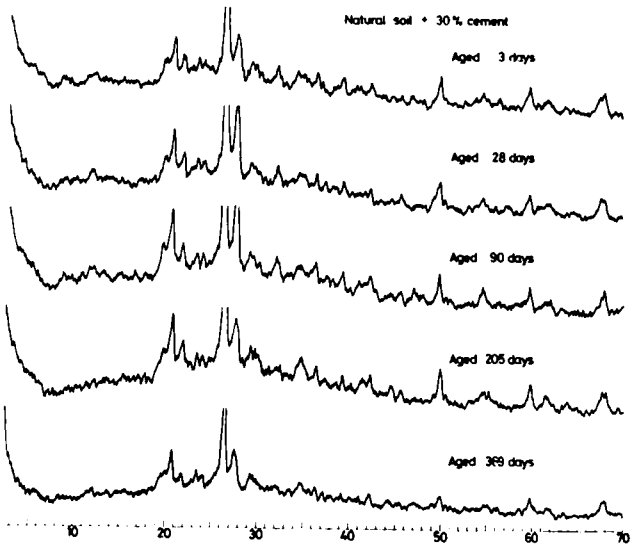

Fig.3.34 X ray diagrams for natural soil + 30% cement samples cured for 3, 28, 90 and 205 and 369 days

pression of cement hydration by the weathered soil particles or to the adsorption onto some amorphous substances in the soil and to the pozzolanic reaction with them.

(3) Thermal Analysis

(a) Kaolinite-cement

Fig. 3.35, Fig. 3.36 and Fig. 3.37 show D.T.A., T.G. and D.T.G. curves of kaolinite(Ka(I))-cement with 30 percent content. As indicated in Fig. 3.35, an endothermic peak of $Ca(OH)_2$ in the vicinity of 500° C co'exists with the peaks due to kaolinite dehydroxylation. This bulge grows until 200 days of curing. However, those at 1 and 2 years become very vague.

A fairly large endotherm in the vicinity of 200° C, found in all samples except 3 days curing one, may be mainly attributed to tetracalcium aluminate hydrate (Green, 1962).

The reaction of kaolinite with $Ca(OH)_2$ in kaolinite-cement mixtures would result in producing a considerably large amount of tetracalcium aluminate hydrate as well as CSH(gel).

T.G. and D.T.G. curves indicate some features due to the dehydroxylation of the clay mineral and the reaction products (Fig. 3.36 and Fig. 3.37).

(b) Bentonite-cement

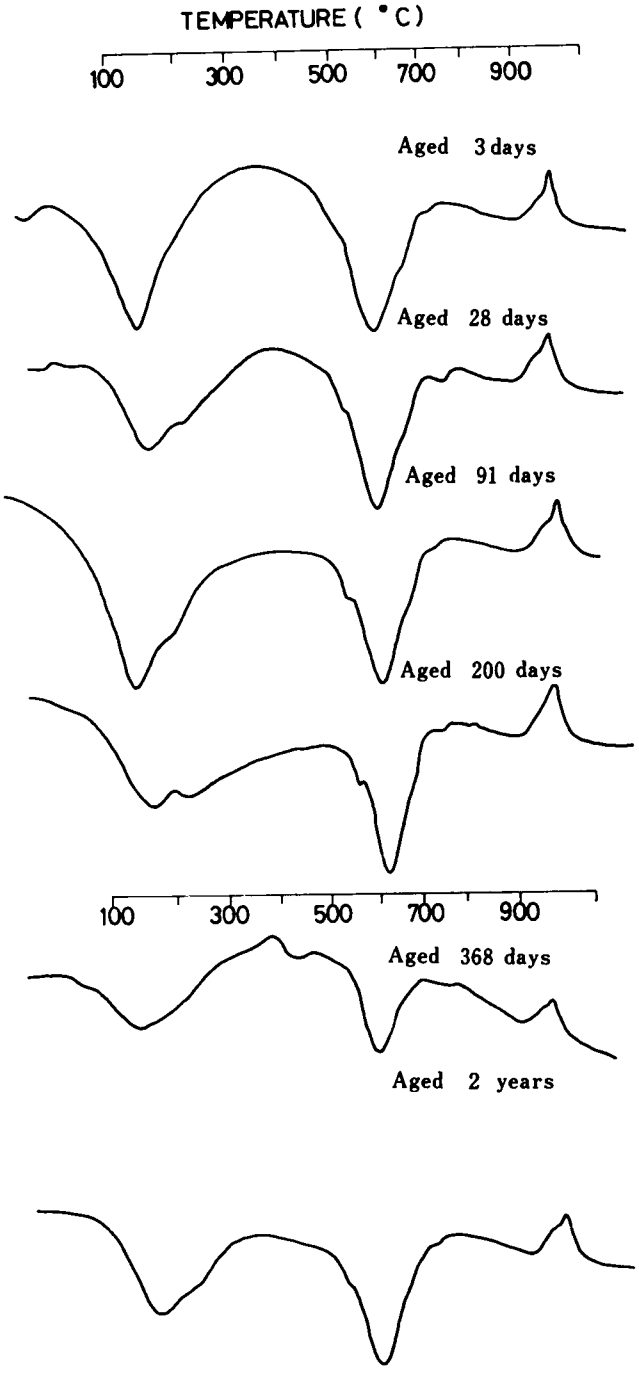

Fig.3.35 D.T.A. curves for kaolinite + 30% cement samples for 3, 28, 91 and 200 days

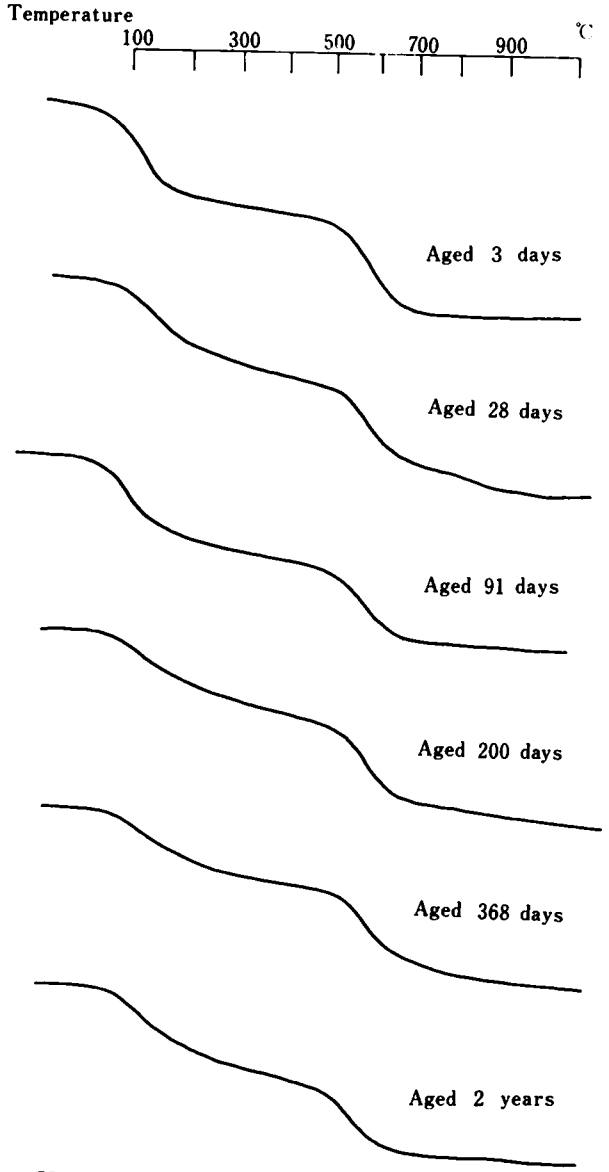

Fig.3.36 T.G. curves for kaolinite + 30% cement samples for 3,28,91,200,368 days and 2 years

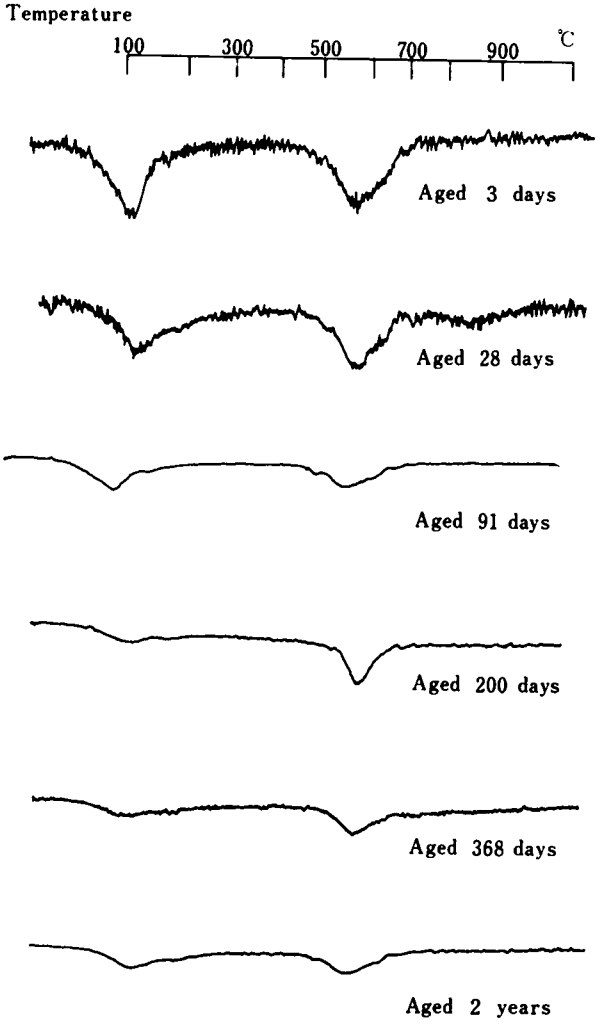

Fig.3.37 D.T.G. curves for kaolinite + 30% cement samples for 3,28,91,200,368 days and 2 years

Fig. 3.38 and Fig. 3.39 show D.T.A. curves of bentonite-cement mixtures with 10 and 30 percent cement content, respectively. All of them exhibit another endothermic peak at about 200° C in addition to an endothermic peak at about 130° C responsible for the adsorbed water in samples.

In calcium montmorillonite, part of the water is more tightly bonded to give a small second peak at about 200° C (Grim, 1953). Since the montmorillonite in bentonite-cement is expected to be saturated with Ca^{++} ions to a considerable extent, it can not be made evident whether a bulge at about 200° C is due to the montmorillonite or to the reaction products such as calcium aluminate hydrate and calcium silicate hydrate.

No endothermic peak of $Ca(OH)_2$ is found in the D.T.A. curves.

(c) Sericite-cement

In the D.T.A. curves of sericite-cement mixture the endothermic peak of $Ca(OH)_2$ at about 500° C seems

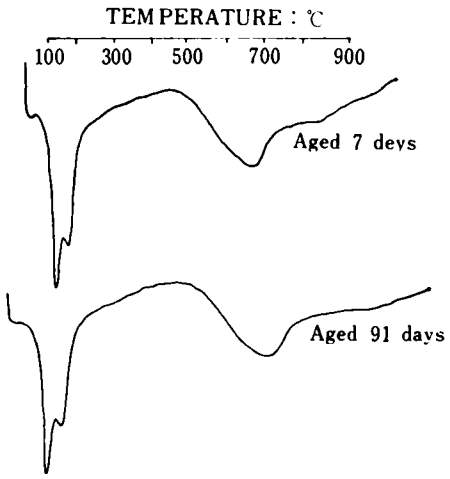

Bentonite + 10% cement

Fig.3.38 D.T.A. curves for bentonite + 10% cement samples cured for 7 and 91 days

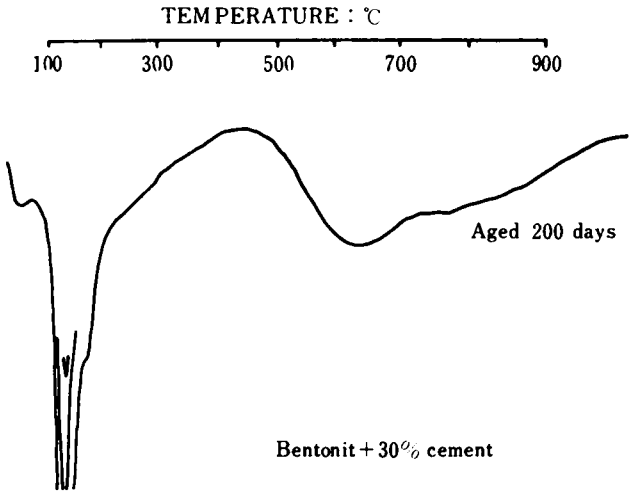

Fig.3.39 D.T.A. curves for bentonite + 30% cement sample cured for 200 days

larger than that in kaolinite-cement(Fig. 3.35, Fig. 3.40). The presence of a greater amount of $Ca(OH)_2$ in sericite-cement mixtures is also confirmed by D.T.G. curves. That is to say, an evident deflection at about 500° C found in D.T.G. curves of sericite-cement (Fig. 3.42) can not be detected in those of kaolinite-cement (Fig. 3.37). No endothermic bulge at about 200° C which is found in kaolinite-cement is observed, indicating that a little or no tetracalcium aluminate hydrate yields in sericite-cement mixtures.

However, a considerable amount of the calcium silicate hydrate would probably be produced. This may be evidenced by a broad exothermic peak at about 900° C in 91 and 200 days curing samples. Fig. 3.41 and Fig. 3.42 are T.G. and D.T.G. curves of this clay-cement mixtures, respectively.

(d) Chlorite-vermiculite mixed-layer mineral-cement

D.T.A., T.G. and D.T.G. curves of mixed-layer mineral-cement are presented in Fig. 3.43, Fig. 3.44 and Fig. 3.45. As expected from the X-ray diffraction results, all curves except 3 days curing exhibit a large peak at about 500° C re-

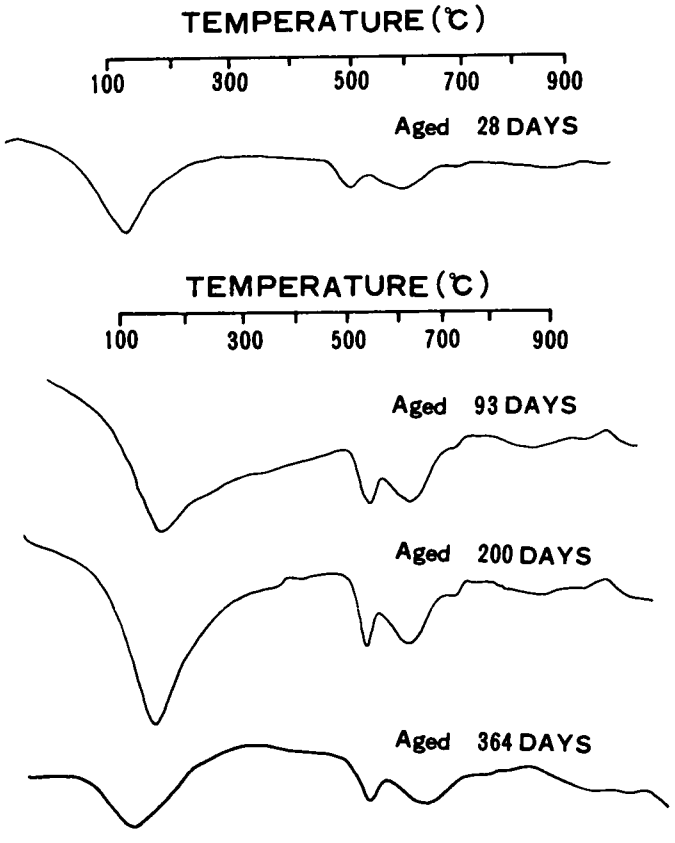

Sericite + 30% cement

Fig.3.40 D.T.A. curves for sericite + 30% cement samples cured for 28, 91 and 200 days

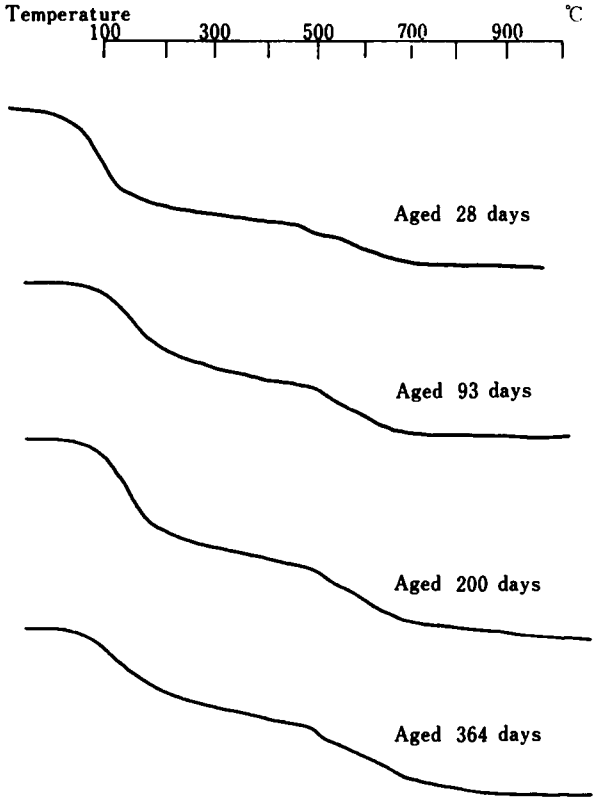

Fig.3.41 T.G. curves for sericite + 30% cement samples cured for 28, 93, 200 and 364 days

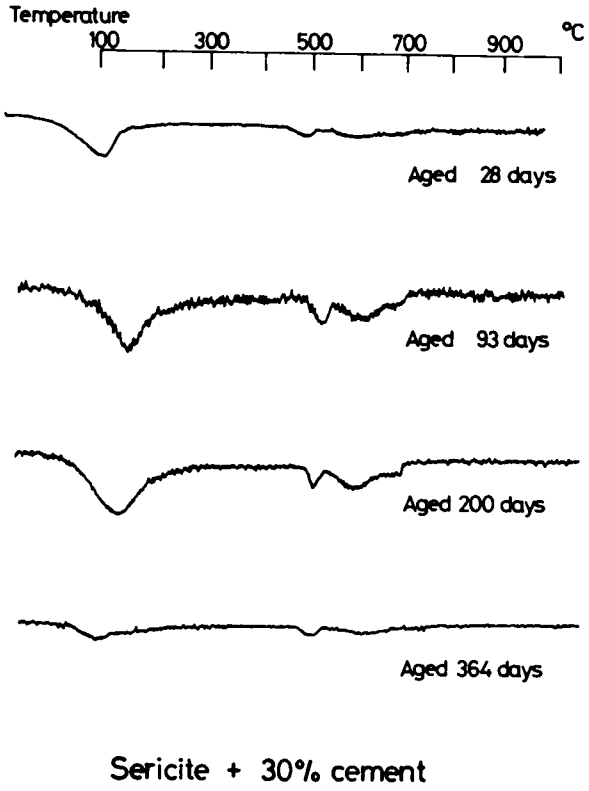

Fig.3.42 D.T.G. curves for sericite + 30% cement samples cured for 28, 93, 200 and 364 days

sponsible for the dehydroxylation of $Ca(OH)_2$. Further, the peak still remains without change in its size even at the end of 182 days curing.

An endotherm at about 780°C found in the D.T.A. curves of 32, 89 and 182 days curing sample may be due to either the calcium silicate hydrate with high CaO/SiO_2 ratio such as γC_2S hydrate or to the calcium carbonate.

The pozzolanic reaction in this clay-cement mixture seems inactive as also indicated by other experimental results.

(e) Allophane-cement

D.T.A., T.G. and D.T.G. curves of allophane(A(I))-cement are presented in Fig. 3.46, Fig. 3.47 and Fig. 3.48. These are almost the same as that of typical allophane clay mineral sample, indicating no progress of cement hydration in this clay-cement.

(4) pH Tests

Fig. 3.49, Fig. 3.50 and Fig. 3.51 show the pH changes with curing time in each clay-cement mixtures (kaolinite(Ka(I))-cement, sericite-cement, bentonite(MB)-cement and natural soil-cement) and cement paste. Furthermore, those of mixed-layer mineral-cement and allophane(A(I), A(II))-cement are given in Fig. 3.52, Fig. 3.53 and Fig. 3.54.

Both the kaolinite- and sericite-cement mixtures show the similar pH vs. curing time curves to that of neat cement paste. They rise slowly until 91 days with a subsequent reduction at 200 days age. On the

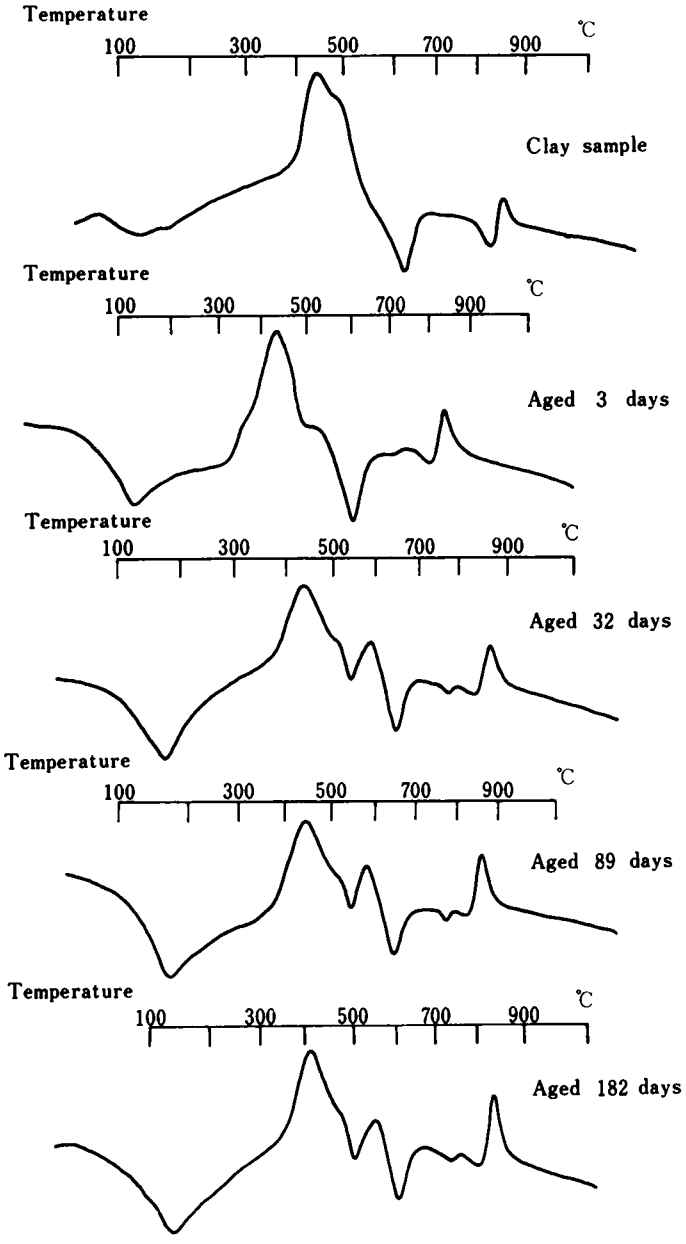

Fig.3.43 D.T.A. curves for mixed-layer mineral +30% cement cured for 3,32,89 and 182 days

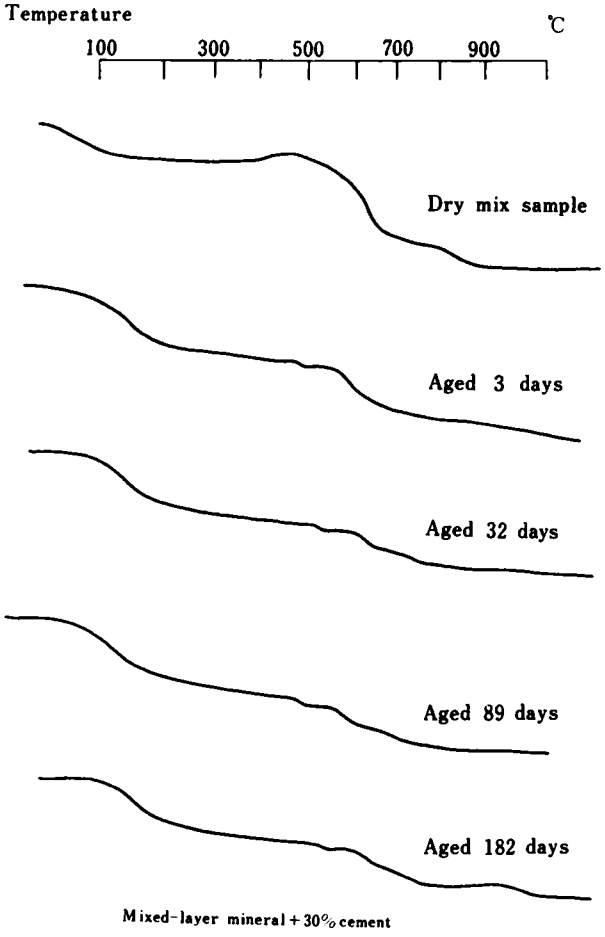

Fig.3.44 T.G.curves for mixed-layer mineral +30% cement cured for 3,32,89 and 182 days

other hand, the pH of the bentonite(MB)-cement mixture rapidly decreases with increasing curing time after 3 or 14 days in 10, 20 and 30 percent cement content samples. All of them approach about 11.0 successively in the order of 10, 20 and 30 percent cement content.

The pH of natural soil-cement with 20 or 30 percent content little changes with curing time. The values of pH of 3 days to 14 days ages samples are considerably low compared with those of other clay-cement samples as a whole. Furthermore, there is found the gradual decrease of the pH with curing time after 14 days in 10 percent cement content ones. This demonstrates that some interaction between clay and cement takes place in natural soil-cement mixtures.

As easily expected from other test results, little changes in pH with curing time are found in the mixed-layer mineral-cement mixtures (Fig. 3.52, Fig. 3.53 and Fig. 3.54). This fact gives an evidence

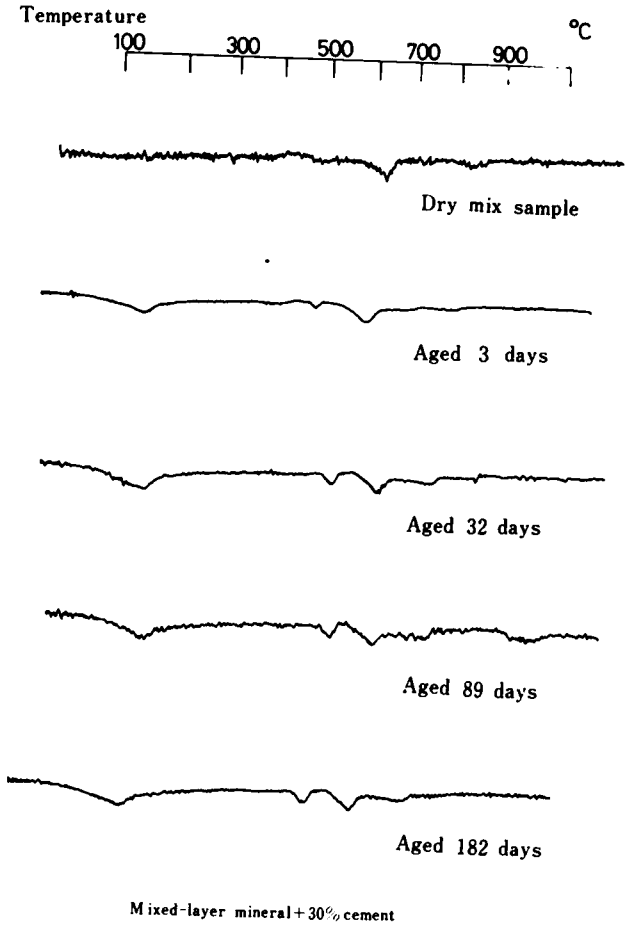

Fig.3.45 D.T.G. curves for mixed-layer mineral +30% cement cured for 3,32,89 and 182 days

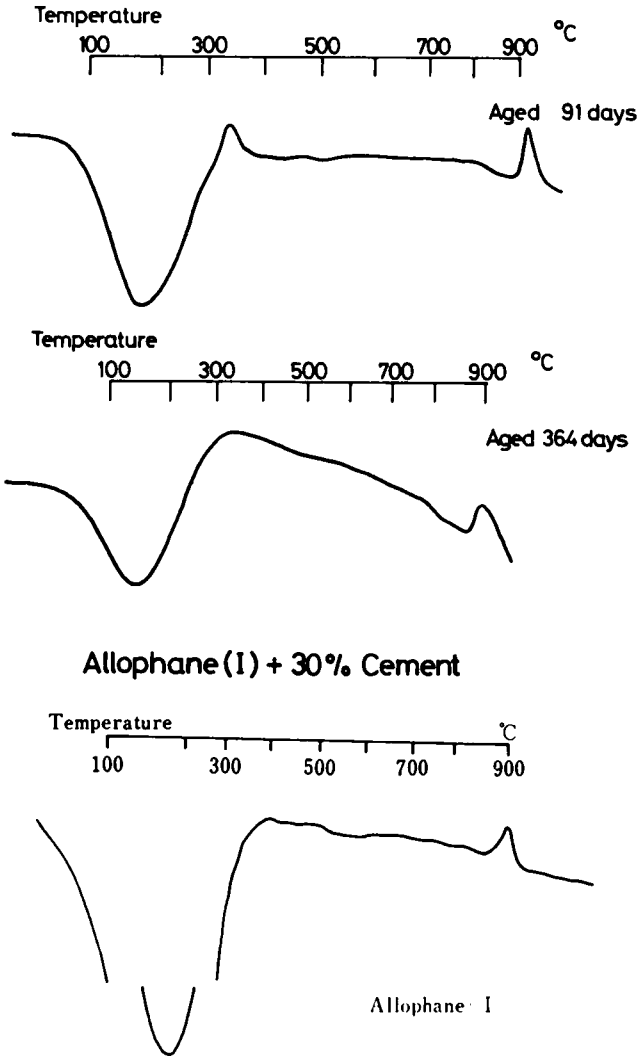

Fig.3.46 D.T.A. curves for allophane(I) +30% cement cured for 91 and 364 days

for the inactivity in the pozzolanic reaction in these clay-cement samples.

The pH value of allophane-cement tends to decrease a little after 28 days ages.

The pH value obtained through the process previously mentioned depends upon the amounts of anhydrous cement and of $Ca(OH)_2$ liberated from cement hydration. Therefore, a slow decrease in pH with ages suggests a slow peogress in the cement hydration and/or the inactivity in the reaction of clay samples with $Ca(OH)_2$ liberated. Little changes in pH of allophane(A(I))-cement may be attributed to the former and those in pH of kaolinite-, sericite- and mixed-layer mineral-cements to the latter.

(5) Unconfined Compression Tests

The results of unconfined compression test for the specimens with 30 percent cement content are presented in Fig. 3.55. Fig. 3.56 to Fig. 3.62 show the relationship between unconfined compressive strength and curing time for each clay-cement mixture. It is found, from these figures, that, exclusive of allophane(A(I))-cements with 10 and 20 percent cement content and of allophane(A(II))-cement with 10 percent cement content, the strength of all clay-cement specimens increases with increasing curing time. All of these results are plotted on semilogarithmic graph paper.

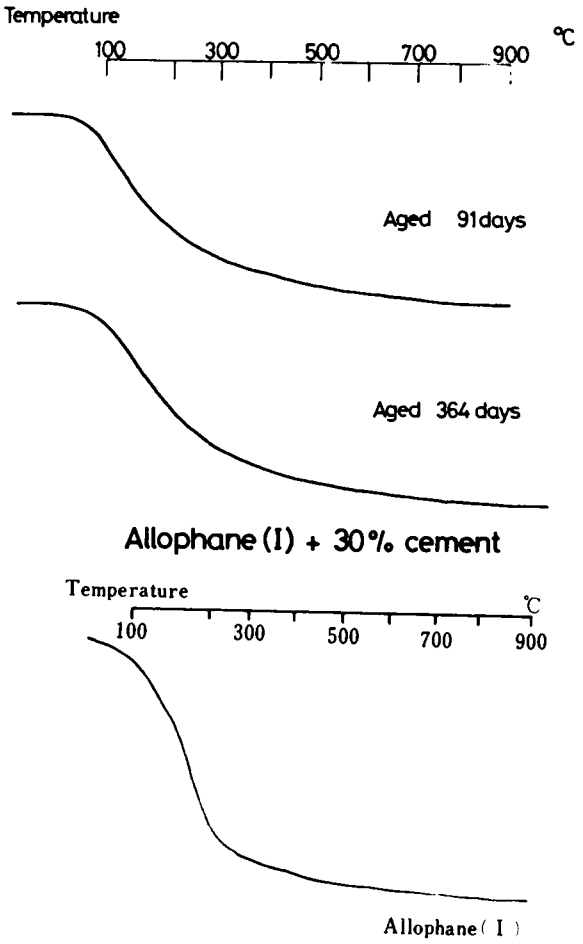

Fig.3.47 T.G. curves for allophane(I) +30% cement cured for 91 and 364 days

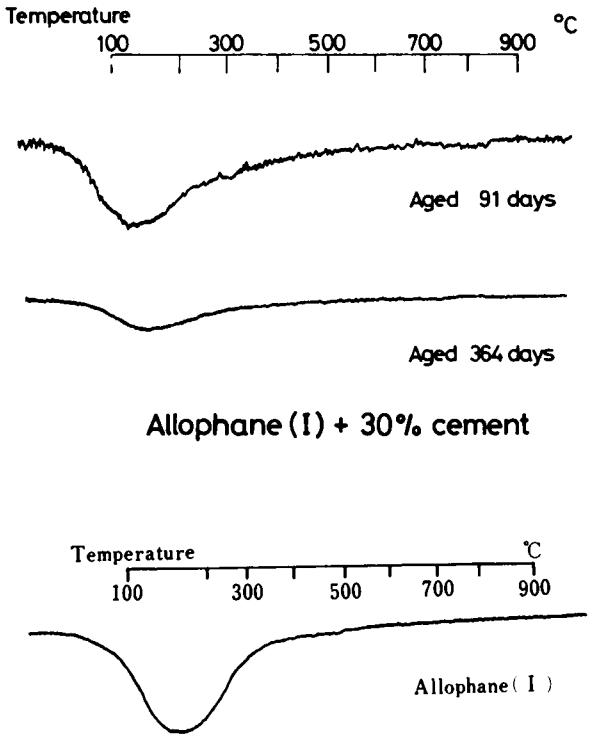

Fig.3.48 D.T.G curves for allophane(I) +30% cement cured for 91 and 364 days

The characteristics in the strength development of each clay-cement mixture are discussed in the following.

(a) Kaolinite-cement

The unconfined compressive strength of kaolinite -cement mixtures approximately linearly increases with curing time (Fig. 3.55). It is remarkably noted that the difference in cement contents of kaolinite-cement brings about a comparatively little difference in their strength compared with those in sericite- and bentonite-cements (Fig. 3. 56, Fig. 3.57 and Fig. 3.58).

Two explanations can be given on such characteristic strength developments.

A considerably great amount of tetracalcium aluminate hydrate is produced in kaolinite-cement, as indicated by X-ray diffraction and D.T.A.. On

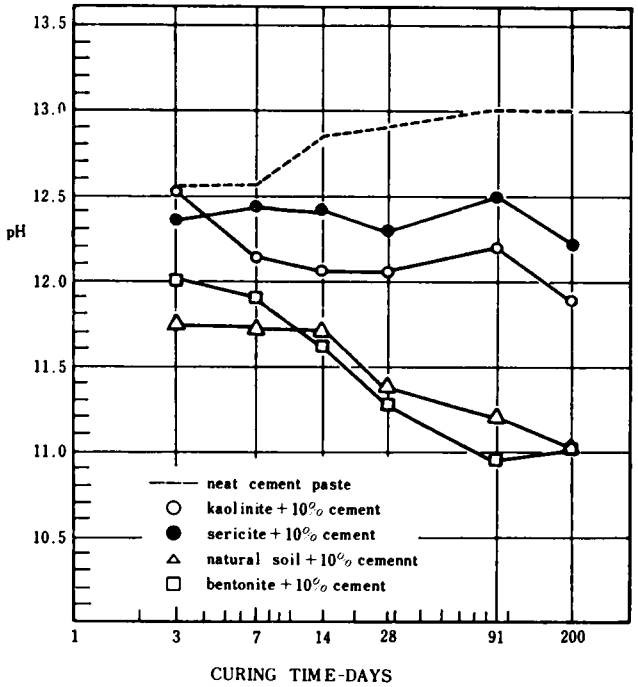

Fig.3.49 pH changes of clay + 10% cement mixtures with curing time

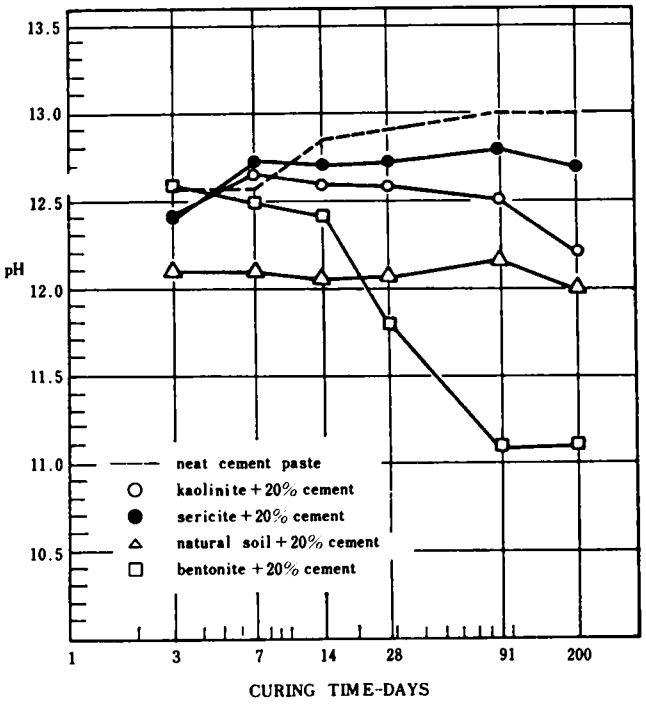

Fig.3.50 pH changes of clay +20% cement mixtures with curing time

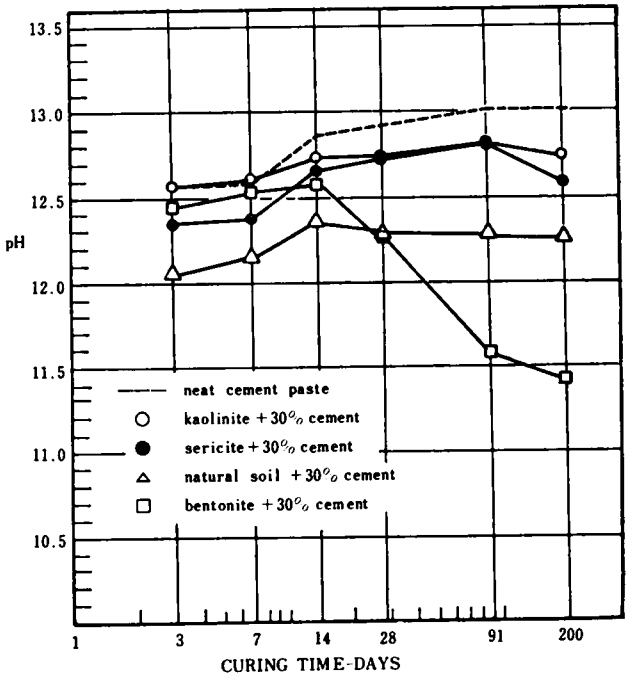

Fig.3.51 pH changes of clay +30% cement mixtures with curing time

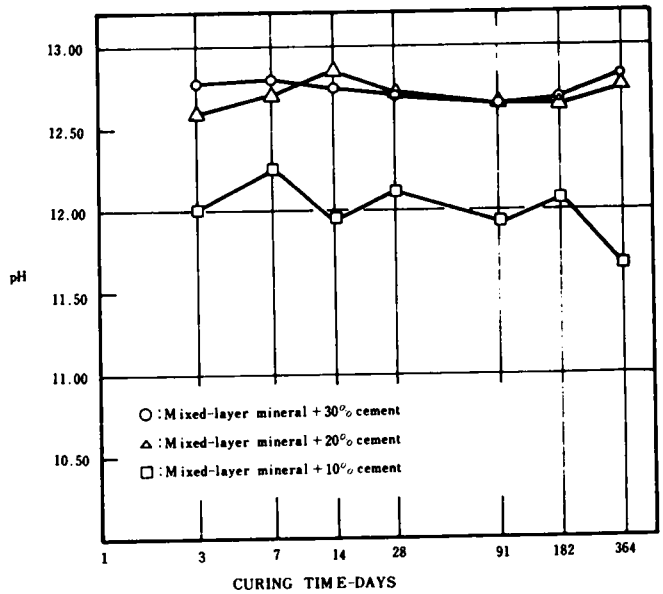

Fig.3.52 pH changes of mixed-layer mineral-cement mixture with curing time

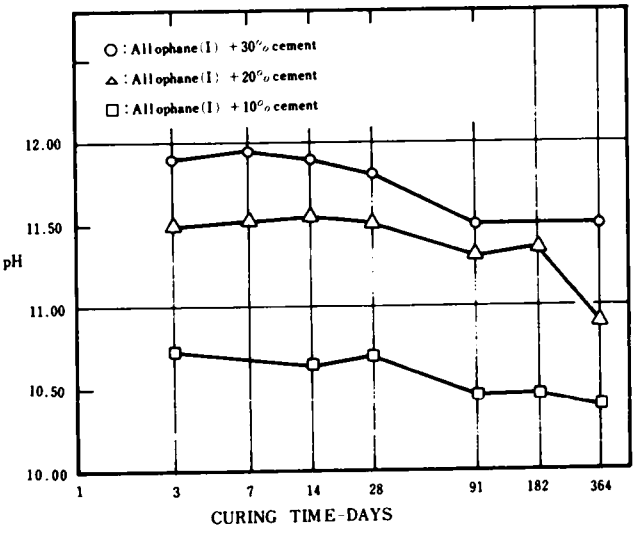

Fig.3.53 pH changes of Allophane(I)-cement mixture with curing time

the contrary, a primary reaction procuct in bentonite- and sericite-cement is tobermorite gel. Thus, there could be the likelihood that the mechanism of the strength development in kaolinite-cement of which the strength primarily comes from tetracalcium aluminate is different from that in bentonite- and sericite-cements in which the origin of cohesion is attributed to tobermorite gel in its most part.

Another factor to be taken into consideration in the strength development of clay-cement is the grain

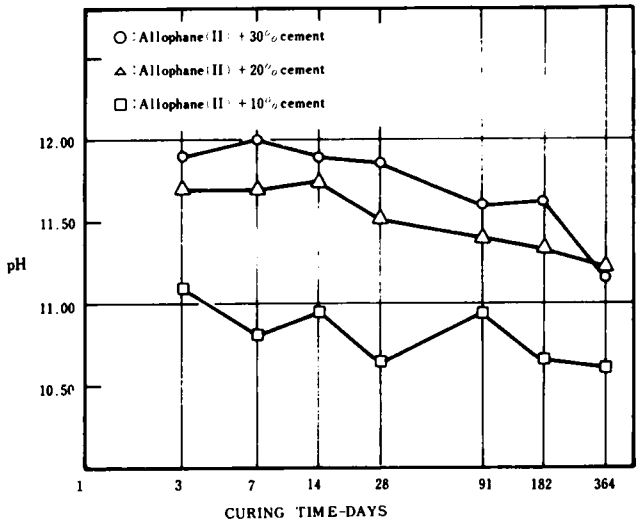

Fig.3.54 pH changes of allophane(II)-cement mixture with curing time

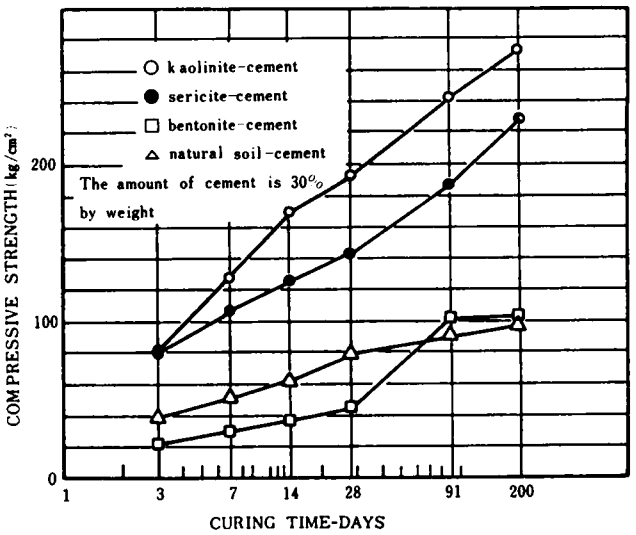

Fig.3.55 Variation in strength with curing time

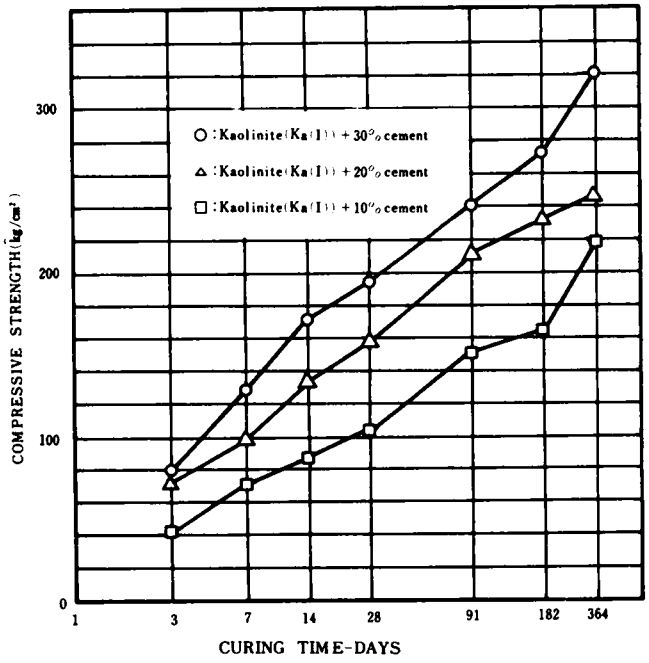

Fig.3.56 Variation of compressive strength with curing time in kaolinite(Ka(I))-cement mixture

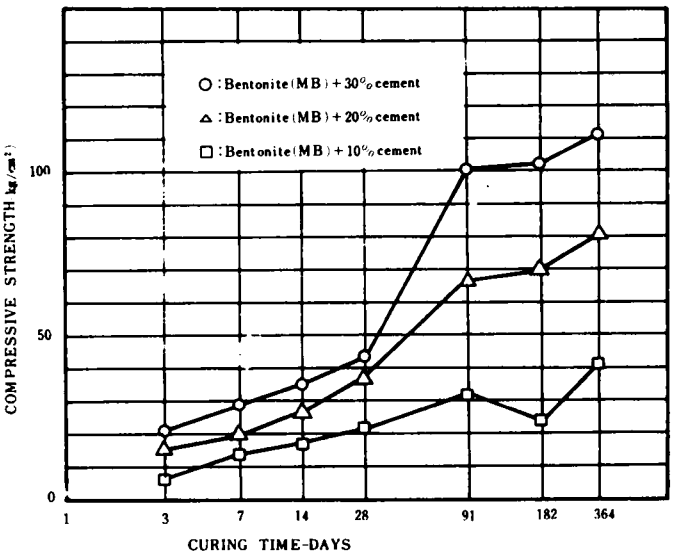

Fig.3.57 Variation of compressive strength with curing time in bentonite(MB)-cement mixture

size distributions of clay samples used. Especially, there is a wide difference in clay content between them (Table 3.3). In this respect, however, it should be noted that kaolinite(Ka(III))-cement specimens using kaolinite clay samples(Ka(III)) having much finer particle (Table 3.3) indicates a little difference in its strength between 10, 20 and 30 percent cement content, in the same manner as in the coarser grained kaolinite(Ka(I))-cement mixtures (Fig. 3.101, Fig. 3.102 and Fig. 3.103).

(b) Bentonite-cement

Until 28 days, little difference is observed in the tendency of the strength increase between these three mixtures (Fig. 3.57). However, between 28 and 91 days of curing, the greater the cement content of

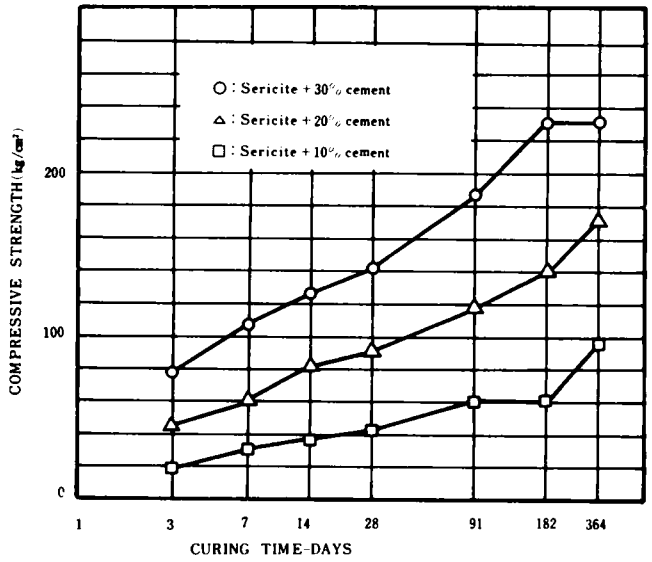

Fig.3.58 Variation of compressive strength with curing time in sericite-cement mixture

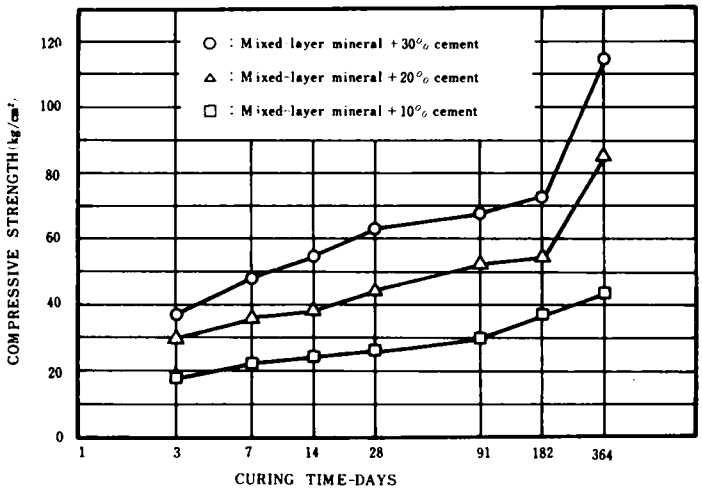

Fig 3.59 Variation of compressive strength with curing time in mixed-layer mineral-cement mixture

the mixture, the greater the strength increase. After 91 days of curing, the strength of each mixture increases a little or little. Despite of a little difference in the strength between 20 and 30 percent cement content specimens at the end of 28 days curing the difference at the curing time of 91 and 200 days becomes almost in proportion to the amount of cement added. This fact seems to suggest that the mechanism of the strength development until 28 days of curing in bentonite-cement may be different from that at later ages.

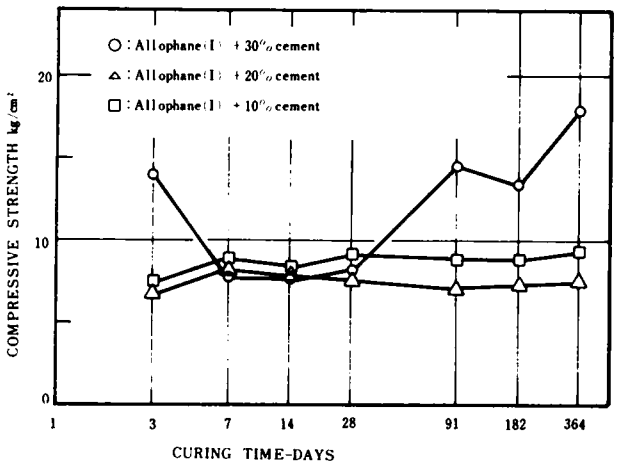

Fig.3.60 Variation of compressive strength with curing time in Allophane(I)-cement mixture

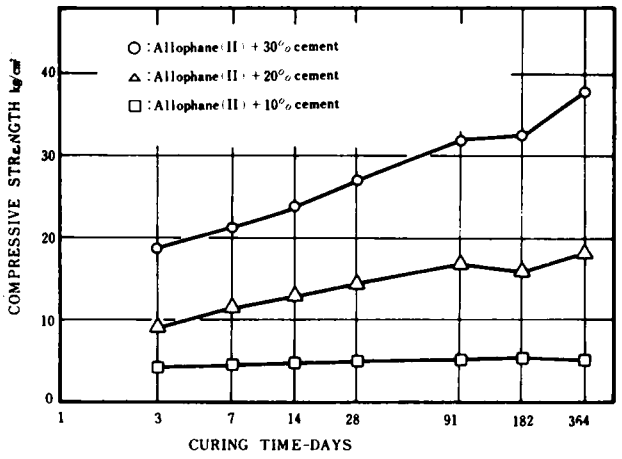

Fig.3.61 Variation of compressive strength with curing time in Allophane(II)-cement mixture

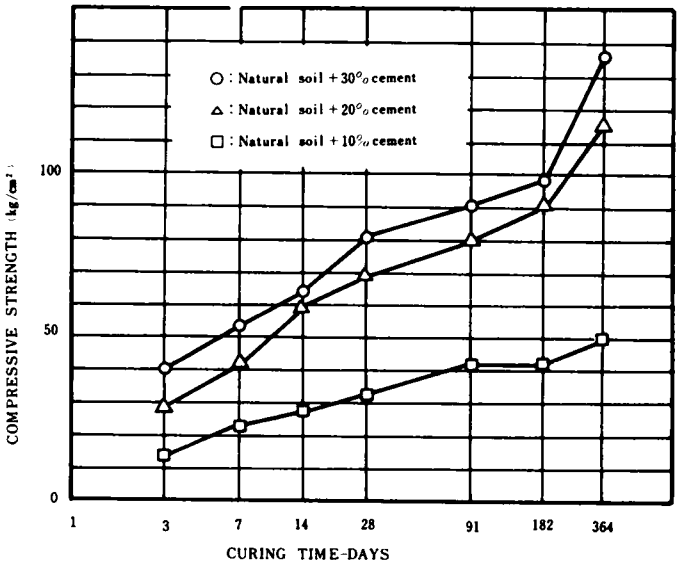

Fig.3.62 Variation of compressive strength with curing time in natural soil-cement mixture

In their studies of lime-montmorillonitic clay reaction, Ho and Handy found that the pozzolanic reaction between $Ca(OH)_2$ and montmorillonitic clays was possible only at the pH higher than 11.0 (Ho and Handy , 1963). The pH value in their investigation was obtained for 30 percent concentration suspension. However, judging from both the characteristic strength vs. curing time curves (Fig. 3.57) and pH tests results in this investigation, a conclusion may be drawn that the pozzolanic reaction between cement and bentonite contributing to the strength increase of the bentonite-cement can occur at the pH higher than a critical value of 11. The liberation of Ca^{++} ions from hydrating cement, and subsequent cation exchange between these calcium ions and the magnesium previously held in the clay sample progress to turn the bentonite into the one saturated with calcium ions up to "lime retention point" at a certain ages after 28 days, followed by the pozzolanic reaction contributing to the strength increase in the alkaline envioronment of the higher than 11. However, the pozzolanic reaction in bentonite-cement can not definitely be related to the pH obtained in this investigation as in Ho and Handy's results of the soil-lime system, because the pH in bentonite-cement is influenced by the anhydrous alite and belite.

It may rightly be supposed that the pozzolanic reaction in bentonite-cement should require the adequate amount of cement to produce the calcium hydroxide beyond the amount needed to attain a lime retention point. If the $Ca(OH)_2$ produced by cement hydration at 28 days of curing is about 25 percent by weight of cement, the amount of $Ca(OH)_2$ produced in the bentonite-cement with 10 percent cement content must be less than a lime retention point confirmed by Eades and Grim (1959) and Handy et al. (1965) from the strength development of bentonite-$Ca(OH)_2$ mixture. According to Handy et al's statement (1965), such a retention point is about 6 percent by weight of a clay sample. It is generally higher than the lime retention point from plasticity tests (2.5 percent)(Handy et al., 1965).

Thus, it may reasonably be presumed that no pozzolanic reaction occurs in the bentonite-cement with 10 percent cement content even after 28 days of curing, resulting in a little increase in its strength. It should be noted that the retention point of the bentonite used in this investigation (about 4.5 percent) is higher than the value of 2.5 percent, because the bentonite sample may be unsaturated with Ca ions.

(c) Sericite-cement

The strength increase tendency with curing time is almost the same as that in kaolinite-cement (Fig. 3. 56 and Fig. 3.58). However, unlike kaolinite-cement mixtures, the strength of the sericite-cement specimens at all ages is approximately in proportion to its cement content.

(d) Mixed-layer mineral-cement

It is a highly interesting phenomenon that the strength of this clay-cement mixture greatly increases between 182 and 364 days of curing (Fig. 3.59).

Such a great increase in strength after the cure of 182 days is not found in other clay mineral-cement mixtures. In this respect, little or no changes in the X-ray diffraction peak height of $Ca(OH)_2$ and in the pH value between both curing times definitely demonstrate that the rapid strength increase is not caused by the pozzolanic reaction between the clay mineral and $Ca(OH)_2$.

Concerning the mineralogical properties of this clay mineral, Sugiura (1962) reported as follows: "Generally, discussion on the diffraction lines at 1.50 to 1.54 Å corresponding to the (060) reflection can lead to the determination of the characteristics of the structural layer constituting a clay mineral. When primarily aluminum is present in the octahedral layer within the structure, this reflection appears at about 1.50 Å. When the major cation in the octahedral layer is magnesium, it does at about 1.54 Å. This mineral is found to belong to the latter, that is, to a trioctahedral mineral, since the reflection in the

randomly oriented specimen of this sample takes place at 1.537 Å."

It is found that this clay sample used includes chlorite-vermiculite mixed-layer mineral rich in magnesium as the predominant component (Table 3.4). Therefore, this clay mineral particles would be presumed to be attacked by $Ca(OH)_2$ resulting from cement hydration at the edges to dissociate magnesia as well as silica and alumina. Consequently, in this clay-cement, a physicochemical reaction process in which magnesium is concerned should be expected to occur in addition to the usual pozzolanic reaction between cement and clay mineral having no brucite layer in the structure.

Two possible processes may be considered. The one is the substitution of silicon by magnesium in the tobermorite lattice, and the other a certain reaction process through which the chrysotile-like magnesium silicate hydrate is formed. This chrysotile ($3MgO,2SiO_2,2H_2O$), a mineral with a layer lattice, which is known to be fibrous in habit, is said to favor the strength development of cement paste (Richartz and Locher, 1965). As stated previously, a new sharp X-ray diffraction peak at 10 Å may suggest the likelihood of the latter.

(e) Allophane-cement

No strength development accompanying with the cure is found in allophane(A(I))-cement with 10 and 20 percent cement contents even in 30 percent cement content specimens, only a little increase in strength occurs after 28 days of curing (Fig. 3.60). However, there is a distinct difference in strength between all cement contents in allophane(A(II))-cement; especially, the strength of 20 and 30 percent cement content specimens increases with increasing curing time (Fig. 3.61). These results concerning the strength development are consistent with those obtained in the X-ray diffraction. The halloysite hydrated included in allophane clay sample seems to have a favorable effect on the strength development of allophane-cement mixtures.

(f) Natural soil-cement

The unconfined compressive strength of this mixture increases during the long periods of curing. There is no characteristic tendency to be noted(Fig. 3.62).

(6) Examination by Optical Microscope

Fig. 3.63, Fig. 3.64 and Fig. 3.65 represent the change with the curing time in the textures of the kaolinite-, bentonite- and sericite-cement, respectively. These are obtained by observing the thin sections under an optical microscope. No groundmass gel as observed in (a) and (b) of Fig. 3.63 and Fig. 3.64 is found in the photomicrographs of the kaolinite- and bentonite-cement mixtures at the end of 91 days and 200 days of curing (Fig. 3.63(c), (d) and Fig. 3.64(c), (d)). Mitchell and Jack (1966), in their reports of the fabric of soil-cement observed with an electron microscope using replicas of the fracture surface, state as follows;"Irregular elongated particles from the hydrating cement at the end of one week appear to have transformed in part to irregular plate-like particles and the distinction between the cement and kaolinite phases becomes virtually impossible at the end of 32 weeks curing." (Mitchell and Jack, 1966).

The disappearance of groundmass gel in the observation of thin sections seems to relate to the above result obtained by Mitchell and Jack. Since the kaolinite clay material used in the present investigations includes relatively coarse particles of quartz, the disappearance of groundmass gel is observed in the interstitial part in kaolinite-cement mixture, as shown in Fig. 3.63.

The Fig. 3.65 shows the existence of the groundmass gel even at the end of 91 days of curing, suggesting that the clay-cement interaction in the sericite-cement mixture is not so active as in the other mix-

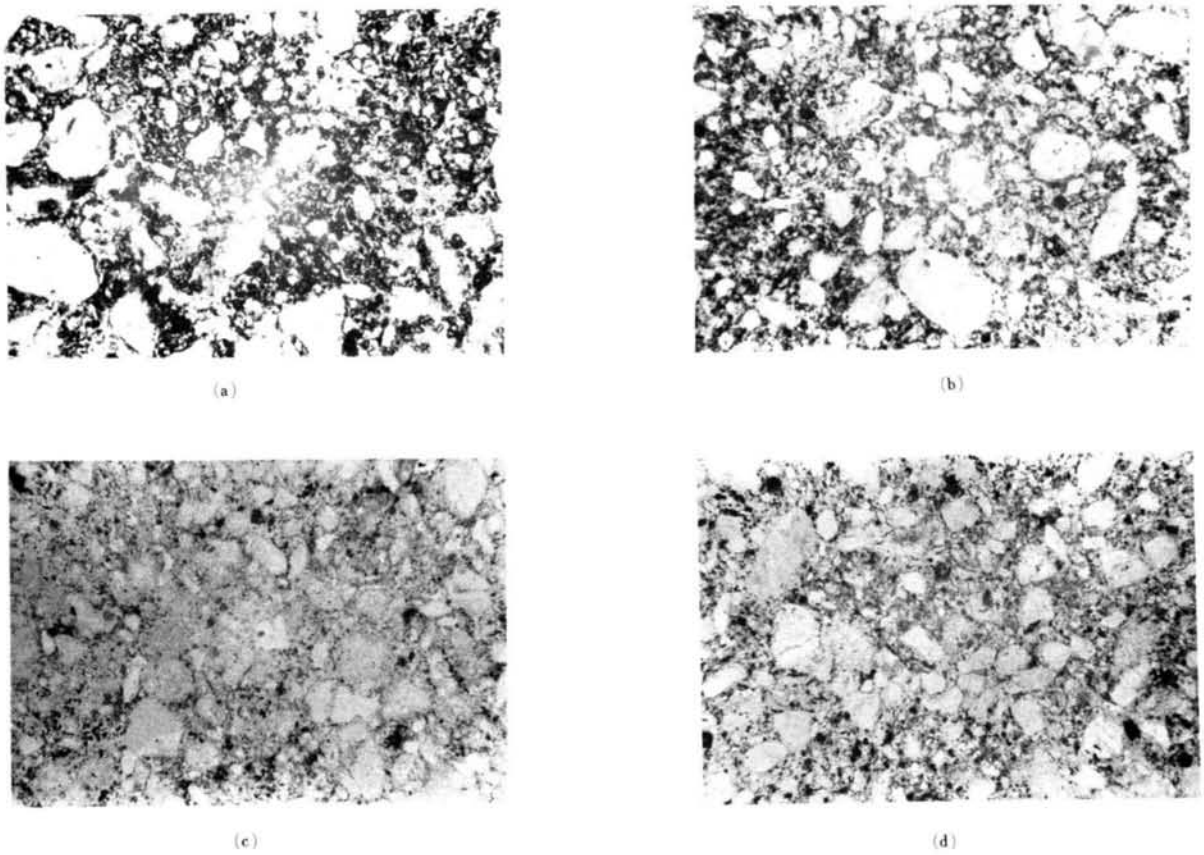

Fig. 3.63 Photomicrographs of thin sections kaolinite +20% cement samples : (a) Aged 3 days, (b) Aged 28 days, (c) Aged 91 days, (d) Aged 200 days (x50)

tures.

In short, the optical observetions lead to a same conclusion as expected by X-ray diffraction, D.T.A. and pH test, described above. The groundmass gel observed in the thin section of clay-cement seems the mixture of CSH(gel) and the amorphous calcium hydroxide.

(7) Summary and Conclusions

A series of experiments demonstrate that the interaction between the clay minerals and cement is active in the order of montmorillonite, kaolinite and sericite, apart from mixed-layer mineral and allophane.

The bentonite-cement seems to produce CSH(gel) more than the kaolinite-cement. The reaction sites of kaolinite with $Ca(OH)_2$ seems to differ from those of sericite and bentonite. This may relate to the sites of cation exchange. Cation exchange due to broken bonds may be important for kaolinite and in part at least, the hydrogens of exposed hydroxyls may be replaced by other cations. Therefore, kaolinite minerals in kaolinite-cement may be attacked at the edges, producing primarily calcium aluminate hydrate and CSH(gel) in part. This is evidenced by the large bulge at about 200°C in the D.T.A. curves of the kaolinite-cement (Fig. 3.35).

On the other hand, in sericite and montmorillonite, where the cation exchange is due to lattice substitution, the cations are mostly on the basal plane surfaces. Thus, sericite and montmorillonite minerals may be attacked in the basal plane surfaces rather than at the edges. Therefore, the interaction of these clay minerals with $Ca(OH)_2$ liberated from hydrating cement must be accompanied by the formation of CSH(gel)

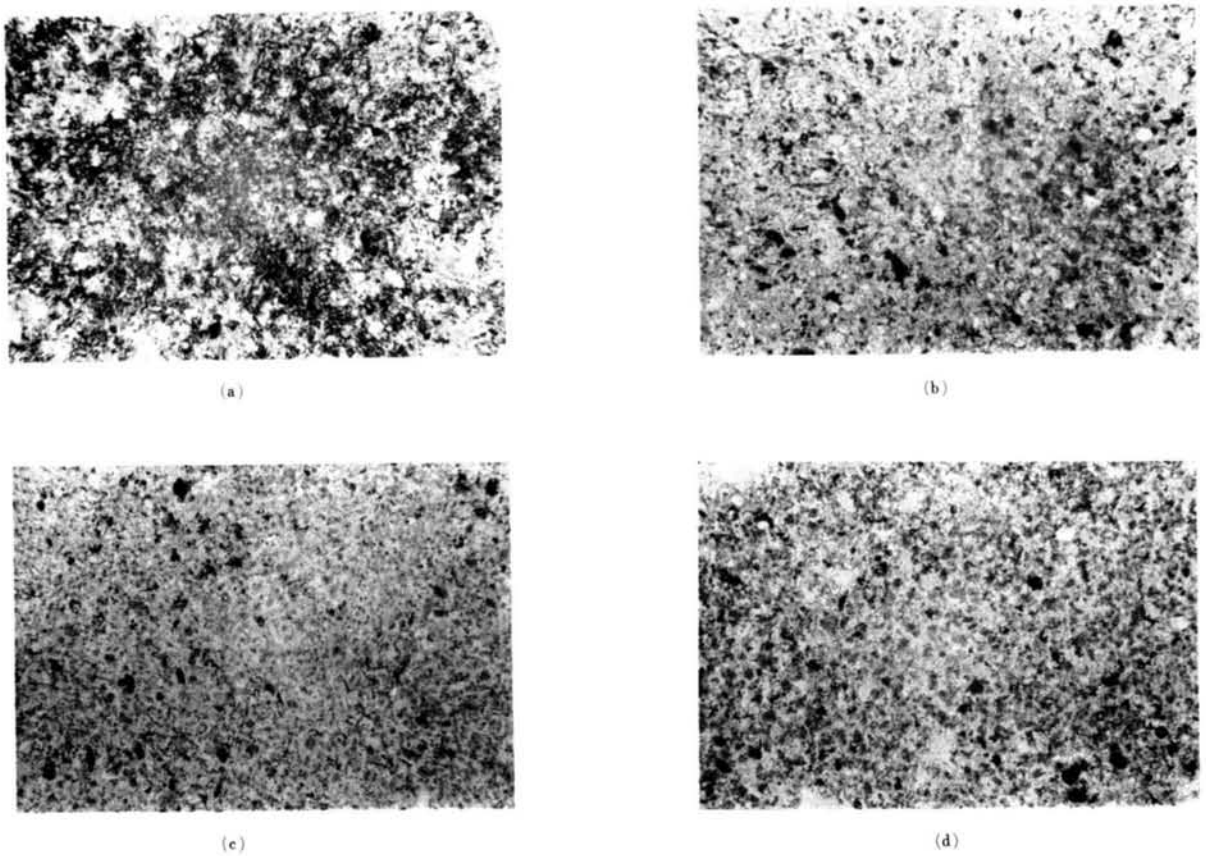

(a)

(b)

(c)

(d)

Fia. 3.64 Photomicrographs of thin sections bentonite +20% cement samples ; (a) Aged 3 days, (b) Aged 28 days, (c) Aged 91 days, (b) Aged 200 days (x 50)

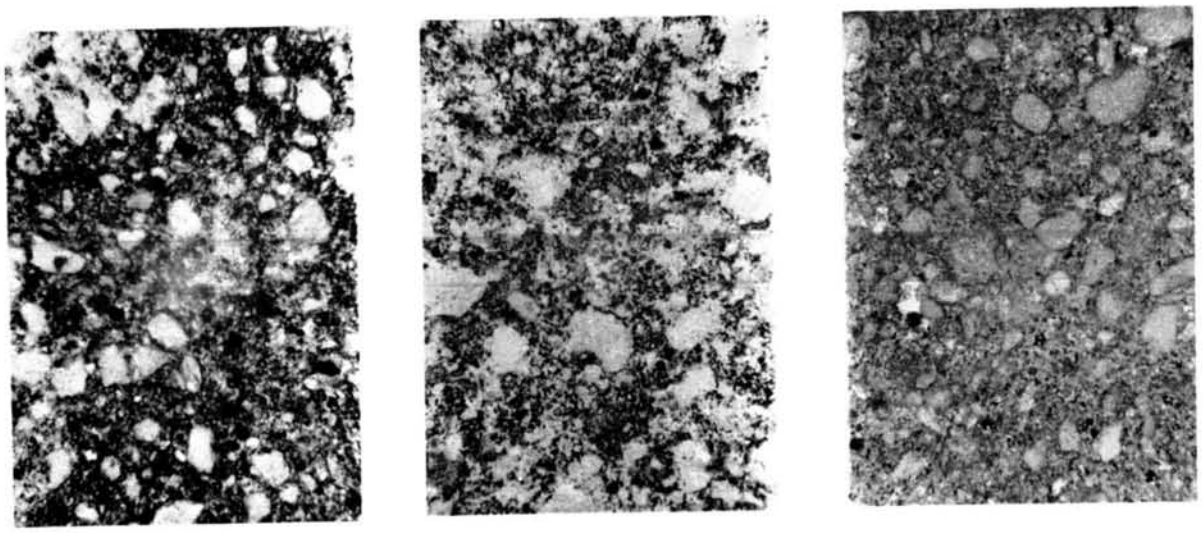

(a)

(b)

(c)

Fig. 3.65 Photomicrographs of thin sections sericite +20% cement samples ;(a) Aged 28 days, (b) Aged 91 days, (c) Aged 200 days (X50)

rather than calcium aluminate hydrate. The broad peak at about 900° C in the D.T.A. curves of the sericite-cement at 91 and 200 days ages and the very high peak of CSH(gel) at 3.07 Å in X-ray diffraction diagrams of bentonite-cement seem to support the above interpretation.

The strength of compacted clay-cement mixtures may come from tobermorite gel and calcium aluminate hydrate resulting from the cement hydration and the secondary clay mineral-$Ca(OH)_2$ interaction. In this respect, the nature of the strength development in chlorite-vermiculite mixed-layer clay mineral-cement appears different from that described above. That is to say, magnesia as well as silica and alumina may be dissolved to a certain extent from these trioctahedral mineral by the attack of $Ca(OH)_2$ at the edges resulting in the formation of fibrous magnesium silicate hydrate contributing to the strength development. Some data were obtained suggesting the formation of such magnesium silicate hydrate.

Furthermore, the possibility that the long-term strength of the mixed-layer mineral-cement is brought about by the magnesium silicate hydrate could be proved by the fact that the rapid increase in strength and the appearance of a sharp X-ray diffraction peak at 10 Å simultaneously occur at the cure of 364 days.

As described above, the mechanism of the interaction between most clay minerals and portland cement may be presumed to be essentially similar to that in the soil-lime system. However, chlorite-vermiculite mixed-layer mineral is found to show a peculiar behavior in its interaction with hydrating cement.

Other conclusions obtained are summarized as follows.

(1) The amount of cement added vs. P.L. curve of bentonite-cement shows a characteristic inflection which has already been found in the soil-lime system.

(2) Despite of the slow increase in the strength of 10 percent cement content specimens, that of the bentonite-cement with 30 and 20 percent cement content rapidly increases after the curing time of 28 days.

(3) The unconfined compressive strength of bentonite- and sericite-cement which primarily depends upon the formation of CSH(gel) is approximately in proportion to the cement content, but in kaolinite-cement mixture in which a great amount of calcium aluminate hydrate is produced, a difference in cement content brings about a little difference in strength.

(4) Allophane seems to suppress the cement hydration.

(5) The inclusion of halloysite hydrated in allophane accelerates the cement hydration, resulting in the increase in the strength of allophane-cement mixtures.

(6) Cation exchange capacity of a clay mineral sample used in clay-cement may relate to whether there exists free lime in the mixtures or not. A clay mineral sample with cation exchange capacity(C.E.C.) of 7 to 10 meq/100g such as kaolinite, sericite and mixed-layer mineral exhibits the presence of $Ca(OH)_2$ in its clay-cement mixture. There is no $Ca(OH)_2$ detected by X-ray diffraction and D.T.A. in a clay-cement using the one with C.E.C. of 25 to 73 meq/100g such as bentonite, allophane and natural soil.

ROLE OF THE CALCIUM HYDROXIDE PRODUCED BY THE CEMENT HYDRATION IN CLAY-CEMENT MIXTURE

A conclusion derived above, as other investigators report, shows that the reaction of clay minerals with calcium hydroxide from the cement hydration plays a significant part in the mechanism of the interaction between clay minerals and portland cement. However, actual functions of $Ca(OH)_2$ in clay-cement mixture have not been revealed yet. Some results were obtained by comparing the experimental results of clay-cement mixtures with those of clay-$Ca(OH)_2$ ones, as stated in the following.

In the preparation of specimens for tests, the calcium hydroxide of 9, 6 and 3 percent by weight of dry clay is added to clay mineral samples correspondingly to the comparable clay-cement mixtures of 30, 20 and

10 percent content, respectively, since the complete hydration of portland cement liberates the calcium hydroxide of about 30 percent by weight of cement.

(1) X-ray Diffraction

Fig. 3.66 and Fig. 3.67 indicate the X-ray diffraction diagrams of bentonite (MB)- and kaolinite(Ka(II))-$Ca(OH)_2$ mixture, respectively.

Only both 9 and 6 percent $Ca(OH)_2$ content samples at the curing time of 3 days indicate the X-ray diffraction peak of $Ca(OH)_2$ at 2.63 Å (Fig. 3.68).

As reported by several investigators (Wang and Handy, 1966)(Diamond, 1963)(Glenn, 1963)(Jack, 1965)(Sloan, 1964), a great amount of CSH(gel) is produced as a reaction product of the bentonite-$Ca(OH)_2$ interaction. The formation of CSH(gel) is evidenced by two sharp peaks at 3.07 Å and 2.08 Å (Fig. 3.66). However, the formation of calcium aluminate hydrate can not definitely be confirmed.

The peak height of $Ca(OH)_2$ (d = 2.63 Å) in kaolinite-$Ca(OH)_2$ mixtures rapidly decreases until 7 days of curing (Fig. 3.69).

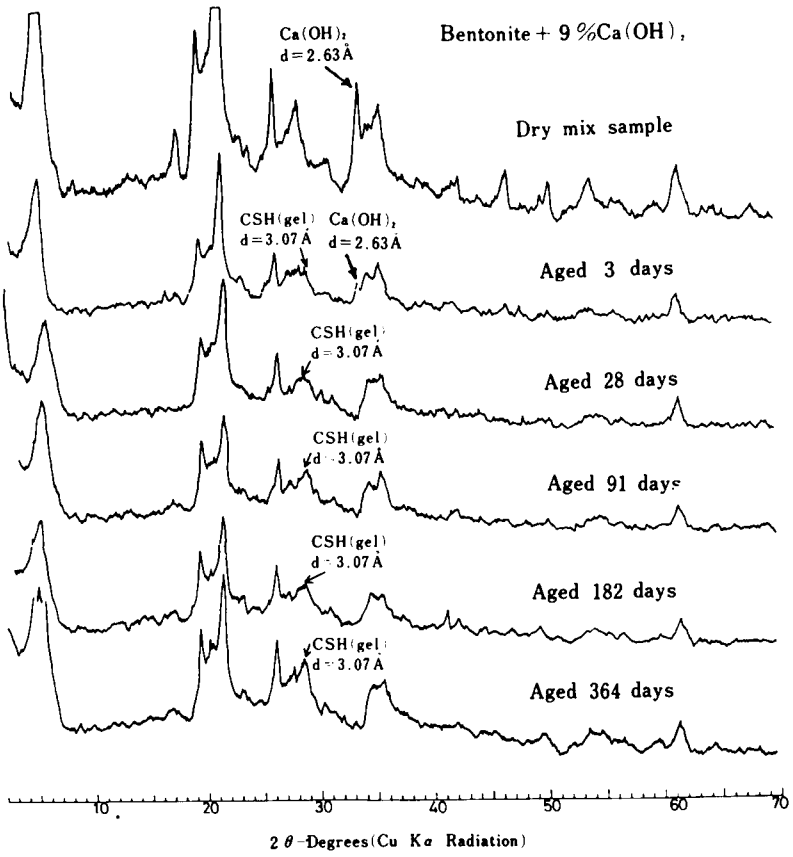

Fig.3.66 X-ray diagrams for bentonite(MB) + 9 % $Ca(OH)_2$ samples cured for 3,28,91,182 and 364 days

The comparison in the changes of the X-ray diffraction peak height between kaolinite-cement and -$Ca(OH)_2$ mixtures (Fig. 3.70) apparently suggests that the liberation of $Ca(OH)_2$ from the cement hydration and the kaolinite-$Ca(OH)_2$ interaction simultaneously progress with curing time.

The X-ray diffraction peak height of CSH(gel) at 3.07 Å in bentonite-cement is considerably great even at 3 days of curing, though not indicating such a gradual increase with curing time as found in kaolinite-cement.

The peaks at 8.2 and 2.9 Å are observed in 9 percent additive content sample of kaolinite-$Ca(OH)_2$ at the end of 3, 7, 14, 28 and 91 days of curing (Fig. 3.67). These peaks may be considered to be the reflections of hillebrandite newly formed. They disappear in the 182 and 364 days curing samples, and a sharp peak is detected at 12.5 Å. This peak may probably be the basal reflection of CSH(I). This fact interpretes that the hillebrandite of high lime-silica ratio is converted to the CSH(I) of the low one after the cure of 91 days. The formation of hillebrandite is evidenced by D.T.A. data as described below.

In this respect, it is mentioned that hillebrandite appears to be formed from the starting materials through the successive intermediate stages of CSH(II) or some other ill-crystallized material and α-C_2S hydrate (Taylor, 1964). The reaction seems to proceed through the following process; kaolinite-$Ca(OH)_2$ mixture ⟶ ill-crystallized CSH(with high lime-silica ratio) ⟶ hillebrandite ⟶ CSH(I)(with low

lime-silica ratio).

Moh(1965) obtained the following result from D.T.A. curves of quartz-C_3S mixtures.

"The two exotherms at 830° and 870° C belong to the CSH with lime-silica ratios of 0.8 to 1.0 and 1.25, respectively. The gradual increase in the size of the lower temperature exotherm and the decrease in size of the other with time definitely indicate that the high-lime member of CSH is transformed to a lower lime member."

On the contrary, none of the X-ray diffraction data of kaolinite-cement shows the presence of hillebrandite and CSH(I).

(2) Differential Thermal Analysis

The endothermic bulge at about 180° C exists in all of D.T.A. curves of kaolinite-$Ca(OH)_2$ mixtures with 9 percent $Ca(OH)_2$ content, as in kaolinite-cement mixtures (Fig. 3.71). This peak belongs to the tetracalcium aluminate hydrate. There is another endotherm at about 630° C in the 28 and 91 days of curing samples as well. This peak can be responsible for the dehydroxylation of hillebrandite. However, no bulge can be found at about 630° C in the D.T.A. curve of 364 days curing samples. Thus, nonexistence of hillebrandite in the 364 days curing sample evidenced by D.T.A. agrees with the X-ray diffraction tests

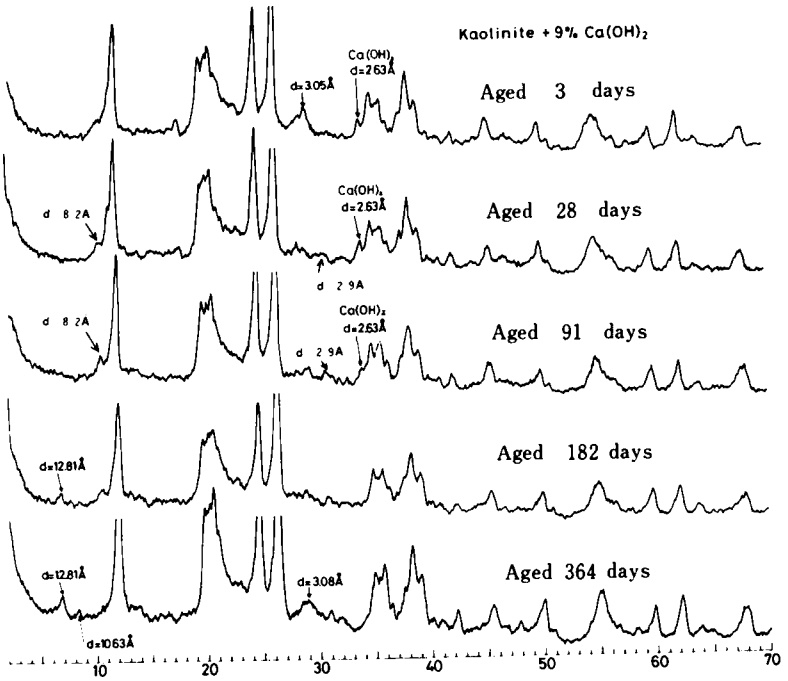

Fig.3.67 X-ray diagrams for kaolinite(Ka(II)) + 9% $Ca(OH)_2$ samples cured for 3,28,91,182 and 364 days

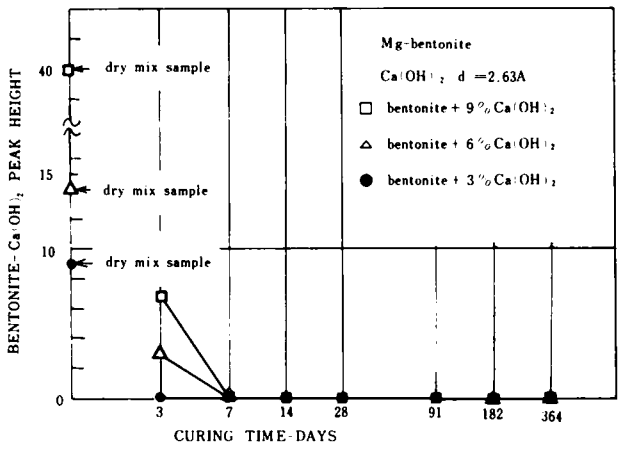

Fig.3.68 X-ray diffraction peaks for hydrating bentonite(MB)-$Ca(OH)_2$ mixtures

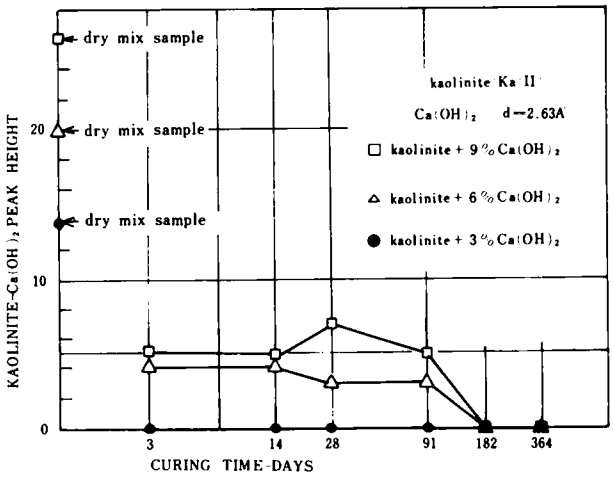

Fig.3.69 X-ray diffraction peaks for hydrating kaolinite(Ka(II))-$Ca(OH)_2$ mixtures

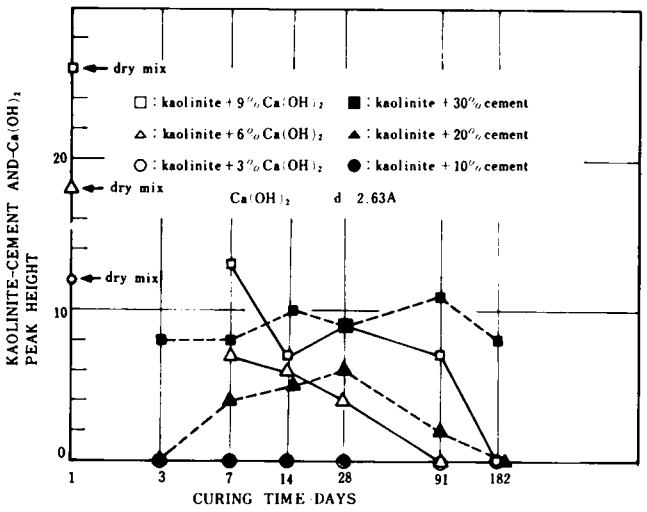

Fig. 3.70 X-ray diffraction peaks for hydrating kaolinite-$Ca(OH)_2$ and -cement mixtures

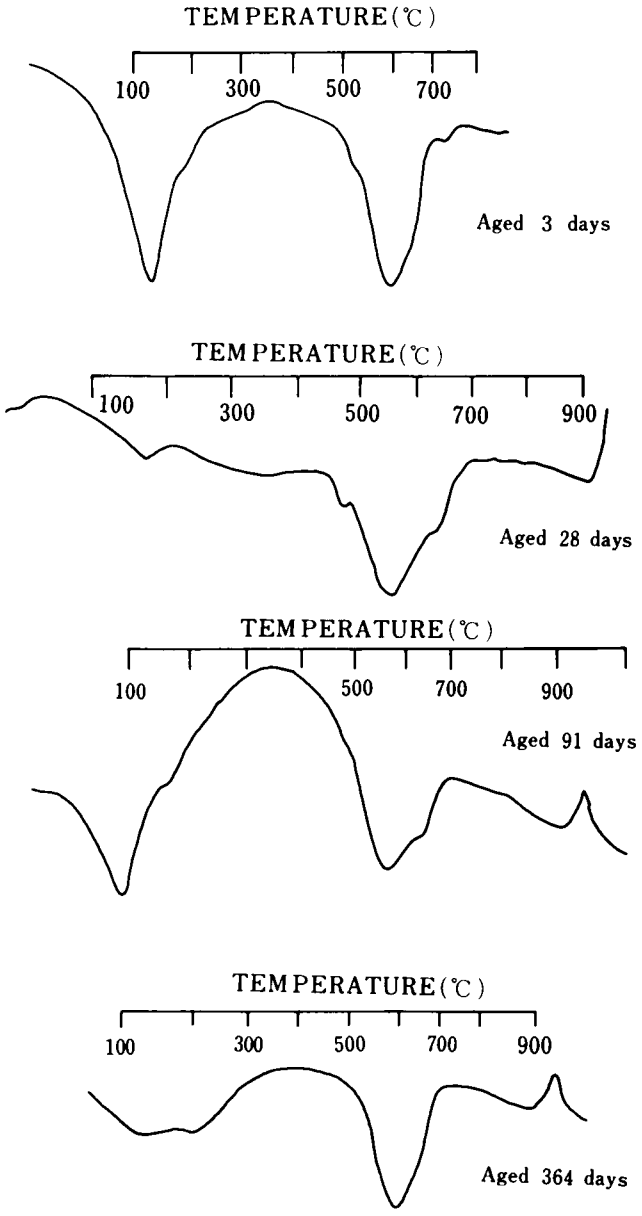

kaolinite(Ka(II))+ 9 %$Ca(OH)_2$

Fig.3.71 D.T.A. curves for kaolinite (Ka(II)) + 9 %$Ca(OH)_2$ cured for 3,28,91 and 364 days

result described above. The D.T.A. curves of kaolinite-cement with 30 percent cement content until 28 days of curing show a very faint endothermic deflection at about 630° C, which disappear after 91 days of curing.

An endothermic bulge due to $Ca(OH)_2$ at about 500° C in kaolinite-$Ca(OH)_2$ has disappeared at 91 days, although that in kaolinite-cement can be detected even at 364 days (Fig. 3.55). This fact demonstrates that the amount of $Ca(OH)_2$ which is consumed by the interaction with kaolinite in the kaolinite-cement is less than that in the kaolinite-$Ca(OH)_2$ mixture. It is very interesting to note that the apparent endothermic bulge due to hillebrandite exists in the kaolinite-$Ca(OH)_2$ mixture consuming far more $Ca(OH)_2$ than the kaolinite-cement mixture.

(3) pH Test

The pH changes with curing time in the bentonite-$Ca(OH)_2$ mixtures are presented in Fig. 3.72. As shown in the figure, the pH in bentonite-$Ca(OH)_2$ mixtures with 6 and 9 percent $Ca(OH)_2$ content rapidly decreases after 3 and 7 days of curing, respectively. The 3 percent $Ca(OH)_2$ content sample shows the pH value of about 11.10 at 3 days age, followed by little change with curing time. This tendency of the pH changes in bentonite(MB)-$Ca(OH)_2$ is different from that in bentonite(MB)-cement (Fig. 3.72, Fig. 3.49, Fig. 3.50, Fig. 3.51). Thus, the comparison in the pH changes between these two different mixtures indicates that little pozzolanic reaction occurs in bentonite-$Ca(OH)_2$ mixtures with 3 percent $Ca(OH)_2$ content. Furthermore, the reduction in pH of the bentonite-cement with 10

percent cement content is found to be not due to the pozzolanic reaction. This conclusion agrees with that drawn by the detailed discussion on the pH changes and unconfined compression test results in bentonite-cement mixtures as previously stated.

The reduction in the pH value of the kaolinite -$Ca(OH)_2$ with curing time is greater than that of the kaolinite-cement (Fig. 3.73, Fig. 3.49, Fig. 3.50, Fig. 3.51). Such reduction in the pH of kaolinite-$Ca(OH)_2$ shows a gradual progress of the kaolinite-$Ca(OH)_2$ reaction.

(4) Unconfined Compression Test

The unconfined compressive strength of kaolinite(Ka(II))-$Ca(OH)_2$ and bentonite(MB)-$Ca(OH)_2$ specimens increases with the lapse of curing time, as shown in Fig. 3. 74 and Fig. 3.75. Little difference in the strength of kaolinite-$Ca(OH)_2$ at 3 and 7 days curing is found between different concentrations of the additive (Fig. 3.74). The strength of kaolinite(Ka(II))-$Ca(OH)_2$ mixture at the end of 28 days of curing decreases, as the amount of the additive increases. The compressive strength of the specimen with 3 percent $Ca(OH)_2$ increases a little after 28 days of curing. At the long-term curing of 91, 182 and 364 days, the kaolinite-6% $Ca(OH)_2$ specimens have the greatest strength of all. The calcium hydroxide of 3 percent by weight of clay may be almost consumed by the pozzolanic reaction contributing to the strength development before 91 days of curing.

On the contrary, only a little development of strength is observed in the bentonite-$Ca(OH)_2$ with 3 percent additive. Further, there is a considerable difference in the compressive strength between different concentrations of the additive at 28, 91, 182 and 364 days of curing. Thus, as stated by Eades and Grim (1959), it can be concluded that the strength of bentonite-cement is not developed without adding the $Ca(OH)_2$ beyond the amount required to attain the lime retention point obtained from strength tests. The three curves in Fig. 3. 75 show that a little or no increase in strength

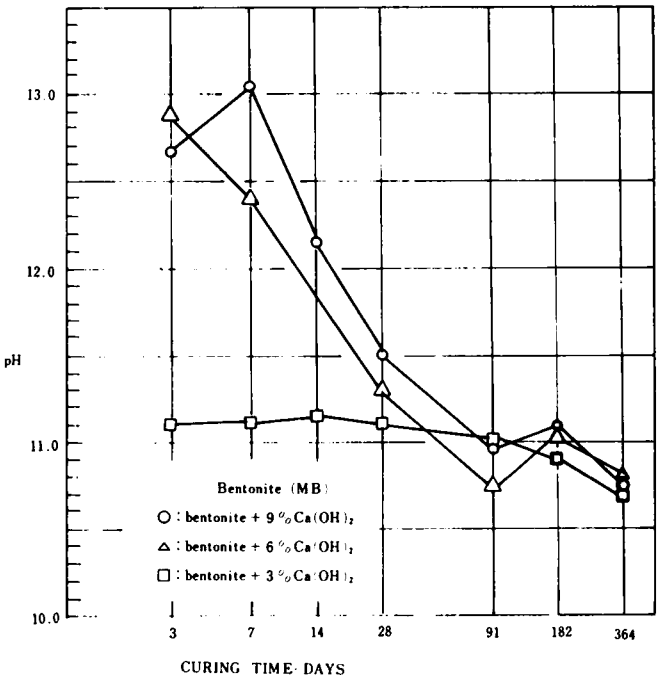

Fig.3.72 pH changes of bentonite-$Ca(OH)_2$ mixtures with curing time

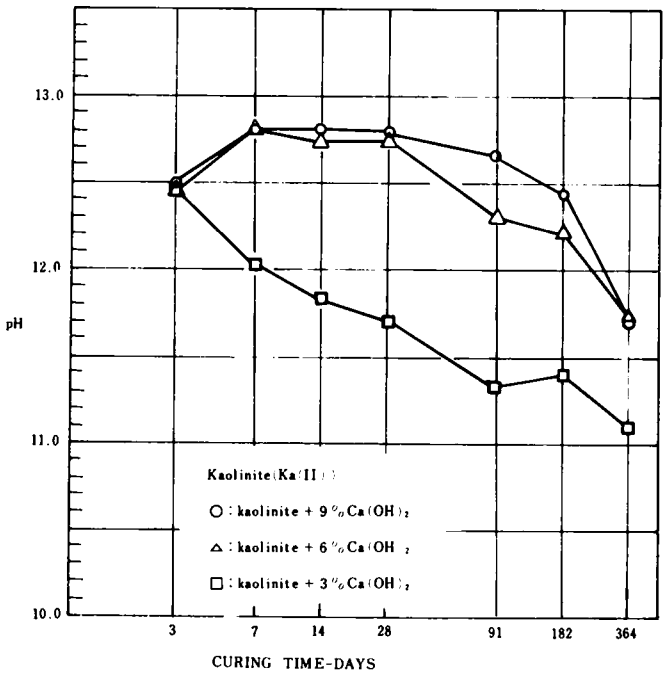

Fig.3.73 pH changes of kaolinite-$Ca(OH)_2$ mixtures with curing time

accompanying with curing time is found after all of $Ca(OH)_2$ added have been consumed by the pozzolanic reaction, i.e., after 182, 91 and 3 days ages for the 9, 6 and 3 percent content specimens, respectively. Plots of the unconfined compressive strength against curing time in clay-cement and -$Ca(OH)_2$ specimens are given in Fig. 3.76, Fig. 3.77, Fig. 3.78, Fig. 3.79, Fig. 3.80 and Fig. 3.81. These pair of curves are comparable one another in their additive concentration. The two curves in each combination of bentonite (MB)-cement and -$Ca(OH)_2$ mixtures show that there is a little difference in strength between them at the initial stage of curing, followed by a great difference at the long-term curing (91, 182 and 364 days of curing). The long-term development of strength in the bentonite-cement is considered to be due to the pozzolanic reaction of bentonite with $Ca(OH)_2$ generated by the cement hydration, as previously concluded. Therefore, such dissimilarity in the tendency of the strength development between bentonite-cement and -Ca $(OH)_2$ could be responsible for the difference between the $Ca(OH)_2$ of reagent and the one liberated by the hydrating cement (Gillot and Sereda, 1966). As another aspect, it may be attributed to the difference in the physicochemical properties of calcium silicate hydrate produced between them, because the calcium silicate hydrate is formed under considerably different environments between clay-cement and -$Ca(OH)_2$ mixtures. In fact, different reaction products were formed between both of them, as shown in the X-ray diffraction test results.

Furthermore, the effect of anhydrous cement particles on the strength can not be out of consideration.

(5) Summary and Conclusions

The results obtained are summarized as follows.

1) Hillebrandite with high lime-silica ratio may be formed at the very initial stage of curing as a reaction product in kaolinite-$Ca(OH)_2$ mixtures, transforming to the CSH(I) with lower lime-silica ratio at the long-term curing (182 and 364 days ages). In this respect, Willoughby et al. (1968) found the formation of hillebrandite in a kaolinite-$Ca(OH)_2$ mixture by means of the X-ray diffraction and electronmicroscopic examination. However, the presence of this mineral seems uncertain in kaolinite-cement mixtures.

2) A large amount of calcium silicate hydrate may be produced in the bentonite(MB)-$Ca(OH)_2$ mixture.

3) The interactions of kaolinite and bentonite with $Ca(OH)_2$ resulting from the cement hydration are not quite equivalent to those with

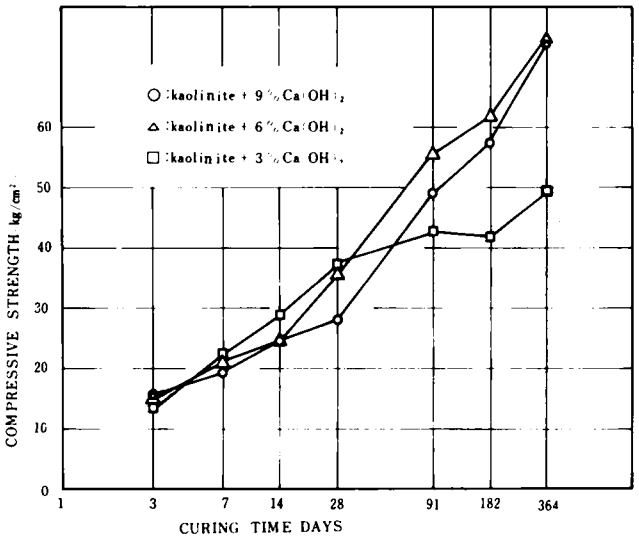

Fig.3.74 Variation in strength with curing time

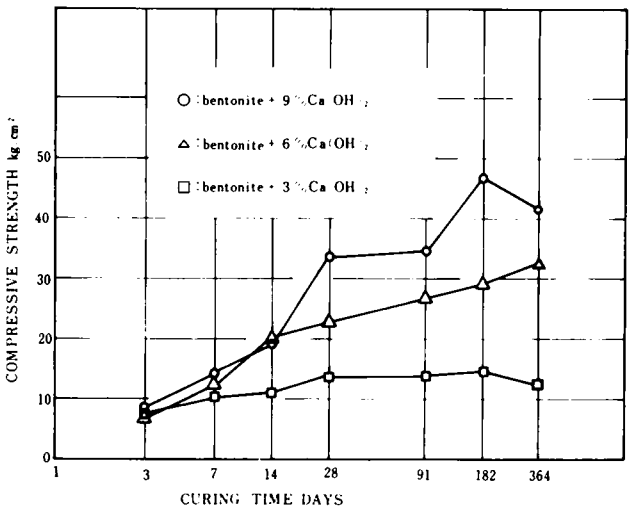

Fig.3.75 Variation in strength with curing time

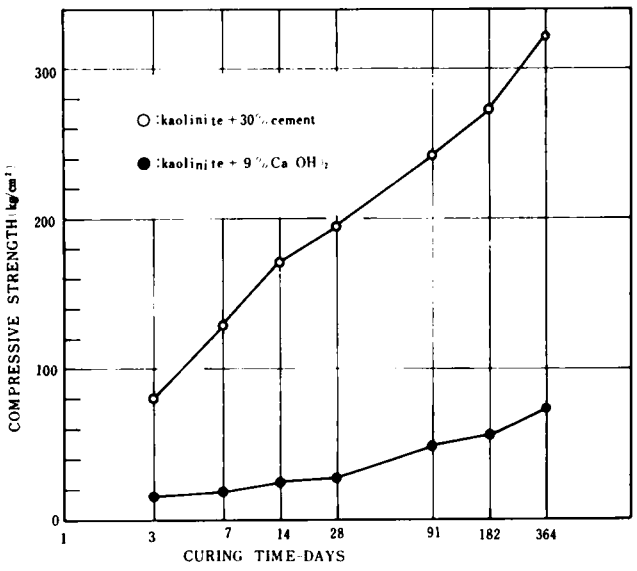

Fig.3.76 Variation in strength with curing time

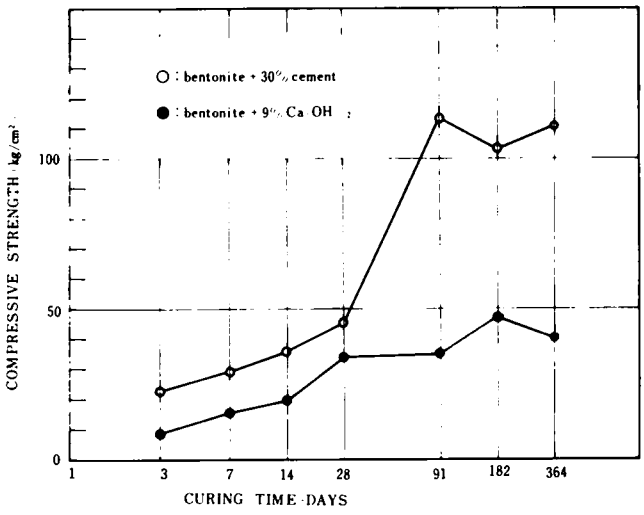

Fig.3.77 Variation in strength with curing time

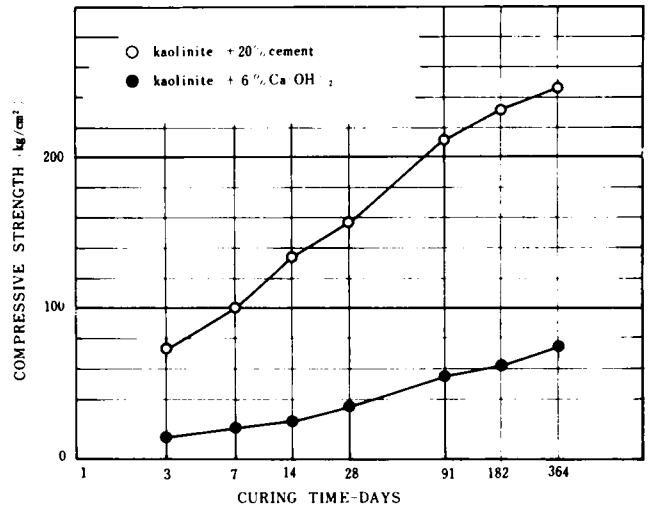

Fig.3.78 Variation in strength with curing time

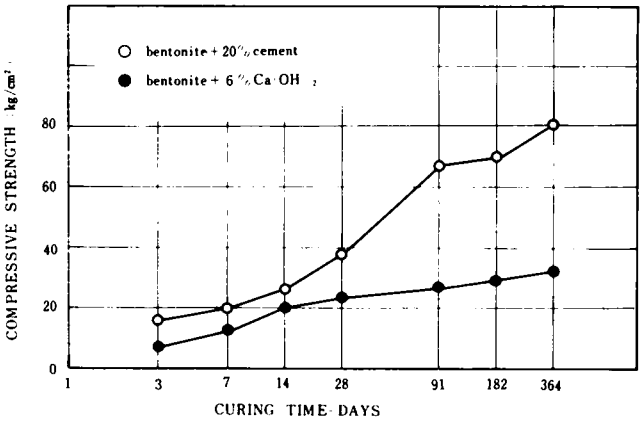

Fig.3.79 Variation in strength with curing time

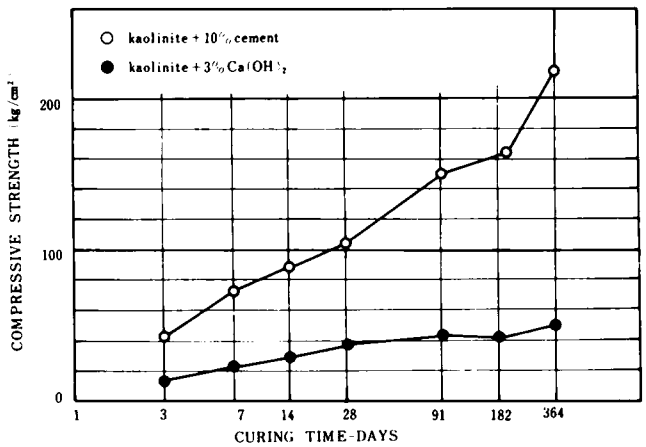

Fig.3.80 Variation in strength with curing time

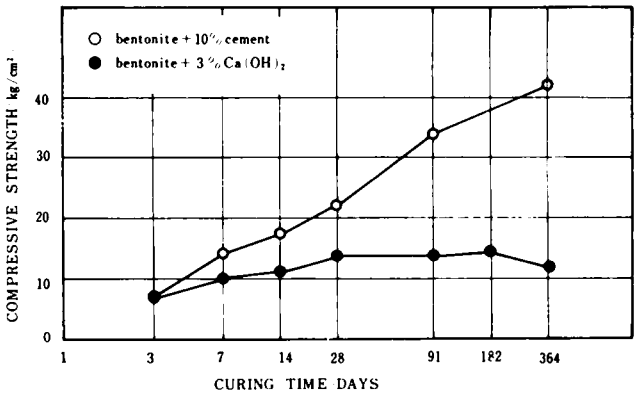

Fig.3.81 Variation in strength with curing time

the $Ca(OH)_2$ of reagent. This discrepancy could be responsible for the following three points; (i) the crystal lattice of $Ca(OH)_2$ in cement paste is distorted and more reactive than the calcium hydroxide grown by the diffusion technique using $CaCl_2$ and NaOH(Gillot and Sereda, 1966), (ii) the calcium hydroxide is generated in the amorphous state at the initial stage of cement hydration, (iii) there is the likelihood that the ionic mobility is different between clay-cement and -$Ca(OH)_2$ systems.

HYDRATION OF ALITE AND BELITE IN COMPACTED CLAY-CEMENT MIXTURES - The Influence of Types of Cement (High Early Strength and Moderate Heat Cement) on the Clay Minerals-Cement Interaction -

It could be expected from the previous parts in this chapter that the rate of hydration of portland cement in compacted clay-cement mixtures is different for different clay minerals used. Then, the rate of reduction in the quantities of alite and belite in kaolinite(Ka(III))- and bentonite(MB)-cement accompanying with their hydration will be discussed in detail using the X-ray diffraction method.

Types of cement selected are high early strength and moderate heat cement having a relatively great amount of C_3S and βC_2S, respectively. The difference between the relative proportions of these constituents (C_3S and βC_2S) included in two types of cement must affect the strength development of clay minerals-cement mixtures and physicochemical interaction between cement and clay minerals.

One of the important problems associated with cement stabilization of soils is the limited amount of time after mixing available for manipulation, testing and possible remanipulation. As a possible solution to this problem, the use of set-retarding admixtures is being investigated by the workers in Virginia Highway Research Council (Tice, 1968)(Noble and Ozol, 1968). In this respect, the subject on the rate of hydration of alite and belite in compacted clay-cement mixtures may be very interesting in practice as well.

(1) X-ray Diffraction

In general, the alite and belite X-ray diffraction patterns overlap each other so that there is no usable peak of one of these materials which is not interfered with by a peak of the other. However, the rate of the hydration of alite and belite in clay-cement mixtures can be determined, as stated below, basing on Kantro et al.'s method for determination of the major compound contents of portland cements by X-ray diffraction (Kantro et al., 1964).

The equations for the alite-belite system are

$$R_1 = \alpha_1 x_1 + \alpha_2 x_2 \qquad (3.1)$$

$$R_2 = \beta_1 x_1 + \beta_2 x_2 \qquad (3.2)$$

where R_1 and R_2 are intensity ratios of two alite-belite lines relative to the standard, α_1, α_2, β_1 and β_2 are constants, and x_1 and x_2 are weight of alite and belite, respectively. In this analysis, an external standard method is used, wherein the intensity standard is a separate specimen, copper, which is checked periodically for beam intensity variations. The diffraction peaks selected for use are those at 1.77 Å(R_1) and 2.20 Å(R_2). The 1.77 Å peak of alite is strong, while that of belite is weak. The peak at 2.20 Å is equally strong for alite and belite. The diffraction intensity of the 1.77 Å peak varies strongly with the relative amounts of alite and belite, while the intensity of 2.20 Å peak is not sensitive to this quantity. The quantity, which is the ratio of the 1.77 Å to the 2.20 Å peak, also varies strongly with the alite-belite ratio. This quantity is given by the ratio of equation (3.1) to equation (3.2).

$$\frac{R_1}{R_2} = R_3 = \frac{\alpha_1 x_1 + \alpha_2 x_2}{\beta_1 x_1 + \beta_2 x_2} \qquad (3.3)$$

The weight fractions of alite and belite in the total silicate are given by

$$w_1 = \frac{x_1}{x_1 + x_2} \qquad (3.4)$$

$$w_2 = \frac{x_2}{x_1 + x_2} \qquad (3.5)$$

In order to evaluate the four parameters in equations (3.1) and (3.2), data must be obtained from alite-belite mixtures of known compositions. Kalosek et al. give the following results in their paper (Kalousek et al., 1964).

$$w_2 = \frac{-(B + CR_3) + \sqrt{(B + CR_3)^2 + 4A(\alpha - BR_3)}}{2A} \qquad (3.6)$$

where $A = -0.0464$, $B = 0.1850$, $C = -0.0298$, $\alpha = 0.1462$, $\beta = 0.1368$

If the x_1, x_2, w_1, w_2 and R_3 in a clay-cement mixture at i days of curing are noted as x_{1i}, x_{2i}, w_{1i}, w_{2i} and R_{3i}, respectively,

$$w_{2i} = f(R_{3i}) = \frac{x_{2i}}{x_{1i} + x_{2i}} \qquad (3.7)$$

$$w_{20} = f(R_{30}) = \frac{x_{20}}{x_{10} + x_{20}} \qquad (3.8)$$

where x_{10}, x_{20}, w_{10}, w_{20} and R_{30} are those for dry mix samples. The ratio of equation (3.7) to equation (3.8) gives equation (3.9).

$$\frac{x_{10} + x_{20}}{x_{11} + x_{21}} \cdot \frac{x_{2i}}{x_{20}} = \frac{f(R_{3i})}{f(R_{30})}$$

$$\frac{x_{2i}}{x_{20}} = \frac{f(R_{3i})}{f(R_{30})} \cdot \frac{R_{1i}}{R_{10}} \left(\text{or } \frac{R_{2i}}{R_{20}} \right) \qquad (3.9)$$

Thus, if the R_3 at each curing time and the ratio of the R_{1i} to the R_{10} are determined, the rate of the decrease in the quantity of belite included in a sample with curing time can be calculated by equation (3.9). Since the sum of w_1 and w_2 is unity, the ratio of weight of alite at a certain time of curing (x_{1i})

to that of dry mix sample (x_{10}) can also be obtained in the same manner.

The intensity of R_1 and R_2 is evaluated as the area covered by the peaks (the shaded area, as indicated in Fig. 3.82).

The X-ray diffraction patterns of the kaolinite(Ka(III))- and the bentonite(MB)-cement indicate the decrease in the intensity of the peaks at 1.77 Å and 2.20 Å with curing time (Fig. 3.83, Fig. 3.84). The ratios of weight of alite and belite in clay-cement and cement paste after the cure of a certain time to that in dry mix samples are plotted as shown in Fig. 3.85 and Fig. 3.86. It may be seen from these figures that, in the initial stage of hydration (within 7 days of curing), the reduction rate in the quantity of alite (x_{1i}/x_{10}) in both kaolinite-cement mixtures is less than in cement paste. However, the a-

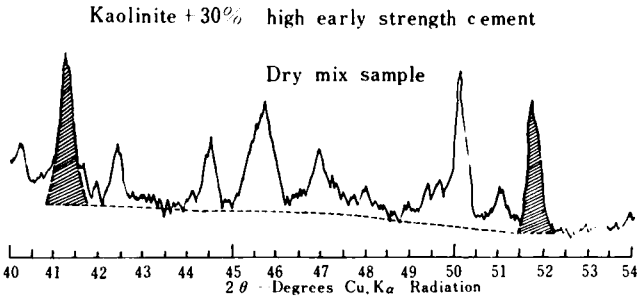

Fig.3.82 X-ray diagram for the dry mix sample of kaolinite and 30% high early strength cement

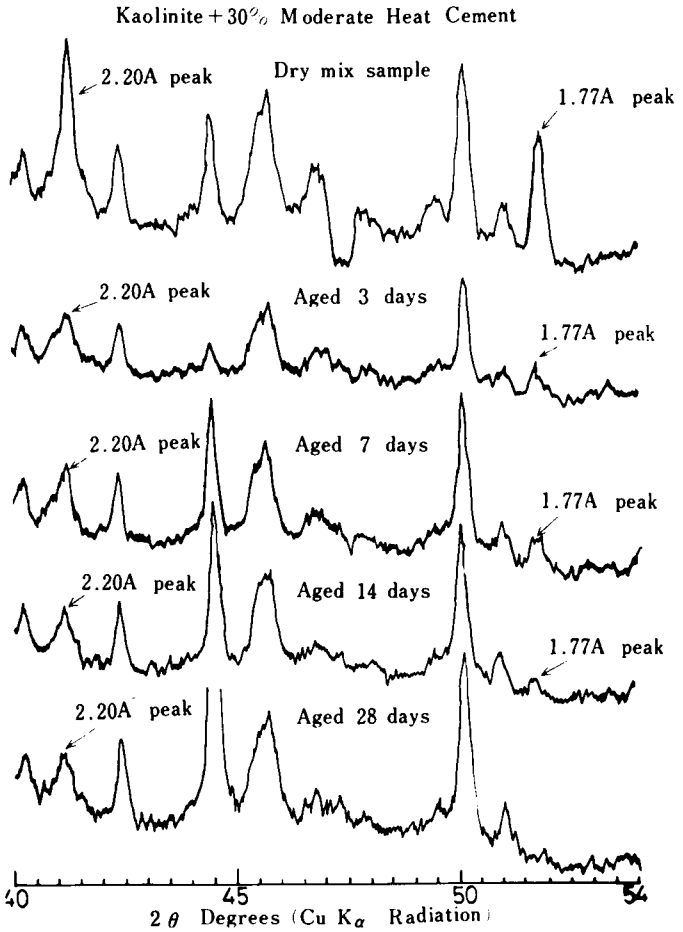

Fig.3.83 X ray diagrams for kaolinite Ka III + 30% moderate heat cement samples cured for 3, 7, 14 and 28 days

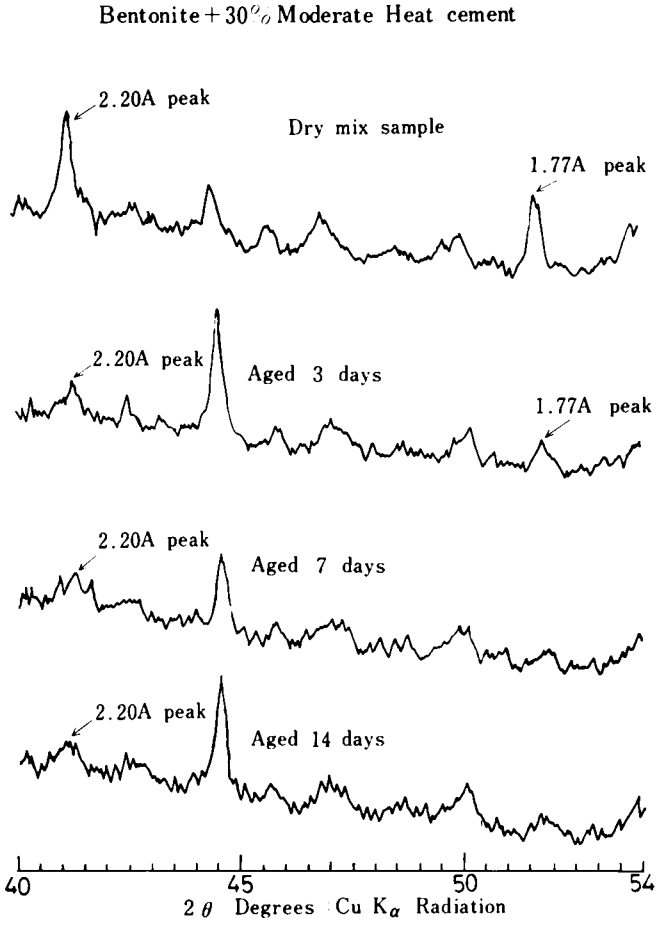

Fig.3.84 X ray diagrams for bentonite MB + 30% moderate heat cement samples cured for 3, 7 and 14 days

mount of alite in cement paste decreases a little or little after the initial hydration (from 1 to 7 days of curing), while that in kaolinite-cement mixtures continues to decrease gradually with curing time.

The hydration of belite in the kaolinite- and bentonite-moderate heat cement mixtures appears to proceed faster than in cement paste (Fig. 3.86). Within 7 days of curing, the hydration of alite in both bentonite-cement mixtures takes place more slowly than in cement paste. However, rapid hydration after 7 days of curing results in the early disappearance of the peak at 1.77 Å. None of the bentonite-cement mixtures shows the 1.77 Å peak at 14 days of curing (Fig. 3.84).

Another fact to be noted as to the X-ray diffraction tests results is that the peak of calcium hydroxide at 2.63 Å can not be detected in any X-ray diagrams of kaolinite(Ka(III))-cement as well as in bentonite(MB)-cement. This result seems to conflict with the presence of an appearent peak of $Ca(OH)_2$ at 2.63 Å in kaolinite(Ka(I))-cement mixtures (Fig. 3.22). This must be attributed to the difference between the amount of clay fraction included in kaolinite clay samples used (Ka(I) and Ka(III))(Table 3.3).

(2) Thermal Analysis

The D.T.A., T.G. and D.T.G. curves of kaolinite- and bentonite-cement mixtures using two types of cements are presented in Fig. 3.87 to Fig. 3. 98.

There is no endotherm due to the dehydroxylation of $Ca(OH)_2$ in all D.T.A. curves of kaolinite-cement. This phenomenon can easily be predicted from the result obtained by the X-ray diffraction. However, a faint deflection at about 500° C is found only in D.T.G. curves of the kaolinite-high early strength cement (H.E.S. cement) mixtures at 91 and 182 days of curing (Fig. 3.89). Thus, the amount of calcium hydroxide liberated in the kaolinite-H.E.S. cement mixtures proves to be more than that in kaolinite-moderate heat cement (M.H. cement) mixtures, because any deflection is not detected at about 500° C in D.T.G. curves of kaolinite-M.H. cement mixtures at all. The kaolinite-cement mixtures display two exotherms at about 900° C in their D.T.A. curves. One is due to kaolinite; the other to CSH(gel). This peak due to CSH(gel) appearing at slightly

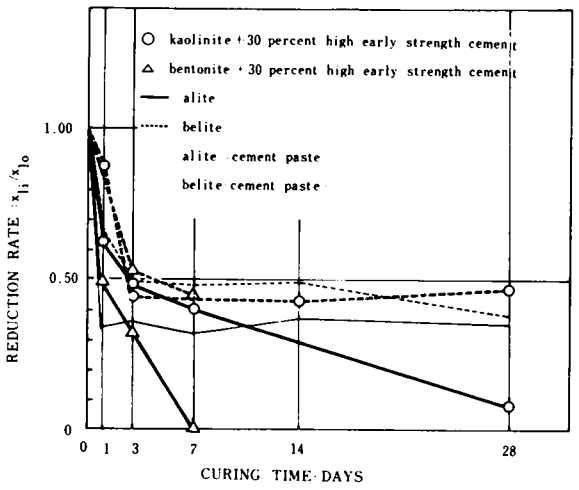

Fig.3.85 Reduction rate in the quantity of alite and belite in kaolinite Ka III and bentonite MB 30% high early strength cement mixtures

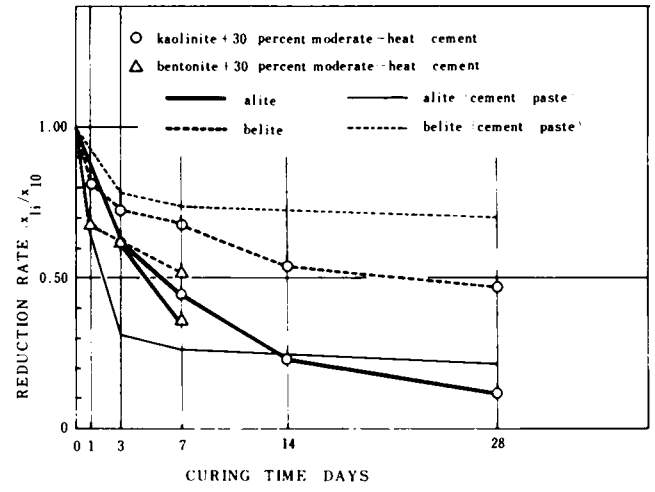

Fig.3.86 Reduction rate in the quantity of alite and belite in kaolinite Ka III and bentonite MB 30% moderate-heat cement mixtures

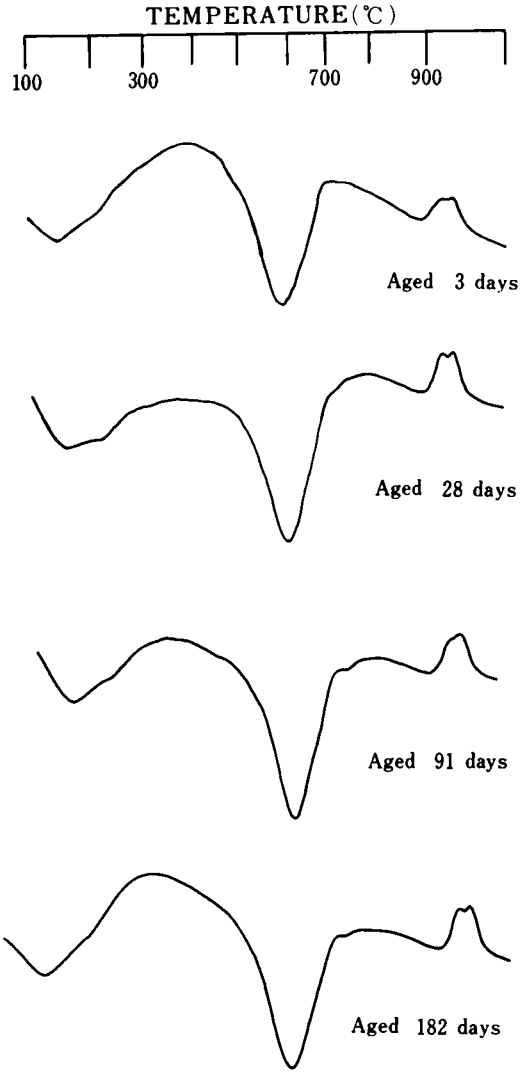

Kaolinte(Ka(III))+30% high early-strength cement

Fig.3.87 D.T.A. curves for kaolinite+30% high-early-strength cement samples cured for 3,28,91 and 182 days

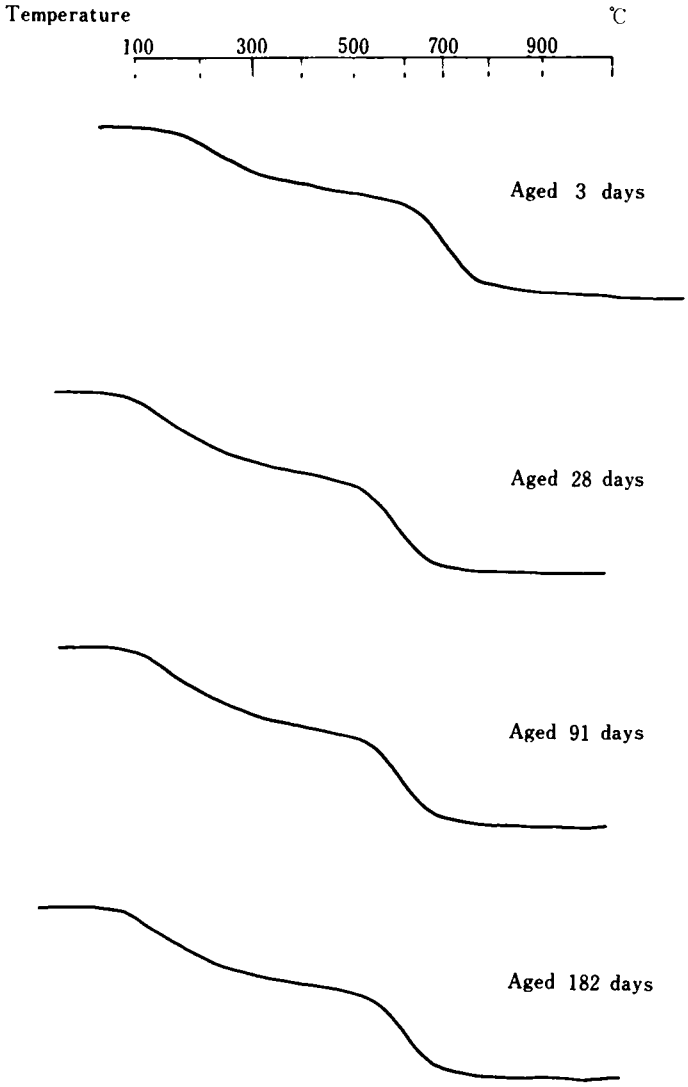

kaolinite(Ka(III))+30% high-early-strength cement

Fig.3.88 T.G.curves for kaolinite+30% high early-strength cement samples cured for 3, 28, 91, and 182 days

lower temperature than the other in the kaolinite(Ka(III))-cement is far greater than that in the kaolinite (Ka(I))-cement (Fig. 3.87, Fig. 3.90, Fig. 3.35). This suggests the formation of a great amount of CSH(gel) in the kaolinite(Ka(III))-cement, which can be attributed to greater quantities of clay fraction included in the Ka(III) than in the Ka(I).

In this respect, the bentonite-cement mixtures present very interesting D.T.A. curves suggesting the changes in lime-silica ratio of calcium silicate hydrates formed with increasing curing time.

The D.T.A. curve of the bentonite-M.H. cement mixtures at 3 days age has a comparatively large exothermic

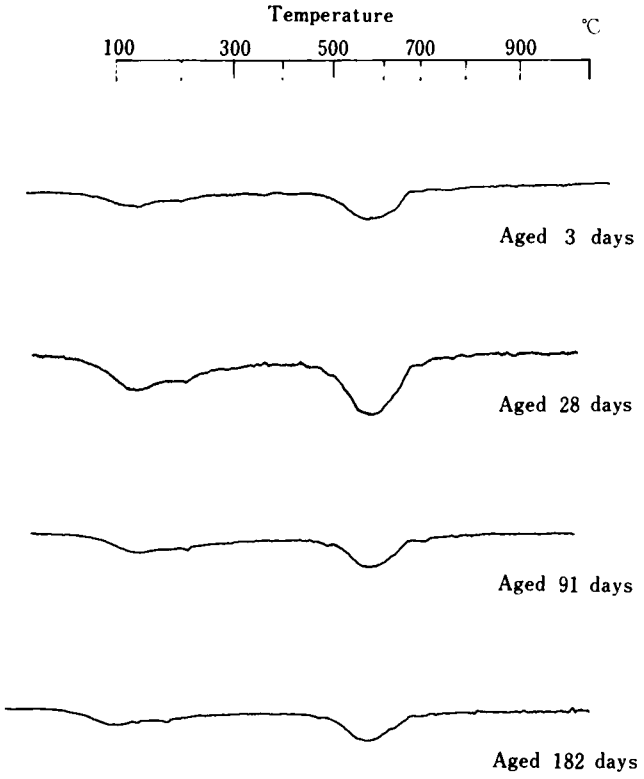

Kaolinite (Ka-III) + 30% high-early strength cement

Fig.3.89 D.T.G. curves for kaolinite + 30% high early strength cement samples cured for 3, 28, 91 and 182 days

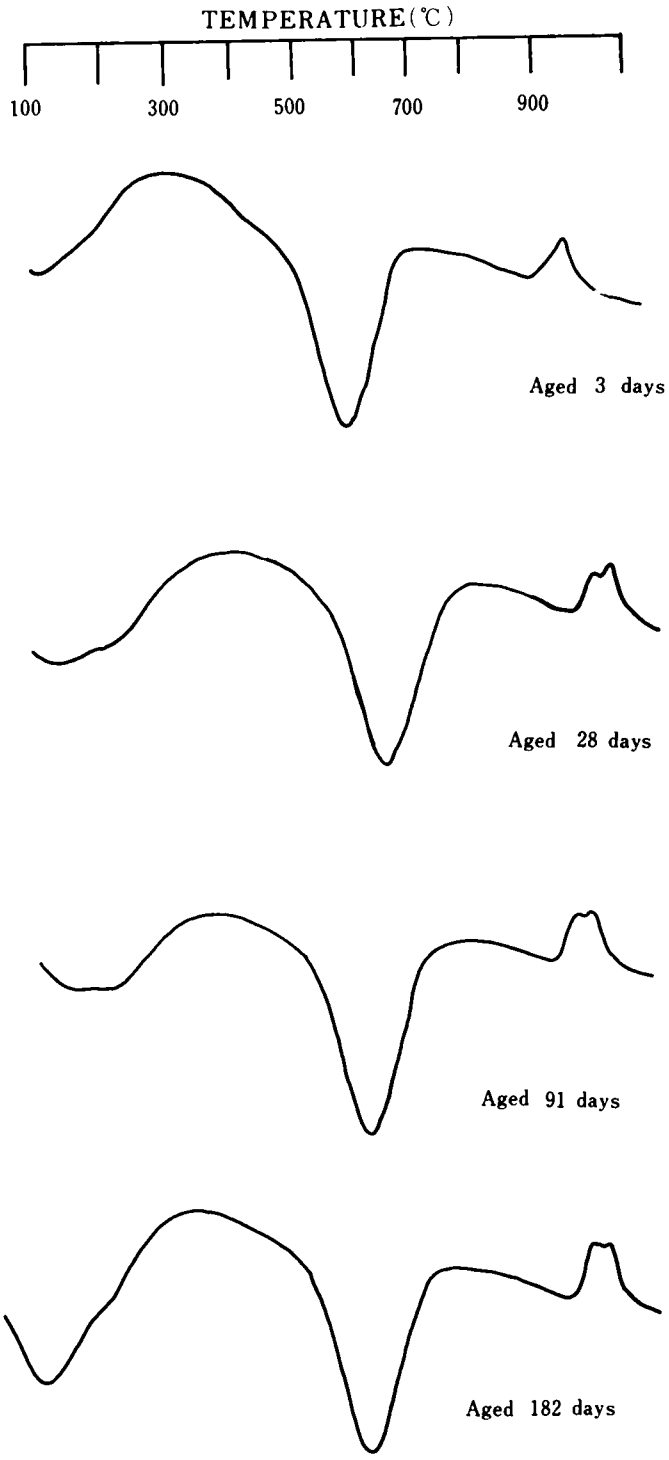

Kaolinite (Ka-III) + 30% moderate heat cement

Fig.3.90 D.T.A. curves for kaolinite + 30% moderate heat cement samples cured for 3, 28, 91 and 182 days

peak at about 900° C, followed by a gradual decrease in its size with curing time (Fig. 3.96). On the other hand, the size of this peak in the bentonite-H.E.S. cement mixture increases during 3 to 28 days of curing (Fig. 3.93). The long-term curing samples (91 and 182 days curing) have no peak at about 900° C in both bentonite-cement mixtures (Fig. 3.93, Fig. 3.96). From these changes in D.T.A. curves accompanying with curing time, the following conclusion can be drawn.

Calcium silicate hydrate with low lime-silica ratio would be produced until 28 days of curing in bentonite-cement mixtures to transform to the one

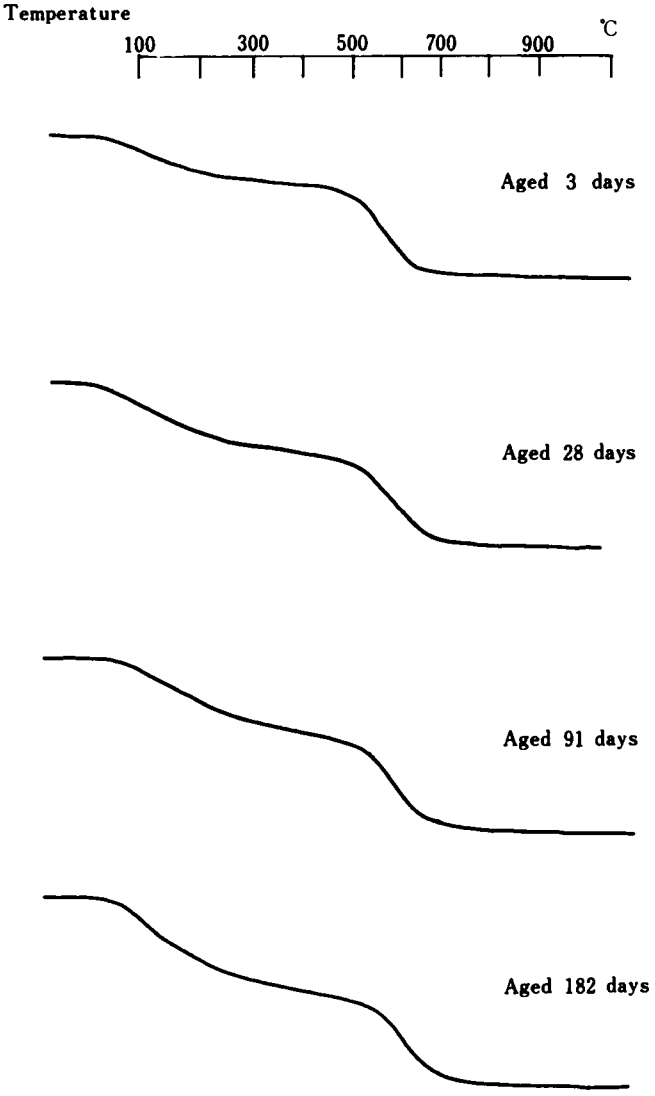

Fig.3.91 T.G. curves for kaolinite+30% moderate-heat cement samples cured for 3,28,91,and 182 days

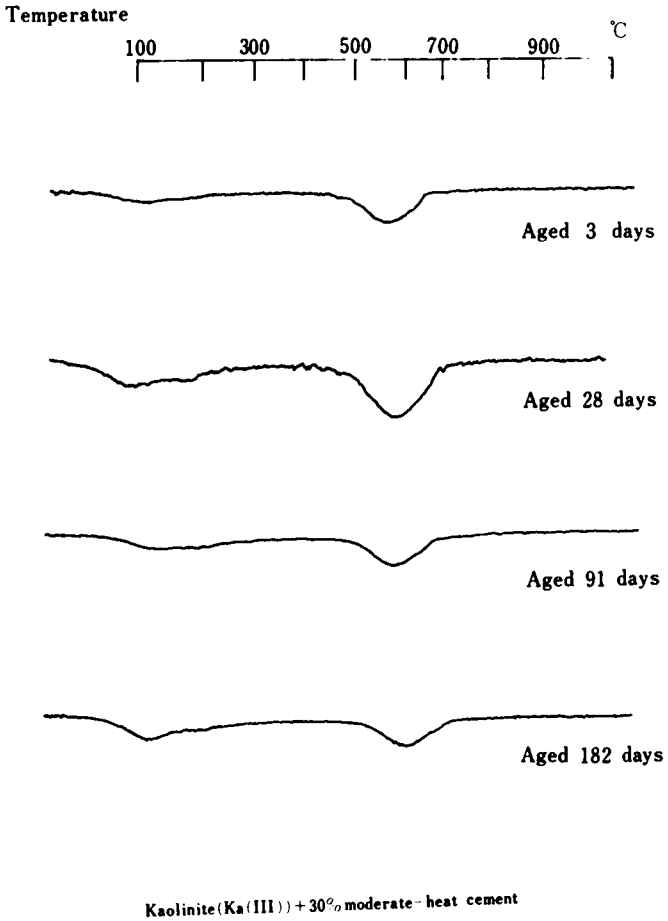

Fig.3.92 D.T.G. curves for kaolinite +30% moderate-heat cement samples cured for 3,28,91 and 182 days

with high lime-silica ratio at least after 91 days of curing, because, according to Kalousek and Prebus(1958), the 0.8 to 1.33 C/S hydrate generally exhibits a strong exothermic effect in D.T.A. at 835°C to 900°C, but the 1.5 to 2.0 C/S one no such exotherm.

(3) pH Test

The pH in kaolinite- and bentonite-cement mixtures using two types of cement of moderate heat and high early strength changes with curing time in the tendency similar to that in these clay minerals-normal cement mixtures as shown in Fig. 3.99 and Fig. 3.100.

The pH of the kaolinite-cement mixtures using high early strength cement is higher than that of the ones with moderate heat cement at all ages.

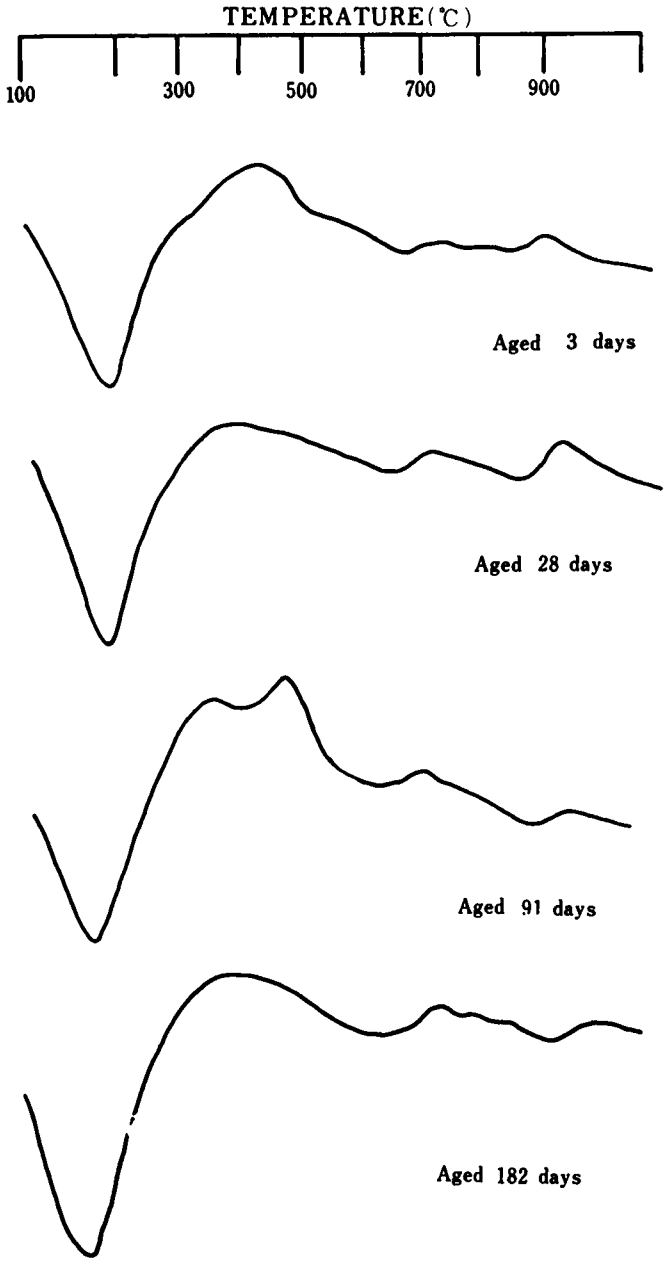

Fig.3.93 D.T.A. curves for bentonite+30% high-early-strength cement samples cured for 3,28,91 and 182 days

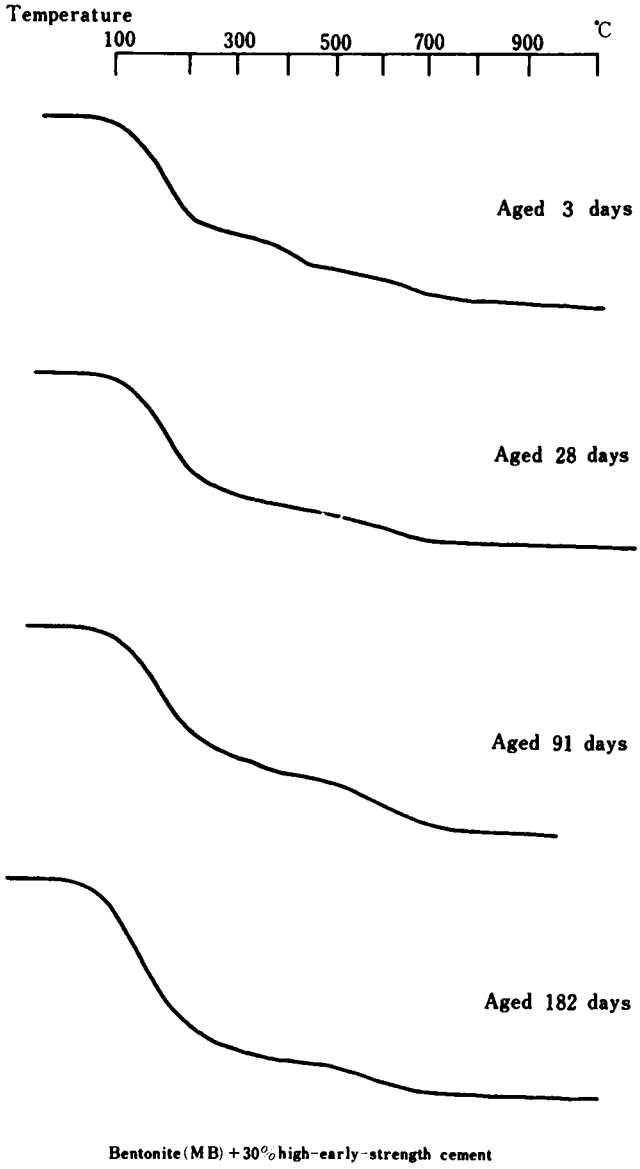

Fig.3.94 T.G. curves for bentonite+30% high-early-strength cement samples cured for 3,28,91 and 182 days

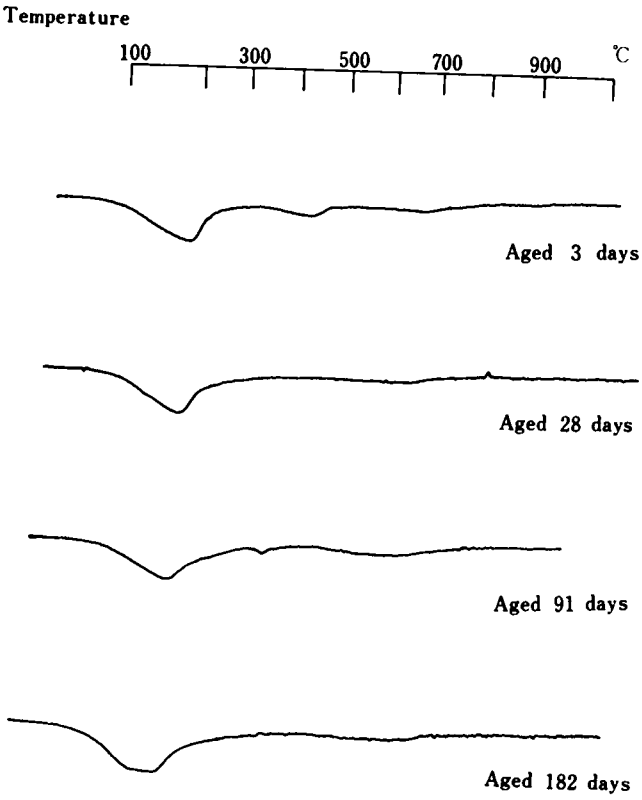

Bentonite(MB)+30% high-early strength cement

Fig.3.95 D.T.G. curves for bentonite+30% high-early-strength cement samples cured for 3, 28, 91 and 182 days

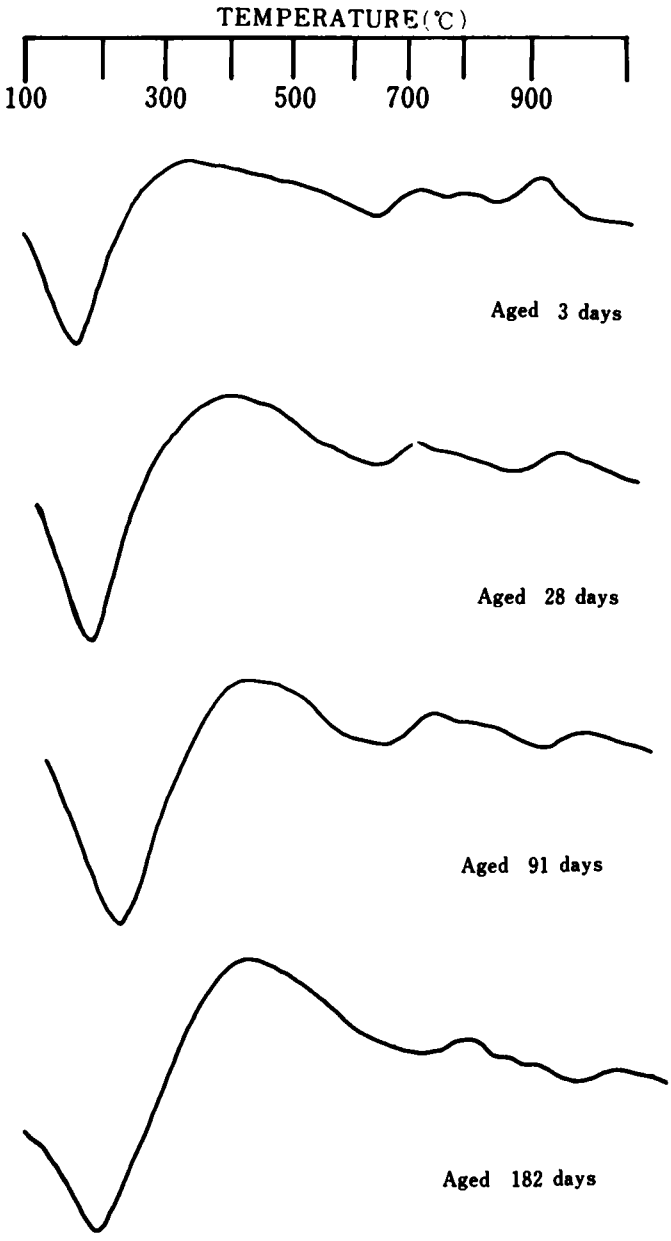

Bentonite(MB)+30% moderate-heat cement

Fig.3.96 D.T.A. curves for bentonite+30% moderate-heat cement samples cured for 3, 28, 91 and 182 days

The rapid reduction in the pH value is found in the bentonite-cement mixtures (Fig. 3.100). The long-term curing (91 and 182 days curing) makes the pH values of the bentonite-M.H. cement mixtures higher than those of the bentonite-H.E.S. cement, although the relationship between both of them at the ages up to 28 days is variable. This phenomena could be interpreted by the presence of a greater amount of anhydrous βC_2S in the bentonite-M.H. cement than in the bentonite-H.E.S. cement. That is to say, hydrolysis of such a greater amount of βC_2S remaining in the bentonite-M.H. cement mixtures at the end of the long-term curing takes place in the course of the preparation of the filtrate for the pH measurement, raising the pH of the mixtures. Lerch and Bogue (1955) described that the amount of lime liberated by hydrolysis of the C_3S and C_3A is greater than that liberated by the other compounds in portland cement, even though the total amount of lime present in the

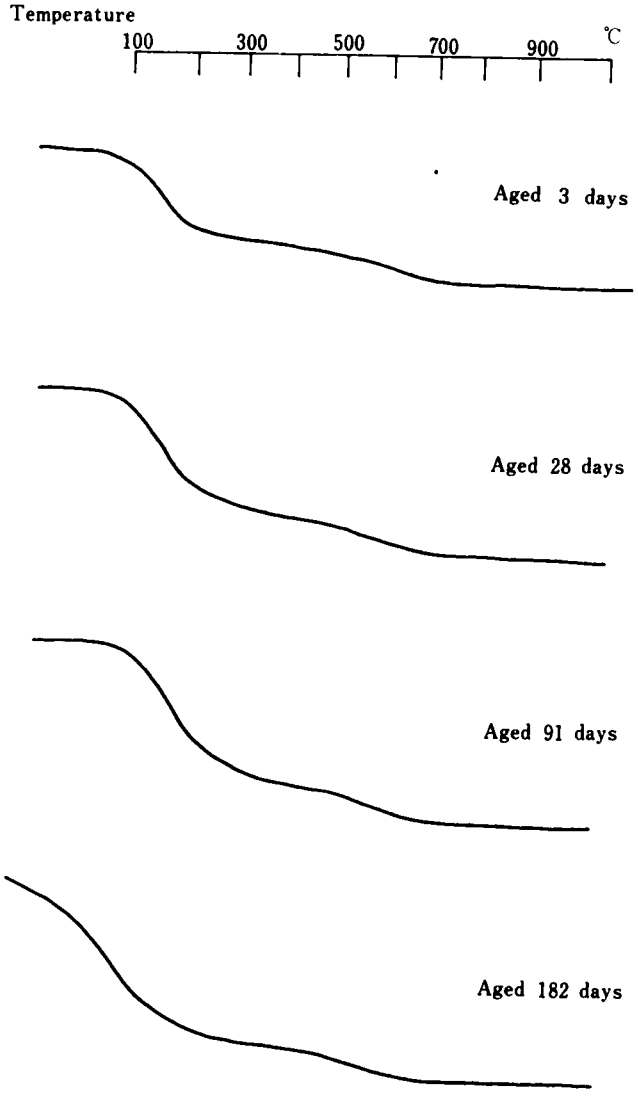

Fig.3.97 T.G. curves for bentonite+30% moderate-heat cement samples cured for 3, 28, 91 and 182 days

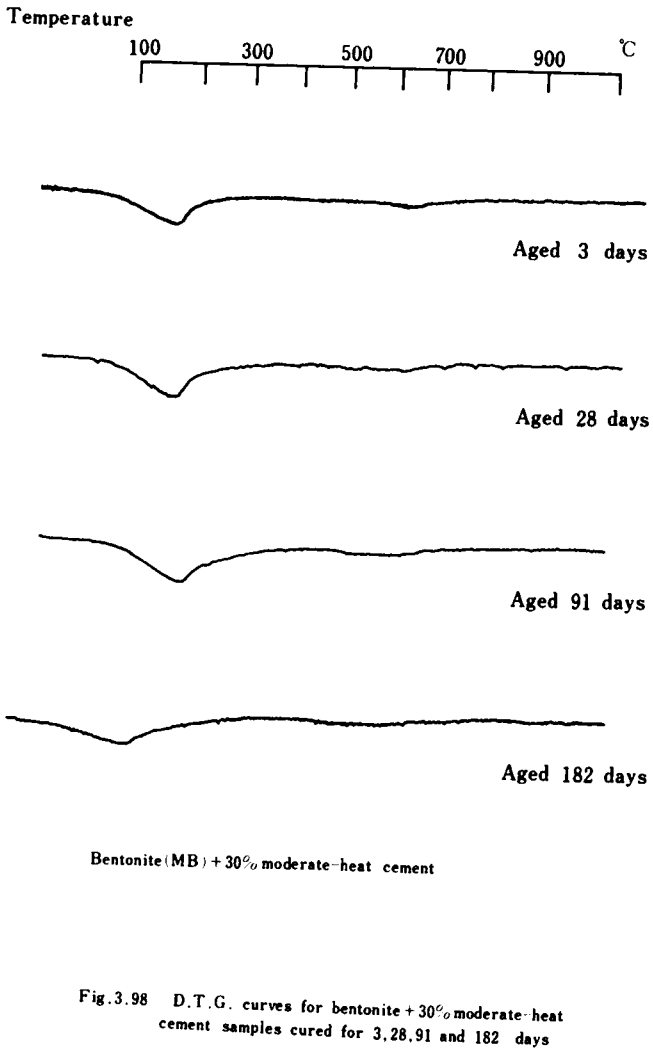

Fig.3.98 D.T.G. curves for bentonite+30% moderate-heat cement samples cured for 3,28,91 and 182 days

system was the same. Therefore, the degree of the effect of compounds in clay mineral-cement mixture on the pH value is great in the order of $Ca(OH)_2$, C_3S and βC_2S, if the $Ca(OH)_2$ exists in a mixture.

The difference between the pH of kaolinite-M.H. and -H.E.S. cement at all ages until 182 days may probably be due to the difference between the amount of $Ca(OH)_2$ present in those mixtures, because the presence of $Ca(OH)_2$ can be detected by the D.T.G. curves only in kaolinite-H.E.S. cement at 91 and 182 days of curing and no difference is seen between the pH of both types of bentonite-cement mixtures cured for less than 28 days, in which no $Ca(OH)_2$ can be detected.

(4) Unconfined Compression Test

The strength increase with curing time in kaolinite(Ka(III))- and bentonite(MB)-cement using two types of cement is shown in Fig. 3.101, Fig. 3.102 and Fig. 3.103 for 30, 20 and 10 percent cement content speci-

mens, respectively. The compressive strength of cement mortar, which is obtained basing on JIS R 5201-1964 is also plotted against each curing time.

As stated in general, the high-early-strength cement mortars exhibit relatively high strength at ages up to 91 days, but thereafter the difference between the strength of high-early-strength and moderate-heat cement decreases with curing time, becoming only a little at the end of 182 days of curing.

Both types of the kaolinite-20 and 30 percent cement mixtures gain strength at greater rate than cement mortars after 28 days of curing. In kaolinite-30 percent cement mixtures, the strength of high-early-strength cement is considerably higher than that of mocerate-heat cement at the ages up to 28 days, but after that there exists only a little difference between their strength.

However, remarkably peculiar tendency is found in the strength development of bentonite-cement mixtures. That is to say, a little or little difference between the compressive strength of bentonite-H.E.S. and -M.H. cement at early curing periods until 28 days is followed by a gradually increasing difference between them. This is the tendency completely reverse to that in the kaolinite-cement and cement mortars.

Since the compressive strength of bentonite-cement greatly depends upon the interaction between bentonite and $Ca(OH)_2$ liberated from hydrating cement, the quantity of $Ca(OH)_2$ available for such interaction should be a significant factor affecting the strength development. Therefore, a relatively less increase in the strength of bentonite-M.H. cement mixtures during the long term curing may be due to the liberation of less $Ca(OH)_2$. The causes for the formation of less $Ca(OH)_2$ in bentonite-M.H. cement are as follows:

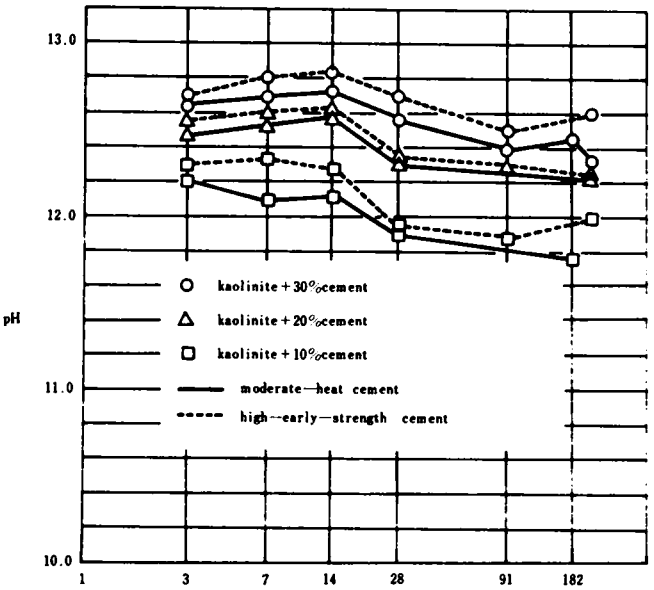

Fig. 3.99 pH changes of kaolinite—cement mixtures with curing time

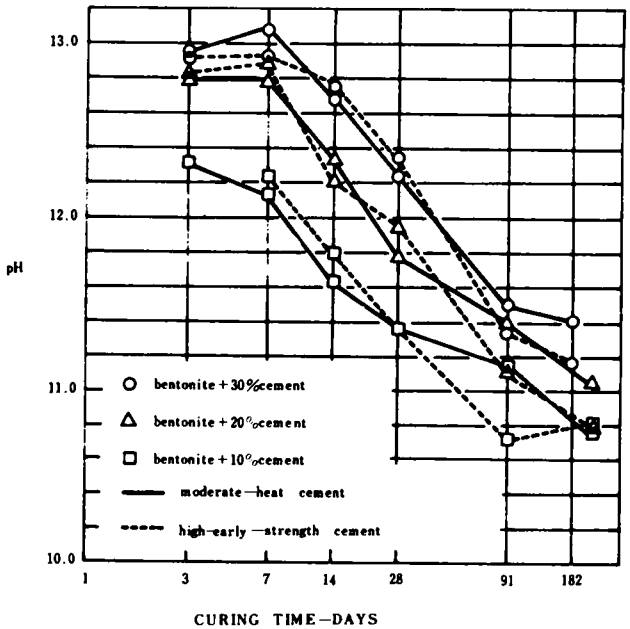

Fig. 3.100 pH changes of bentonite—cement mixtures with curing time

The βC_2S produces much less $Ca(OH)_2$ than C_3S because of the lower Ca/Si ratio of the starting material. Furthermore, much βC_2S remains even after 91 and 182 days, as indicated by the higher pH in bentonite-M.H. cement than in bentonite-H.E.S. cement at these ages.

(5) Summary and Conclusions

The quantitative analysis by X-ray diffraction gives several findings on the rate of hydration of alite and belite in the compacted kaolinite- and bentonite-cement mixtures. Further, other experiments show that the different type of cements have different interactions characteristics with clay minerals.

The results obtained are summarized as follows:

1) In the initial stage of hydration (within 7 days of curing), the rate of the decrease of the quantity of alite with curing time in both kaolinite-high-early-strength and moderate-heat cement is less than in cement paste. However, the quantity of alite in cement paste decreases a little or little after the initial hydration (from 1 to 7 days of curing), while that in kaolinite-cement mixtures continues to decrease gradually with curing time.
2) The hydration of belite in the kaolinite- and bentonite- moderate-heat cement mixtures appears to proceed faster than in cement paste.
3) Within 7 days of curing, the hydration of alite in bentonite-cement takes place more slowly than in cement paste, but the more rapid hydration after 7 days of curing results in the earlier disappearance of the peak at 1.77 Å than in kaolinite-cement mixtures and cement pastes.
4) From the changes in D.T.A. curves accompanying with curing time, it is found that the calcium silicate hydrate with low lime-silica ratio would be produced in bentonite-cement until 28 days of curing, followed by the transformation to the one with high lime-silica ratio at least after 91 days of curing.
5) The long-term curing leads to the greater decrease in pH of the bentonite-high-early-strength cement, while to less decrease in

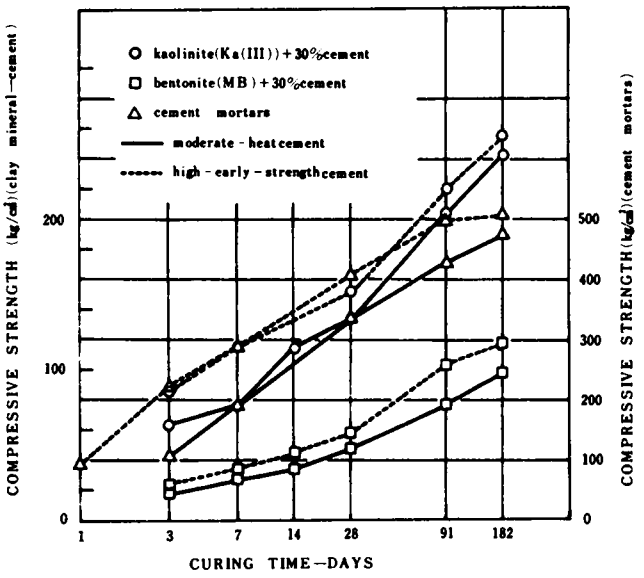

Fig.3.101 Variation in strengtth with curing time

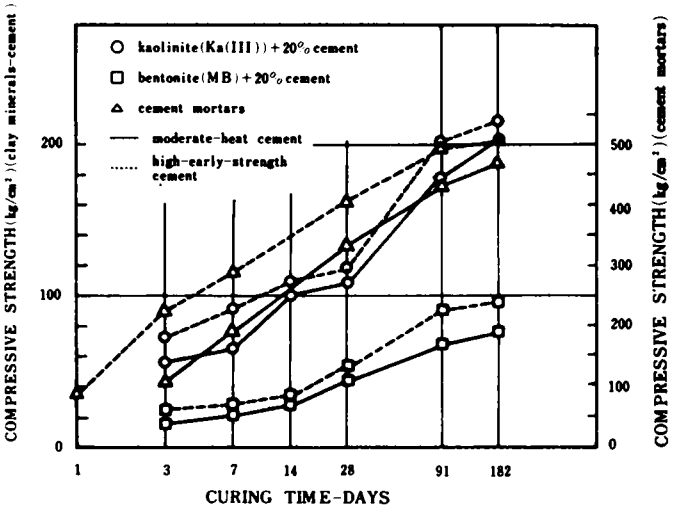

Fig.3.102 Variation in strength with curing time

the bentonite with moderate-heat cement. Consequently, the pH of the former is somewhat less than that of the latter at the end of 182 days of curing.

6) A little or little difference between the compressive strength of bentonite-high-early-strength and -moderate-heat cement at early curing periods until 28 days is followed by a gradually increasing difference between them. This is the tendency completely reverse to that in the kaolinite-cement and cement mortars.

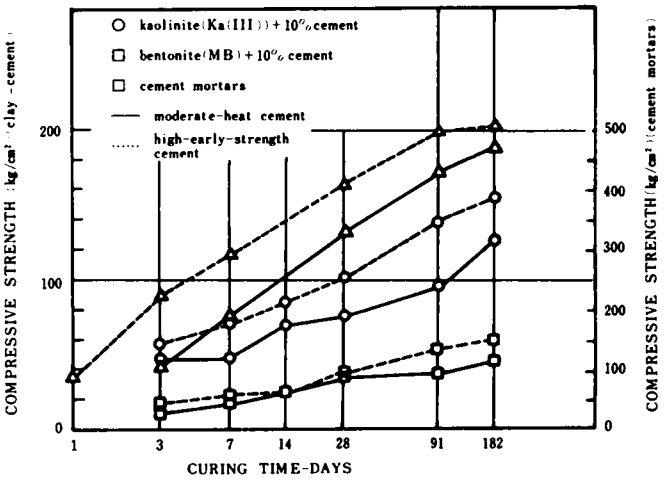

Fig.3.103 Variation in strength with curing time

INFLUENCE OF EXCHANGEABLE CATIONS (Na^+, Mg^{++}, Ca^{++}) HELD ON BENTONITE ON THE BENTONITE-CEMENT INTERACTION

As previously revealed, in clay-cement mixture (especially, montmorillonitic clay-cement mixtures), ion exchange reaction proceeds between montmorillonite and cement hydration products until the montmorillonite is finally saturated with Ca ions as far as sufficient Ca ions are supplied. Therefore, cations held on the original bentonite sample should have a certain effect on the physicochemical process in the clay mineral-hydrating cement interaction.

(1) X-ray Diffraction

The basal spacing of montmorillonite in the Na-bentonite-cement mixture changes with curing time, as shown in Fig. 3.104. The X-ray diffraction experiments were made for the samples with the moisture content equilibrated at room conditions. Such samples were prepared as follows:

The original samples with optimum moisture content (about 40 percent) were dried in a vaccum desiccator at room temperature of about 15°C for about 8 hours and left in a room atmosphere.

As to the relationship between the degree of the calcium saturation of montmorillonite and its basal spacing, Lagulos and Handy (1962) state as follows: "The basal d-spacing of montmorillonite reflects the amount of interlayer water. Previous investigators have reported the tendency for a sodium montmorillonite to retain one layer of water between the mineral sheets when dried under room conditions, and the tendency for calcium montmorillonite to retain two layers. This is essentially true for sample 1 (the percent calcium saturation: 19.4 %) and 5 (the percent calcium saturation: 94.0 %) equilibrated at 50 percent relative humidity, the basal d-spacings being 12.6 Å and 14.9 Å, respectively. Of particular interest is that the intermediate samples show intermediate spacings according to d = 0.031 Ca + 12.0 in which Ca is the percent calcium saturation."

The Na-bentonite sample produced by exchanging Mg^{++} in the Mg-montmorillonite for Na^+ shows its basal reflection at 12.6 Å (see Fig. 3.1). Considerably broad (001) peaks at 7 and 14 days ages, as shown in Fig. 3.104, appear that various peaks ranging that at 12.6 Å to 15 Å overlap one another. This may indicate that montmorillonite in the specimens at 7 and 14 days ages are varied in the degree of the calcium saturation. That is to say, the clay-cement mixtures compacted under a very limited moisture content such as optimum moisture content have an non-homogeneous structure in the respect of the degree of the calcium

saturation, when the diffusion of Ca ions progresses only to an insufficient extent. However, the X-ray diagram of the 28 days age sample has the sharp (001) peak at 15.5 Å, indicating that the complete transformation of the original Na-montmorillonite to the calcium one extends over the interior of the specimens at the end of 28 days curing. Plots of the d-spacings of the (001) peak against curing time are given in Fig. 3.105. The scale of the percent calcium saturation in Fig. 3.105 is noted according to Lagulos and Handy's formula described above.

(2) Unconfined Compression Test

The strength vs. curing time curves for three types of bentonite-cement mixtures are plotted in Fig. 3.106, Fig. 3.107 and Fig. 3.108. The characteristic of the strength gain of bentonite-cement is found to vary with cations held on the original bentonite samples used.

It may be impossible to compare the strength development characteristic of the Ca-bentonite-cement mixtures with other two types of Na- and Mg-bentonite-cement mixtures, because the physical properties and mineral compositions of the Ca-bentonite sample are somewhat different from those of Na- and Mg-bentonite.

The lower compressive strength of Ca-bentonite-cement mixtures may be due to the poorer reactivity in the $Ca(OH)_2$-bentonite interaction and/or to the slower progress in cement hydration in the mixture, as expected from the pH tests results to a certain extent.

The effect of exchangeable magnesium and sodium ions held on the bentonite on the strength development may obviously be characterized by the relationship between the cement content and strength at 91 days age; the compressive strength of the Mg-bentonite-30% cement mixtures at 91 days age is markedly greater than that of the Na-bentonite-30% cement

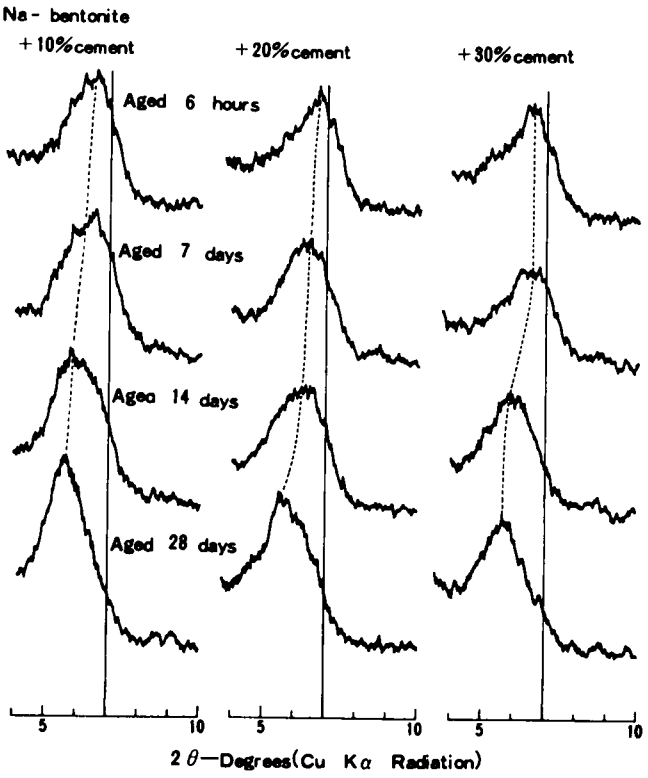

Fig. 3.104 (001)peaks for Na—bentonite+30 20 and 10% cement samples cured for 6 hours, 7, 14 and 28 days

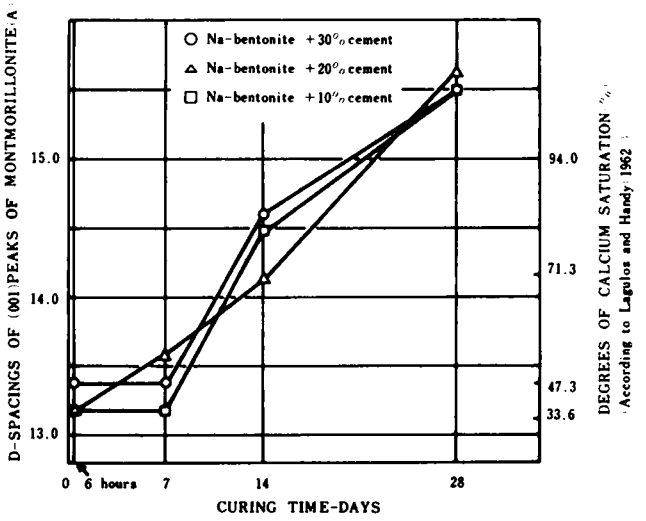

Fig. 3.105 Changes in d-spacings of (001) peaks of montmorillonite in Na-bentonite+30%, 20% and 10% cement samples with curing time

mixture; on adding 20 percent cement, there is a little difference between them; contrary to 30% cement content specimens, the addition of 10 percent cement gives the Na-bentonite-cement greater strength than the magnesium one (Fig. 3.106, Fig. 3.107 and Fig. 3.108). Such greater strength of the Na-bentonite-cement mixtures at the low cement content may be due to the effect of the coarsened clay grains produced as a result of the cation exchange treatment. Since such "new" grains may be capable of withstanding mechanical dispersion to a certain extent, they should behave themselves like silt particles. As cement hydration proceeds, sodium and magnesium ions originally retained on the bentonite must be exchanged by calcium ions. Especially, it is evidenced by the X-ray diffraction test that the Na-montmorillonite in the Na-bentonite-cement is almost completely changed to the Ca-montmorillonite during the 28 days curing (Fig. 3.104). Thus, the amount of $Ca(OH)_2$ consumed by the cation exchange and the behavior of sodium or magnesium ions substituted by calcium ions should greatly affect the strength development of the bentonite-cement mixtures. As to the former, more $Ca(OH)_2$ certainly seem to be consumed in sodium-bentonite-cement than in magnesium-bentonite-cement, because the replacing power of the common ions is Li < Na < NH_4 < K < Mg < Rb < Ca < Co < Al (Gedroiz, 1922). Concerning the latter, the possibility of the substitution of silicon by magnesium in the tobermorite lattice could be expected. Such an effect of Mg ions would favor the strength of the bentonite-cement. In this respect, it is much interesting to note the following statement for the reaction in the $Ca(OH)_2$-MgO-bentonite system: "A possibility is that large amounts of magnesium ions have entered

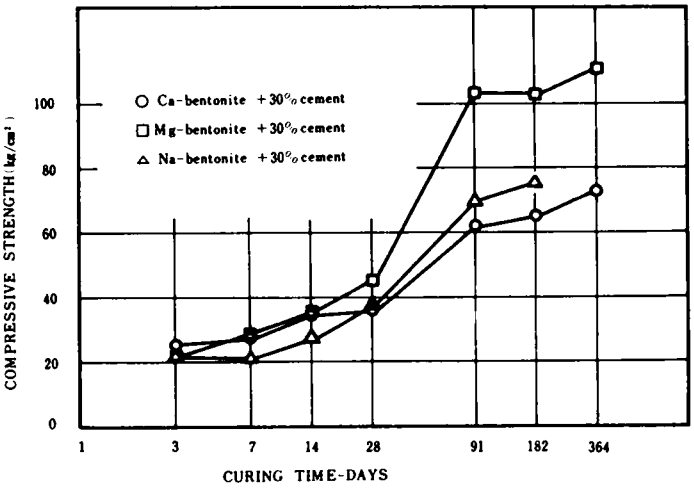

Fig.3.106 Variation of compressive strength with curing time in Na-, Mg- and Ca-bentonite+30% cement mixture

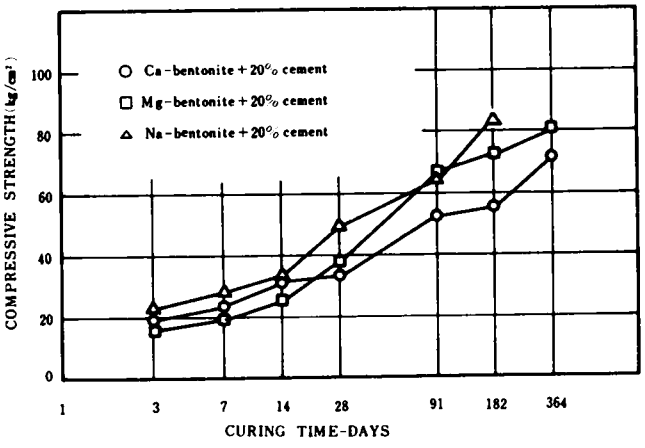

Fig.3.107 Variation of compressive strength with curing time in Na-,Mg- and Ca-bentonite+20% cement mixture

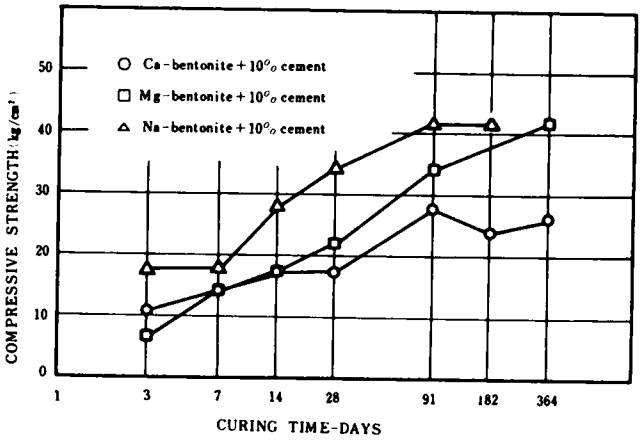

Fig.3.108 Variation of compressive strength with curing time in Na-,Mg- and Ca-bentonite+10% cement mixture

the tobermorite structure and thus made more calcium ions available for further pozzolanic reactions." (Wang and Handy, 1966) A great difference in the strength between the Na- and Mg-bentonite-cement mixtures at 91 days age could be explained by two effects described above.

All Na-bentonite-cement specimens gain strength even before 28 days curing. This strength development appears to contradict with the concept of retention point, since, before 28 days curing, montmorillonite in the Na-bentonite-cement mixtures is considered not to attain a retention point beyond which further $Ca(OH)_2$ liberated is consumed by the pozzolanic reaction contributing to strength gain. However, as stated in the X-ray diffraction results, the degree of the calcium saturation of montmorillonite in the Na-bentonite-cement specimens at 3, 7 and 14 days ages is non-homogeneous through over the interior of the specimens. Therefore, even at the ages until 28 days, a part of the montmorillonite in the Na-bentonite-cement may participate in the pozzolanic reaction with $Ca(OH)_2$ through the calcium saturation and subsequent attainment of a retention point. Naturally, calcium silicate hydrate resulting from cement hydration also serves the strength development.

(3) pH Tests

Fig. 3.109 shows pH changes of Ca-, Mg- and Na-bentonite-cement mixture with curing time. The pH values of the Ca-bentonite-cement mixtures for every cement contents are greater than the comparable ones of the Mg- and Na-bentonite-cement mixtures, more slowly decreasing with curing time. Such higher pH values in the Ca-bentonite-cement mixtures are due to the poorer reactivity in the $Ca(OH)_2$-bentonite interaction and /or to the slower progress in the cement hydration in the mixture. Such differences between the Ca-bentonite-cement and other two mixtures would be responsible for the effect of the crystallinity of montmorillonite and non-clay minerals included in the bentonite samples rather than for the effect of the exchangeable cations held.

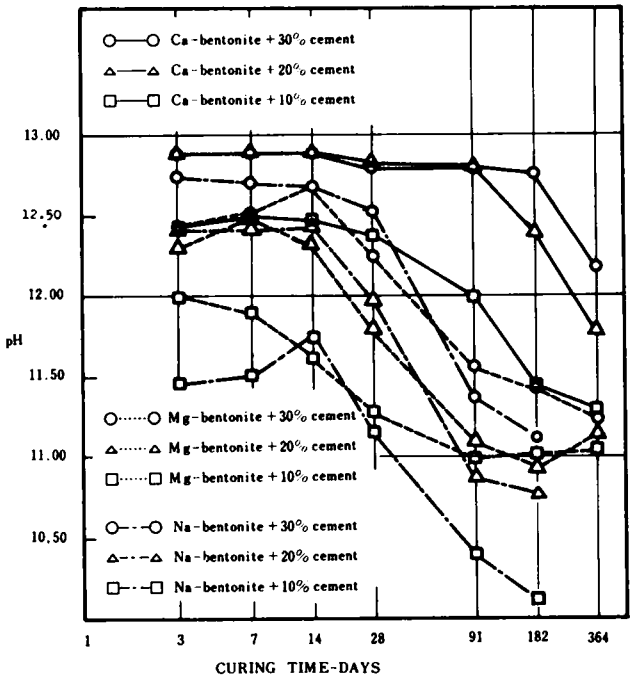

Fig.3.109 pH changes of Ca-,Mg- and Na-bentonite-cement mixture with curing time

(4) Differential Thermal Analysis

Fig. 3.110 and Fig. 3.111 show the D.T.A. curves of the Ca- and Na-bentonite-cement mixtures at various ages, respectively.

The changes of the peak at about 900° C with curing time in the Ca- and Na-bentonite-cement mixtures are different from those of the Mg-bentonite-cement mixtures (Fig. 3.93 and Fig. 3.96). That is to say, the former has a large exothermic peak at about 900° C in the D.T.A. curves at all ages. On the other hand, the latter mixtures at the end of 91 and 182 days curing, as previously described, exhibit no such a large peak found in those at 3 and 28 days ages. Concerning the calcium silicate hydrate synthesized in the laboratory, Kalousek and Prebus (1958) stated as follows : "The 1.5 C/S sample showed a rounded exothermic peak between 880° and 910° C in differential thermal analysis, but the 1.75 C/S product exhibited no

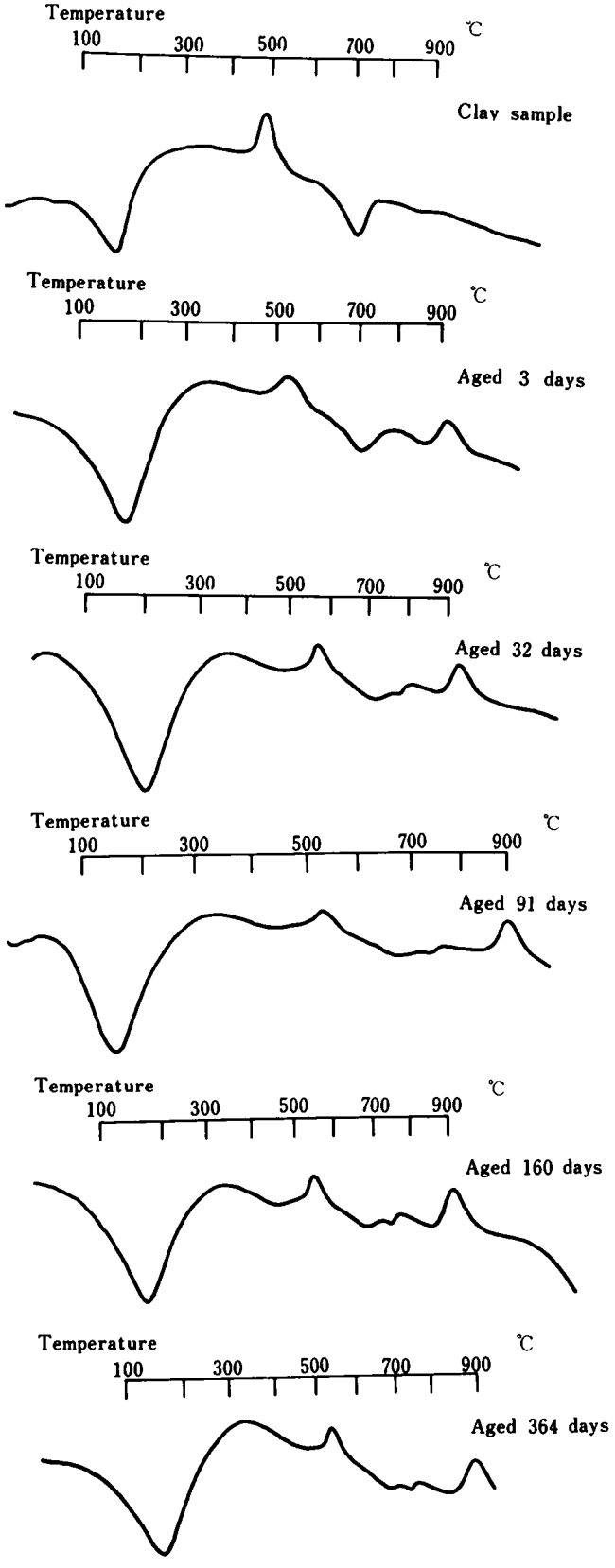

Ca-Bentonite + 30% Cement

Fig. 3.110 D.T.A. curves for Ca-bentonite + 30% samples cured for 3, 32, 91, 160 and 364 days

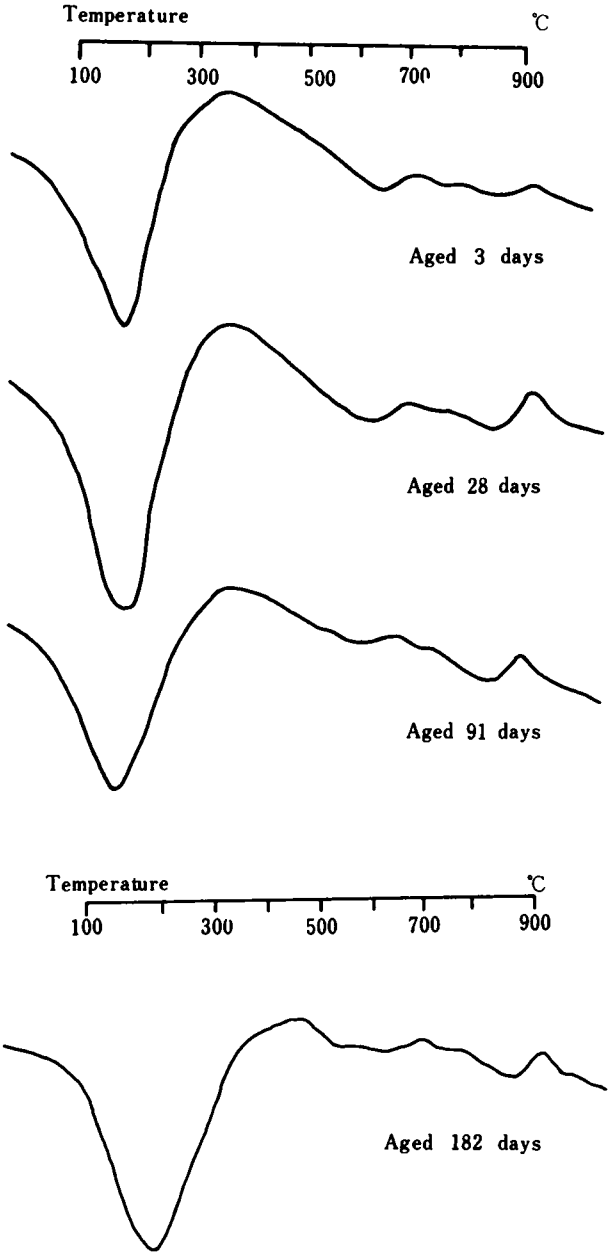

Na-bentonite + 30% cement

Fig.3.111 D.T.A. curves for Na-bentonite + 30% cement sample cured for 3, 28 and 91 days

such thermal change." Thus, the calcium silicate hydrate produced in the bentonite-cement mixtures at the initial stage of curing (until 28 days) is of the low lime-silica ratio. However, the calcium silicate hydrate with low lime content produced at the initial ages in the Mg-bentonite-cement changes to the high lime one during the long-term curing; that in the Ca- and Na-bentonite-cement mixtures remains the low lime content one even at the end of the long-term curing. Since, in the Na-bentonite-cement, a comparatively large amount of lime is consumed by the cation exchange reaction in the initial stage of curing, the amount of lime available for pozzolanic reactions occuring during the long-term curing would not be enough to convert the low lime-CSH(gel) to the high lime one.

The formation of the low lime product in the Ca-bentonite-cement mixture can not be interpreted by the effect of the exchangeable cation (Ca^{++}). This mixture may be lacking in free lime compared with the Mg-bentonite-cement, because of the suppression of the cement hydration.

It should bear in mind that the substitution of silicon by magnesium in the tobermorite lattice takes part in the formation of the high lime-CSH(gel) by the pozzolanic reaction occuring over the long-term. Furthermore, special attention should be paid to the fact that the long-term strength of the Mg-bentonite-cement mixtures with the high lime-silica ratio-CSH(gel) is far greater than that of the Na- and Ca-bentonite-cement with the low lime-silica ratio one.

(5) Summary and Conclusions

The physicochemical reaction processes in the Mg-bentonite-cement interaction are remarkably different from those in the Na-bentonite-cement interaction. Especially, the compressive strength of the Mg-bentonite-30% cement mixtures at 91 days age is markedly greater than that of the Na-bentonite-30% cement mixtures. Such differences may be attributed to the lime-silica ratio of CSH(gel) formed in the mixtures. The exchangeable cations (Na^{+}, Mg^{++}) held on the original bentonite greatly affect the physicochemical pro cesses in the cement hydration and subsequent pozzolanic reactions, CSH(gel) having different lime-silica ratios being formed according to the exchangeable cations.

The results obtained are summarized as follows:

1) Clay-cement mixtures compacted under a very limited moisture content such as optimum moisture content have an non-homogeneous structure in the respect of the degree of the calcium saturation, when the diffusion of Ca ions progresses only to an insufficient extent. The X-ray diagram of the 28 days age sample has the sharp (001) peak at 15.5 Å, indicating that the complete transformation of the original Na-montmorillonite to the calcium one extends over the interior of the specimens at the end of 28 days of curing.
2) The behavior of sodium or magnesium ions substituted by calcium ions should greatly affect the strength development of the bentonite-cement mixtures. In this respect, the possibility of the substitution of silicon by magnesium in the tobermorite lattice could be expected. Such an effect of Mg ions would favor the strength of the bentonite-cement.
3) Higher pH values in the Ca-bentonite-cement mixtures are considered to be due to the poorer reactivity in the $Ca(OH)_2$-bentonite interaction and/or to the slower progress in the cement hydration in the Ca-bentonite-cement mixtures.
4) The Ca- and Na-bentonite-cement mixtures have a large exothermic peak at about 900° C in their D.T.A. curves at all ages. On the other hand, the D.T.A. curves of the Mg-bentonite-cement mixtures exihibit no such a large peak found in those at 3 and 28 days ages. The calcium silicate hydrate produced in the bentonite-cement mixtures at the initial stage of curing is found to be of the low lime-silica ratio.

However, such a calcium silicate hydrate changes to the high lime one during the long-term curing in the Mg-bentonite-cement; that in the Ca- and Na-bentonite-cement mixtures remains the low lime content one even at the end of the long-term curing.

7. SUMMARY AND CONCLUSIONS

In this chapter, four subjects concerning the clay minerals-portland cement interaction were experimentally discussed. It was elucidated that the interaction between the clay minerals and cement hydration products plays an important role in the formation of the microcopic structure of clay mineral-cement mixtures, and further, in their strength development. Consequently, the factors which affect the physicochemical process of the clay mineral-cement interaction are as follows: a) Species of clay minerals, b) Degree of crystallinity of clay minerals, c) Grain sizes of clay minerals samples used, and species and quantity of non-clay minerals included in the samples, d) Exchangeable cations (Na^{+}, Ca^{++}, Mg^{++}) held on the original clay minerals, e) Compound compositions of portland cement.

Tremendously complex phenomena may take place because of the mutual interference of these factors. Furthermore, the relationship between the physicochemical phenomena and strength of the compacted clay-cement mixtures is far more complex. In this respect, it is interesting to note the fact that the substances from which the strength originates are varied according to the species of clay minerals used. The strength of kaolinite-cement mixtures seems to be developed by both the calcium aluminate hydrate and calciun silicate hydrate; that of bentonite-cement is almost indebted to a great amount of CSH(gel) produced. Especially, it is very interesting new finding that the lime-silica ratio of the CSH(gel) formed in the bentonite-cement specimens cured for the long-term varies with the exchangeable cations held on the original bentonite, greatly affecting their strength. In chlorite-vermiculite mixed-layer mineral-cement, the strength increase by the long-term curing after 182 days age is remarkable. However, it is difficult, from various experimental results, to suppose that such a strength increase is responsible for CSH(gel) resulting from a usual pozzolanic reaction. Magnesia constituting this mineral probably takes part in the great strength gain at the long-term ages. In fact, several X-ray diffraction peaks suggesting the formation of a magnesium silicate hydrate are detected.

In general, it is certain that the pozzolanic reaction between clay minerals and $Ca(OH)_2$ resulting from cement hydration plays a significant role in clay minerals-cement mixtures. However, this study reveals that the reaction products in clay minerals-cement mixtures are considerably different from those in clay minerals-$Ca(OH)_2$ ones. For example, no hillebrandite which is formed in kaolinite-$Ca(OH)_2$ mixtures can be confirmed in kaolinite-cement mixtures. Such a difference between them may be attributed to the nature of reactions occuring in both systems. That is to say, in the former system, the hydration of cement and $Ca(OH)_2$-clay minerals interaction take place interacting each other; the latter includes only a reaction process of the more simplified system, i.e., $Ca(OH)_2$-clay minerals system.

REFERENCES

Ariizumi, A. (1967): "Reaction of Hydrated Lime with Clay Minerals in Soil Stabilization", Jour. of the Clay Science Society of Japan (in Japanese), Vol. 6, No. 2, 3 pp. 74 - 80.

Ariizumi, A. and Iwai, T. (1969): "Utilization of Halloysite as a Strength - Improving Agent for Concrete", Proc. Int. Clay Conf. Vol. 1, Tokyo, pp. 835 - 841.

Arnould, F. (1967a): "La Tobermorite: Partie Principale de la Pate de Ciment Portland", Le Genie Civil-

T. 144 - N 1 -Janvier, pp. 51 - 58.

Arnould, F. (1967b): "Questions Relatives à la "Tobermorite" et Théorie des "Pseudo-Solides" ", Le Génie Civil T. 144 - N 6, Juin, pp. 485 -495.

ASTM (1968): "Inorganic Index to the Powder Diffraction File" ASTM Publication PD 1s - 18i

Bezruk, V.M. (1950): "Soil-Cement Mixes - A New Structural Material" Dorizdat, Gushosdor-MVD-USSR, Moscow, pp. 143 - 172

Bogue, R.H. (1955): "The Chemistry of Portland Cement" 2nd Ed., New York, Reinhold.

Brindley, G.W. (1965): "Discussions and Recommendations concerning the Nomenclature of Clay Minerals and Related Phyllosilicates" Clay and Clay Minerals, Proc. Natl. Conf. Clays and Clay Minerals Vol. 14, pp. 27 - 34,

Brunauer, S., Kantro, D.L., and Weise, C.H. (1959): "The Surface Energy of Tobermorite", Canadian Journal of Chemistry, Vol. 37, pp. 714 - 724

Cement Association of Japan (1968): Proc. 5th Int. Symp. Chemistry of Cements, 4 vols,

Chatterji, S. and Jeffery, J.M. (1966): "Three Dimensional Arrangement of Hydration Products in Set Cement Paste", Nature Vol. 19, pp. 1233 - 1234,

Copeland, L.E., Kantro, D.L. and Verbeck, G. (1960): "Chemistry of Hydration of Portland Cement", Nat. Bur. Std. Monograph, 43, Vol. 1, pp.429 - 465

Croft, J.B. (1967): "The Influence of Soil Mineralogical Composition on Cement Stabilization", Geotechnique Vol. 17, No. 2, pp. 119 - 135

Deer, W.A., Howie, R.A. and Zussman, J. (1963): "Rock Forming Minerals", Wiley, New York, N.Y., 5 vol. 1125 pp.

Diamond, S. (1963): "Tobermorite and Tobermorite-Like Calcium Silicates Hydrates: Their Properties and Relation to Clay Minerals", Ph. D. thesis, Purdue Univ. Lafayette, Indiana

Diamond, S. and Kinter, E.B. (1966): "Mechanisms of Soil-Lime Stabilization - An Interpretive Review", Highway Research Record No. 92, pp. 83 - 92

Eades, J.L. and Grim, R.E. (1959): "Reaction of Hydrated Lime with Pure Clay Minerals in Soil Stabilization", H.R.B. Bull. 262, pp. 51 - 63

Farran, J. (1956): "Contribution Minéralogique à l'Etude de l'Adhérence entre les Constituants Hydratés des Ciments et les Matériaux enrobés", Revue des Matériaux de Construction, N 490 - 491, p. 155

Fujii, K. (1952): "$Ca(OH)_2$ Produced Accompanying with Hardening of Portland Cement", Proc. Japan Cement Engineering Association (in Japanese), Vol. 6, pp. 167 - 173

Gard, J.A., Howison, J.W. and Taylor, H.F.W. (1959): "Synthetic Compounds Related to Tobermorite: an Electronmicroscope, X-ray, and Dehydration Study", Magazine of Concrete Research Vol. 11, pp. 151 - 158

Geodroiz, K. (1922): "On the Absorptive Power of Soils", Translated by S. Waksman and Distributed by U.S. Department of Agriculture

Green, K.T. (1962): "Chemistry of Hydration of Portland Cement",Chemistry of Cement, Nat. Bur. Std. Monograph 43 - Vol. 1, pp. 359 - 374

Gillot, J.E. and Sereda, P.J. (1966): "Strain in Crystals Detected by X-ray", Nature Vol. 209, No. 5018, pp. 34 - 36, Jan.

Gillot, J.E. (1968): "Clay in Engineering Geology", Elsevier

Glenn, G.R. (1963): "X-ray Studies of Lime-Bentonite Reaction Products", Ph. D. thesis, Iowa State Univ., Ames, Iowa

Grim, R.E. (1968): "Clay Mineralogy", McGraw-Hill 2 nd ed.

Handy, R.L. (1956): "Stabilization of Iowa Loess with Portland Cement" Unpublished Ph. D. thesis, Iowa State College Library, Ames.

Handy, R.L. (1958): "Cementation of Soil Minerals with Portland Cement or Alkalis", H.R.B. Bull. 198, pp. 55 - 64

Handy, R.L., Demirel, T. Ho, C., Nady, R.M. and Ruff, C.G. (1965): "Mechanisms of Soil-Lime Stabilization Discussion", Highway Research Record No. 92, pp. 96 - 98

Herzog, A. and Mitchell, J.K. (1962): "X-ray Evidence for Cement-Clay Interaction", Nature 195, pp. 989 - 990

Herzog, A. and Mitchell, J.K. (1963): "Reactions Accompanying Stabilization of Clay with Cement", Highway Research Record No. 36, pp. 146 - 171

Ho, C. and Handy, R.L. (1963): "Characteristics of Lime Retention by Montmorillonite Clays", Highway Research Record No. 29, pp. 55 - 69

Ingles, O.G. and Frydman, S. (1966): "The Effect of Cement Lime on the Strength of Some Soil Minerals, and Its Relevance to the Stabilization of Australian Soils", Procs. of the Third Conference of the Australian Road Research Board Vol. 3 Part 2, pp. 1504 - 1528

EL Jack, S.A. (1965): "A Study of Cement-Clay Interaction" Ph. D. thesis, University of Califormia, Berkeley

Jambor, I.J. (1963): "Relation between Phase Composition, Over-All Porosity and Strength of Hardened Lime -Pozzolana Pastes" Magazine of Concrete Research Vol. 15, No. 45, pp. 131 - 142

Jong, J.G.M., Stein, H.N. and Stevels, J.M. (1968): "Influence of Aluminium Hydroxide and Lime on the Hydration of Tricalcium Silicate", Jour. Applied Chemistry Vol. 18 No. 1, pp. 9 - 17, Jan.

Kalousek, G.L. and Prebus, A.F. (1958): "Crystal Chemistry of Hydrous Calcium Silicates: III, Morphology and Other Properties of Tobermorite and Related Phases", Jour. of the American Ceramic Society Vol. 41, No. 4, pp. 124 - 132

Kantro, D.L., Weise, C.H., Brunauer, S. and Copeland, L.E. (1964): "Determination of the Major Compound Contents of Portland Cements by X-ray Diffraction", S.C.I. Monograph No. 18, pp. 346 - 349

Kawamura, M., Hasaba, S., Nakano, H. and Sugiura, S. (1969): "A Role of the Interaction of Clay Minerals with Portland Cement in Soil-Cement Mixture", Transactions of the Japan Society of Civil Engineers Vol. 1, Part 2, pp.

Kawamura, M., Hasaba, S. and Sugiura, S. (1970a): "A Function of Free Lime and Characteristics of Cement Hydration in Compacted Clay-Cement Mixtures", in the course of preparation

Kawamura, M., Hasaba, S. and Sugiura, S. (1970b): "The Influence of Exchangeable Cations (Na^{+}, Mg^{++}, Ca^{++}) Held on Bentonite on the Bentonite-Cement Interaction", in the course of preparation

Laguros, J.G. and Handy, R.L. (1962): "Effect of Exchangeable Calcium on Montmorillonite Low-Temperature Endotherm and Basal Spacing", H.R.B. Bull. 349, pp. 51 - 58

Lerch and Bogue, R.H. (1955): "The Chemistry of Portland Cement", 2nd Ed., New York, Reinhold.

Lipowski, L. (1968): "Physikochemishe Ersheinungen beim Erhärten von Zement-Lehm-Gemischen", Zement-Kalk-Gips, Nr, 11 pp. 476 - 483

Marshall, C.E. (1964): "The Physical Chemistry and Mineralogy of Soils", John Wiley and Sons, New York

Mitchell, J.K. and Jack, S.A.E. (1966): "The Fabric of Soil-Cement and its Formation", Proc. the 14th Natio. Conf. on Clay and Clay Minerals, pp. 279 - 305, Pergamon Press

Moh, Z.C. (1962): "Soil Stabilization with Cement and Sodium Additives", Proc. of A.S.C.E., Jour. Soil Mechanics and Foundation Div., 88, pp. 81 - 105

Moh, Z.C. (1965): "Reactions of Soil Minerals with Cement and Chemicals", Highway Research Record No. 86, pp. 39 - 61

Noble, D.F. (1967): "Reactions and Strength Development in Portland Cement-Clay Mixtures", Highway Research Record No. 198, pp. 39 - 56

Noble, D.F. and Ozol, N.A. (1968): "Use of Retarders with Cement Treated Soils" Interim Report No. 2, Virginia Highway Research Council, pp. 13

Powers, T.C. and Brownyard, T.L. (1947): "Studies of the Physical Properties of Hardened Cement Paste", Proc. A.C.I. Vol. 43, pp. 101 - 132, pp. 249 - 336, pp. 469 - 504, pp. 549 - 602, pp. 669 - 712, pp. 845 - 880

Powers, T.C. (1960): "Properties of Cement Paste and Concrete", Proc. 4th Intern. Symp., Washington, p. 557

Richartz, W. and Locher, F.W. (1965): "Ein Beitrag zur Morphologie und Wasserbindung von Calciumsilicathydraten und zum Gefüge des Zement Steins", Zement-Kalk-Gips, Heft 9, pp. 449 - 459, Sept.

Royer, L. (1954): "De l'Épitaxie; Quuelques Remarques sur les Problèms Qu'elle Soulève", Bulletin de la Société Francaise de Mineralogie, T. 77, p. 1004

Sierra, R. (1968): "Étude au Microscope Électroni ue de L'Hydratation des Silicates Calciques du Ciment Portland", Jour. de Microscopie Vol. 7, n 4 - pp. 491 - 508

Sloan, R.S. (1964): "Early Reaction Determination in two Hydroxide-Kaolinite Systems by Electron Microscopy and Diffraction", Clays and Clay Minerals, 13th Conf. pp. 331 - 339, Pergamon Press. New York

Sugiura, S. (1962): "Chlorite-Vermiculite Mixed-Layer Clay Mineral from the Noto Mine, Ishikawa Prefecture ", Jour. of the Mineralogical Society of Japan Vol. 5, No. 5 (in Japanese), pp. 311 - 323

Taplin, J.H. (1959): "A Method for Following the Hydration Reaction in Portland Cement Paste", Australian J. Appl. Sci. 10, pp. 329 - 345

Taylor, H.F.W.(ed.) (1964): "The Chemistry of Cements", 2 vols, London and New York: Academic Press

Tice, J.A. (1968): "Use of Retarders with Cement Treated Soils" Interim Report No. 3, Virginia Highway Research Council, p. 37

U.S. Department of Commerce, (1962): Proc. 4th Int. Symp. Chemistry of Cements, 2 vols, National Bureau of Standards Monograph 43

Van Olphen, H. (1963): "Clay Colloid Chemistry", Interscience, New York

Wang, J.W.H. and Handy, R.L. (1966): "Role of MgO in Soil-Lime Stabilization", H.R.B. Special Report 90, pp. 475 - 492

Weyl, W.A. (1953): "Wetting of Solids as Influenced by the Polarizability of Surface Ions", In Gomer, Robert Smith, Eds, Structure and Properties of Solid Surfaces, pp. 147 - 181, The University of Chicago Press

Willoughby, D.R., Gross, K.A., Ingles, O.G., Silva, S.R. and Spiers, V.M. (1968): "The Identification of Reaction Products in Alkali-Stabilized Clays by Electron Microscopy, X-ray and Electron Diffraction ", Proc. of the 4th Conference of the Australian Road Research Board

Winchell, A.N. (1951): "Elements of Optical Mineralogy 2 Description of Minerals" 4th ed. Wiley, New York, N.Y., 551 pp.

Winterkorn, H.F., Gibbs, H.J. and Fehrmann, R.G. (1942): "Surface Chemical Factors of Importance in the

Hardening of Soil by Means of Portland Cement", Procs. H.R.B. Vol. 22, pp. 385 - 414

Yoshida, M. (1953): see "Clay Handbook (in Japanese)" pp. 576 - 577, Gihodo Co. 1966

CHAPTER III VISCOELASTIC PROPERTIES OF SOIL-CEMENT MIXTURE

1. INTRODUCTION

From microscopic aspect, the physicochemical interaction of cement with extremely fine soil particles smaller than 2 μ is very important phenomenon to be investigated in order to relate the mechanical properties of soil-cement mixtures to their structures. In this respect, several findings are obtained, as mentioned in Chapter II.

From more macroscopic aspect, the quantity, size distribution and physical properties of clay pockets contained in soil-cement specimens have a significant effect on the mechanical properties of soil-cement. The latter subject, with which the phenomenon of ions diffusion is associated (Davidson, Demirel and Handy 1965), is not quite independent of the former.

On the other hand, shrinkage cracking as well as durability against repeated freezing and thawing, and wetting and drying, are significant problems in the soil-cement base course. In this respect, all over the world keenly desired better understanding of shrinkage cracking in nature. In New Zealand, shrinkage- and tensile strength tests appear to be actively recommended as essential tests to be carried out for the design of soil-cement pavement (Dunlop, 1970).

As to the soil-cement, each soil produces its own crack pattern. Clays develop higher total shrinkage but cracks are finer and more closely spaced. Granular soils produce less shrinkage but larger cracks spaced at greater intervals (National Academy of Science, 1961).

Such difference between crack patterns of clays and granular soils should be attributed to their shrinkage characteristic and mechanical properties, especially viscoelastic properties. Thus, the significance of viscoelastic properties in soil-cement mixtures must be emphasized especially for a better understanding of shrinkage cracking.

In this chapter, firstly, the influence of the size distribution and the original moisture content of clay pockets on the creep deformation characteristics will be discussed experimentally. Simultaneously, an effect of a physical property (moisture content) of clay pockets at the production of specimens on the subsequent alteration of macroscopic structure of clay-cement mixtures will also be estimated from their viscoelastic behavior.

Finally, several experimental discussions will be made on viscoelastic characteristics of granular soil -cement mixtures for the purpose of further elucidation of role of clay pockets in soil-cement mixtures.

2. REVIEW OF THE LITERATURE

There are an extremely few papers referring to viscoelastic properties of soil-cement. Dunn's unpublished paper (1960) seems the first to mention the creep characteristics of soil-cement. A series of paper were published, on which this paper is made basing (Okada and Kawamura, 1964)(Okada and Kawamura, 1965)(Okada and kawamura, 1967)(Hasaba, Kawamura and Ofuka, 1970).

Recently, George (1969) reported an interesting paper concerning several viscoelastic characteristics of soil-cement for the purpose of a better understanding of shrinkage cracking of pavement. Brief mentions will be made on these Dunn's and George's papers in the following.

Viscoelastic behavior of soil-cement is discussed on the basis of the creep test results obtained for specimens loaded in uniaxial compression to a constant stress for a relatively short time (about two weeks) (Dunn, 1960). He states a phenomenon that every specimen exhibits the change in rate of creep at about 17 hours after the start of the test. According to his statement, most possible explanation for this phenome-

non may be the "secondary time effects" of soils containing some amount of clay when subjected to sustained load. He concluded that the creep characteristics of soil-cement appear to be more similar to the consolidation of soils than to the sustained compression of concrete. The soils used in his experiments are granular soils.

In the creep tests carried out under the surrounding condition allowing evaporation of moisture from specimens, it is a very difficult problem whether the creep deformation can be separated from drying shrinkage.

In this respect, George experimentally evidenced that shrinkage and creep was interdependent phenomena. The creep results obtained in his experiment revealed that the creep of the test specimens exposed in a 55 percent relative humidity condition was about 4 or 6 times that of the specimen sealed against moisture gain or loss (George, 1969). Furthermore, he described that a mixture which exhibited high shrinkage generally also showed high creep (George, 1969).

In the description regarding shrinkage cracking in soil-cement base course, George pointed out that Burgers model showed the greatest promise in mechanical simulation of actual soil-cement behavior.

3. INFLUENCE OF "CLAY POCKETS" ON THE VISCOELASTIC PROPERTIES OF CLAY-CEMENT MIXTURE

(1) Outline of Experiments

Apparatus

The machine which disintegrates clay lumps was used to produce clay-cement mixtures involving clay pockets with various moisture contents and size distributions. Photograph 4.1 shows the disintegrating machine, of which a section is schematically drawn in Fig. 4.1. The mould and the rods shown in Photograph 4.2 were employed to produce cube-shaped clay lumps. These machine and the mould used in laboratory were made for the following purpose.

Cohesive clays lumps which were dried up to a certain moisture content can be disintegrated by the machine to produce the soil material available for soil-cement. The soil-cement using these disintegrated clay lumps was found to have enough unconfined compressive strength for the practical application of pavement (Hasaba, and Kawamura, 1968).

The creep test apparatus used to apply a constant load to the specimens is shown schematically in Fig. 4.2. Load was held constant by a spring.

Materials and their Mix Proportions

Cement used is normal portland cement. Cohesive clayey soil is from Utatsuyama hill in Kanazawa; its physical properties are shown in Table 4.1. Cement content is 10 percent by weight of dry soil; moisture content the optimum moisture content (31.5 percent) determined basing on JIS A 210.

Preparation of Cohesive Clay Lumps Sample and Indication of its Lumps Size Distributions

The clayey soil from the field was dried under the room conditions, and then disintegrated by the machin as finely as possible. Disintegrated soil material to which water had been added to equal the optimum moisture content was placed in the 40 cm x 40 cm x 4 cm mold in two layers. Each layer was rodded 200 times uniformly over the mold. Such plate-like clay lump obtained was subdivided into the 4 cm cubes with a knife-edge plate. These cube-shaped clay lumps were dried to a given moisture content in a drying oven at about 110°C. Moisture contents of the clay lumps selected in this experiment was 0, 10, 20 and 30 percent. Such dried clay cubes were dropped at the rate of one lump per five seconds from a height of 40 cm above the inlet of the machine. The revolution velocity of the machine was varied in the five steps of

125, 250, 375, 500 and 625 r.p.m. to disintegrate the clay cubes into various size destributions of clay lumps material. Sieve analyses, from which clay lump-size distribution and specific surface area can be estimated, were carried out for all of disintegtated soil samples.

The specific surface area is defined as total surface area of clay lumps per unit volume (i.e. 1 cm^3) as follows:

$$S = f\ (\Sigma nd^2/\Sigma nd^3) \qquad (4.1)$$

where S : specific surface area (cm^2/cm^3), f : shape factor, d : particle diameter (mm), n : number of the particles of d in diameter.

Assuming that the spherical particles of $(d_n + d_{n+1})/2$ in diameter are substituted for the particles ranging from d_n to d_{n+1} in diameter, the specific surface area of a disintegrated clay lumps sample can be calculated from the sieve analysis as follows:

$$S \doteqdot f\ \Sigma \frac{Y_{n+1,\ n}}{100\ d_m} \qquad (4.2)$$

where $Y_{n+1,\ n}$: percentage of size group $(d_n - d_{n+1})$

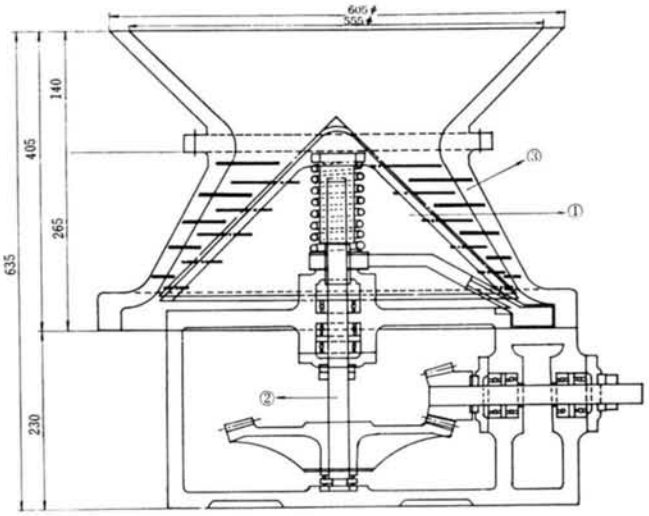

Unit : mm

Fig. 4.1 Cross section of disintegrating machine

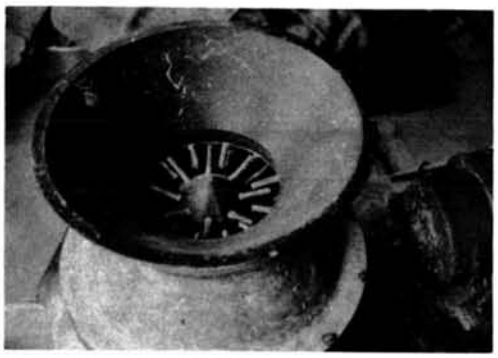

Photo. 4.1 Disintegrating machine

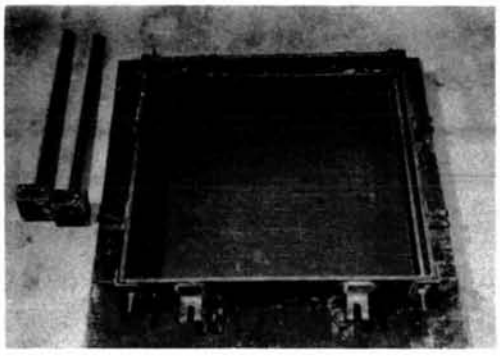

Photo. 4.2 The mould and the rods for producing the cube-shaped clay lumps

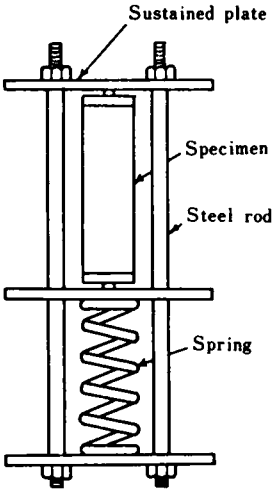

Fig. 4.2 Creep test apparatus

Table 4.1 Physical properties of soil used

Properties		Soil
Size Ranges:	>74 μ (%)	4
	74-5 μ (%)	93
	< 5 μ (%)	3
Liquid Limit (%)		63.4
Plastic Limit (%)		30.9
Plastic Index		32.5
Maximum Dry Density (g/cm^3)		1.37
Optimum Moisture Content (%)		31.5

$$d_m = (d_n + d_{n+1})/2$$

f : 6 for sphere

Preparation of Soil-Cement Specimens

A certain amount of Cement and the disintegrated clayey soil were first mixed and followed by the subsequent mixing for five minutes per 5 kg of the mixture by mixer adding water until an uniform mixture with the optimum moisture content was obtained. The mixture was then placed in the cylinder mold in six layers. Each layer was rodded 19 times. The finished cylinder specimens are 8 cm in diameter and 30 cm in height.

The compactive effort for cylinder soil-cement specimens was determined based on JIS A 1210. That is to say, the rodding numbers per unit volume of soil-cement mixtures were determined so as to equal those specified in JIS A 1210.

Curing Condition of Specimens and Condition of Surrounding Atmosphere in Creep Test

All of specimens tightly closed with polyethylene sacks were cured for 7 and 28 days in the moist room in which the temperature was maintained at 20° C.

The relative humidity and temperature of the environment in creep test were 85 ± 2 percent and 20° C, respectively.

Procedure of Creep Test

Three of five specimens (five specimens were made for each type of the mixture) were broken in compression so that the loads for the sustained load tests could be determined.

Immediately after the prescribed compressive stresses (corresponding to 30 percent of the unconfined compressive strength) were applied to the specimens, the deformation measurement was initiated.

The Berry strain meter was used to determine axial strains of the cylinder specimens. A following special device was attached on the specimens to measure large deformation, because the increasing deformations by far exceeded the measurable limit of the strain meter. Two caps in which many holes of 0.7 mm diameter were made at equal distances of 0.9 mm on their sides, was set at the both ends of the specimens in order that strains could continuously be determined by measuring the change of the distances between an appropriate pair of holes of the two caps (see Photograph 4.3).

The load applied to the specimen decreased with increasing deformation of the specimen. When the sustained load was reduced to about 90 percent, the specimen was re-loaded to the initial level.

Shrinkage was obtained for the specimens allowed to stand under the same environment as the sustained load tests.

The creep strain in this investigation was determined on the basis of the assumption that creep strain could be separated from shrinkage.

Photo.4.3 Creep test apparatus

(2) Analyses of Test Results

(a) Analysis by the Concept of Distribution Function of Retardation Time

In general, informations on the stress-strain relation of a material are indispensable for its practical application as an engineering material. An attempt has been made on the estimation of microscopic structure of a material from its mechanical behavior as well (Sawaragi and Tokumaru, 1955).

This chapter aims not only at discussing the viscoelastic characteristics of soil-cement using disintegrated clay lumps samples, but also at estimating the change of the structure due to the migration of calcium ions, though the system discussed here is considerably macroscopic compared with that on which generally such an attempt is made. For this purpose, the distribution functions of retardation time were determined from creep data obtained for the soil-cements using various types of clay lumps samples.

The fundamental equation corresponding to the mechanical model indicated in Fig. 4.3 is given as follows (Sawaragi and Tokumaru, 1955)(Ogishi, 1963):

$$J_c(t) = \int_0^\infty \Phi(\tau_k)d\tau_k - \int_0^\infty \Phi(\tau_k)\, e^{-t/\tau_k}\, d\tau_k \qquad (4.3)$$

where $J_c(t)$: creep compliance

$\Phi(\tau_k)$: distribution function of retardation time (τ_k)

The distribution function $\Phi(\tau_k)$ can be obtained by solving the integral equation (Eq.(4.3)).

If the kernel function e^{-t/τ_k} in Eq.(4.3) is approximately substituted for a step function, the function $\Phi(\tau_k)$ can be determined by Eq.(4.4)(Alfrey and Doty, 1945):

$$\Phi(\tau_k) \fallingdotseq d(J_c(t))/dt \qquad (4.4)$$

The value of $\Phi(\tau_k)$ can be obtained by differentiating numerically the experimental curves of $J_c(t)$. The numerical differentiation is based on Rutledge's equation (Tanaka, 1959).

(b) Determination of Burgers Model Constants

The distribution function of retardation time definitely represents the difference of the structure in soil-cement mixtures, as shown later. However, a clear physical interpretation for the function may be impossible.

On the contrary, each constants of Burgers model(Fig. 4.4) has the physical meaning respectively. Furthermore, this model can favorably be used not only to describe the viscoelastic behavior of soil-cement,

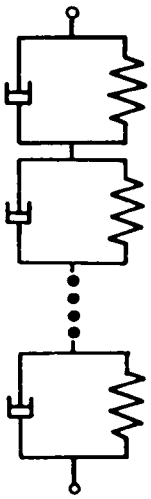

Fig. 4.3 Mechanical model

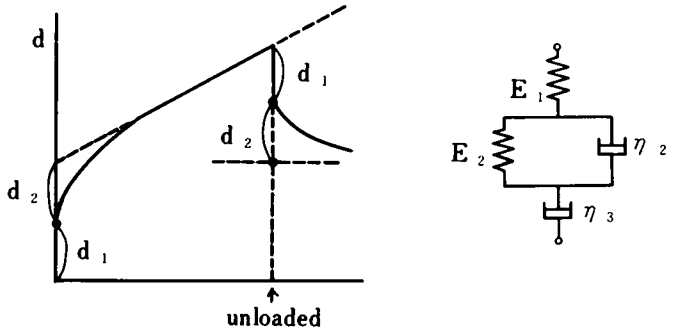

Fig. 4.4 Burgers model analysis of creep curve

but also to discuss shrinkage cracking in soil-cement base course (George, 1969).

Burgers model constants are determined from creep tests data as follows:

When a constant stress is applied to this model, the deformation (ε_c) is represented by Eq. (4.5).

$$\varepsilon_c = (\sigma/E_1) + (\sigma/E_2)(1 - e^{-t/\tau_k}) + (\sigma/\eta_3)t \qquad (4.5)$$

where $\tau_k = \eta_2/E_2$

Burgers model constants could be determined by considering the corresponding relationship between Eq. (4.5) and creep curve (Fig. 4.4) as follows:

(i) When t is extremely small,

$$\varepsilon_{ct\to 0} = \sigma/E_1 \qquad (4.6)$$

Thus, instantaneous elastic deformation gives the constant E_1.

(ii) After a elapse of sufficient time the stationary creep, as indicated by a dotted line, progresses;

$$\varepsilon_{ct\to\infty} = \text{const.} + (p/\eta_3)t \qquad (4.7)$$

Therefore, creep viscosity, η_3, can be determined from the gradient of the dotted line.

(iii) From Eq. (4.7),

$$(\varepsilon_{ct\to\infty})_{t\to 0} = (\sigma/E_1) + (\sigma/E_2) \qquad (4.8)$$

When the dotted line is extrapolated back to t = 0, the intercept ($d_1 + d_2$) on d-coordinate axis corre-

sponds to $\{(\sigma/E_1)+(\sigma/E_2)\}$. Therefore, E_2 is obtained from d_2 (Fig. 4.4).

(iv) From Eq. (5)

$$-\varepsilon_c + (\sigma/E_1) + (\sigma/E_2) + (\sigma/\eta_3)t = (\sigma/E_2)e^{-t/\tau_k}$$

$$\ln\{-\varepsilon_c + (\sigma/E_1) + (\sigma/E_2) + (\sigma/\eta_3)t\} = \ln(\sigma/E_2) - (t/\tau_k) \qquad (4.9)$$

When the value of $\ln\{-\varepsilon_c + (\sigma/E_1)+(\sigma/E_2)+(\sigma/\eta_3)t\}$ are plotted against time (t), the graidient of the line obtained gives $(-1/\tau_k)$.

(c) Determination of Constants in a Creep-Time Equation, i.e. Hyperbolic Expression

There is a hyperbolic form as one of various types of creep-time equations proposed with concrete (Lorman, 1940). In this paper, the hyperbolic expression will be used in order to predict the ultimate creep strains of soil-cement mixtures.

$$\varepsilon_c = f(t)\ \sigma \qquad (4.10)$$

Where ε_c is the creep strain, σ is the stress in kilograms per square centimeter, and the coefficient f(t) is a function of time.

Assuming f(t) in Eq. (4.10) in the hyperbolic form, one has

$$\varepsilon_c = \{mt/(n_c + t)\}\sigma \qquad (4.11)$$

where t is the time in days reckoned from the instant when the load is applied, and m and n_c are constants whose significance is explained below.

m : ultimate creep strain per unit of stress

n_c : the time at which 50 percent of the ultimate creep strain is obtained.

(3) Result and Discussion

Structure of Soil-Cement and its Distribution Function of Retardation Time

Fig. 4.5 shows creep compliance ($J_c(t)$) curves of soil-cement specimens compacted using three different specific surfaces of clay lumps samples with 10 percent moisture content. The soil-cement specimens made using different fineness of clay lumps samples are found to have different $J_c(t)$ curves. The distribution functions of retardation time (τ_k) can be obtained from these $J_c(t)$ curves, as stated previously. For example, those for the specimens made using zero percent moisture content clay lumps samples are given in Fig. 4.6 and Fig. 4.7, in which the ages at applying a constant load are 7 and 28 days, repectively. It is found that the shape of the distribution functions $\Phi(\log \tau_k)$ differs with the specific surfaces of clay lumps samples used. Thus, the shape of the functions ($\Phi(\log \tau_k)$) may considerably be affected by moisture content and specific surface of clay lumps used, and by the age of the soil-cement specimens.

Firstly, as shown in Fig.4.6, the curves of those made using the zero percent moisture content clay lumps, when a constant load is applied at 7 days age, appear to be built by superimposing two curves of the distribution functions each having the maximum value at different retardation time. Especially, the specimens made using the finest clay lumps sample (its specific surface is the largest of all) show the curve having distinct "double hill-like shape". These superimposed "hill-like" curves are obtained only in the

7 days age specimens made using the zero percent clay lumps samples, and not at all in the specimens to which a constant load is applied at 28 days age.

This "double hill-like shape" curve would allow us to presume that this type of soil-cement specimens are composed of two phases having considerably different mechanical properties. That is to say, it may be supposed that the volume fraction occupied by "clay pockets" in 7 days age specimens made with the zero percent clay lumps is so great as to be equal to that of the skeleton part (in which soil particles are bonded each other by cementitious calcium silicate hydrate gel). Further, the machanical properties of clay pockets in this soil-cement with the zero percent clay lumps may be not similar to those of clay pockets in another type of clay lumps sample-cement mixtures.

The conclusion can be drawn that the volume fraction of clay pockets in a specimen highly affects the shape of its distribution function Φ, as indicated by the difference between the curves for the specific surface of 290 cm^2/cm^3 and 86 cm^2/cm^3.

As shown in Fig. 4.8 and Fig. 4.9, the effect of the specific surface on the characteristics of the function, $\Phi(\log \tau_K)$, in 10 percent moisture content clay lumps samples used, is not so remarkable as in those of zero percent moisture content. Such difference between both moisture contents may be responsible for the difference in the diffusion rate of Ca ions from the hydrating cement. The diffusion of Ca ions in 10 percent moisture content clay lumps samples may probably be more rapid than in zero percent ones. Therefore, the volume fraction of clay pockets in the structure of soil-cement mixtures made with 10 percent moisture clay lumps may gradually decrease during the curing periods, even if the original soil samples used include considerably coarse clay lumps. In consequence, the shape of the distribution function of the 10 percent moisture content clay lumps samples-cement mixtures would not reflect the difference in the specific surface of the original clay lumps materials.

Little difference may be found in the shape of distribution function between the

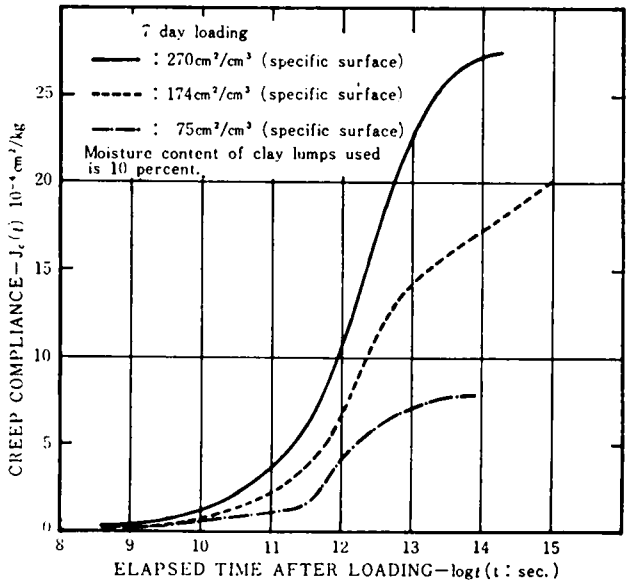

Fig. 4.5 Creep compliance of soil-cement mixtures using clay lumps sample

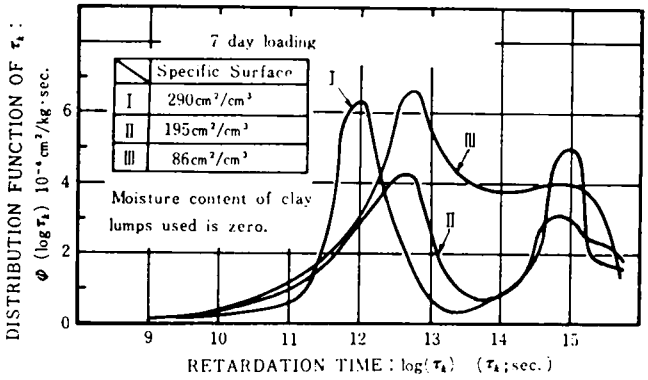

Fig. 4.6 Distribution function of τ_K in soil-cement mixture using clay lumps sample

specific surfaces of the samples with 20 and 30 percent moisture content (Fig. 4.10, Fig. 4.11), though there is only a little difference in their specific surface. Further, the values of the function in the range of short retardation time in high moisture content such as 30 and 20 percent are greater than in low ones of 0 and 10 percent moisture content (compare Fig.4.10 and Fig. 4.11 with Fig. 4.7, Fig. 4.8 and Fig. 4.9).

The relationships between the specific surfaces, and the maximum value ($\Phi(\log \tau_k)$) and the retardation time ($(\tau_k)_{\Phi max.}$) giving the maximum value of $\Phi(\log \tau_k)$ are plotted as shown in Fig. 4.12 and Fig. 4.13 (for the " double hill-like shaped " function, the smaller value of $(\tau_k)_{\Phi max.}$ are taken). At 7 days age loading, the maximum value of the distribution function decreases with increasing specific surface in the specimens using 0 and 10 percent moisture content samples. Conversely, at 28 days age loading, the maximum values a little or little increase with specific surface, as shown by broken lines (Fig. 4.12). Thus, the characteristic values of the function ($\Phi_{max.}$, $(\log \tau_k)_{\Phi max.}$) at 7 days age loading are highly affected by the specific surface of clay lumps samples used, but those at 28 days loading little dependent upon the original clay lumps size. Further, as a whole, the sharp mountainous curves (0 and 10 percent moisture content) shift towards the greater retardation time and decrease in their height during the cure of 7 to 28 days. These changes between both ages at loading reveal that, even after 7 days ages, the diffusion of Ca ions and the subsequent pozzolanic reaction take place in the soil-cement specimens made using these two types of clay lumps samples, resulting in the change in their internal structure.

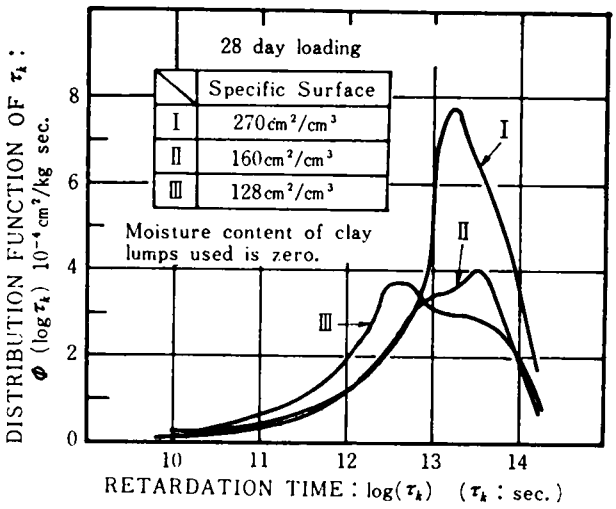

Fig. 4.7 Distribution function of τ_K in soil-cement mixture using clay lumps sample

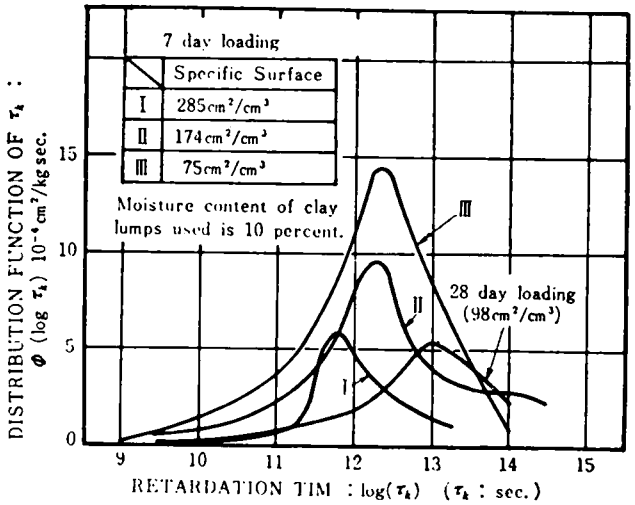

Fig. 4.8 Distribution function of τ_K in soil-cement mixture using clay lumps sample

On the other hand, using the 30 percent moisture content clay lumps samples, no remarkable changes in the height and shape of curves are found between 7 and 28 days age

loading. Furthermore, despite of the coarse clay lumps included, none of the functions shows such "double hill-like shape" as in zero percent moisture content samples-cement mixtures.

These experimental results would lead to the suggestion that the more rapid diffusion of Ca ions in soil-cement made using 30 percent moisture content clay lumps make the structure considerably homogeneous at least at 7 days age.

Thus, the structure of clay lumps -cement mixtures could be inferred from their distribution functions as follows:

The constituent phases (clay pockets and skeleton parts) distribution in clay lumps sample-cement mixture varies during the cure depending upon moisture content and size distribution of clay lumps sample used. When clay lumps samples used are same in its size distribution, the higher the moisture content of clay lumps samples used, the more rapid the diffusion of Ca ions occurs, the stable and homogeneous structure being formed at the earlier curing time.

Such difference between the finished internal structures in the various types of specimens after a certain curing time may be confirmed to some extent even by examining the longitudinal sections of specimens by the naked eye (see Fig. 4.14*).

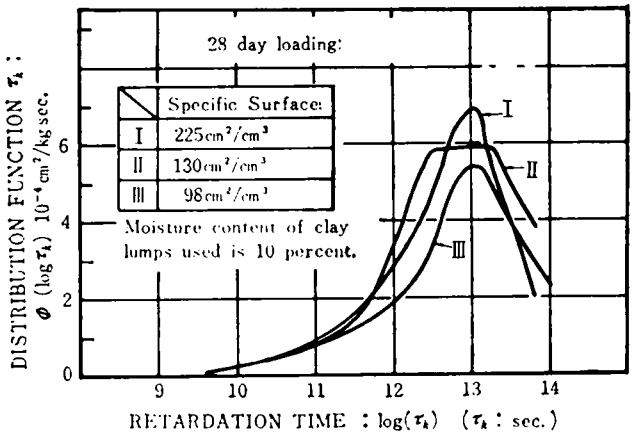

Fig. 4.9 Distribution function of τ_K in soil-cement mixture using clay lumps sample

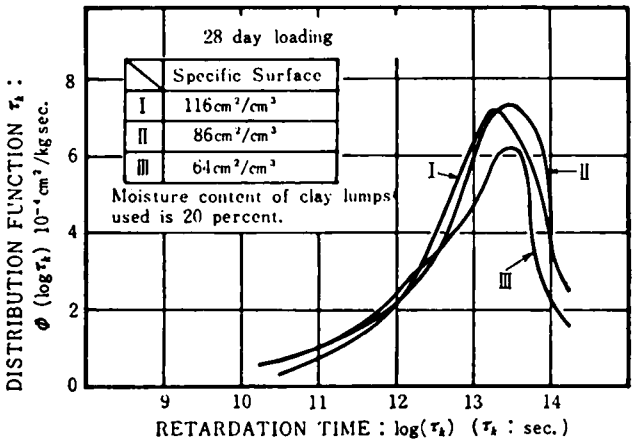

Fig. 4.10 Distribution function of τ_K in soil-cement mixture using clay lumps sample

The Structure of Soil-Cement Mixtures and their Burgers Model Constants

* Specimens after the completion of creep test were longitidinally cut in two by the saw. Then, phenolphthalein 1% ethyl alcohol solution is sprinkled on the cut faces. The various distributions of clay pockets in the specimens are seen in these plates. Further, it is found that carbonation proceeds towards the interior of the specimens.

Burgers model constants of soil-cement mixtures made using clay lumps samples at 7 and 28 days age loading are represented in Table 4.2 and Table 4.3, respectively.

The constant E_1 shows the characteristic of the response of a specimen to stresses applied in a short time. The η_3 is an indication of the creep viscosity of a specimen over the long term.

The relationship between specific surface and these two constants (E_1, η_3) are given in Fig. 4.15 and Fig. 4.16.

E_1 increases with increasing specific surface irrespective of the moisture content of clay lumps samples used , but η_3 differs with the moisture content of them. This fact indicates that E_1 gives an indication of elastic properties of skeleton parts and that η_3 is predominantly influenced by the properties of clay pockets rather than of skeleton parts.

As previously suggested by the analysis of distribution functions and examination of the sections of specimens by naked eye, the finished structures of the 30 percent moisture content clay lumps samples-cement mixtures are so homogeneous comparing with others that the concentration of cementitious calcium silicate hydrates in skeleton parts probably becomes less. The relatively smaller values of E_1 in the 30 percent moisture content clay lumps samples-cement mixtures could be interpreted by the less concentration of cementitious materials in skeleton parts.

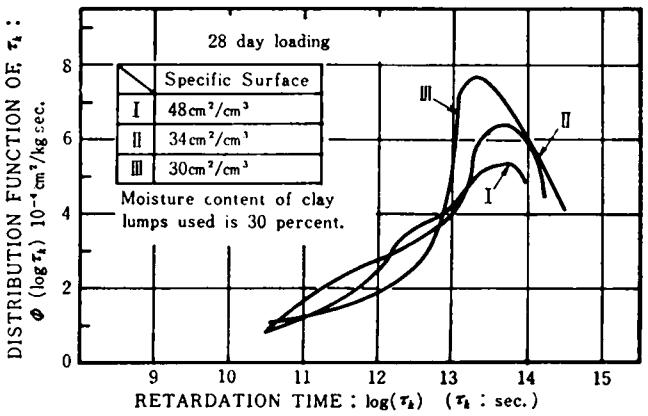

Fig. 4.11 Distribution function of τ_K in soil-cement mixture using clay lumps sample

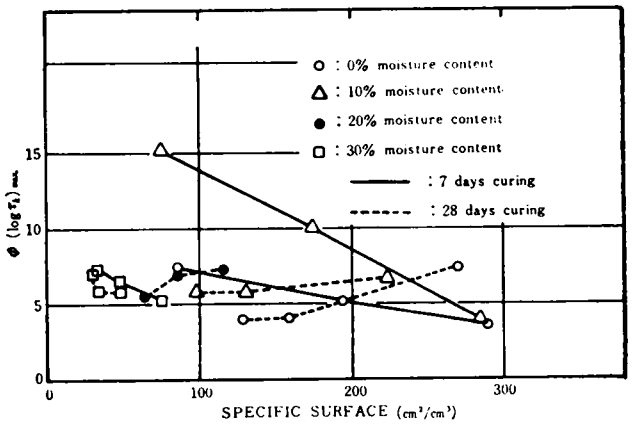

Fig. 4.12 Relationship between the maximum value of the distribution function and the specific surface of clay lumps sample used

On the other hand, none of the relationship between η_3 and specific surface seems to show a definite tendency (Fig. 4.16). The value of η_3 is supposed to depend primarily upon the volume fraction of clay pockets and their characteristic of viscosity. However, at present, it may be impossible to relate the experimental results obtained to these two factors.

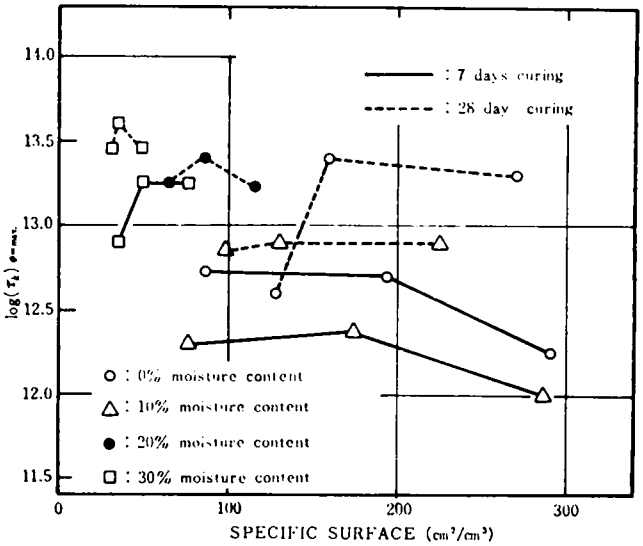

Fig. 4.13 Relationship between the retardation time taking the maximum value of Φ and the specific surface of clay lumps sample used

Table 4.2 Four-element model constants of each soil-cement mixture using clay lumps (7 day loading)

Moisture Content (%)	Specific surface (cm^2/cm^3)	E_1 (x 10^4 kg/cm^2)	E_2 (x 10^3 kg/cm^2)	η_2 (x 10^3kg. day/cm^2)	η_3 (x 10^5kg. day/cm^2)
0	86	0.79	0.98	3.27	0.43
	195	0.88	1.59	2.80	1.03
	290	0.67	1.00	1.50	1.12
10	75	0.58	0.39	0.96	0.78
	174	0.71	0.67	1.45	0.45
	285	0.95	1.38	2.97	0.48
30	33	0.72	0.70	2.06	1.30
	49	0.73	0.77	2.88	0.63
	75	0.62	0.66	2.68	0.57

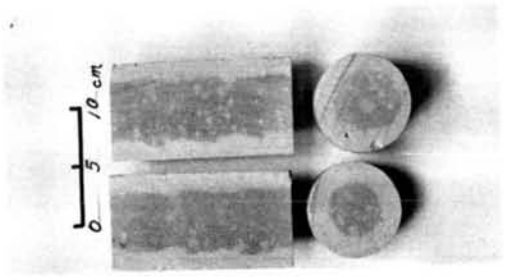

Moisture content : 0%
Specific surface : 128cm²/cm³

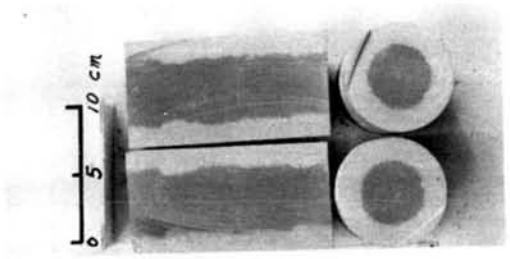

Moisture content : 0%
Specific surface : 270cm²/cm³

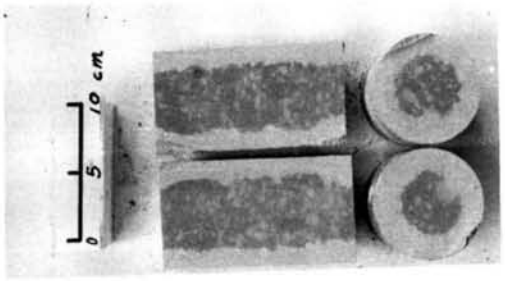

Moisture content : 10%
Specific surface : 98cm²/cm³

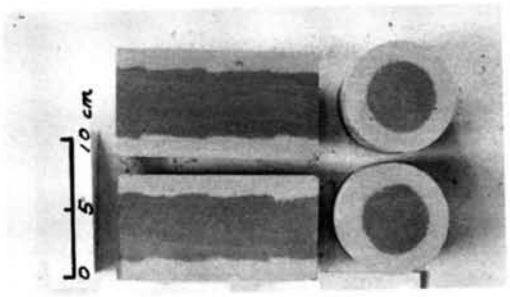

Moisture content : 10%
Specific surface : 225 cm²/cm³

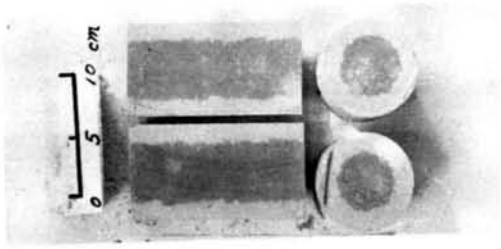

Moisture content : 20%
Specific surface : 56cm²/cm³

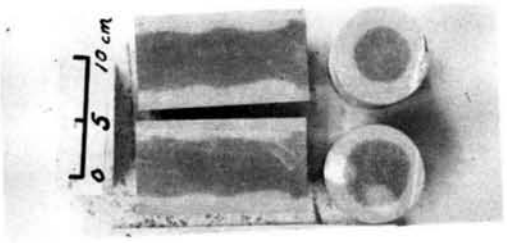

Moisture content : 20%
Specific surface : 116 cm²/cm³

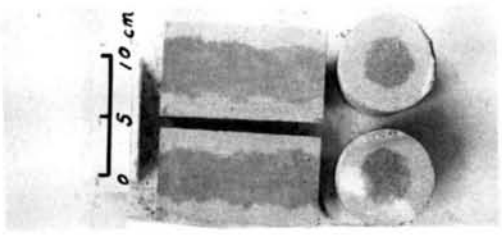

Moisture content : 30%
Specific surface : 33cm²/cm³

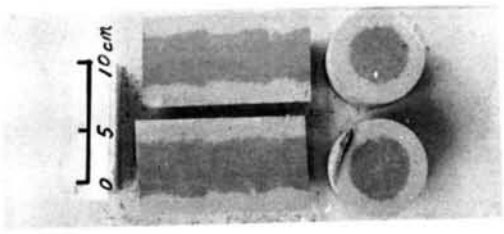

Moisture content : 30%
Specific surface : 48cm²/cm³

Fig. 4.14 Indication of sections of soil-cement specimens on which phenolphthalein 1% ethyl alcohol is splinkled

Table 4.3 Four-element model constants of each soil-cement mixture using clay lumps (28 day loading)

Moisture Content (%)	Specific Surface (cm^2/cm^3)	E_1 (x 10^4 kg/cm^2)	E_2 (x 10^3 kg/cm^2)	η_2 (x 10^3kg. day/cm^2)	η_3 (x 10^5kg day/cm^2)
0	128	0.87	1.44	6.00	1.39
	160	1.31	1.51	7.61	1.58
	270	1.38	1.06	5.00	0.95
10	98	1.31	1.15	3.84	1.21
	130	1.11	0.91	3.29	1.24
	225	1.30	0.89	2.88	1.78
20	64	1.26	1.11	4.28	0.96
	86	0.98	0.99	4.58	0.94
	116	1.14	0.91	4.06	0.84
30	30	0.99	0.94	5.04	0.48
	34	0.94	1.04	5.61	0.43
	48	0.93	0.81	4.72	1.14

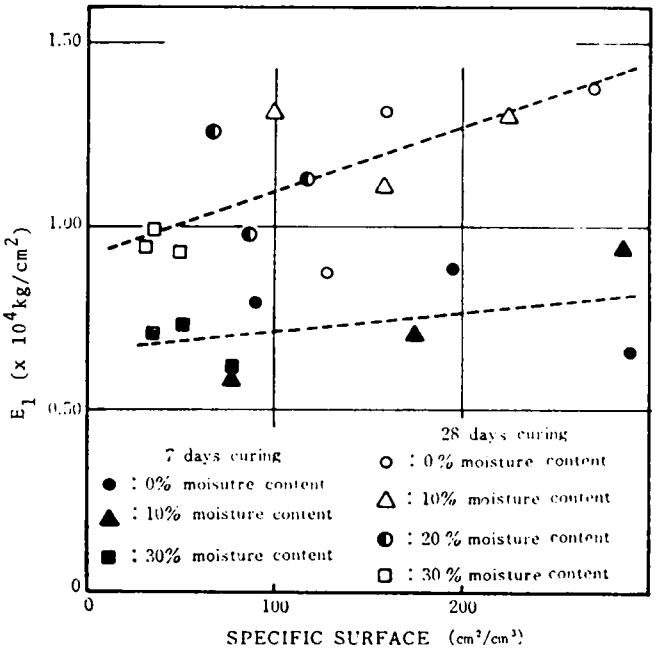

Fig. 4.15 Relationship between E_1 and the specific surface of clay lumps sample used

The Structure of Soil-Cement and the Ultimate Creep Strain

The ultimate creep strain(m) for the 7 and 28 days age loading are plotted against specific surface (Fig. 4.17, Fig. 4.18).

At 7 days age loading, the use of finer-disintegrated clay lumps samples greatly reduces the ultimate creep strain.

However, at 28 days age loading, the ultimate creep strain tends to increase a little with specific surface. There is little difference between moisture contents of clay lumps samples used, though it should be noted that the ultimate creep strains in the 30 percent moisture content samples-cement mixtures are great in comparison with other ones. As a whole, at 28 days age loading, all of the ultimate creep strains except those of 30 percent moisture content are in the range of 1.0 to 1.5 x 10^{-4}(cm^2/kg) irrespective of clay lumps size and of their moisture content. This result can also be attributed to the homogeneous structure of 28 days age specimens which is brought about by the diffusion of Ca ions during the curing periods of 7 to 28 days. Thus, the results concerning the ultimate creep strain are compatible with those obtained by other analyses such as distribution function and Burgers model.

(4) Summary and Conclusions

This section deals with two subjects. The first of these is to investigate the influence of the size and moisture content of clay lumps samples on the viscoelastic properties of soil-cement mixtures. The second is to reveal the change in the structure of soil-cement due to the diffusion of calcium ions by means of creep tests.

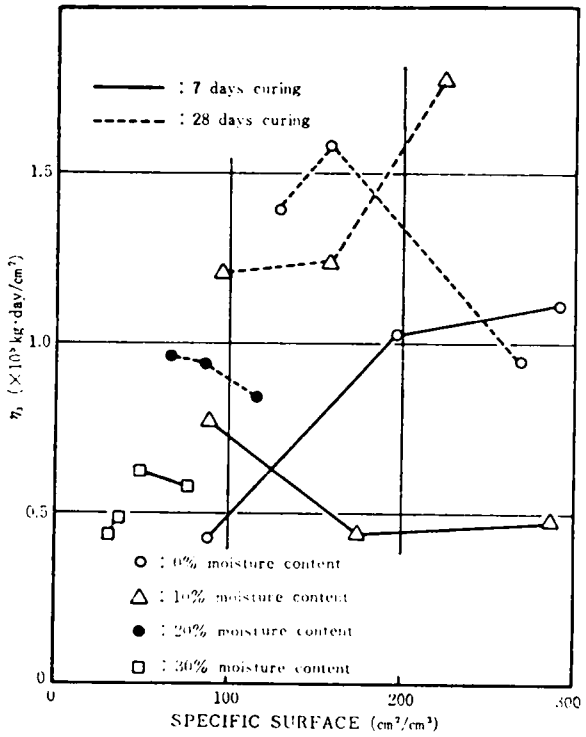

Fig. 4.16 Relationship between η_3 and the specific surface of clay lumps sample used

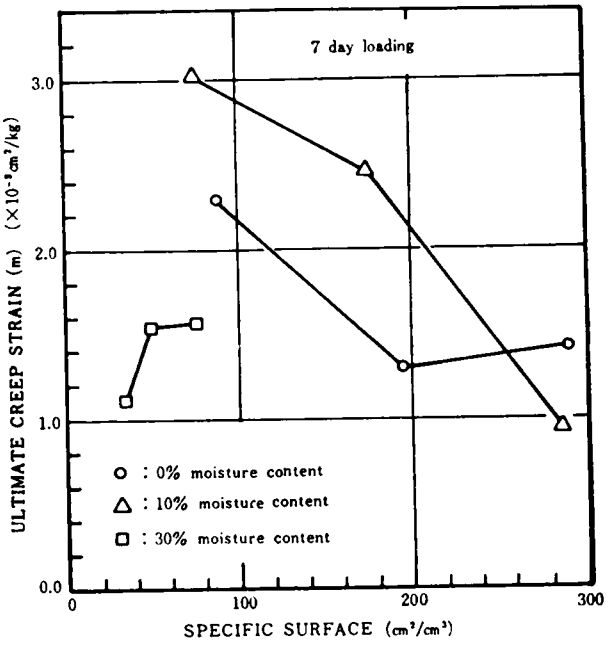

Fig. 4.17 The variation of ultimate creep strain with the specific surface of clay lumps sample used

The major conclusions obtained are summarized in the following.

1) The distribution functions of retardation time(τ_k) of soil-cement mixtures made using clay lumps samples of zero percent moisture content appear to consist of two "hill-like" curves having a distinct sharp peak. On the contrary, all of others have only one sharp peak.

2) The Burgers model constant E_1, which is the modulus of elasticity characterizing the elastic property of soil-cement mixture, increase with decreasing size of clay lumps used, irrespective of their moisture content. On the other hand, the value of η_3 showing creep viscosity greatly depends on the moisture content of clay lumps samples.

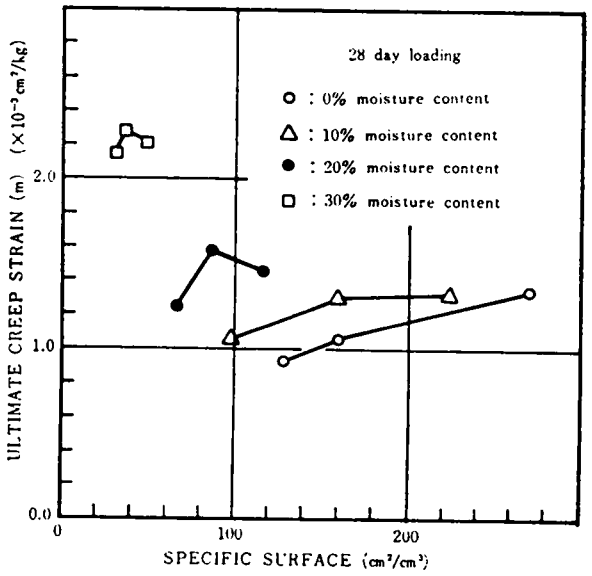

Fig. 4.18 The variation of ultimate creep strain with the specific surface of clay lumps sample used

3) The ultimate creep strains of 7 days age loading specimens decrease with decreasing size of clay lumps samples. The relationship between the ultimate creep strains and the specific surface shows a different tendency for a different moisture content of the original clay lumps samples used. However, those of 28 days age loading ones, independently of moisture content, increase a little with the specific surface.

4) The distribution of constituent phases (clay pockets and skeleton parts) in the clay lumps sample-cement mixtures varies during the cure dependently upon moisture content and size distribution of the sample used. When clay lumps samples used are same in their size distribution, the higher the moisture content of clay lumps samples used, the more rapid the diffusion of Ca ions occurs, the stable and homogeneous structure being formed at earlier curing periods.

4. VISCOELASTIC PROPERTIES OF SOIL-CEMENT USING GRANULAR SOILS

The structure of granular soil-cement mixtures, in which a soil including sand (>74 μ) of more than 80 percent is used, should be different from that of clay lumps-cement mixtures such as discussed in the previous paragraph. It may be reasonable to postulate that there is little clay pockets in such a granular soil-cement mixture.

In this paragraph, mainly in order to clarify the function of clay pockets in mechanical properties of soil-cement and to obtain more data for better understanding of shrinkage cracking, the viscoelastic characteristics of granular soil-cement mixtures having little clay pockets will be discussed. The major subjects are as follows:

(1) The causes of creep in soil-cement are discussed using a mechanical model, which was proposed by Freudenthal et al. (Freudenthal et al., 1958) to explain the characteristics of creep of concrete under high compressive stresses.

(2) The dynamic modulas of elasticity and the logarithmic decrement of soil-cement are determined by the sonic method, and the changes in the damping of vibration with increasing silt content in the soils are examined.

(3) Burgers model constants are given for several soil-cement mixtures made using different soils in silt content. Comparison of those of clay lumps-cement mixtures is also made to obtain some basic information for discussing shrinkage cracking due to shrinkage stresses.

(1) Outline of Experiments

Materials and their Mix Proportions

Cement used is normal portland cement. Soils used are from a hill in Kyoto and Awaji; their physical properties are shown in Table 4.4. Two 3:1 mixtures of soil S_1 and soil S_2, and soil S_3 give soil S_4 and soil S_5, respectively. Furthermore, the 1:1 mixture of soil S_1 and soil S_3 gives soil S_6. Cement contents selected are 10, 7.5 and 5 percent by weight of dry soil. The moisture contents of the specimens are less than optimum moisture content by 1 and 2 percent and greater than by 2 percent.

Preparation of Specimens

The size of cylinder specimens for creep test is 10 cm in diameter, and 30 cm in height; the one for sonic test specimens 7.5 in diameter and 15 cm in height.

Materials were mixed by hand until a uniform mixture was obtained.

The compactive effort for cylinder soil-cement specimens was determined based on JIS A 1210, as stated in the previous section (p.75).

Curing Condition of Specimens and Surrounding Atmosphere Condition in Creep Tests

All of specimens tightly closed in polyethylene sacks were cured for given periods in the moist room in which the temperature was maintained at 20° C. The relative humidity and the temperature of the environment in creep test were 80 percent and 20° C, respectively.

Table 4.4 Physical properties of soils

Properties	S_1	S_2	S_3	S_4	S_5	S_6
Size Ranges:						
> 74 μ(%)	84.0	93.0	9.0	——	——	——
74 - 5 μ(%)	13.5	5.0	83.5	——	——	——
< 5 μ(%)	2.5	2.0	2.5	——	——	——
Liquid Limit (%)	N.L.	N.L.	42.3	24.0	——	——
Plastic Limit (%)	N.P.	N.P.	25.6	19.5	——	——
Plastic Index			16.7	4.5	——	——
Maximum Dry Density (g/cm^3)	1.860	1.996	——	1.850	1.828	1.790
Optimum Moisture Content (%)	12.5	10.8	——	13.5	13.9	14.5

Apparatus and Procedure of Creep and Sonic Tests

The creep test apparatus are same as described in paragraph 3.. Huggenberger strain meter was used to measure axial strains of the cylinder specimens. The prescribed compressive stresses applied to the specimens at 7 days age was 20, 40, 60 and 80 percent of the unconfined compressive strength.

The sonic apparatus used in this investigation is manufactured according to JIS A 1127. Resonant frequency (f_0) and frequencies (f_1, f_2) on either side of the resonance where the amplitude of vibration is 0.707 times the maximum were determined.

The strains for determination of static modulus of elasticity were measured by Marten's mirror extensometer.

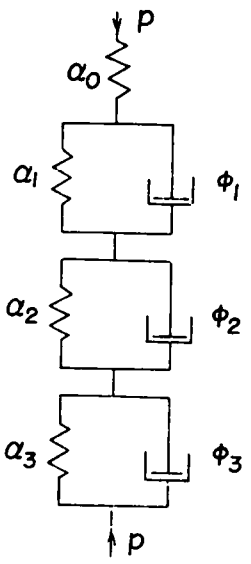

Fig. 4.19 Mechanical model.

(1) A Hooke element represents the linear instantaneous deformation.
(2) A Kelvin element (I) represents the irrecoverable deformation due to internal, partially destructive readjustment within the granular mass of the soil-cement
(3) A Kelvin element (II) represents the recoverable creep or "delayed elasticity".
(4) A Kelvin element (III) represents "consolidation" effects of irrecoverable pore water motion towards the surface and subsequent evaporation

α_0, α_1, α_2, α_3=spring constants of Hooke element, Kelvin element (I),(II) and(■) respectively

ϕ_1, ϕ_2, ϕ_3=fluidity coefficients of Kelvin elements (I), (II) and (■) respectively

(2) Analyses of Tests Results

(a) Mechanical Model Analysis According to Freudenthal et al.'s concept

A mechanical model, shown in Fig. 4.19, is used to analyze the creep test results of soil-cement mixtures.

Following procedure was adopted for determining these model constants:

When a constant load is applied to this model, the total deformation ($\varepsilon_c(t)$) is represented by Eq. (4.12).

$$\dot{\varepsilon}_c(t) = \sigma\alpha_1 e^{-t/\tau_1} + \sigma\alpha_2 e^{-t/\tau_2} + \sigma\alpha_3 e^{-t/\tau_3}$$

$$\varepsilon_c(t) = \sigma\alpha_1(1 - e^{-t/\tau_1}) + \sigma\alpha_2(1 - e^{-t/\tau_2}) + \sigma\alpha_3(1 - e^{-t/\tau_3}) + \sigma\alpha_0 \qquad (4.12)$$

The total creep deformation can be separated into the recoverable (ε_{cr}) and irrecoverable component (ε_{ci}), as described in Fig. 4.19. Such separation makes it possible to determin all of these model constants. α_2 and τ_2 can easily be obtained from an anlysis of the ε_{cr} - $\dot{\varepsilon}_{cr}$ curves; constants α_1, τ_1, α_3 and τ_3 from two linear parts having different slope in the ε_{ci} - $\dot{\varepsilon}_{ci}$ curves.

First, the procedure for the determination of constants α_2, τ_2 from recoverable component is as follows:

Recoverable creep strain (ε_{cr}) is represented by Eq. (4.13).

$$\varepsilon_{cr} = \sigma\alpha_2(1 - e^{-t/\tau_2}) \qquad (4.13)$$

Therefore,

$$\varepsilon_{cr} = \varepsilon_{r\infty} - \tau_2\dot{\varepsilon}_{cr} \qquad (4.14)$$

where $\varepsilon_{r\infty}$ (= $\sigma\alpha_2$) : recoverable component of the total ultimate creep strain

The slope of a line obtained by plotting ε_{cr} against $\dot{\varepsilon}_{cr}$ gives a retardation time (τ_2). Further, when the line is extrapolated back to $\varepsilon_{cr} = 0$, the intercept on ε_{cr}-cordinate axis corresponds to $\sigma\alpha_2$.

Next, α_1, τ_1, α_3 and τ_3 are determined as follows;

Irrecoverable creep strain (ε_{ic}) is expressed by Eq. (4.15) or Eq. (4.16).

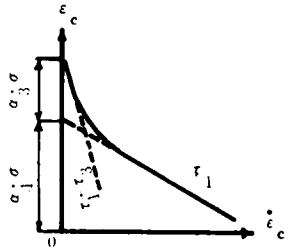

Fig. 4.20 Schematic diagram of $\varepsilon_c - \dot{\varepsilon}_c$ relation

$$\varepsilon_{ci} = \sigma\alpha_1(1 - e^{-t/\tau_1}) + \sigma\alpha_3(1 - e^{-t/\tau_3}) \qquad (4.15)$$

$$\dot{\varepsilon}_{ci} = (\alpha_1/\tau_1)\sigma e^{-t/\tau_1} + (\alpha_3/\tau_3)\sigma e^{-t/\tau_3} \qquad (4.16)$$

Let us suppose that the τ_3 and α_1 values are several times the values for τ_1 and α_3, respectively.

The relation between ε_{ci} and $\dot{\varepsilon}_{ci}$ is non-linear, as shown by Eq.(4.15) and Eq.(4.16). This relation may be rewritten as Eq.(4.17) for very small values of t, since the effect of the second terms in Eq.(4.15) and Eq.(4.16) are so small as to be negligible comparing with those of the first terms ($\alpha_3/\tau_3 \ll \alpha_1/\tau_1$).

$$\varepsilon_{ci} \doteqdot \sigma\alpha_1 - \tau_1\dot{\varepsilon}_{ci} \qquad (4.17)$$

With increasing value for t, the effect of the second term in Eq.(4.15) gradually increases until the relation between ε_{ci} and $\dot{\varepsilon}_{ci}$ becomes non-linear. The curvilinear part appearing as a transition from one straight line to the other in the experimental curve (Fig. 4.20) definitely indicates such non-linearity between ε_{ci} and $\dot{\varepsilon}_{ci}$.

The Eq.(4.15) is transformed into a more convenient form:

$$\varepsilon_{ci} = \sigma(\alpha_1 + \alpha_3) - \sigma(\tau_1 + \tau_3)[\{\alpha_1/(\tau_1 + \tau_3)\}\, e^{-t/\tau_1} + \{\alpha_3/(\tau_1 + \tau_3)\}e^{-t/\tau_3}] \qquad (4.18)$$

Further increase in the value t passing through the transition intensifies the decreasing effects of the $\{\alpha_1/(\tau_1 + \tau_3)\}e^{-t/\tau_1}$ term in Eq.(4.18) and of the first term in Eq.(4.16). Consequently, Eq.(4.18) and Eq.(4.16) approximately become Eq.(4.19) and Eq.(4.20), respectively.

$$\varepsilon_{ci} \doteqdot \sigma(\alpha_1 + \alpha_3) - \sigma(\tau_1 + \tau_3)\{\alpha_3/(\tau_1 + \tau_3)\}e^{-t/\tau_3} \qquad (4.19)$$

$$\dot{\varepsilon}_{ci} \doteqdot (\alpha_3/\tau_3)\sigma e^{-t/\tau_3} \qquad (4.20)$$

Eq.(4.21) is derived from Eq.(4.19) and Eq.(4.20).

$$\varepsilon_{ci} \doteqdot \sigma(\alpha_1 + \alpha_3) - (\tau_1 + \tau_3)\dot{\varepsilon}_{ci} \qquad (4.21)$$

where $\alpha_3/(\tau_1 + \tau_3)$ is approximately used for α_3/τ_3.

As easily understood from the above correlation between the characteristic ε_{ci} - $\dot{\varepsilon}_{ci}$ curve (Fig. 4.20), and Eq. (4.17) and Eq. (4.21), the slopes of the initial and the latter linear part, and their intercepts on the ε_{ci}- coordinate axis give τ_1 and $(\tau_1 + \tau_3)$, and α_1 and $(\alpha_1 + \alpha_3)$(Fig. 4.20).

(b) Analysis of Sonic Test Results

Transversal Vibration of a Viscoelastic Beam

The resonant frequency and band width determined by the transversal vibration of a viscoelastic beam are utilized to compute the dynamic Young's modulus and viscosity coefficient of soil-cement mixtures.

The following equation of motion is obtained for the transversal vibration of a viscoelastic beam of which the mechanical behavior can be represented by Kelvin's model and which has a transversal dimension small compared with both its length and wavelength (Horio and Onogi, 1951).

$$\rho(\partial^2 y/\partial t^2) + E_d k^2(\partial^4 y/\partial x^4) + \eta_d k^2(\partial^5 y/\partial x^4 \partial t) = 0 \qquad (4.22)$$

where the axis of the beam in the position of equilibrium is represented as x and an axis perpendicular to it and parallel to the plane of symmetry as y. Furthermore, t = time, ρ = density, E_d = modulus of elasticity, η_d = viscosity coefficient, and k^2 = moment of inertia of the cross section.

When the Eq. (4.22) is solved so as to satisfy the boundary conditions at the free end, the formulas for the dynamic modulus of elastisity and viscosity coefficient are obtained.

$$E_d = \{(4\pi^2 \ell^4 \rho)/(m^4 k^2)\} f_0^2 \qquad (4.23)$$

where the secondary term is neglected because of its little effect. Furthermore, ℓ = the length of the beam, f_0 = resonant frequency (cycle/sec.), m = a factor which depends upon the mode of vibration; 4.7004 for the fundamental vibration of beam freely supported on both end.

$$\eta_d = \{(2\pi \ell^4 \rho)/(m^4 k^2)\} \Delta f \qquad (4.24)$$

where η_d : viscosity coefficient (poise), $\Delta f = f_2 - f_1$, f_1, f_2 = frequencies on either side of resonance at which the amplitude of vibration is 0.707 times the maximum.

Since the diameter of the cylinder (7.5 cm in diameter, 15 cm in height) used in this investigation is not small compared with its length, the dynamic modulus of elasticity should be modified using a factor (T') expressed by Eq. (4.25).

$$T' = T[\{1 + (0.26\nu + 3.22\nu^2)(k/\ell)\}/\{1 + 0.1328(k/\ell)\}] \qquad (4.25)$$

where T = a factor which depends upon the value of k/ℓ; 2.11 for the specimen of 7.5 cm in diameter and 15 cm in height, ν : Poisson's ratio (1/7 for the soil-cement specimen in this experiment)

Eq. (4.23) and Eq. (4.24) are transformed into more convenient forms;

$$E_d = k_1 W f_0^2 \qquad (4.26)$$

where $k_1 = 3.676 \times 10^{-3}$, E_d: kg/cm^2, W = the weight of a specimen(kg), f_0: cycle/sec.

$$\eta_d = k_2 W \Delta f \tag{4.27}$$

where $k_2 = 0.2728$, W; the weight of a specimen(kg), Δf: cycle/sec., η_d: poise

Energy Loss due to Internal Friction

A part of mechanical energy applied to a viscoelastic body is changed into thermal energy. When a sinusoidal stress is applied to Kelvin body, the energy loss per one cycle is as follows:

$$H = \pi \eta_d w \gamma_0^2 = \pi C \gamma_0^2$$

where $C = \eta_d w$, H = energy loss per one cycle, γ_0 = the maximum amplitude, w = angular frequency.

Therefore, a factor of C can be regarded as a constant which is proportional to the energy loss per one cycle. For the transversal vibration, the value of C can be computed according to Eq.(4.28).

$$C = 2\pi k_2 W f_0 \Delta f \tag{4.28}$$

The logarithmic decrement (δ) was determined as follows:

$$\delta = \pi \Delta f / f_0 \tag{4.29}$$

Therefore, the following relation between δ and C should hold.

$$\delta = \pi C / E_d \tag{4.30}$$

That is to say, δ can be regarded as a measure of the ratio of the energy loss due to internal friction to the elastic strain energy stored during one cycle.

(3) Results and Discussions

I) The Mechanism of Creep in Soil-Cement

Fig. 4.21 shows an example of creep strain-time curve. The total creep deformations are separated into the recoverable (ε_{cr}) and irrecoverable component (ε_{ci}) as follows: The recoverable creep strain was determined by measuring the increasing elongation of a specimen immediately after the time at which a constant load had been released (after the loading of 100 days). Further, the differnce between the total and recoverable creep gave the irrecoverable component.

The ε_{cr}-$\dot{\varepsilon}_{cr}$ and ε_{ci}-$\dot{\varepsilon}_{ci}$ curves obtained are shown in Fig. 4.22 (a), (b) and (c). Furthermore. the values of ultimate creep strain (ε_{cu}) and model constants (α_1, τ_1, α_2, τ_2, α_3 and τ_3 for the soil S_6-cement mixture can not be determined because none of their ε_{ci}-$\dot{\varepsilon}_{ci}$ curves satisfy the assumption ($\alpha_3/\tau_3 << \alpha_1/\tau_1$) made on determination of these constants (Fig. 4.22 (c)).

There are two linear parts in the ε_{cr}-$\dot{\varepsilon}_{cr}$ curve of the soil-cement made using a soil composed of approximately 80 percent sand (>74μ)(Fig. 4.22 (a)). This behavior conflicts with the concept that the recoverable creep mechanism is responsible only for "delayed elastisity". The recoverable creep of the soil-cement seems responsible not only for "delayed easticity" of the skeleton part, but also for the other cause

having a different retardation time. This cause would be attributed to the absorption of moisture from the atmosphere. Thus, a part of the consolidetion mechanism may be reversible, although it is assumed that a Kelvin element (III) represents "consolidation" effects of irrecoverable pore water motion towards the surface and resulting in subsequent evaporation. In this table, the constants having the larger retardation time are noted as α_2, τ_2; the smaller one as α_2', τ_2'.

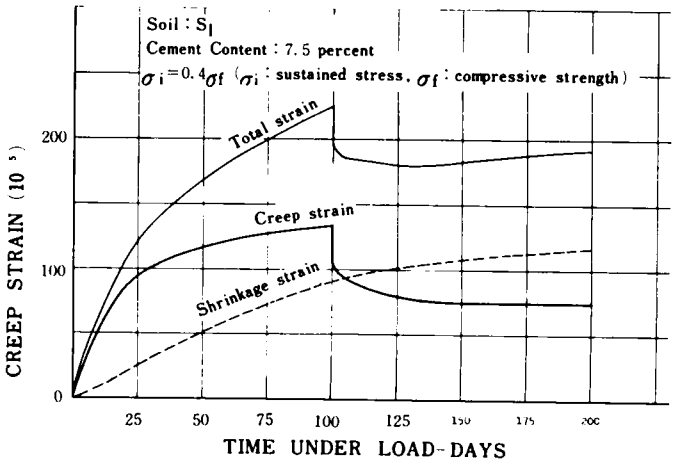

Fig · 4.21 Creep curve obtained with 10×30 cm cylinders stressed at 40 percent of 7 day age compressive strength.

On the contrary, in the soil S_4- and soil S_6-cement mixtures, plotting ε_{cr} against $\dot{\varepsilon}_{cr}$ generates only one straight line. There appears no recoverable component having the larger retardation time which is found in soil S_1-cement mixtures. This may show that almost of the recoverable creep in such soil-cement is due to "absorption of moisture". As shown in Table 4.6, the retardation time (τ_2') of the recoverable creep in soil S_4- and soil S_6-cement is somewhat greater than that in soil S_1-cement. Thus, the creep recovery due to moisture absorption in the soil-cement containing the greater amount of silt is found to occur over during the longer period after release of load.

The constants α_1 and τ_3 representing the irrecoverable creep characteristic of soil S_1-cement mixture are considerably greater than α_3 and τ_1, respectively. That is, the irrecoverable creep deformation of the soil S_1-cement during the initial stage would mainly be caused by internal, partially destructive readjustment within the granular mass of the soil-cement, followed by gradually increasing consolidation effects due to pore water motion towards the surface of the specimens.

The constants α_1 and τ_1 in the soil S_4-cement are several times α_3 and approximately equal to τ_3, respectively. The addition of 25 percent silty clay to the original soil sample S_1 increases the retardation time of the mechanism due to internal, partially destructive effects. Further addition of 50 percent silty clay brings about a substantial change in the ε_{ci}- ε_{ci} curves. The difference in the tendency of the ε_{ci}-$\dot{\varepsilon}_{ci}$ curves between soil S_1-cement and less silt included-soil S_4 and S_6-cement mixtures suggests that the structure of the former is quite different from that of the latter two mixtures. There probably seem to exist a comparatively great volume fraction of clay pockets in the soil S_6-cement.

With regard to the effect of the sustained stresses, both of the constants α_1 and τ_1 are almost independent of the stresses in the range of 0.2 to 0.6 σ_f (σ_f: unconfined compressive strength). However, the constants α_1 and τ_1 obtained from the creep tests carried out under an extremely high compressive stress (0.8 σ_f) are considerably great compared with others (Table 4.6). Although the irrecoverable creep mechanism due to internal, partially destructive effects is not substantially affected by the sustained stress level in the range of comparatively low stresses, the application of an extremely high sustained stress seems to cause a certain partial failure even in the skeleton phase which is relatively stable under lower stresses. Thus, generally speaking, creep characteristic of soil-cement may be highly dependent upon st-

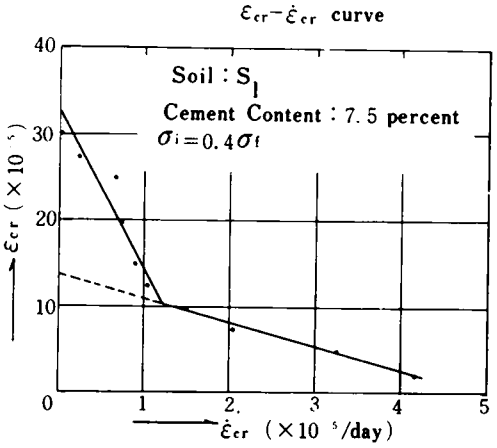

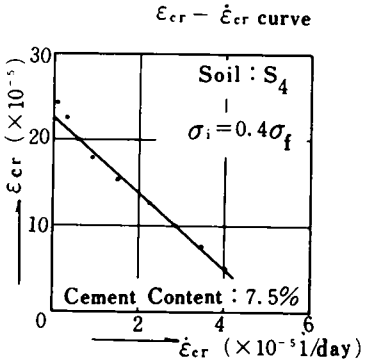

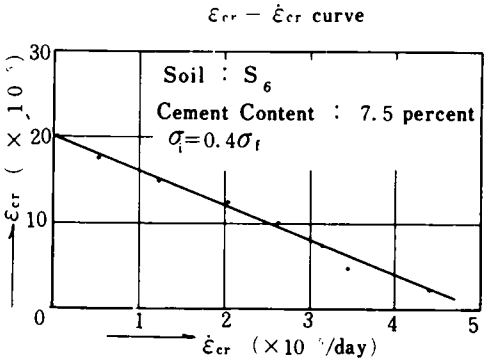

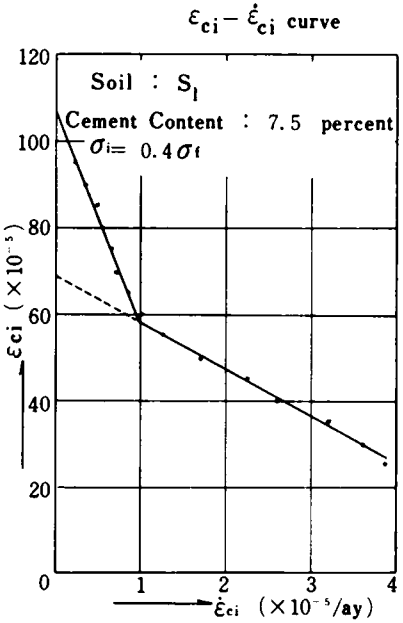

(a)

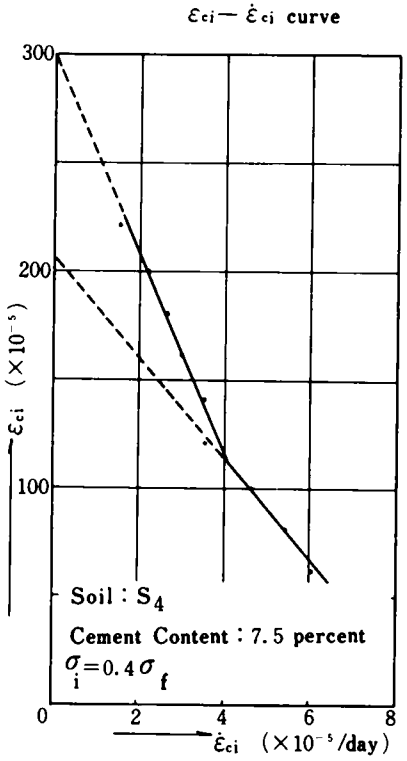

(b)

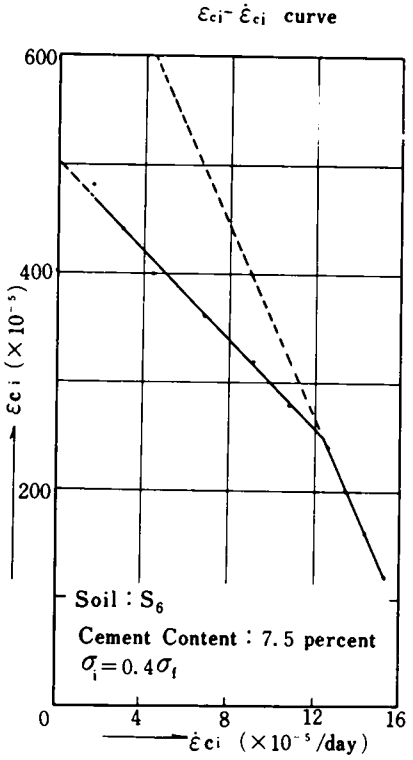

(c)

Fig. 4.22 $\varepsilon_{cr}-\dot{\varepsilon}_{cr}$ and $\varepsilon_{ci}-\dot{\varepsilon}_{ci}$ curves for soil S_1—cement ((a)), soil S_4—cement ((b)) and soil S_6—cement ((c))

Table 4.5 Mechanical model constants of granular soil-cement mixtures

Soils	Sustained stresses (kg/cm^2)	Consolidation		Breakedown		Recovery				ε_{cu} (10^{-5})	
		α_3 ($10^{-5}cm^2/kg$)	τ_3 (days)	α_1 ($10^{-5}cm^2/kg$)	τ_1 (days)	α_2 ($10^{-5}cm^2/kg$)	τ_2 (days)	α_2' ($10^{-5}cm^2/kg$)	τ_2' (days)	Total	Recovery
S_1	25.5 (0.4 σ_f)	1.51	39.2	2.71	10.8	0.74	15.3	0.54	2.7	158	31
S_1	25.5 (0.4 σ_f)	1.46	39.5	2.93	9.0	0.62	12.2	0.64	2.3	150	32
S_4	18.5 (0.4 σ_f)	6.38	32.0	13.51	36.0	—	—	1.42	6.8	322	26
S_4	18.5 (0.4 σ_f)	4.97	22.4	11.19	23.6	—	—	1.22	4.4	308	24
S_6	10.8 (0.4 σ_f)	—	—	—	—	—	—	2.06	4.0	625	22
S_6	10.8 (0.4 σ_f)	—	—	—	—	—	—	1.85	3.8	650	20

Cement content: 7.5 percent σ_f: Unconfined compressive strength at 7 days age, ε_{cu}: Ultimate creep strain

Tabel 4.6 Mechanical model constants of granular soil-cement mixtures

Soils	Sustained stresses (kg/cm^2)	Consolidation		Breakedown		Recovery				ε_{cu} (10^{-5})	
		α_3 ($10^{-5}cm^2/kg$)	τ_3 (days)	α_1 ($10^{-5}cm^2/kg$)	τ_1 (days)	α_2 ($10^{-5}cm^2/kg$)	τ_2 (days)	α_2' ($10^{-5}cm^2/kg$)	τ_2' (days)	Total	Recovery
S_1	12.7 (0.2 σ_f)	1.00	14.0	2.38	15.0	0.73	12.5	1.04	4.5	64	20
S_1	12.7 (0.2 σ_f)	0.43	12.8	2.90	13.7	0.82	20.1	1.24	4.7	68	23
S_1	25.5 (0.4 σ_f)	1.51	39.2	2.71	10.8	0.74	15.3	0.54	2.7	158	31
S_1	25.5 (0.4 σ_f)	1.46	39.5	2.93	9.0	0.62	12.2	0.64	2.3	150	32
S_1	38.2 (0.6 σ_f)	8.74	191.7	2.77	8.3	0.87	21.0	0.92	6.3	390	63
S_1	38.2 (0.6 σ_f)	10.94	216.8	2.72	11.2	0.80	19.6	0.89	5.8	415	59
S_1	51.0 (0.8 σ_f)	8.08	55.0	4.98	18.0	0.46	12.9	1.09	7.4	1280	78
S_1	51.0 (0.8 σ_f)	7.12	67.2	9.20	40.8	0.63	18.8	0.92	5.4	1310	76

Cement content: 7.5 percent, σ_f: Unconfined compressive strength at 7 cays age, ε_{cu}: Ultimate creep strain

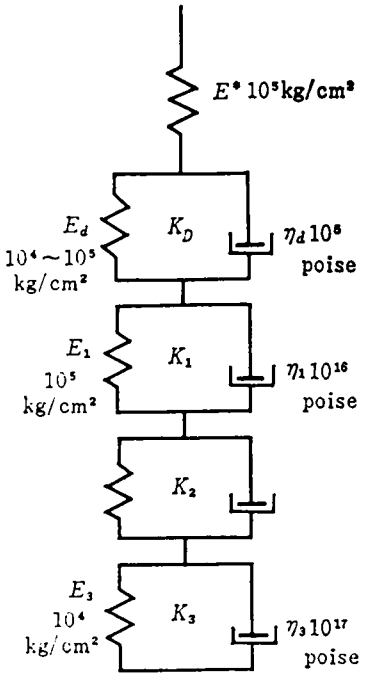

Fig. 4.23 Mechanical model

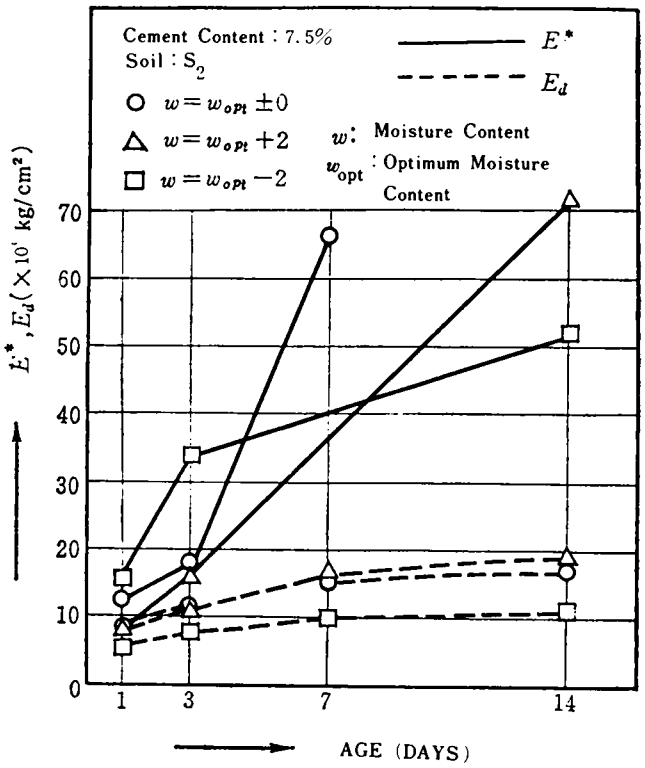

Fig. 4.24 Variation in Ed, E* with age

ress.

II) Characteristics of Damping of Vibration in Soil-Cement

Discussions on Modulus of Elasticity

Spring constants (E_1, E_2 and E_3) and viscosity coefficients (η_1, η_2 and η_3) of the mechanical model shown in Fig. 4.23 were determined by creep tests, as described above; they were of the order of 10^4 - 10^5 kg/cm^2 and 10^{16} - 10^{17} poise, respectively. The values of these viscosity coefficients are far greater than the dynamic ones, η_d (having the order of 10^5), which are determined by sonic test. None of these Kelvin elements (K_1, K_2 and K_3) having such great viscosity coefficients responds to vibraion applied in sonic test. In this section, in order to discuss the relation between the static (E_s) and dynamic modulus of elasticity (E_d) in soil-cement mixtures, another combination of one Kelvin element (K_D) and one Hooke element (H) in series is used; their model constants are noted as E^*, E_d and η_d, as shown in Fig. 4.23.

The stress(σ)-strain(ε) relationship in this model is expressed as follows:

$$\varepsilon = \sigma\{(1/E^*) + (1/E_d)(1 - e^{-t/\tau_d})\} \qquad (4.31)$$

where $\tau_d = \eta_d/E_d$

It is impossible to determine model constants E^*, E_d and η_d by the vibration analysis of such a model. Assuming that the value of the constant E^* is several times that of E_d, E_d and η_d could approximately be

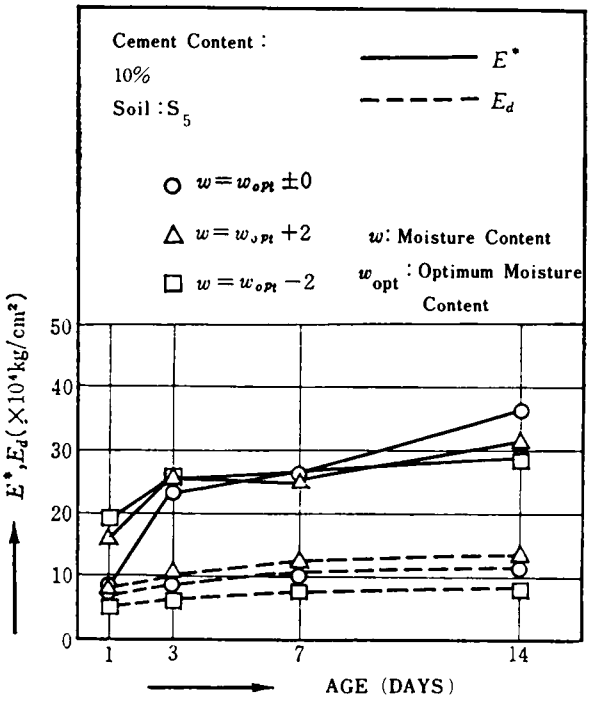

Fig. 4.25 Variation in Ed and E* with age

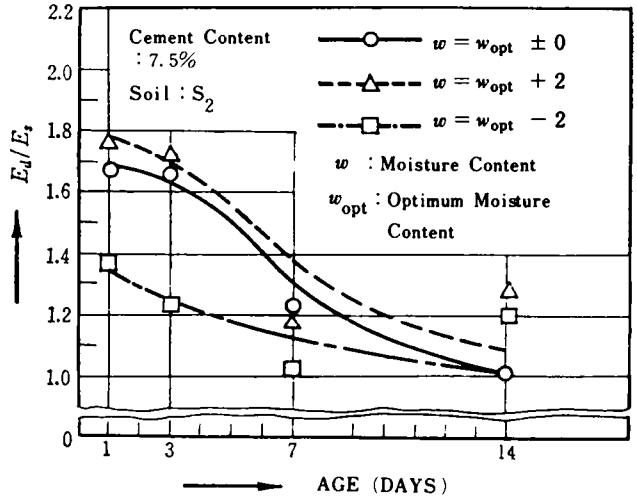

Fig. 4.26 Variarion in Ed/Es with ages

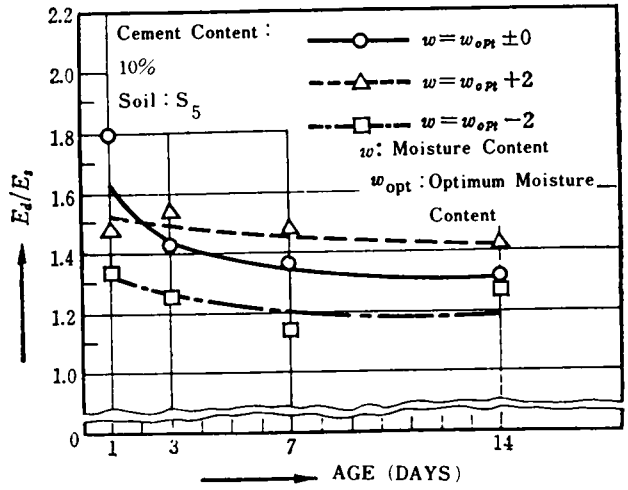

Fig. 4.27 Variation in Ed/Es with age

determined by the vibration analysis of a viscoelastic beam previously described. The e^{-t/τ_d} term in Eq. (4.31) can be neglected in the short-term loading test for determining the static modulus of elasticity, because the retardation time (τ_d) of the K_D element is extremely small, only 10^{-6} second more or less, according to the sonic test results obtained.

When the static modulus of elasticity[¶] (E_s) is taken as the initial tangent of the stress-strain curves obtained in the short-term loading tests for a body of which mechanical behavior can be represented by the model indicated in Fig. 4.23, Eq. (4.32), Eq. (4.33) and Eq. (4.34) are given.

$$\varepsilon = \sigma\{(1/E^*) + (1/E_d)\} = \sigma(1/E_s) \tag{4.32}$$

$$(1/E_s) = (1/E^*) + (1/E_d) \tag{4.33}$$

$$(E_d/E_s) = (E_d/E^*) + 1 \tag{4.34}$$

The moduli of E_d and E^* increase with increasing curing time, as shown in Fig. 4.24 and Fig. 4.25. Further, the E_d/E_s vs. ages relationships are presented in Fig. 4.26 and Fig. 4.27. The less the moisture content of specimens, the smaller the value of E_d/E_s in all ages (1 - 14 days ages). The E_d/E_s value of soil S_2-cement mixture rapidly approaches unity eith increasing curing time; the value of E_d/E^* rapidly decreases (see Eq. (4.34)).

The soil S_5-cement is approximately equal to the soil S_2-cement in the E_d/E_s value at the initial ages of 1 and 3 days. Thereafter, however, the E_d/E_s values of the soil S_5-cement are followed by a relatively slow reduction with ages, indicating the high value (1.2 to 1.4) even at 7 and 14 days of curing. Further , the E^* value of the soil S_5-cement more slowly increases with curing time compared with that of the soil S_1-cement. Thus, the addition of silt affects the characteristic of the changes in the value of E^* and E_d/E_s with ages. Especially, the E^* value is highly reduced by the addition of a silty clay; its development with curing time is singificantly retarded (Fig. 4.25).

The E^* is likely to give an indication of elasticity of a skeleton phase which also plays a predominant role in the strength of the soil-cement. It may be the skeleton phase composed of cement gel and/or calcium silicate hydrates and only sand particles (>74 μ) that exists in the soil-cement made using a sandy soil S_2. However, there must be the other type of skeleton phase made up of cement gel and/or calcium silicate hydrates and silt particles (<74 μ) in the soil S_5-cement. The modulus of elasticity of the former would be extremely high in comparison with that of the latter.

Discussions on Characteristic of Damping of Vibration

a) Changes in the Value of C and δ with Ages

Both values of C and δ decrease with ages (Fig. 4.28 and Fig. 4.29). This indicates the decrease in the energy loss due to internal friction among the soil particles. Such decrease in energy loss may be brought about by gradually strengthening the bonding of soil particles with calcium silicate hydrates resulting from the cement hydration and the secondary $Ca(OH)_2$-silicates interaction. The greater value of δ and C in the soil S_5-cement than in the soil S_2-cement evidences the presence of the greater amount of

¶ The tangent modulus of elasticity at stress zero(E_s) was determined by the extrapolated intercept of the stress(σ) vs. tangent modulus(E) curves with E-axis.

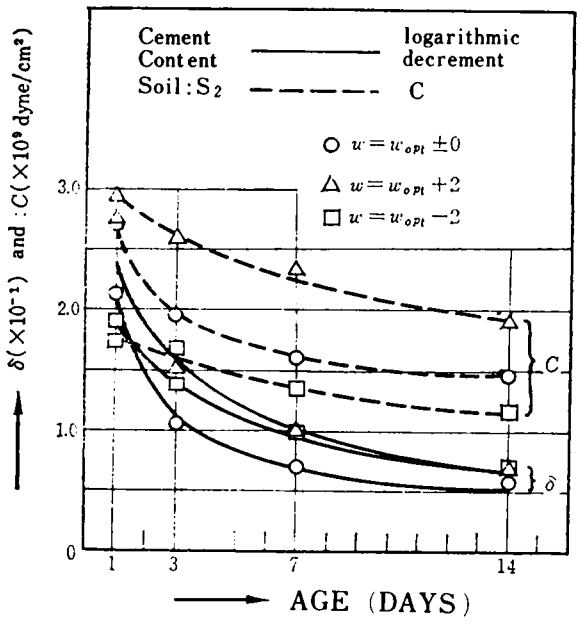

Fig.4.28 Variation in δ and C with age

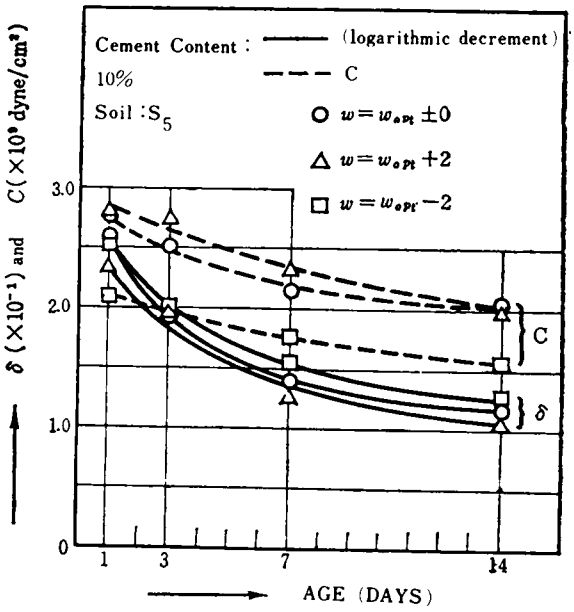

Fig. 4.29 Variation in δ and C with age

the unbonded soil particles; the reduction in the value of δ with cement content could also be explained in the same manner (Fig. 4.30).

b) Influence of Moisture Content on the Value of δ and C

The value of C and δ in the soil S_5-cement mixtures increases and decreases, respectively, as their moisture content increases (Fig. 4.29). The presence of a certain amount of clay pockets in the soil S_5-cement is presumed, as described above. Therefore, it is found that the higher the moisture content of the clay pockets phases, the greater the energy loss due to this phase.

The tendency found in the δ vs. moisture content relation is completely contrary to that in the C vs. moisture content relation. This phenomenon could be interpreted by the fact that the increase in the E_d value accompanying with increasing moisture content exceeds the increase in the energy loss due to internal friction(C), because δ can be regarded as a measure of the ratio of the energy loss(C) to the elastic strain energy (E_d).

According to the vibration analysis for the system of one Hooke-one Kelvin element combination in series, the following expressions are derived (Kosaka, 1959)(Kolsky, 1963):

$$\delta = \pi C(E_s/E_d^2) \qquad C/E^* << 1 \qquad (4.35)$$

$$\delta = \pi(E^*/C) \qquad C/E^* >> 1 \qquad (4.36)$$

The C/E^* value of soil-cement is about 10^{-3}. Therefore,

$$\delta_B = \delta_K(E_s/E_d) \tag{4.37}$$

where δ_K = the logarithmic decrement in Kelvin body

δ_B = the logarithmic decrement in the one Hooke-one Kelvin element combination system

Consequently, the strict solution of the vibration analysis of one Hooke-one Kelvin element system is found to give the smaller value of δ, because the E_s/E_d value is usually smaller than unity (Eq.(4.37)).

The δ value of the soil S_2-cement mixture at 1 day curing is great in the order of increasing moisture content. However, such order is reversed in the course of curing until 14 days age (Fig. 4.30). The energy loss due to anelasticity in soil S_2-cement mixtures as well as in soil S_5-cement mixtures decreases, as their moisture content decreases. However, the higher the moisture content, the greater the increasing rate of the E_d value with ages in the former, compared with the latter. This fact suggests that there would be a considerable difference between their structures.

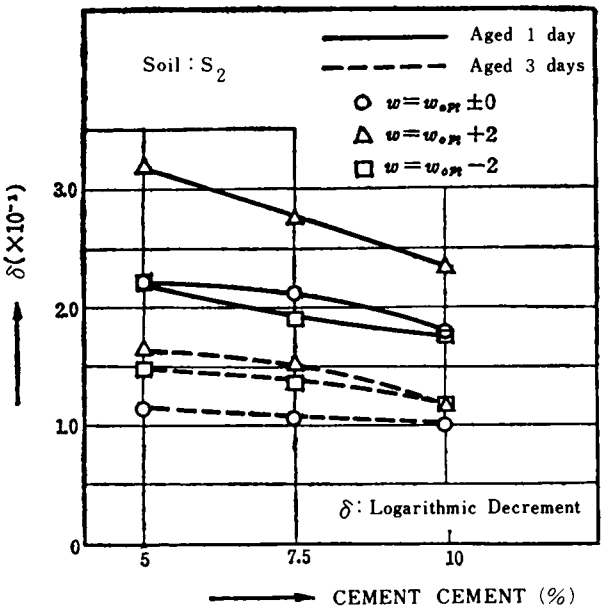

Fig. 4.30 Relationship between logarithmic decrement and cement content

III) Influence of Silt Content and Clay Pockets on Burgers Model Constants

Burgers model constants of soil S_1-, soil S_4- and soil S_6-7.5 percent cement mixtures are repre-

Table 4.7 Burgers model constants of granular soil-cement mixtures

Model Constants	Soil S_1-cement	Soil S_4-cement	Soil S_6-cement
E_1 (10^4 kg/cm^2)	6.69	5.19	2.89
η_3 (10^7 kg day/cm^2)	0.977	0.542	0.092
E_2 (10^4 kg/cm^2)	2.51	0.790	0.252
η_2 (10^5 kg day/cm^2)	2.07	1.89	0.224

Table 4.8 Ratios of Burgers model constants in granular soil-cement to the comparable ones in clay lumps-cement mixtures

Model Constants	Soil S_1-cement	Soil S_4-cement	Soil S_6-cement
E_1	5.9	4.6	2.6
η_3	90	50	8.5
E_2	24	7.5	2.4
η_2	44	39	4.7

sented in Table 4.7 (the sustained stress $\sigma_i = 0.4\ \sigma_f$). The value of E_1 and η_2 proportionally decreases, as the amount of a silty clay added increases. However, as indicated in Table 4.7, the reduction rate of the value E_2 and η_2 is not proportional to the amount of the clay added.

These results would be compared with those of clay lumps-cement mixtures in the following.

Table 4.8 shows the ratios of Burgers model constants in granular soil-cement to the corresponding constants (the average of all data) in clay lumps-cement mixtures.

It should be noted that the ratios in the creep viscosity coefficient(η_3) are remarkably high compared with the ratios in the instantaneous modulus of elasticity(E_1). Such a little difference in the value E_1 reveals that clay lumps-cement mixtures have comparatively similar skeleton phase to that in granular soil-cement in their elastic properties, since the value of E_1 predominantly depends upon the elasticity of the skeleton phase. On the other hand, great difference in the creep viscosity may possibly be attributed to the effect of clay pockets. That is, a considerably great volume fraction of clay pockets in clay lumps-cement mixtures plays a significant part in decreasing their creep viscosity, though their skeleton phase is so rigid as to compete with that of granular soil-cement.

Moreover, a significant decrease in the value η_3 accompanying with the addition of a silty clay(S_3) suggests the presence of a considerable amount of clay pockets in the soil S_6-cement mixture.

(4) Summary and Conclusions

Several viscoelastic properties of granular soil-cement mixtures were investigated by the creep test and the sonic test. Consequently, it was found that the viscoelastic properties of the soil-cement made using a soil including much silt fraction were substantially different from those the sandy soil-cement with less silt. Changes in the viscoelastic properties of granular soil-cement with increasing silt fraction in soils used are summarized as follows:

1) The recoverable creep of the soil-cement made using a soil composed of approximately 80 percent sand seems responsible not only for "delayed elasticity" of the skeleton part, but also for the absorption of moisture from atmosphere. However, almost of the recoverable creep in the soil-cement with much silt may be due only to "absorption of moisture".

2) An analysis of the creep tests results suggests that there seem a relatively great volume fraction of

clay pockets in the soil-cement made using a soil with much silt.

3) Creep characteristic of soil-cement may be highly dependent upon stress.

4) The addition of silt to the soil material affects the characteristic of the changes in the value of E^* and E_d/E_s with ages. Especially, the E^* value is greatly reduced by the addition of a silty clay.

5) The energy loss due to anelasticity in soil-cement mixtures decreases, as their moisture content decreases.

6) Clay lumps-cement mixtures have comparatively similar skeleton phase to that in granular soil-cement in their elastic properties.

7) A considerably great volume fraction of clay pockets in clay lumps-cement mixtures plays a significant part in decreasing their creep viscosity, though their skeleton phase is so rigid as to compete with that of granular soil-cement.

5. SUMMARY AND CONCLUSIONS

The objictive of this chapter is to elucidate the relationship between the viscoelastic properties and the comparatively macroscopic structure in soil-cement. In this paper, among a great number of factors controling the internal structure of soil-cement, size and moisture content of clay lumps, and the amount of silt included in the granular soil used are dealt with.

The creep and sonic tests results indicate that the viscoelastic properties of soil-cement are greatly affected by volume fraction and moisture content of clay pockets in the soil-cement specimens. The volume fraction of clay pockets gradually changes during the periods of curing, so that the volume fraction of skeleton parts increases. Naturally, no clay pockets would be present in the soil-cement made using a soil composed of more than 80 percent sand. The viscoelastic behavior of such soil-cement mixtures is substantially different from that of the soil-cement with clay pockets. Thus, grain size of soil material and, size and moisture content of clay lumps are significant factors to control the macroscopic structure and mechanical properties of soil-cement. Therefore, it may be significant to discuss what structure of soil-cement is more capable of withstanding shrinkage cracking, considering its shrinkage characteristics discussed in the next chapter.

REFERENCES

Alfrey, T. and Doty, T. (1945): J. Appl. Phys. 16. 700

Davidson, L.K., Demirel, T. and Handy, R.L. (1965): "Soil Pulverization and Lime Migration in Soil-Lime Stabilization", Highway Research Record No. 92, pp. 103 - 126

Dunlop, R.J. (1970): "Laboratory Testing for Cement and/or Lime Stabilization of Soils" Personal Communication

Dunn, Francis Patrick (1960): "The Effect of Sustained and Repeated Loads on Soil-Cement, and an Analysis of its Viscoelastic Behavior", Thesis, M.S. Degree, Ohio Univ., Columbus, 85 pp

Freudenthal, A.M. and Roll, Frederic (1958): " Creep and Creep Recovery of Concrete Under High Compressive Stress", Proc. ACI Vol. 54, June, pp. 1111 - 1142

George, K.P. (1969): "Cracking in Pavements Influenced by Viscoelastic Properties of Soil-Cement", Highway Research Record 263, pp. 47 - 59

Hasaba, S. and Kawamura, M. (1968): "Disintegration of Cohesive Clay Lumps Used as Soil-Cement", Transactions of the Japan Society of Civil Engineers No. 155 (in Japanese), pp. 25 - 31

Hasaba, S., Kawamura, M. and Ofuka, N. (1970): "The Influence of Disintegration of Clay Lumps on Shrinkage Characteristics and Viscoelastic Properties of Soil-Cement Mixtures", Proc. the Japan Society of Civil Engineers No. 177 (in Japanese), pp. 33 - 42

Horio, M. and Onogi, S. (1951): "Forced Vibration of Reed as a Method of Determining Viscoelasticity", Jour. Applied Phys. 22, p. 977

Kolsky, H. (1963): " Stress Wave in Solids", Dover

Kosaka, Y. (1961): "A Study on Decrement Characteristic of Vibration in Mortar", Transactions of the Architectural Institute of Japan (in Japanese) No. 63

Lorman, W.R. (1940): "The Theory of Concrete Creep", Proc. ASTM, Vol. 40, pp. 1082 - 1102

National Academy of Science (1961): "Soil Stabilization with Portland Cement", H.R.B. Bull. 292, pp. 14 - 15

Ogishi, S. (1963): "On the Rheological Behavior of Hardened Concrete (Report No. 2)" Transactions of Architectural Institute of Japan No. 86, pp. 1 - 6.

Okada, K. and Kawamura, M. (1964): "Some Considerations of Load Deformation Characteristics of Soil-Cement ", Journal of the Society of Material Science, Japan (in Japanese) Vol. 13, No. 132, Sep. pp. 705 - 710

Okada, K. and Kawamura, M. (1965): "Vibrational Characteristic of Soil-Cement", Journal of the Japan Society of Civil Engineers (in Japanese) Vol. 50, No. 10, pp. 28 - 34.

Okada, K. and Kawamura, M. (1967): "Some Considerations on Drying Shrinkage Stresses of Soil-Cement", Transactions of the Japan Society of Civil Engineers (in Japanese) No. 142, pp. 37 - 45

Sawaragi, Y. and Tokumaru, H. (1955): "On the Distribution Functions Characterizing the Mechanical Behavior of the Linear and Non-Linear Visco-elastic Bodies", Journal of the Japan Society of Aeronautical Engineering (in Japanese) Vol. 2, No. 12, pp. 317 - 322

Tanaka, A. (1959): "Applied Mathematics" (in Japanese)

CHAPTER IV SHRINKAGE CHARACTERISTICS AND SHRINKAGE STRESSES IN SOIL-CEMENT

1. INTRODUCTION

The mechanism of shrinkage in soil-cement has little been revealed. Further, there seems no definite explanation for shrinkage cracking as well. However, shrinkage cracking of soil-cement pavements is recognized as a serious problem. The prevention against shrinkage cracking is indispensable for a more extensive use of soil-cement. As described in the introduction of the preceding chapter, shrinkage cracking of a material depends greatly upon its shrinkage characteristics and mechanical properties. Hence, in order to "design" a material so as to reduce its shrinkage cracking, its structure-mechanical behavior and -shrinkage characteristics relationships are the fundamental problems to be disclosed.

The relationship between the macroscopic structure and viscoelastic properties in several soil-cement mixtures has been discussed in the preceding chapter.

In this chapter, first, the effect of clay pockets on the shrinkage characteristics will be discussed.

When the shrinkage tensile stress on the exposed surface of soil-cement mass exceeds the ultimate tensile strength of the material, surface cracking occurs. Theoretical estimation of the shrinkage stress in soil-cement involves great difficuties because of its non-linear viscoelasticity.

In paragraph 4 of this chapter, an attempt will be made experimentally to estimate the stress, supposing that the progress of drying shrinkage in soil-cement can be represented by the diffusion equation. The changes in the shrinkage characteristics and stresses of sandy soil-cement with increasing silt fraction will also be discussed.

The formulas for shrinkage stresses in the viscoelastic body (Burgers body) such as concrete and soil-cement show that the shrinkage stress on the exposed surface of such a viscoelastic beam (or slab) is proportional to the value of $E_1 S_\infty$ (S_∞: the ultimate shrinkage strain)(Kawamura, 1969). In the last paragraph , basing on the formulas, a consideration is given on the relationship between shrinkage cracking and the factors influencing the structure of soil-cement.

2. REVIEW OF THE LITERATURES

Although shrinkage cracking is considered to be a very serious problem in soil-cement pavements, only a few studies have been reported. Especially, the paper by Okada and Kawamura (1967), on which a part of this chapter is based, appears the first to discuss problems on shrinkage cracking in soil-cement.

In this paragraph, to begin with, George's papers recently published, in which shrinkage characteristics and cracking are discussed from the different aspects from this paper, will be reviewed. Nagayama and Handy's report (1965) is also stated. Further, it may be expected that the formulas for shrinkage stresses in linear viscoelastic body recently derived by the auther may be used for estimating the shrinkage cracking in soil-cement. Finally, a comparison of the formulas with George's concept is made.

George made an attempt to explain the shrinkage in soil-cement by capillary tension, liquid adsorption and lattice shrinkage (George, 1968a). The shrinkage of sandy soil-cement would be caused by the different mechanism from that of clayey soil-cement including a great amount of clay fraction (<5 μ), because the former may be responsible primarily for the shrinkage of cement paste phase involved and the latter predominantly for the shrinkage of the clay-water system.

He states that, since the loss of moisture is the primary reason for shrinkage, cement hydration causes a kind of self-desiccation and shrinkage; further, he evidenced this hypothesis by the experimental result that the waxed beam shrank without any appreciable loss of water. It was concluded that whereas the sh-

rinkage of clayey soil was primarily a function of the fine fraction in the soil, this was not true of sands and sandy soil, where the main reason was probably due to shrinkage of the hydrated cement paste.

According to Nakayama and Handy's study (1965), montmorillonitic clay in a mix greatly increased total shrinkage, kaolinitic clay increased shrinkage less. They concluded that minimization of shrinkage required reduction of the initial water content and, more important, the amount of clay.

George's concepts (George, 1969) regarding to shrinkage cracking in soil-cement pavements will be summarized in the following.

Basing on the concept that, cracks are formed, when the tensile stresses set up in cement-treated base slabs due to the restraint resulting from the friction between the slab and subgrade exceed the tensile strength of the material, he derived the formulas for determining crack width and crack spacing. According to the formulas, the crack spacing(L) is influenced by the tensile strength, the coefficient of sliding(μ) and specific weight of the material(γ); the crack width, primarily a function of the total maximum shrinkage, is to some degree influenced by μ, γ, L and the modulus of elasticity in tension. So far as crack width was concerned, however, the agreement between the predicted and observed values was extremely poor. He considered that such disparity in results could be attributed to the fact that in deriving these formulas, it was tacitly assumed that cement-treated soil was perfectly elastic. Then, he discusses the crack width and spacing assuming that the stress-strain behavior of the material can reasonably be represented by Burgers model, concluding that the viscous properties of soil-cement are important in reducing crack width. Further, the conclusions were drawn that stress computed according to viscoelastic theory was on the avarage 50 percent smaller than that computed by the elastic theory and that insofar as the rate of shrinkage was concerned, rapid shrinkage caused larger stresses.

Thus, George's discussions are based on the tensile stresses caused by restraining the average shortening per unit length due to shrinkage in base slab. However, the shrinkage stress in soil-cement slab is not uniformly distributed over a longitudinal cross section. Such shrinkage stress distributions in concrete beam (or slab) were discussed in detail by Pickett (1946a)(1946b). Further, the shrinkage distribution across a cross section of a drying concrete mass has also been experimentally confirmed by some investigators.

Recently, following Pickett's theory, formulas for shrinkage stresses in linear viscoelastic bodies represented by Burgers model were derived by the auther(Kawamura, 1969). From the discussion of an example of shrinkage stresses computed using the formulas derived, the following conclusions can be drawn:

1. The tensile shrinkage stresses on the exposed surface of a concrete beam drying from one face only have the maximum value at the initial time of drying (1 to 2 days), followed by the comparatively rapid decrease, irrespective of the condition of restraint.
2. The computed results show that the maximum shrinkage stress is about $0.3\ E_1 S_\infty$.

Thus, it may be assumed that the behavior of shrinkage stresses varies with Burgers model constants and shrinkage characteristics of a given material. It is definitely concluded that shrinkage cracking characteristics greatly depend upon the product of the tensile modulus of elasticity and ultimate shrinkage strain, and upon the tensile strength.

3. INFLUENCE OF "CLAY POCKETS" ON SHRINKAGE CHARACTERISTICS OF SOIL-CEMENT MIXTURES

(1) Outline of Experiments

Materials and their Mix Proportions

Cement used is normal portland Cement. Cohesive clayey soil is from Utatsuyama hill in Kanazawa; its physical properties are shown in Table 4.1 (see p. 75). Cement content is 10 percent by weight of dry soil; moisture content the optimum moisture content (31.5 percent) is determined basing on JIS A 210.

Preparation of Cohesive Clay Lumps Sample

See CHAPTER III, Paragraph 3 (p. 73).

Preparation of Soil-Cement Specimens

The 10 by 10 by 40 cm test beams were prepared. The mixture was placed in the prism mold in two layers. Each layer was rodded 150 times. The direction of the compaction with a rod is perpendicular to the direction of the shrinkage measurement. As to mixing of materials and to the determination of compactive effort, see CHAPTER III, Paragraph 3 (p. 75).

Curing Condition of Specimens and Condition of Surrounding Atmosphere in Shrinkage Test

All of specimens tightly closed with polyehtylene sacks were cured for 7 and 28 days in the moist room in which the temperature was maintained at 20° C until the shrinkage measurements were initiated. The relative humidity and the temperature of the environment in shrinkage test were 85 ± 2 percent and 20° C, respectively.

Procedure of Shrinkage Test

The Berry strain meter was used to determin drying shrinkage of the beams with 30 cm gage length. Immediately after the completion of the curing, the specimens were exposed to the atmosphere. Each type of specimens were made in duplicate; the experimental results are their average.

(2) Analysis of Test Results

In order to characterize the shrinkage (ε_s) vs. drying time (t) curves of the specimens, the hyperbolic assumption expressed by Eq. (5.1) was made.

$$\varepsilon_s = S_\infty t/(n + t) \tag{5.1}$$

where S_∞: ultimate shrinkage, n: the time at which 50 percent of the ultimate shrinkage is obtained.

The Eq. (5.1) is transformed into;

$$t = vS_\infty - n \tag{5.2}$$

where $v = t/\varepsilon_s$

(3) Result and Discussion

The $v(=t/\varepsilon_s)$ vs. t relations are approximately linear in concrete and sandy soil-cement cured in the moist atmosphere before testing, while a plot of v against t in clay lumps-cement mixtures gives more complex curves as schematically drawn in Fig. 5.1, especially in the initial stage of drying time. During the initial drying periods, the shrinkage-time curves in clay lumps-cement have four periods of time during which shrinkage rate is different. For example, a v-t curve of the mixture (7 days age) made using the clay sample with the 30 percent moisture content and with specific surface of 74.7 cm^2/cm^3 is shown in Fig. 5.2.

Shrinkage (ε_s) in the primary period proceeds in the form of hypabolic function with increasing drying time. The secondary is transient period followed by the tertiary period during which shrinkage rate is constant. The last period has the same hyperbolic ε_s - t curve as the primary period. The constants S_∞

and n obtained from the slope and intersection of the plotted line in the last period and the shrinkage rate (k_0) in the tertiary period are shown in Fig. 5.3 and Table 5.1.

The influence of the lumps size (specific surface, see CHAPTER III p. 74) and moisture content on the shrinkage characteristics would be discussed on the basis of these data.

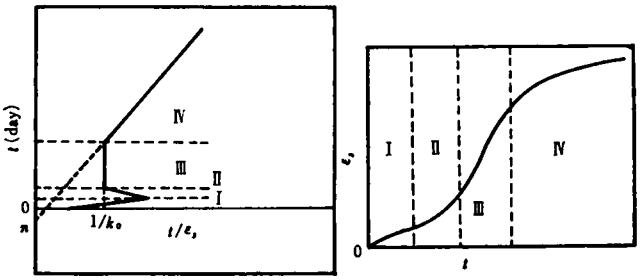

Fig.5.1 Schematic diagram for the progression of shrinkage strain (ε_s) with drying time (t)

Relationship between Physical Properties of Clay Pockets and Ultimate Shrinkage

The ultimate shrinkage of the 10 percent moisture content clay lumps-cement cured for 7 days decreases with increasing specific surface of clay samples used (Fig.5.3(a)), while that of the zero percent moisture content clay lumps-cement is independent of specific surface.

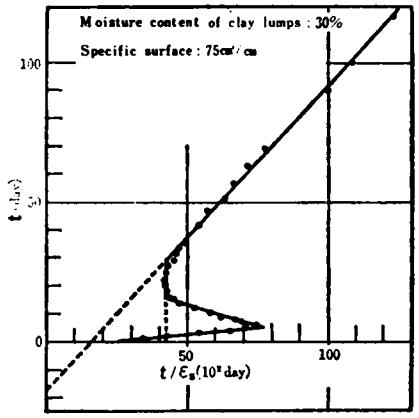

Fig.5.2 An example of the relationship between drying time (t) and t/ε_s (ε_s : shrinkage strain)

In general, the shrinkage characteristics of clay lumps-cement mixtures are considered to be greatly influenced by the shrinkage of clay pockets distributed throughout the soil-cement mass and by their volume fraction. As suggested by the distribution funtions and examination of cross sections of specimens by naked eye (see CHAPTER III, p. 84), the volume fractions of clay pockets in the zero and 10 percent moisture content clay lumps-cement mixtures seem different for different size distribution of clay lumps samples used. It may be reasonable to suppose that the coarser the clay lumps sample used, the greater the volume fraction of clay pockets involved in the finished clay lumps-cement specimens after the cure of a given period. Therefore, the difference in the shrinkage characteristics between the zero and 10 percent moisture content clay lumps-cement can be attributed to the difference in the shrinkage of clay pockets between them. The shrinkage of clay pockets in the zero percent moisture content clay lumps-cement mixtures may be presumed to be so small as approximately to equal the shrinkage of the skeleton phase, compared with that in the 10 percent moisture content clay lumps-cement mixtures. This presumption could reasonably interprete the above fact that the ultimate shrinkage of the zero percent moisture content clay lumps-cement cured for 7 days is almost independent of specific surface.

The ultimate shrinkage of the 30 percent moisture content clay lumps-cement mixtures cured for 7 days is comparatively small compared with others (Fig. 5.3 (a)). As stated in the preceding chapter, the shape of the distribution functions of the 30 percent moisture content clay lumps-cement mixtures suggested that their structures become comparatively homogeneous, i.e. of less clay pockets during the cure of 7 days. Thus, even if the soil-cement specimens are made using the clay lumps samples with the specific surface of

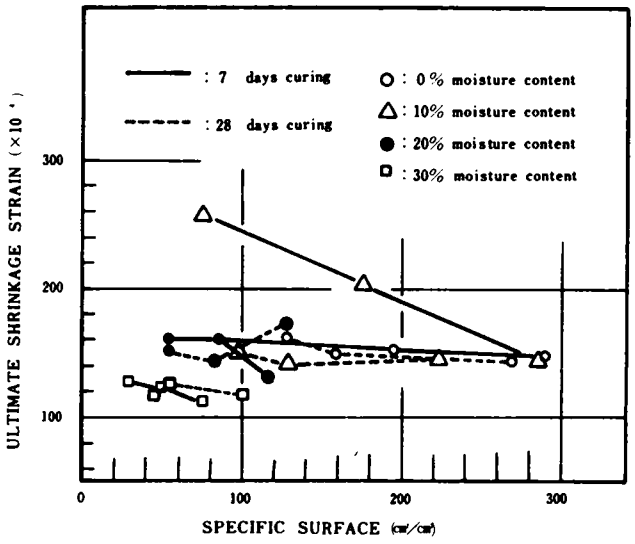

(a)

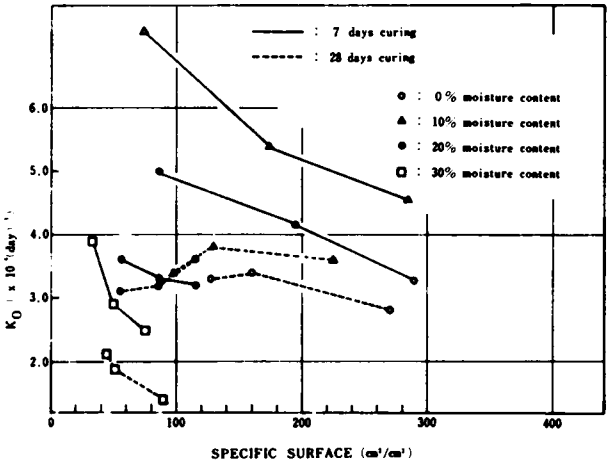

(b)

Fig. 5.3 Relationship between shrinkage characteristics of soil-cement ((a) : ultimate shrinkage strain, (b) : shrinkage rate (K_0)) and the specific surface of clay lumps sample used

Table 5.1 Relationship between n and the specific surface of clay lumps samples used

Moisture Content (%)	Specific Surface (cm^2/cm^3)	n (days)	Ages of Specimens (days)
0	86	5	7
	195	6	
	290	6	
10	75	12	7
	174	15	
	285	14	
20	56	18	7
	86	20	
	116	17	
30	33	12	7
	49	14	
	75	17	
0	128	20	28
	160	20	
	270	22	
10	98	19	28
	130	17	
	225	16	
20	56	24	28
	86	24	
	116	23	
30	45	28	28
	51	35	
	90	49	

about 80 cm^2/cm^3, the use of different moisture content clay lumps sample gives different shrinkages at 7 days age. However, the ultimate shrinkage of the 28 days age specimens is almost independent of the moisture content and specific surface of clay lumps samples used (Fig. 5.3 (a)). This tendency, further, may imply that the homogeneous sturcture is formed in the course of 28 days curing even in the mixture made using the zero percent moisture content clay lumps.

Consequently, it may be concluded that the degree of diffusion of calcium ions is also a significant factor affecting the shrinkage of clay lumps-cement mixtures. Therefore, in practice, the use of the clayey soil completely dried up or with considerably high moisture content (about 30 percent) appears to reduce ultimate shrinkage, even if clay lumps included in the soil are to only a little degree disintegrated. However, the shrinkage of soil-cement made using the moderate moisture content clay lumps, such as 10 percent, can not be reduced without disintegrating the original clayey soil lumps into considerably fine clay lumps samples.

There is the ultimate shrinkage of 27×10^{-4} obtained as an example in sandy soil-cement mixtures (Okada and Kawamura, 1967). The ultimate shrinkage for clay lumps-cement mixtures obtained in this experiment ranges from 112×10^{-4} to 258×10^{-4}. Thus, the maximum shrinkage of clay lumps-cement mixtures is about 10 times that of sandy soil-cement. However, a pertinent control of the internal structure, for example, the use of the high moisture content clay lumps would be able to reduce shrinkage to a considerable extent.

Relationship between Physical Properties of Clay Pockets and Shrinkage Rate (k_0)

The value k_0 of 7 days age specimens made using the zero and 10 percent moisture content clay lumps samples decreases with increasing specific surface (Fig. 5.3 (b)). That is, the finer the clay lumps samples with a given moisture content, the smaller the shrinkage rate (k_0) of 7 days age specimens in the tertiary period (Fig. 5.3 (b)). Further, the value k_0 as well as the ultimate shrinkage is different for different clay lumps samples in their moisture content, even if the clay lumps samples of the same specific surface are used.

Naturally, the value k_0 of the 28 days age specimens is smaller than the comparable value of the 7 days age specimens, almost independently of the specific surface and moisture content. However, there is an exception that the value k_0 of the 30 percent moisture content clay lumps-cement mixtures is considerably smaller than that of other mixtures. Such a characteristic difference between these two ages is considered to be due to the homogenization of the internal structure during the cure of 7 to 28 days ages. From these experimental phenomena, considerable part of the shrinkage in the tertiary period is found to be attributed to the shrinkage of clay pockets.

Relationship between Physical Properties of Clay Pockets and the Value of n

No definite tendency can be found in the relation between the specific surface and the value of n, as shown in Table 5.1. The value, n, of the zero percent moisture content clay lumps-cement at 7 days age is remarkably small compared with others. This indicates that the shrinkage of the zero percent moisture content clay lumps-cement more rapidly proceeds than that of other types of mixtures. Such rapid shrinkage would probably be due to an extremely small shrinkage of the clay pockets in the specimens. Naturally, the value, n, of the specimens cured for 28 days is far greater than the comparable one at 7 days age (Table 5.1).

(4) Summary and Conclusions

The moisture content of clay lumps samples may greatly affect the ultimate shrinkage of the soil-cement

mixtures. The shrinkage of soil-cement was found greatly to depend upon the shrinkage characteristics and volume fraction of clay pockets included in it.

In practice, the use of the clayey soil completely dried up or with considerably high moisture content (about 30 percent) appears to reduce ultimate shrinkage, even if clay lumps included in the soil are to only a little degree disintegrated. However, the shrinkage of soil-cement made using the moderate moisture content clay lumps, such as 10 percent, is not reduced without disintegrating the original soil into considerably fine lumps.

Consequently, the physical properties of the original material, such as moisture content and lumps size , should be controlled so as to reduce the shrinkage and/or volume fraction of clay pockets for reducing the shrinkage of clay lumps-cement mixtures, because the shrinkage of clay lumps-cement greatly depends upon the shrinkage of clay pockets included.

4. SHRINKAGE STRESSES IN SOIL-CEMENT MIXTURES

Generally, creep plays an important role in reducing the shrinkage stress in soil-cement or concrete which is susceptible to cracking on account of its low tensile strength. As discussed in detail in CHAPTER III, the ultimate creep strain of soil-cement is far greater than that of concrete. Although the shrinkage of soil-cement is about 4 to 40 times that of concrete, the shrinkage stresses in soil-cement could be offsetted to a considerable extent by its greater creep deformation. Further, the ratio of tensile strength to compressive strength in soil-cement is about a fourth to a fifth, which is about two times that in concrete.

Mechanical properties and shrinkage characteristic of soil-cement mixtures greatly vary with the compositions of the soil used, as described in the preceding part of this chapter. Therefore, it is a fundamental problem to be understood in the discussion of shrinkage cracking what structure of soil-cement induces less shrinkage stresses.

(1) Application of Pickett's Theoty to the Discussion of Shrinkage Stress in Soil-Cement

Pickett derives theoretical expressions for deformations of concrete beams and slabs that occur during the course of drying and expressions for distribution of the accompanying shrinkage stresses (Pickett, 1946a). In the derivation of the formulas, he assumed that the laws govering the development of shrinkage stresses in concrete during drying were analogous to those govering the development of thermal stresses in an ideal body during cooling. However, it is pointed out that the flow of water is different from that indicated by the diffusion equation, and that the relationship between the change in moisture content and unrestrained shrinkage is not linear as required by these equations. Shrinkage may be assumed to be proportional to moisture content for practical purposes.

Pickett's formulas are incapable of estimating the shrinkage stresses in concrete or soil-cement quantitatively, because the stress-strain relations of these materials are not elastic, but rather viscoelastic.

This chapter aims at determining the stresses in soil-cement pavements resulting from drying shrinkage over during comparatively long term. Therefore, the stress-strain relationship to be introduced in such a stress analysis should not be that which is obtained by the short-term loading tests, but that which is obtained by creep tests. That is, in order to estimate shrinkage stresses, creep deformation characteristics should be introduced into the basic stress-strain relation.

As stated in CHAPTER III, creep deformations of soil-cement, which are far greater than those of concrete, differ with silt fraction, moisture content and properties of clay pockets. Thus, shrinkage stres-

ses and the accompanying shrinkage cracking in soil-cement are found to be affected by the factors such as amount of silt, moisture content and properties of clay pockets.

In this investigation, assuming that the development of unrestrained shrinkages produced in soil-cement accompanying with loss of moisture follows the diffusion equation, shrinkage stresses in soil-cement pavements are experimentally estimated using sustained stress-strain (including creep and instantaneous elastic deformations) relation.

(2) Solution of Equation for Diffusion of Unrestrained Shrinkage in Slab or Beam Drying from One Face Only

Provided the assumption of proportionality between moisture content and shrinkage strain is acceptable , the progress of shrinkage strain in concrete can be represented by the diffusion equation. The diffusion equation for the beam shown in Fig. 5.4 is given by Eq. (5.3).

$$k\partial^2 S/\partial y^2 = \partial S/\partial t \tag{5.3}$$

The boundary conditions at y = 0 and b are represented by Eq. (5.4) and Eq. (5.5), respectively.

$$\partial S/\partial t = 0 \tag{5.4}$$

$$\partial S/\partial y = (f/k)(S_\infty - S) \tag{5.5}$$

The boundary condition at the exposed surface (Eq. (5.5)) is based on the analogy of Newton's law of radiation.

A general solution for S satisfying Eqs. (5.3), (5.4) and (5.5) is expressed by Fourier series as follows;

$$S = S_\infty - \sum_1^\infty A_n e^{(-kt/b^2)\beta_n^2} \cos \beta_n (y/b) \tag{5.6}$$

where β_n: the nth root of $\beta \tan \beta = fb/k$

From the initial condition of $(S)_{t=0} = 0$

$$A_n = (S_\infty/\cos \beta_n)(2fb/k)/\{(fb/k)^2 + (fb/k) + \beta_n^2\}$$

There is the other solution which is obtained by the analogy of Newton's law of radiation from the semi-infinite solid surface instead of considering the surface at y=0 to be sealed.

The solution is expressed by Eq. (5.7) using probability integral.

$$S/S_\infty = \Phi[\{1 - (y/b)\}/2\sqrt{T}] - \Phi[\{1 - (y/b)\}/2\sqrt{T} + B\sqrt{T}]e^{B\{1 - (y/b)\} + B^2T} \tag{5.7}$$

Notation

S = free, unrestrained unit linear shrinkage strain

S_∞ = value of S when t = ∞

t = time in days

k = diffusivity coefficient of shrinkage in sq. cm. per day

f = surface factor in cm per day

x, y = coordinates

l, b = the dimension of the specimen (Fig. 5.4)

B = fb/k

T = kt/b^2

erfc(u) = $(2/\sqrt{\pi})\int_x^\infty e^{-u^2}du$

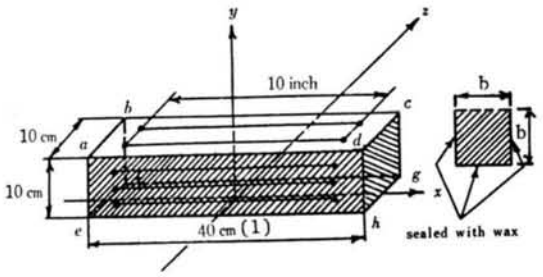

Fig.5.4 Beam drying one face only (shading shows sealed surfaces)

According to Pickett's calculation results (1946 a), Eq. (5.7) gives somewhat different S/S_∞ value at y=0 from that given by the exact solution of Eq. (5. 6); therefore, Eq. (5.7) may be used in place of Eq. (5.6) whenever T is so small that S/S_∞ at y=0 is less than the permissible error. In this study, since the value of S/S_∞ at y=0 is to be discussed and T small enough, Eq. (5.7) is used for the evaluation of S/S_∞.

(3) Determination of Diffusivity Coefficient of Shrinkage (k) and Surface Factor (f)

The value of k and f are required for the evaluation of shrinkage (S). When T is so small that Eq. (5.7) may be used in place of Eq. (5.6), k and f are determined as follows:

The shortening of a beam can be expressed by Eq. (5.8)(Pickett, 1946a).

$$\text{unit shortening} = S_{av} = (1/b)\int_0^b S\,dy \qquad (5.8)$$

The following equation (Eq. (5.9)) is obtained by substituting Eq. (5.7) into Eq. (5.8).

$$S_{av}/S_\infty = (1/B)\{e^{B^2T}\Phi(B\sqrt{T}) - 1 + (2B\sqrt{T}/\sqrt{\pi})\} \qquad (5.9)$$

Furthermore, if the parameter $B\sqrt{T}$ is very small, the following equation (Eq. (5.10)) is obtained by expanding the expression in the brackel of Eq. (5.9).

$$S_{av}/S_\infty = BT[1 - (4B\sqrt{T}/3\sqrt{\pi}) + (1/2)(B\sqrt{T})^2 - \{8(B\sqrt{T})^3/15\sqrt{\pi}\} + \cdots] \qquad (5.10)$$

If T is less than about 0.05 and B is less than about 5, the value of S_{av}/S_∞ can be calculated with a considerably high accuracy using Eq. (5.10)(Pickett, 1946a). Eq. (5.10) is rewritten as follows:

$$\sqrt{k}\,xt(1 - 0.752\sqrt{t}\,x + 0.500\,t\,x^2 - 0.301\,t\sqrt{t}\,x^3) = 10(S_{av}/S_\infty) \qquad (5.11)$$

where $x = f/\sqrt{k}$, b = 10 cm

When S_{av}^* and S_∞ are experimentally obtained, the value of S_{av}/S_∞ is determined for various drying times (t).

The factors of k and x in Eq. (5.11) are unknown. When the values of S_{av} are known for two different drying times, they can be determined by solving simultaneous equations of two unknowns. Finally, we can determin them by solving the third order of equation for x.

(4) Experimental Determination of Shrinkage Stresses in Soil-Cement during Drying

Pickett's basic concept concerning shrinkage stresses in elastic solids is cited from his paper (1946a) as follows:

"The shrinkage S given as a function of time (t) and coordinate (y) is defined as the linear unit deformation that would occur if each infinitesimal element were unrestrained. However, the properties of a continuous solid will not permit an arbitrary distribution of deformations; therefore, unless the distribution of shrinkage given by Eq. (5.7) happens to be compatible with the conditions of continuity, stresses will be produced that will modify the deformations so as to make them compatible (if the distribution of shrinkage is compatible with the conditions of continuity, stresses will not be produced). The term e_x is defined as the resultant unit deformation in the x-direction (the direction of length). It is therefore the algebraic sum of shrinkage, S, and the strain produced by stresses."

The three principal stresses in wide slabs and in narrow beams will be in the directions of length, width and depth, respectively, if the bodies are under uniform exposure either from one or from two opposite faces and are without external restaint. And now σ_y is obviously zero; and if Poisson's ratio is assumed as zero and when the discussion is confined to narrow beams, σ_z is negligible. Therefore,

$$e_x = \varepsilon_s - S \tag{5.12}$$

$$\text{or } \varepsilon_s = e_x + S \tag{5.13}$$

where e_x: resultant unit deformation in the x-direction

ε_s: strains produced by stresses

S: drying shrinkage in the x-direction

e_x can experimentally be obtained as stated in the next paragraph; S can be determined using the theoretical formuls of Eq. (5.7). Therefore, strains produced by stresses are given as a function of t and y. It is desirable to determin experimentally both e_x and S. However, since it is almost impossible to determin shrinkage strain S experimentally, Eq. (5.7) is used for estimating S. The procedures for estimating σ_x from ε_s obtained as described above are as follows:

---

* In this investigation, S_{av} is the unit shortening measured at y/b = 0.5 in a rectangular prism specimen (10 x 10 x 40 cm) drying from one face only. The validity of such determination is proved as follows:

When the long narrow beams of homogeneous, isotropic solids that follow Hooke's law dry from one face only without any restriction, the following equation is derived so as to satisfy the conditions of compatibility ($\partial^2 e_x/\partial y^2 = 0$) and the equations of equilibrium ($\int_0^b \sigma_x\, dy = 0$, $\int_0^b \sigma_x y\, dy = 0$).

$$e_x = \{(6y/b) - 4\}(1/b)\int_0^b S\, dy + \{6 - (12y/b)\}(1/b^2)\int_0^b Sy\, dy$$

where e_x and σ_x are elongation in x-direction and normal component of stress parallel to x-axis- positive if tensile, negative if compressive; b: thickness of specimens (see Fig. 5.4).

When y/b = 0.5, $e_x = -(1/b)\int_0^b S\, dy = -S_{av}$. This indicates that the elongation e_x at y/b = 0.5 experimentally obtained gives $-S_{av}$. It is questionable whether these equations obtained based on theory of elasticity are valid for soil-cement beams. However, as described later (Fig. 5.7 and Fig. 5.8), there is a fairly good agreement between the experimental S_{av} vs. drying time curves and the calculated ones.

Assuming that strain (ε) of hardened soil-cement at a certain time (t) after the application of a sustained stress (σ) is expressed by a function of σ/σ_f (σ: sustained stress, σ_f: strength of soil-cement specimens),

$$\varepsilon = \varepsilon_i + \varepsilon_c \tag{5.14}$$

where ε_i: instantaneous elastic strain

ε_c: creep strain

$$\varepsilon = f(\sigma/\sigma_f) \tag{5.15}$$

Further, both σ and σ_f are functions of time (t):

$$\sigma = \sigma(t),\ \sigma_f = \sigma_f(t) \tag{5.16}$$

The minute change ($\Delta\sigma$) in stress produced by the minute change ($\Delta\varepsilon$) in strain is represented as follows: Differentiating both sides of Eq. (5.15) by t,

$$d\varepsilon/dt = (df/d\zeta)\{(d\sigma/dt)\sigma_f - \sigma(d\sigma_f/dt)\}/\sigma_f^2 \tag{5.17}$$

where $\zeta = \sigma/\sigma_f$

If minute change of ε and σ during unit time (t_1) are noted as $\Delta\varepsilon$ and $\Delta\sigma$, the relation between $\Delta\varepsilon$ and $\Delta\sigma$ at a given time $t = t_i$ is expressed by Eq. (5.18)

$$(\Delta\sigma)_{t=t_i} = (d\zeta/df)_{t=t_i} \cdot (\sigma_f)_{t=t_i} \cdot (\Delta\varepsilon)_{t=t_i} + (\sigma/\sigma_f)_{t=t_i} \cdot (\Delta\sigma_f)_{t=t_i} \tag{5.18}$$

The stresses $\sigma_{t=t_i + t_1}$ at the time ($t = t_i + t_1$) are given as follows:

$$\sigma_{t = t_i + t_1} = \sigma_{t=t_i} + (\Delta\sigma)_{t=t_i} \tag{5.19}$$

$d\zeta/df$ is determined by the numerical differentiation of the ε vs. σ/σ_f curve experimentally obtained at each time. There are also experimental curves of σ_f vs. t (ages). The stress σ_x at t = 1 day can be directly obtained from the ε vs. σ/σ_f curve using the strain (ε_s) produced at t = 1 day. The subsequent stresses are calculated one after another, as indicated by Eq. (5.18) and Eq. (5.19).

(5) Outline of Experiments

(a) Shrinkage Tests

Materials and their Mix Proportions

See the corresponding item in creep tests of sandy soil-cement mixtures (p. 88, Table 4.4).

Preparation of Soil-Cement Specimens

See the corresponding item in shrinkage tests of clay lumps-cement mixtures (p. 106).

Procedure

Specimens cured for 1 day in the moist room were waxed in their all surfaces except only one face abcd (Fig. 5.4) to prevent the evaporation from these five surfaces, as shown in Fig. 5.4.

In order to determine the distribution of e_x in y-direction, unit shortening at y/b = 0, 0.25, 0.50, 0.75 and 1.00 were measured by Huggenberger strain meter with 10 inch gage length. Specimens were stored in the room which the temperature and relative humidity were maintained at 20° C and 50 percent, respectively. Each type of specimens were made in duplicate; the experimental results were their average.

(b) Creep Tests

See the corresponding item included in CHAPTER III (pp. 88 - 89).

(6) Assumptions Made in Actual Stresses Calculations

Tensile and compressive strength vs. ages curves and sustained stress vs. strain curves of each type of soil-cement are required for determining the shrinkage stresses in these soil-cement specimens.

Several assumptions are made on the use of these experimental curves.

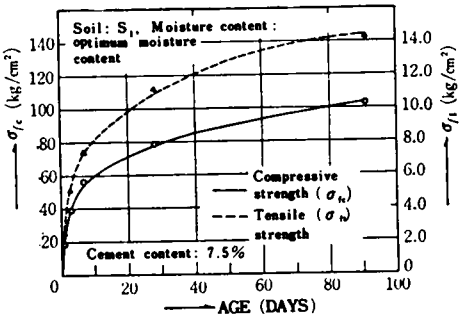

Fig.5.5 Relationship between strength and age

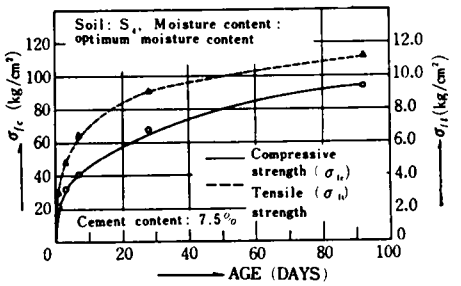

Fig.5.6 Relationship between strength and age

1) Tensile strength was obtained basing on JIS A 1113, i.e. splitting-tension test.

2) Tensile strength- and compressive strength-ages curves of soil S_1- and soil S_4-7.5 percent cement mixtures are presented in Fig. 5.5 and Fig. 5.6, respectively. These plots on semi-logarithmic graph paper give straight lines. Strength vs. ages relations of their mixtures are estimated from the data at 3 and 14 days ages using the above characteristic.

Table 5.2 Value of k and f obtained from the data at 1 and 5 days

Soil	Cement content (%)	k (cm²/day)	f (cm/day)	$S\infty$ ($\times 10^{-5}$)
S_1	5	1.11	0.34	186
	7.5	0.77	0.28	222
	10	1.32	0.32	265
S_4	5	1.14	0.43	247
	7.5	0.93	0.30	290
	10	1.18	0.36	282

Moisture content : Optimum moisture content

3) The following three assumptions are made on the ε-σ/σ_f relation used in stresses calculation.

(a) The ε-σ/σ_f curves obtained by compression creep tests are applicable to tensile stresses calculation.

(b) The same ε-σ/σ_f curve is used for the stresses calculation of mixtures made using the same soil, irrespective of cement contents. This assumption is based on the experimental fact that the creep deformation characteristics of soil-cement are little affected by cement content (Okada and Kawamura, 1964).

(c) The sustained stress-strain curves of soil S_4-cement are estimated from creep strain-time curve under the application of only a constant load, σ_c, (σ_c/σ_f = 0.4). The estimation is made on the basis of the assumption that the sustained stress-strain relation at each time is logarithmic.

(7) Results and Discussion

Diffusivity Coefficient of Shrinkage(k) and Surface Factor(f) in Soil-Cement

The values of k and f obtained using the data at 1 and 5 days are given in Table 5.2. Pickett reported an example of these values in concrete; k = 0.23 cm^2/day, f = 0.18 cm/day and $S_\infty = 280 \times 10^{-5}$ (temperature : 24.4°C, relative humidity: 50 percent). Comparing these values (k and f) between both materials, the value, k, in sandy soil-cement mixtures is about 3 to 5 times that in concrete; the value, f, about 1.5 to 2.5 times.

If the shrinkage tendency of each elemental volume is linearly related to the moisture content in soil-cement, moisture in soil-cement is found far more easily to move than in concrete, because diffusivity coefficient of shrinkage(k) means the quantity of water moving through an arbitrary cross-section of area, 1 cm^2, per unit time, 1 day. However, the ultimate shrinkages(S_∞) of these soil-cement mixtures are equal to or smaller than the value in cement mortar.

Average Drying Shrinkage

Plots of the value, S_{av}, obtained by the experiments and theoretical calculations against drying time (t) give the curves represented in Fig. 5.7 and Fig. 5.8. As shown in these figures, an initial good agreement between the experimental and theoretical curves is followed by a gradually increasing difference

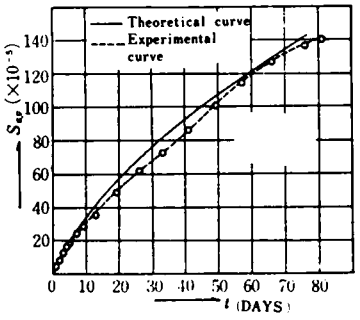

Fig.5.7 Average shrinkage vs. drying time curves (soil: S_1, cement content: 7.5 percent)

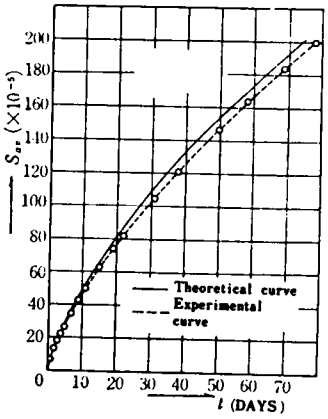

Fig.5.8 Average shrinkage vs. drying time curves (soil: S_1, cement content: 7.5 percent)

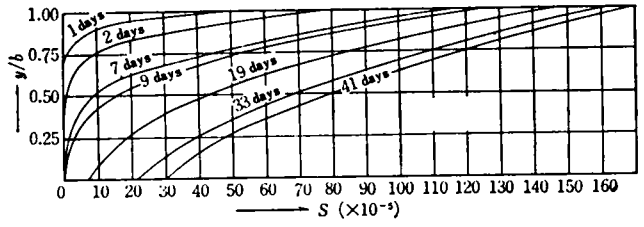

Fig. 5.9 Theoretical shrinkage distribution in the soil-cement specimen at various time (soil : S_1, cement content :7.5 percent)

between them. Experimental values of k at long drying times are a little smaller than the comparable theoretical values. This fact indicates that the value of k decreases with increasing drying time.

Calculation Results of Drying Shrinkage Strain (S(t,y)) and Measured Values of Resultant Strain (e_x)

Theoretical drying shrinkages (S(t,y)) calculated using Eq. (5.7) are shown in Fig. 5.9 and Fig. 5.10. Extremely large shrinkage occurs on the exposed surface and in its neighborhood at the initial drying stages, followed by its extensive progress into more interior parts until moisture near the sealed face (y/b=0) begins to move at about 10 days drying time.

The results of e_x experimentally measured are plotted in Fig. 5.11 and Fig. 5.12. At the initial stages of drying time, the closer to the exposed surface a given region, the more rapidly the value of e_x in the region increases. Difference between e_x at y/b=0 and y/b=1.0 becomes the largest at about 50 days of drying. After the time, the e_x near the sealed face gradually increases, while there is a little or little increase in the e_x on the exposed surface. Further drying makes the values of e_x at all positions gradually approach to a value of S_∞.

Results of Shrinkage Stresses Calculations and their Discussions

a) Sustained Stress-strain Curve

A sustained stress-strain curve used in stresses calculation is given in Fig. 5.13.

b) Drying Shrinkage Stresses Distributions in Soil-Cement Beam Drying from One Face Only

Fig. 5.14 shows an example of shrinkage stresses distributions in the soil S_4-7.5 percent cement mixtures specimen.

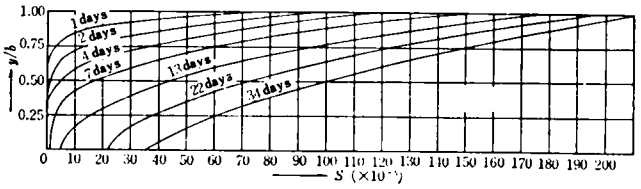

Fig.5.10 Theoretical shrinkage distribution in the soil-cement specimen at various time (soil : S_4, cement content : 7.5 percent)

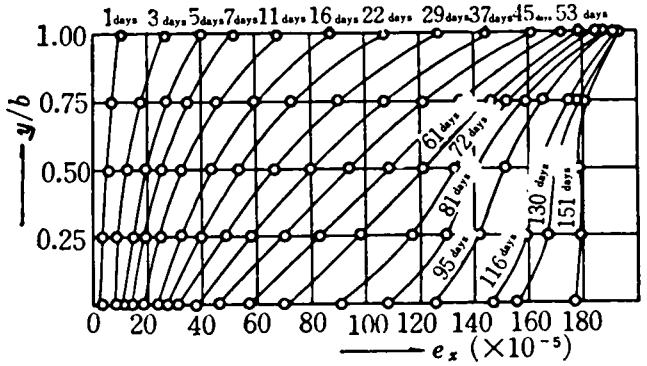

Fig. 5.11 Variations of e_x distribution with drying time (soil : S_1, cement content : 7.5 percent)

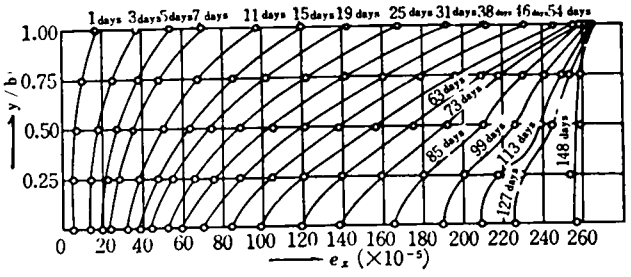

Fig. 5.12 Variations of e_x distribution with drying time (soil : S_4, cement content : 5 percent)

Tensile stresses are produced in the region near the exposed surface; compressive stresses in the region near the sealed face. In soil-cement beam unrestrained, the following equation should be satisfied: $\int_0^b \sigma_x \, dy = 0$.

However, none of the stresses distributions experimentally obtained in this investigation satisfies such an equation, as definitely shown in Fig. 5.14.

Pickett's theoretical calculations for elastic solids show that tensile stresses are produced in the region, $0<y/b<0.2$ and $0.8<y/b<1.0$ and that compressive stresses in the region, $0.2<y/b<0.8$. It goes without saying that stresses distributions such elastic solids satisfy $\int_0^b \sigma_x \, dy = 0$.

Fig. 5.15 shows an example of σ_x/σ_f vs. drying time(t) curves at the positions of y/b = 0, 0.25, 0.50, 0.75 and 1.00. The ratios of tensile stresses on the exposed surface (y/b = 1.00) to tensile strength (σ_f) in all types of soil-cement specimens investigated in this paper vary with drying time as shown in Fig. 5.16 and Fig. 5.17. The value of σ_x/σ_f of all specimens has the maximum at about 5 days after initiation of drying. The maximum value of σ_x/σ_f in soil S_1-5 percent cement mixture is considerably smaller than that of soil S_1-7.5 and 10 percent cement mixtures. On the other hand, the maximum value of soil S_4-cement mixtures is almost independent of cement content. Thus, addition of a small quantity of cement (about 5 percent) to sandy soil such as soil S_1 favors the reduction of the value, σ_x/σ_f, comparing with the mixtures with high cement contents such as 7.5 and 10 percent. Therefore, it may be desirable for reducing shrinkage cracking to use cement as a little as possible. However, shrinkage cracking in soil S_4-cement mixtures including somewhat more amount of silt fraction may be independent of cement contents. As a while, soil S_4-cement mixtures may be more susceptible to shrinkage cracking than soil S_1-cement.

c) Drying Shrinkage Stresses Distributions in Completely Restrained Beam or Slab Drying from One Face Only

An actual soil-cement pavement slab is rather analogous to a slab completely restrained against warping and longitudinal unit shortening than an unrestrained slab. Shrinkage stresses distributions in a completely restrained slab should be required to understand shrinkage cracking in soil-cement pavement better. Since e_x is zero in a completely restrained slab, shrinkage stresses are produced only by shrinkage strain S. In a completely restrained slab, tensile stresses are produced over through all cross-sections from the

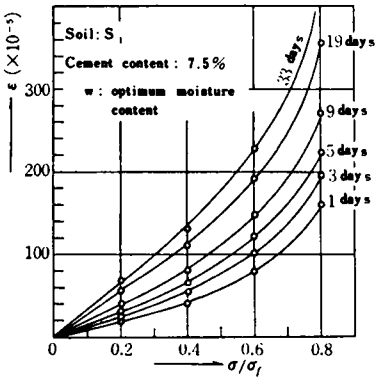

Fig.5.13 Sustained stress-strain curves

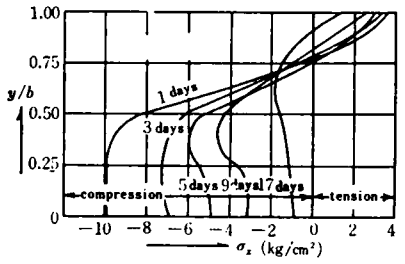

Fig.5.14 Stress distributions in the soil-cement specimen unrestrained (soil: S_4, cement content: 7.5 percent)

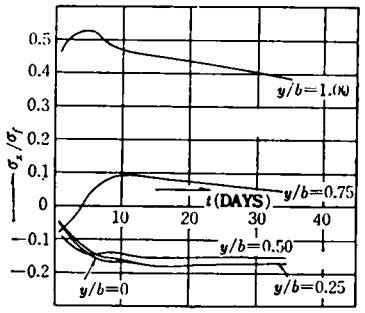

Fig.5.15 Variations of σ_x/σ_f with drying time at various positions (soil: S_4, cement content : 7.5 percent)

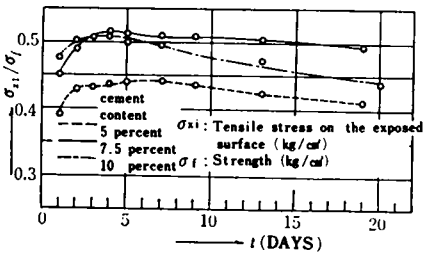

Fig.5.16 σ_x/σ_f vs. t curves at y/b = 1.00 (soil: S_1)

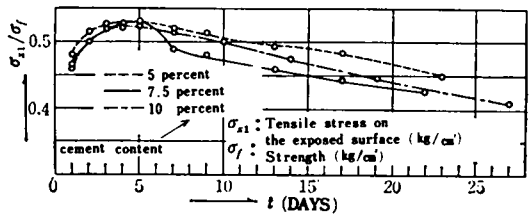

Fig.5.17 σ_x/σ_f vs. t curves at y/b = 1.00 (soil: S_4)

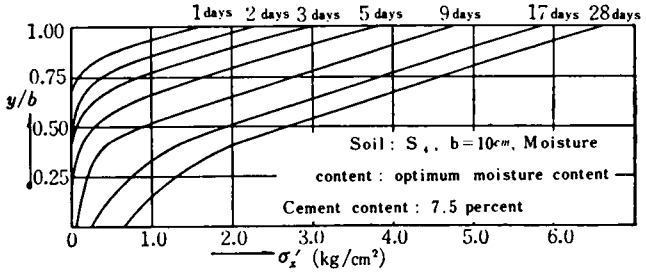

Fig.5.18 Stress distribution in the soil-cement specimen completely restrained

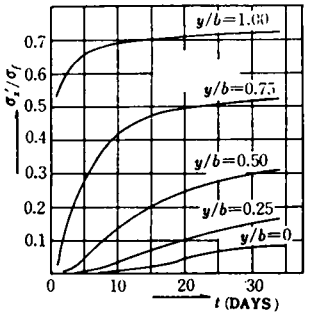

Fig.5.19 Variations of $\sigma_{x/\sigma f}$ with drying time at various positions (soil: S_4, cement content : 7.5 percent)

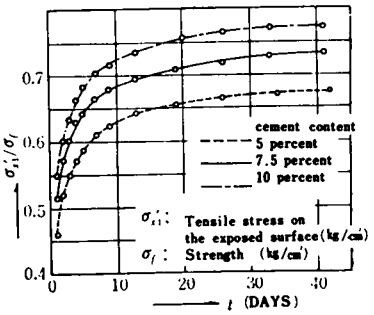

Fig.5.20 σ_{x1}/σ_f-t curves (soil: S_1)

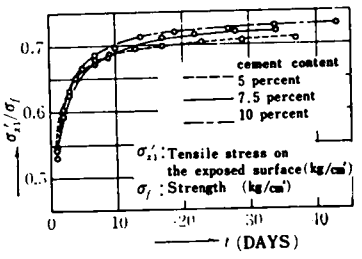

Fig.5.21 σ_{x1}/σ_f - t curves (soil: S_4)

exposed surface to the sealed face, increasing with drying time (Fig. 5.18). Plots of the value, σ'_x/σ_f (σ'_x: stresses produced in a completely restrained slab) against drying time at each cross section of y/b = 0, 0.25, 0.50, 0.75 and 1.00 give the curves, for example, shown in Fig. 5.19. The σ'_x/σ_f on the exposed surface vs. drying time in various types of soil-cement are plotted (Fig. 5.20 and Fig. 5.21). All of these curves continue to rise with drying time without the maximum value followed by the subsequent reduction unlike those for other different conditions of restraint. A great increase in the value of σ_x/σ_f is found during the initial 10 days of drying; thereafter a little or little increase.

Several conclusions can be drawn from these two figures:

(a) the sandy soil-cement mixtures become more susceptible to shrinkage cracking, as the amount of cement added increases, (b) there is little difference in shrinkage cracking characteristic between cement contents in the soil S_4-cement mixtures having more silt fraction, (c) the addition of the more amount of cement to sandy soils such as soil S_1 may enhance the possibility of shrinkage cracking, while with low cement content, the use of a soil containing more silt fraction makes a soil-cement more susceptible to shrinkage cracking.

(8) Summary and Conclusions

1) The diffusivity coefficient of shrinkage (k) in sandy soil-cement mixtures is about 3 to 5 times that in concrete; the surface factor (f) about 1.5 to 2.5 times.
2) The sandy soil-cement mixtures become more susceptible to shrinkage cracking, as the amount of cement added increases.
3) There is little difference in shrinkage cracking characteristic between cement contents in the soil S_4 -cement mixtures containing more silt fraction.
4) The addition of the more amount of cement to sandy soils such as soil S_1 may enhance the possibility of shrinkage cracking, while with low cement content, the use of a soil containing more silt fraction is more susceptible to shrinkage cracking.
5) It may be considered that increasing silt fractions in soils used decrease the compressive strength of soil-cement for a given cement content. Therefore, in practice, in order to produce a soil-cement developing a given compressive strength, the use of the soil with less silt fraction is desired for reducing shrinkage cracking of soil-cement. However, when soils containing comparatively much silt fraction are used, even an addition of a great amount of cement does not make the mixture susceptible to cracking.

Thus, the characteristics of shrinkage stresses produced on the exposed surface greatly depend upon the amount of silt fraction included in the soil used. The presence of a comparatively great amount of silt fraction is not necessarily an undesirable factor to reduce its shrinkage cracking.

5. A CONSIDERATION ON SHRINKAGE CRACKING IN SOIL-CEMENT AS A VISCOELASTIC MATERIAL

The evaluation of shrinkage stresses in soil-cement and concrete is much complicated in the following two points.

The first of these is the mathematical expression of shrinkage strain in the body which is a function of time. Carlson proposed that the diffusion equation could be applied to the process of progression of shrinkage strain in concrete (Carlson, 1937). Subsequent works on this subject were conducted by Pickett, (1946a,b), Rostasy (1960) and Wischers (1960) so on.

The second is the time-dependent stress-strain relationship of the material which is very important es-

pecially in the estimation of the internal stresses resulting from the volume change progressing with time from surface to interior of the mass. Thus, for estimation of internal stresses due to shrinkage, the expression which relates shrinkage strain, stress-strain relationship and time should be derived.

Hansen (1965) derived the formula of the tensile shrinkage stress for a constant strain rate using the four-element model. In the previous paragraph, shrinkage stresses in soil-cement pavement were estimated by experimental method. In this method, nonlinear creep deformation of the material was introduced.

Many investigators have indicated that stress-strain relation in concrete and soil-cement can be considered as viscoelastic.

Zienkiewicz (1961) illustrates the development of thermal stresses in a simple concrete slab due to the heat of hydration and boundary cooling in which he regards concrete as a viscoelastic material. His method is based on the elastic-viscoelastic analogy of which method was used by Alfrey (1948) in stress analysis in high polymers and by McHenry (1943) in concrete. The elastic-viscoelastic analogy method requires the relaxation function of a material which much difficulty is accompanied to obtain. However, if shrinkage stresses can be predicted from creep data, surface cracking and loss of flexural strength due to shrinkage can be estimated easier.

In this paper, expressions for shrinkage stresses in viscoelastic materials such as soil-cement and concrete are derived using stress analysis in viscoelastic bodies proposed by Lee (1955). According to Lee's theory (1955), stress and strain in linear viscoelastic bodies can be dealt with as an associated elastic one, if the time can be removed by the Laplace transform. Formulas for shrinkage stresses in linear viscoelastic bodies represented by Burgers model can be derived using the formulas in elastic beams or slabs given by Pickett (1946). The assumptions made in this derivation and the procedure followed by Pickett in deriving the equation for shrinkage strain are described in paragraph 4 (pp. 110 - 111).

(1) Derivation of Formulas

Stresses are considered in linear viscoelastic body expressed by Burgers model. A long narrow beam shown in Fig. 5.22 has the only longitudinal stresses which are independent of coordinate x, if Poisson's ratio were zero. Mathematical stress analysis will be made for a beam drying from one face only. Equations for stresses resulting from shrinkage strain represented by Eq. (5.7) will now be derived.

For the convenience of the derivation of formulas, Eq. (5.7) is transformed to the following Eq. (5.20).

$$S/S_\infty = \operatorname{erfc}(\beta/2\sqrt{t}) - \operatorname{erfc}\{(\beta/2\sqrt{t}) + \alpha\sqrt{t}\}e^{\alpha\beta+\alpha^2 t} \qquad (5.20)$$

where $\alpha = f/\sqrt{k}$, $\beta = \{(1 - (y/b)\}(b/\sqrt{k})$

Stresses and Strains

For long narrow beams, the condition of compatibility is as follows:

$$\partial^2 e_x/\partial y^2 = 0$$

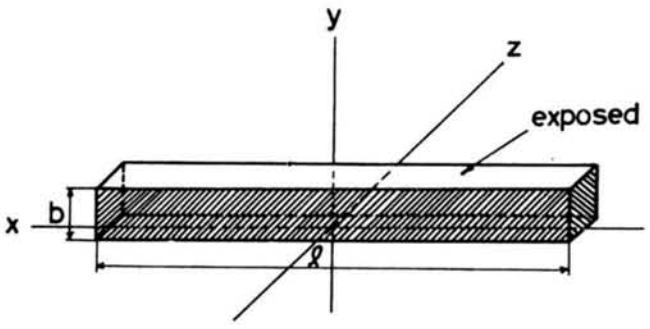

Fig. 5.22 Beam drying from one face only (shading shows sealed surfaces)

e_x is defined as the resultant unit deformation in the direction of length, which is the sum of shrinkage (S) and the strain (ϵ_x) produced by stresses, as represented by Eq. (5.21).

$$e_x = \epsilon_x - S \tag{5.21}$$

When the stress(σ_x) and strain(ϵ_x) can be represented by a single component x, a linearly viscoelastic relation can be written in the form:

$$P(\sigma_x) = Q(\epsilon_x) \tag{5.22}$$

where P and Q are linear differential operators of the form:

$$P = \sum_0^p p_r \partial^r/\partial t^r, \qquad Q = \sum_0^q q_r \partial^r/\partial t^r$$

For no external restraint the equation of equilibrium become

$$\int_0^b \sigma_x \, dy = 0 \tag{5.23}$$

$$\int_0^b \sigma_x y \, dy = 0 \tag{5.24}$$

The time dependence is removed by operating with the Laplace transform on all these equations. The transform is denoted by a star on the corresponding function.

$$\overset{*}{e}_x = \overset{*}{\epsilon}_x - \overset{*}{S} \tag{5.25}$$

$$P(p)\overset{*}{\sigma}_x = Q(p)\overset{*}{\epsilon}_x \tag{5.26}$$

$$\partial^2 \overset{*}{e}_x/\partial y^2 = 0 \tag{5.27}$$

$$\int_0^b \overset{*}{\sigma}_x \, dy = 0 \tag{5.28}$$

$$\int_0^b \overset{*}{\sigma}_x y \, dy = 0 \tag{5.29}$$

where p is the transform parameter. Eq. (5.25) to (5.29) represent the problem for an elastic body of the same shape as the viscoelastic one with elastic constants which are a function of the parameter p. When the stresses $\overset{*}{\sigma}_x(y,p)$ have been determined, the expressions for the stresses $\sigma_x(y,t)$ of viscoelastic body are given by the inversion of the Laplace transform. The solution for this elastic problem is obtained by Pickett (1946a) as follows:

$$\overset{*}{\sigma}_x = \{Q(p)/P(p)\}[\overset{*}{S} + \{(6y/b) - 4\}(1/b)\int_0^b \overset{*}{S} \, dy + \{6 - (12y/b)\}(1/b)^2 \int_0^b \overset{*}{S} y \, dy] \tag{5.30}$$

Pickett (1946a) also derived the more usable expression, which are easier to understand, by means of superposition of the elementary solutions. This second derivation is based on the fact that the resultant stresses $\overset{*}{\sigma}_x$ consist of three parts described below.

The first part is the stress $\overset{*}{\sigma}'_x$ which is produced by complete restraint against the longitudinal deformation. The second part is a uniform stress $\overset{*}{\sigma}'_x$ equal to and opposite in sign to the average of the first part. The third is a stress resulting from a simple moment that is equal to and opposite in sign to the moment produced by the sum of the first two parts. Using the expressions derived by Pickett (1946), each stress in viscoelastic body is represented by Eq. (5.31), (5.32) and (5.33).

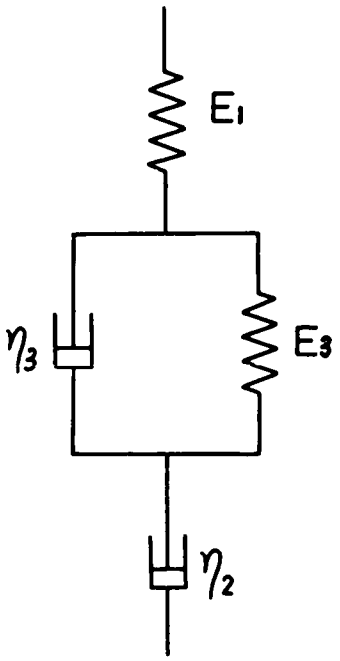

Fig. 5.23 Burgers model

For complete longitudinal restraint (the first part of $\overset{*}{\sigma}_x$)

$$\overset{*}{\sigma}'_x = \{Q(p)/P(p)\}\overset{*}{S} \tag{5.31}$$

For restraint against warping only (sum of the first and second parts of $\overset{*}{\sigma}_x$)

$$\overset{*}{\sigma}''_x = \{Q(p)/P(p)\}(\overset{*}{S} - \overset{*}{S}_{av}) \tag{5.32}$$

$$\overset{*}{S}_{av} = (1/b)\int_0^b \overset{*}{S}\, dy \tag{5.33}$$

For no external restaint (sum of all three parts)

$$\overset{*}{\sigma}_x = \{Q(p)/P(p)\}[\overset{*}{S} - \overset{*}{S}_{av} + \{6 - (y/b)\}(2b\overset{*}{v}_{max}/3\ell^2)] \tag{5.34}$$

where $\overset{*}{v}_{max}$ is the maximum deflection that occurs at $x = \ell/2$, as expressed by Eq. (5.35).

$$\overset{*}{v}_{max} = (3\ell^2/2b)\{(1/b)\int_0^b \overset{*}{S} y\, dy - (1/2b)\int_0^b \overset{*}{S}\, dy\} \tag{5.35}$$

Further, S_{av} and v_{max} are also given by the more convenient form of Eq. (5.36) and Eq. (5.37), respectively.

$$S_{av}/S_\infty = (1/B)\{ e^{\alpha^2 t}\mathrm{erfc}(\alpha\sqrt{t}) - 1 + (2/\sqrt{\pi})\alpha\sqrt{t}\} \tag{5.36}$$

$$(2b/3\ell^2)(v_{max}/S_\infty) = \{(1/2B) + (1/B^2)\}\{e^{\alpha^2 t}\mathrm{erfc}(\alpha\sqrt{t}) - 1 + (2/\sqrt{\pi})\alpha\sqrt{t}\} - (\alpha^2/B^2)t \tag{5.37}$$

Operators P(p) and Q(p) of Burgers Model

For the prescribed material with known operators P(p) and Q(p), the inversion of Eq. (5.31), (5.32) and (5.34) gives shrinkage stress in each condition of restraint.

P(p)/Q(p) of Burgers model (Fig. 5.23) is expresses by Eq. (5.38) or Eq. (5.39), because σ_x, ε_x and $(\sigma_x/E_1)-\varepsilon_x$ equal to zero, when t = 0.

$$Q(p)/P(p) = \{p^2 + (E^3/\eta^3)p\}/[(1/E_1)p^2 + \{(E_3/E_1\eta_3) + (1/\eta_2) + (1/\eta_3)\}p + \{E_3/(\eta_2\eta_3)\}] \tag{5.38}$$

$$Q(p)/P(p) = E_1[1 - \{(\phi_1 + \phi_2)p + \phi_1\phi_3\}/\{(p - \phi_1)(p - \phi_2)\}]$$

$$E_1/\eta_2 = \phi_1,\ E_1/\eta_3 = \phi_2,\ E_3/\eta_3 = \phi_3$$

$$\phi_1 = \{-(\phi_1 + \phi_2 + \phi_3) + \sqrt{(\phi_1 + \phi_2 + \phi_3)^2 - 4\phi_1\phi_3}\}/2$$

$$\phi_2 = \{-(\phi_1 + \phi_2 + \phi_3) - \sqrt{(\phi_1 + \phi_2 + \phi_3)^2 - 4\phi_1\phi_3}\}/2$$

Shrinkage Stresses in Three Different Conditions of Restraint

Each resultant stresses σ_x', σ_x'' and σ_x are derived in the following.

(1) For complete longitudinal restraint

From Eq. (5.31),

$$\overset{*}{\sigma}_x' = \{Q(p)/P(p)\}\overset{*}{S}$$

Applying the Laplace transform (Carslaw and Jaeger, 1963)(Churchill, 1958) to Eq. (5.20),

$$\overset{*}{S}/S_\infty = (e^{-\beta\sqrt{p}}/p) - \{e^{-\beta\sqrt{p}}/(p + \alpha\sqrt{p})\}$$

$\overset{*}{\sigma}_x'/S_\infty$ is expressed by Eq. (5.40) using parameter p.

$$\overset{*}{\sigma}_x'/S_\infty = E_1[1 - \{(\phi_1 + \phi_2)p + \phi_1\phi_3\}/(p - \phi_1)(p - \phi_2)]\cdot [\{e^{-\beta\sqrt{p}}/p\} - \{e^{-\beta\sqrt{p}}/(p + \alpha\sqrt{p})\}] \tag{5.40}$$

The inversion of Eq. (5.20) gives the shrinkage stress for complete longitudinal restraint, as represented by Eq. (5.41):

$$\sigma_x'/S_\infty E_1 = (S/S_\infty) - \{A(t)e^{\phi_1 t} + B(t)e^{\phi_2 t})\} \tag{5.41}$$

where

$$A(t) = \{\phi_1/(\phi_1 - \phi_2)\}\{\phi_1 + \phi_2 + (\phi_1\phi_3/\phi_1)\}(I_{\beta 1} - e^{\alpha\beta}I_{\alpha 1})$$

$$B(t) = -\{\phi_2/(\phi_1 - \phi_2)\}\{\phi_1 + \phi_2 + (\phi_1\phi_3/\phi_2)\}(I_{\beta 2} - e^{\alpha\beta} I_{\alpha 2})$$

$$I_{\alpha 1} = \int_0^t e^{(\alpha^2 - \phi_1)\tau} \operatorname{erfc}\{\alpha\sqrt{\tau} + (\beta/2\sqrt{\tau})\}d\tau$$

$$I_{\alpha 2} = \int_0^t e^{(\alpha^2 - \phi_2)\tau} \operatorname{erfc}\{\alpha\sqrt{\tau} + (\beta/2\sqrt{\tau})\}d\tau$$

$$I_{\beta 1} = \int_0^t e^{-\phi_1\tau} \operatorname{erfc}(\beta/2\sqrt{\tau})d\tau$$

$$I_{\beta 2} = \int_0^t e^{-\phi_2\tau} \operatorname{erfc}(\beta/2\sqrt{\tau})d\tau$$

(II) For restraint against warping only (or for a beam dried from two opposite faces)

$$\overset{*}{\sigma}''_x = \{Q(p)/P(p)\}(\overset{*}{S} - \overset{*}{S}_{av}) \qquad (5.32)$$

According to Pickett, if T is less than about 0.05 and B is more than about 5, Eq. (5.36) is applicable for the evaluation of S_{av}/S_∞ to a fair degree of accuracy. Applying the Laplace transform to Eq. (5.36),

$$\overset{*}{S}_{av}/S_\infty = (1/B)[\{1/(p + \alpha\sqrt{p})\} - (1/p) + \alpha p^{-3/2}]$$

$\overset{*}{\sigma}''_x/S_\infty$ is expressed by Eq. (5.42):

$$\overset{*}{\sigma}''_x/S_\infty = \{Q(p)/P(p)\}\overset{*}{S}/S_\infty - \{Q(p)/P(p)\}\overset{*}{S}_{av}/S_\infty \qquad (5.42)$$

The inversion of Eq. (5.42) gives the shrinkage stress σ''_x for restraint against warping only (Eq. (5.43).

$$\sigma''_x/E_1 S_\infty = S/S_\infty - (S_{av}/S_\infty)\{A(t)e^{\phi_1 t} + B(t)e^{\phi_2 t}\}$$

$$+ (1/B)\{C(t)e^{\phi_1 t} + D(t)e^{\phi_2 t}\} \qquad (5.43)$$

where

$$C(t) = \{\phi_1/(\phi_1 - \phi_2)\}\{\phi_1 + \phi_2 + (\phi_1\phi_3/\phi_1)\}\{I'_{\alpha 1} - I'_{\beta 1} + (2\alpha/\sqrt{\pi})I_{R1}\}$$

$$D(t) = -\{\phi_2/(\phi_1 - \phi_2)\}\{\phi_1 + \phi_2 + (\phi_1\phi_3/\phi_2)\}\{I'_{\alpha 2} - I'_{\beta 2} + (2\alpha/\sqrt{\pi})I_{R2}\}$$

$$I'_{\alpha 1} = \int_0^t e^{(\alpha^2 - \phi_1)\tau} \operatorname{erfc}(\alpha\sqrt{\tau})d\tau$$

$$I'_{\alpha 2} = \int_0^t e^{(\alpha^2 - \phi_2)\tau} \operatorname{erfc}(\alpha\sqrt{\tau})d\tau$$

$$I_{R1} = \int_0^t e^{-\phi_1\tau} d\tau$$

$$I_{R2} = \int_0^t \sqrt{\tau} e^{-\Phi_2 \tau} d\tau$$

(III) For no external restraint

From Eq. (5.34),

$$\overset{*}{\sigma}_x = \{(Q(p)/P(p)\}[\overset{*}{S} - S_{av} + \{6 - 12(y/b)\}(2b/3\ell^2)\overset{*}{v}_{max}]$$

According to Pickett's paper (1946a), if T is less than about 0.05 and B is more than 5, Eq. (5.37) is applicable for the evaluation of $(2b/3\ell^2)v_{max}$. Applying the Laplace transform to Eq. (5.37),

$$(2b/3\ell^2)(\overset{*}{v}_{max}/S_\infty) = \{(1/2B) + (1/B^2)\}[\{1/\sqrt{p}(\sqrt{p} + \alpha)\}$$

$$- (1/p) + (1/p\sqrt{p})] - (\alpha^2/B^2)(1/p^2)$$

$$\overset{*}{\sigma}_x/S = \{Q(p)/P(p)\}\{(\overset{*}{S}/S_\infty) - (\overset{*}{S}_{av}/S_\infty)\} +$$

$$\{Q(p)/P(p)\}\{6 - 12(y/b)\}(2b/3\ell^2)(\overset{*}{v}_{max}/S_\infty) \qquad (5.44)$$

The inversion of Eq. (5.44) gives the shrinkage stress σ_x for no external restraint (Eq. (5.45)).

$$\sigma_x/E_1S_\infty = (S/S_\infty) - (S_{av}/S_\infty) - \{A(t)e^{\Phi_1 t} + B(t)e^{\Phi_2 t}\} + (1/B)\{C(t)e^{\Phi_1 t} +$$

$$D(t)e^{\Phi_1 t}\} + \{6 - 12(y/b)\}[(2b/3\ell^2)(v_{max}/S_\infty) - \{(1/2B) + (1/B^2)\}\{C(t)e^{\Phi_1 t}$$

$$+ D(t)e^{\Phi_2 t}\}] + (\alpha^2/B^2)(K_1e^{\Phi_1 t} + K_2e^{\Phi_2 t} + K_3t + K_4) \qquad (5.45)$$

where

$$K_1 = \{(\phi_1 + \phi_2)(\phi_1 + \phi_1\phi_3)\}/\{\phi_1^2(\phi_1 - \phi_2)\}$$

$$K_2 = -\{(\phi_1 + \phi_2)(\phi_2 + \phi_1\phi_3)\}/\{\phi_2^2(\phi_1 - \phi_2)\}$$

$$K_3 = \phi_1 + \phi_2$$

$$K_4 = \{(\phi_1 + \phi_2)(1 + \phi_1 + \phi_2)\}/(\phi_1\phi_2)$$

(2) Constants Available for the Computation of Shrinkage Stresses

In order to compute stresses using the formulas derived in the preceding section, constants of four-element model, diffusivity coefficient of shrinkage and surface factor must be determined. Constants of four-element model can be easily obtained from creep strain-time curves. These constants for various types of soil-cement are given in Table 4.2, Table 4.3 (p.83, p.85), Table 4.7 and Table 5.2. However, only a few

reports on these constants of concrete seem available. These constants of concrete are summarized below.

(a) Constants of four-element model

The rheological properties of concrete were analyzed by Ogishi (1963). Hansen (1965) determined constants of four-element model of a 3 to 7 days old concrete, as shown below, using the experimental results obtained by Theuer.

$$E_1 = 2.5 \times 10^5 \text{ kg/cm}^2, \quad E_3 = 2.1 \times 10^5 \text{ kg/cm}^2,$$

$$\eta_2 = 0.81 \times 10^6 (\text{kg/cm}^2)\text{day}, \quad \eta_3 = 1.12 \times 10^5 (\text{kg.cm}^2)\text{day}$$

There is considerable difference between constants obtained by Ogishi (1963) and those by Hansen (1965). Such difference may primarily be due to the properties of concrete and to the ambient condition in creep test. Furthermore, in evaluating η_2 graphically from creep strain-curve, different value may be obtained for different part of the curve which is regarded as linear, because four-element model does not exactly represent the viscoelastic properties of concrete. It can be understood, from preceding equations derived , that the value of η_2 has a great effect on the shrinkage stress. Therefore, much care should be given on the determination of η_2 in the evaluation of shrinkage stress.

(b) Diffusivity coefficient of shrinkage and surface factor

It may be supposed that the diffusivity coefficient of shrinkage (k) is the amount of moisture moving through a cubic centimeter per day in the mass of concrete. Surface factor (f) expresses the degree of resistance against the emanation of moisture from the solid mass to the atmosphere. The resistance is considered to be caused by the filmy air around the surface of the mass with higher humidity than in the outer air. Therefore, the value of k and f depends upon the surrounding condition, the shape and dimensions of the mass and the porosity of concrete. Diffusivity coefficients of shrinkage are obtained by Rostasy (1960) for various porosity of concrete and mortar. His tests conducted at 20° C and a relative humidity of 65 % give the following diffusivity coefficients:

$0.00001 - 0.00002 \times 10^4 \text{cm}^2/\text{day}$ for cement mortar 1:3 to 1:5

$0.000005 - 0.00001 \times 10^4 \text{cm}^2/\text{day}$ for concrete

Pickett (1946b) computes the shrinkage strain using the following value:

$$k = 0.23 \text{ cm}^2/\text{day}, \qquad f = 0.18 \text{ cm/day}$$

where the surrounding condition is at 24°C and a relative humidity of 50 %.

(3) The Computation of the Shrinkage Stress on the Exposed Surface

The expression of tensile stresses on the exposed surface of a beam completely restrained longitudinally is represented by Eq. (5.46), which is obtained by substituting zero for β in Eq. (5.41).

$$\{\sigma_x'/(S_\infty E_1)\}_{y=b} = (S/S_\infty) - \{A'(t)e^{\phi_1 t} + B'(t)e^{\phi_2 t}\} \qquad (5.46)$$

where

$$A'(t) = \{\phi_1/(\phi_1 - \phi_2)\}\{\phi_1 + \phi_2 + (\phi_1\phi_3/\phi_1)\}(I'_{\beta 1} - I'_{\alpha 1})$$

$$B'(t) = -\{\phi_2/(\phi_1 - \phi_2)\}\{\phi_1 + \phi_2 + (\phi_1\phi_3/\phi_2)\}(I'_{\beta 2} - I'_{\alpha 2})$$

$$I'_{\beta 1} = \int_0^t e^{-\phi_1 t} d\tau$$

$$I'_{\beta 2} = \int_0^t e^{-\phi_2 t} d\tau$$

The tensile stresses of a beam restrained against warping only and with no external restraint are also expressed by Eq. (5.47) and Eq. (5.48), respectively.

$$(\sigma''_x/E_1 S_\infty)_{y=b} = (S/S_\infty) - (S_{av}/S_\infty) - \{A'(t)e^{\phi_1 t} + B'(t)e^{\phi_2 t}\} + (1/B)\{C(t)e^{\phi_1 t} + D(t)e^{\phi_2 t}\}$$

$$(\sigma_x/E_1 S_\infty)_{y=b} = (S/S_\infty) - (S_{av}/S_\infty)\{A'(t)e^{\phi_1 t} + B'(t)e^{\phi_2 t}\} + (1/B)\{C(t)e^{\phi_1 t} + D(t)e^{\phi_2 t}\} - 6[(2b/3\ell^2)(V_{max}/S_\infty) - \{(1/2B) + (1/B^2)\}\{C(t)e^{\phi_1 t} + D(t)e^{\phi_2 t}\} + (\alpha^2/B^2)(K_1 e^{\phi_1 t} + K_2 e^{\phi_2 t} + K_3 t + K_4)] \quad (5.48)$$

Little difficulty may be accompanied in the computation of tensile stresses on the exposed surface, if the value of $I'_{\alpha 1}$ and $I'_{\alpha 2}$ can be computed by the computer.

(4) An Example of the Shrinkage Stresses Computed by the Use of the Formulas Derived

The tensile stresses on the exposed surface of concrete beams drying from one face only, completely restrained are computed for three different values of α ($= f/\sqrt{k}$) using the viscoelastic constants obtained by Hansen and Theuer previously stated (Fig. 5.24).

The variations of the tensile shrinkage stress with drying time in concrete beams restrained against warping only and with no external restraint are also shown in Fig. 5.25 and Fig. 5.26. The tensile shrinkage stresses have the maximum value at the initial stage of drying time (1 to 2 days), followed by the comparatively rapid decrease, irrespective of the condition of restraint. The maximum value of the stresses is different a little for a different value of α.

In general, it is supposed that the tensile strength of concrete is probably affected by the tensile shrinkage stress on the exposed surface of concrete specimens. This is experimentally evidenced by some investigators (Nagataki, 1963)(Hanson, 1968). Nagataki (1963) obtained experimental curves showing the variation of the flexural strength of cement mortar beams drying from two opposite faces. In his report, it was stated that the minimum flexural strength is attained at about 24 hours of drying time and that such initial loss in strength is followed by a gain with an increase in drying time.

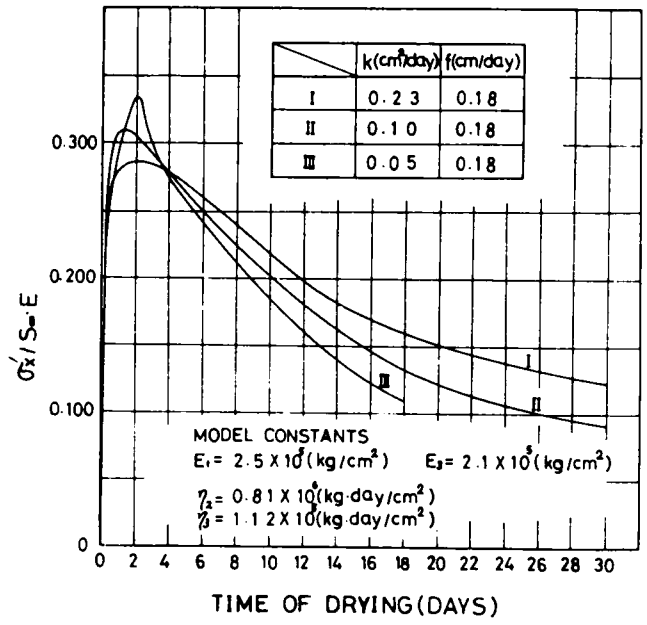

Fig. 5.24 Shrinkage stress on the exposed surface versus drying time for several values of α $(=f/\sqrt{k})$ in a completely restrained beam, drying from one face only

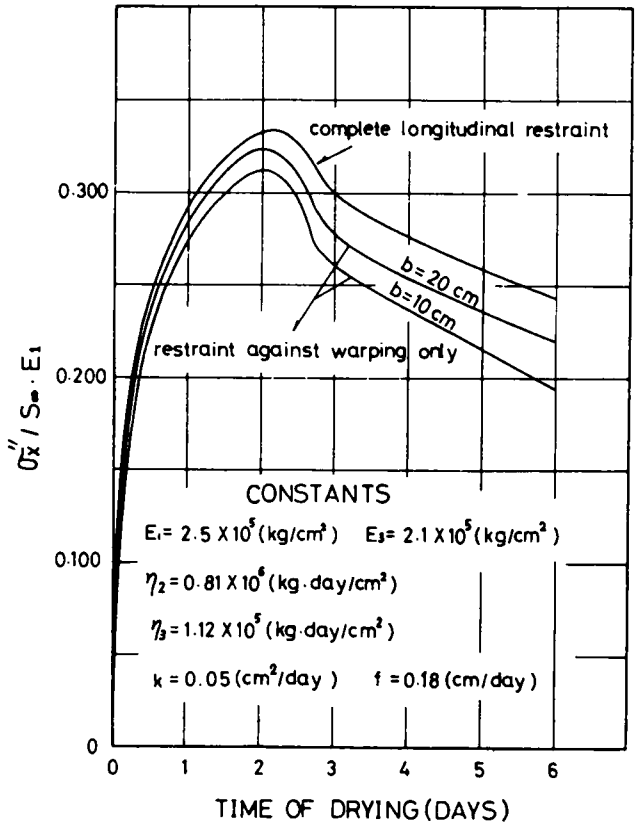

Fig. 5.25 Shrinkage stress on the exposed surface versus drying time in a beam restrained against warping only, drying from one face

The tensile shrinkage stress versus drying time curves (see Fig. 5.25) show that such initial loss in flexural strength is caused by the shrinkage stress on the exposed surface.

Surface cracking occurs when such tensile stresses exceed the tensile strength of concrete. From the computation results (see Fig. 5.24, Fig. 5.25 and Fig. 5.26), it is found that the maximum shrinkage stress is about 0.3 E_1S_∞. Thus, it may be concluded that the value of E_1S_∞ shows the measure of surface cracking of concrete due to shrinkage. Eq. (5.46), Eq. (5.47) and Eq. (5.48) may be useful for estimating the influence of various factors on the surface shrinkage cracking of the viscoelastic materials such as concrete and soil-cement, although four-element model does not necessarily represent the exact stress-strain-time behavior of the materials, especially at failure.

(5) A Consideration on Shrinkage Cracking in Soil-Cement

As concluded from the mathematical works described above, the maximum shrinkage stress on the exposed surface is proportional to the value of E_1S_∞. Therefore, the value of $E_1S_\infty/\sigma_{cf}(=\alpha)$($\sigma_{cf}$: compressive strength) can be regarded as a measure to predict shrinkage cracking.

The values, α, of soil S_1- soil S_4-cement mixtures are 3.7 and 4.7, respectively. The value, $\alpha(3.7)$, of the sandy soil S_1-cement is fairly small comparing with the 4.7 of soil S_4-cement and with those for clay lumps-cement mixtures, as will be described in the following (Fig. 5.27). Increase in silt fraction of the soil used increases the value, α, i.e. makes the soil-cement susceptible to shrinkage cracking. This results agree with that obtain-

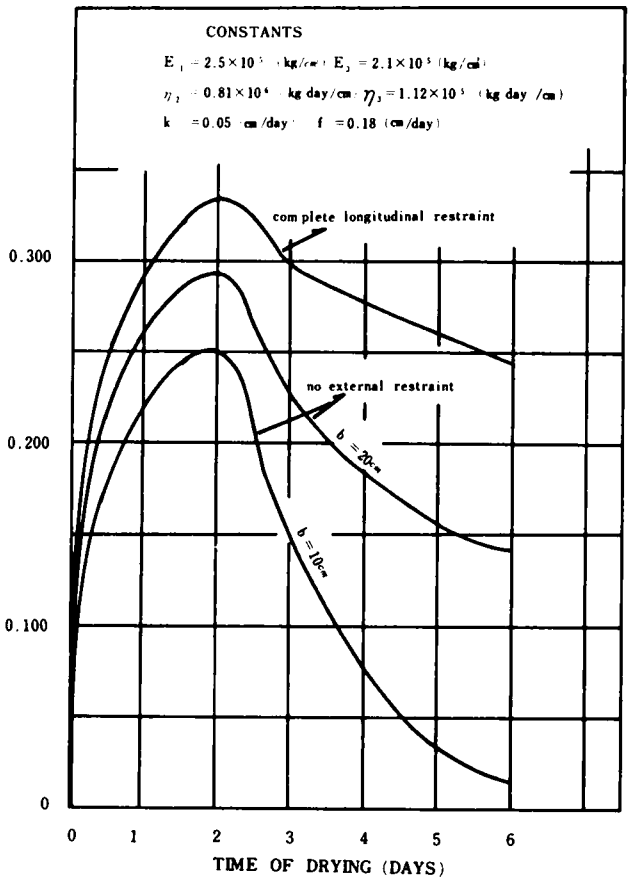

Fig.5.26 Shrinkage stress on the exposed surface vs. drying time curves in a beam with no external restraint, drying from one face only

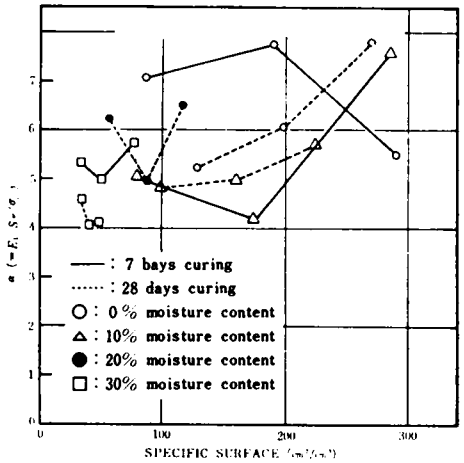

Fig.5.27 Relationship between $\alpha(=E_1 \cdot S/\sigma_{cf})$ and the specific surface of clay lumps sample used

ed by the experimental shrinkage stresses calculation in paragraph 3.

Plots of α against specific surfaces of clay lumps samples used in clay lumps -cement mixtures are shown in Fig. 5.27. The value, α, increases with increasing specific surface with a few exceptions. The values , α, of 10 percent moisture content clay lumps samples-cement mixtures are smaller than those of zero percent ones except for that of specific surface 290 cm^2/cm^3 at 7 days age.

Generally, the value, α, of the 7 days age specimens made using zero percent moisture content clay lumps samples are extremely great and the 28 days age specimens of 30 percent moisture content show considerably small value of α. It may be found that the use of high moisture content clay lumps and the cure of the specimens over during long periods make it possible to reduce shrinkage cracking of clay lumps-cement mixtures. Thus, in order to reduce shrinkage cracking, the original material should be controlled so as to produce the soil-cement with homogeneous structure. In this respect, clay pocket is deleterious element in reducing shrinkage cracking of soil-cement.

As expressed by Eq.(5.46), the shrinkage stresses on the exposed surface of a viscoelastic beam (or slab) greatly depend upon the value of Φ_1 and Φ_2. Further, these parameter (Φ_1, Φ_2) are affected almost by η_3, because η_2 is far greater than η_3, especially in soil-cement (see Table 4.2, Table 4.3 and Table 4.7).*

Eq.(5.46) shows that the shrinkage stresses decrease, as the value of η_3 decrease. Therefore, the value of η_3 as well as $E_1 S_\infty$ may be a significant factor for reducing shrinkage cracking.

(6) Summary and Conclusions

From the discussion of the formulas derived, the following conclusions can be drawn:

1) Eq.(5.46), (5.47) and (5.48) may be useful for the estimation of the surface cracking due to shrinkage in soil-cement.
2) The tensile shrinkage stresses on the exposed surface of a concrete beam drying from one face only have the maximum value at the initial time of drying (1 to 2 days), followed by the comparatively rapid decrease, irrespective of the condition of restraint.
3) The tensile shrinkage stress versus drying time curves (see Fig. 5.25) show that the initial loss in flexural strength of concrete is caused by the tensile shrinkage stress on the exposed surface.
4) The computation results show that the maximum shrinkage stress is about 0.3 $E_1 S_\infty$.
5) In order to reduce shrinkage cracking, the original soil material should be prepared so as to produce the soil-cement with homogeneous structure. In this respect, clay pocket is a deleterious element in reducing shrinkage cracking of soil-cement.
6) The value of η_3 (see Fig. 5.23) as well as $E_1 S_\infty$ may be a significant factor for reducing shrinkage cracking.

6. SUMMARY AND CONCLUSIONS

As to the relationship between macroscopic structure and shrinkage characteristics in soil-cement, discussion is made concentrating on the relationship between properties of clay pockets and shrinkage. In consequence, it is found that distribution and physical properties of clay pockets have an important effect on the ultimate shrinkage and shrinkage rate of a mixture. Therefore, it may be possible to design the material so as to reduce its shrinkage as far as possible. However, in discussing shrinkage cracking, the

---

* An attention should be paid to the fact that η_3 and η_2 in this discussion corresponds to η_2 and η_3 in Table 4.2, Table 4.3 and Table 4.7, respectively.

determination of shrinkage stresses is more significant than shrinkage itself. In this chapter, two attempts are made on the determination of shrinkage stresses. One is an experimental analysis in which nonlinear creep deformation can be introduced, and the other is based on stress analysis in viscoelastic bodies. These stresses calculation results show that grain size of soil has a sifnificant effect on shrinkage stresses and that the presence of clay pockets is a deleterious element for reducing shrinkage cracking of soil-cement.

REFERENCES

Alfrey, T. (1948): "Mechanical Behavior of High Polymers", Interscience, New York

Carlson, R.W. (1937): "Drying Shrinkage of Large Concrete Members", ACI Journal, Proc. Vol. 33, No. 2, pp. 327 - 336

Carslaw and Jaeger (1963): "Operation Methods in Applied Mathematics" Dover, New York

Churchill, R.V. (1958): "Operational Mathematics", McGraw-Hill

George, K.P. (1968a): "Shrinkage Characteristics of Soil-Cement Mixtures", Highway Research Record 255, pp. 42 - 58

George, K.P. (1968b): "Cracking in Cement-Treated Bases and Means for Minimizing It", Highway Research Record 255, pp. 51 - 71

George, K.P. (1969): "Cracking in Pavements Influenced by Viscoelastic Properties of Soil-Cement", Highway Research Record 263, pp. 47 - 59

Hansen, T.C. (1965): "Surface Cracking of Mass Concrete Structures at Early Form Removal", Extrait du Bulletin Rilem n 28, Sept. pp. 145 - 153

Hanson, J.A. (1968): "Effects of Curing and Drying Environments on Splitting Tensile Strength of Concrete", ACI Journal, Proc. Vol. 65, No. 7, pp. 535 - 543

Kawamura, M. (1969): "Shrinkage Stresses in Concrete as a Viscoelastic Material", ACI Journal, Proc, Vol. 66, No. 12, pp. 968 - 971

Lee, E.H. (1955): "Stress Analysis in Viscoelastic Bodies", Quarterly of Applied Mathematics, Vol. 13, No. 2, pp. 183 - 190

McHenry, D. (1943): "A New Aspect of Creep in Concrete and its Application to Design", Proc. ASTM, Vol. 43 , pp. 1069 - 1087

Nagayama, H. and Handy, R.L. (1965): "Factors Influencing Shrinkage of Soil-Cement", Highway Research Record No. 86, pp. 15 -27

Nagataki, S. (1963): "A Basic Study of Drying Shrinkage Stresses in Concrete", Informative Abstracts, 18th annual Meeting of JSCE 4th division), pp. 129 - 130, (in Japanese)

Okada, K. and Kawamura, M. (1967): "Some Considerations on Drying Shrinkage Stresses of Soil-Cement", Transactions of the Japan Society of Civil Engineers (In Japanese) No. 142, pp. 37 - 45

Okada, K. and Kawamura,M.(1964): "Some Considerations of Load-Deformation Characteristics of Soil-Cement", Journal of the Society of Material Science, Japan (in Japanese) Vol. 13 No. 132, Sep. pp.705 - 710

Pickett, G. (1946a): "Shrinkage Stresses in Concrete", ACI Journal, Vol. 17, No. 3, pp. 165 - 195

Pickett, G. (1946b): "Shrinkage Stresses in Concrete", ACI Journal, Vol. 17, No. 4, pp. 361 - 398

Rostasy, F.S. (1960): "Zur Theorie der Austrocknung und des Schwindens Zementgebundener Massen", Zement-Kalk-Gips, 13, Heft 3, pp. 93 - 103

Wischers, D.I.G.,: "Die Mathematische Erfassung der Spannung infolge Schwindens", BETONSTEIN-ZEITUNG 26,

Heft 11, pp. 470 - 472

Zienkiewicz, O.C. (1961): "Analysis of Visco-Elastic Behavior of Concrete Structure with Particular Reference to Thermal Stresses", ACI Journal, Proc. Vol. 58, No. 10, pp. 383 - 394

CHAPTER V SUMMARY AND CONCLUSIONS

This paper aims at discussing the relationship between the structure and mechanical properties in soil-cement mixtures from both microscopic and macroscopic aspects.

Firstly, in CHAPTER II, the effect of the interaction between clay minerals and cement on the strength characteristics of compacted clay minerals-cement mixtures is experimentally discussed from rather microscopic aspects. In this respect, the following four problems are investigated.

1. Characteristics of the various species of clay minerals-cement interaction. Clay minerals selected here are montmorillonite, kaolinite, sericite, chrolite-vermiculite mixed layer and allophane.
2. A role of calcium hydroxide resulting from cement hydration in the formation of clay-cement structure and in its progressive strength development.
3. The influence of exchangeable cations held on a clay mineral on the strength of clay-cement mixtures, hydration of cement and reaction products.
4. The hydration rate of C_3S and βC_2S in bentonite- and kaolinite-cement.

These problems are discussed by the use of X-ray diffraction, thermal analysis (D.T.A., T.G., D.T.G.), pH tests and an examination with optical microscope and unconfined compression test.

The major conclusions obtained are as follows:

1. The bentonite-cement seems to produce CSH(gel) more than the kaolinite-cement.
2. The strength of almost compacted clay minerals-cement mixtures may come from tobermorite gel and calcium aluminate hydrate resulting from the cement hydration and the secondary clay mineral-$Ca(OH)_2$ interaction. However, in chrolite-vermiculite mixed-layer clay mineral-cement mixture, magnesia as well as silica and alumina may be dissolved to a certain extent from these trioctahedral mineral by the attack of $Ca(OH)_2$ at the edges, resulting in the formation of fibrous magnesium silicate hydrate contributing to the strength development.
3. Allophane seems to suppress the cement hydration.
4. Hillebrandite with high lime-silica ratio may be formed at the considerably initial stage of curing as a reaction product in kaolinite-$Ca(OH)_2$ mixtures, transforming to the CSH(I) with lower lime-silica ratio at the long-term curing (182 and 364 days ages). However, the presence of this mineral seems uncertain in kaolinite-cement mixtures.
5. The interaction of kaolinite and bentonite with $Ca(OH)_2$ resulting from the cement hydration is not quite equivalent to that with the $Ca(OH)_2$ of reagent. This discrepancy could be attributed to the following three causes; (i) the crystal lattice of $Ca(OH)_2$ in cement paste is distorted and more reactive than the calcium hydroxide grown by the diffusion technique using $CaCl_2$ and NaOH, (ii) at the initial stage of cement hydration, the calcium hydroxide is generated in the amorphous state, (iii) there is the likelihood that the ionic mobility is different between clay-cement and -$Ca(OH)_2$ system.
6. From the changes in D.T.A. curves accompanying with curing time, it is found that the calcium silicate hydrate with low lime-silica ratio would be produced in bentonite-cement until 28 days of curing, followed by the transformation to the one with high lime-silica ratio at least after 91 days of curing.
7. A little or little difference between the compressive strength of bentonite-high-early-strength and moderate-heat cement at early curing periods until 28 days is followed by a gradually increasing difference between them. This is a tendency completely reverse to that in the kaolinite-cement

and cement mortars.

8. Clay-cement mixtures compacted under a very limited moisture content such as optimum moisture content have an non-homogeneous structure in the respect of the degree of the calcium saturation, when the diffusion of Ca ions progresses only to an insufficient extent. The X-ray diagram of the 28 days age sample has the sharp (001) peak at 15.5 Å, indicating that the complete transformation of the original Na-montmorillonite to the calcium one extends over the interior of the specimens at the end of 28 days of curing.
9. The behavior of sodium or magnesium ions substituted by calcium ions greatly affects the strength development of the bentonite-cement mixtures. In this respect, the possibility of the substitution of silicon by magnesium in the tobermorite lattice can be expected. Such an effect of Mg ions may favor the strength of the bentonite-cement.
10. The Ca- and Na-bentonite-cement mixtures have a large exothermic peak at about 900°C in their D.T.A. curves, and those of the Mg-bentonite-cement mixtures exihibit no such a large peak found in those at 3 and 28 days ages. The calcium silicate hydrate produced in the bentonite-cement mixtures at the initial stage of curing is found to be of the low lime-silica ratio. However, such a calcium silicate hydrate changes to the high lime one during the long-term curing in the Mg-bentonite-cement; that in the Ca- and Na-bentonite-cement mixtures remains the low lime content one even at the end of the long-term curing.

From a macroscopic aspect, the quantity, size distribution and physical properties of clay pockets contained in soil-cement specimens have a significant effect on the mechanical properties of soil-cement. In CHAPTER III, the influence of these factors on the creep deformation characteristics is experimentally discussed. Furthermore, an effect of a physical property (moisture content) of clay pockets existing at the production of specimens on the subsequent formation of macroscopic structure of clay-cement mixtures is also estimated from their viscoelastic behavior. In addition, several experimental discussions are made on viscoelastic properties of granular soil-cement mixtures for the purpose of further elucidation of a role of clay pockets in soil-cement mixtures.

The major conclusions drawn are described as follows:

1. The distribution functions of retardation time (τ_K) of soil-cement mixtures made using clay lumps samples of zero percent moisture content appear to consist of two hill-shaped curves having a distinct sharp peak. On the contrary, all of others have only one sharp peak.
2. The distribution of constituent phases (clay pockets and skeleton parts) in the clay sample-cement mixtures varies during the cure depending upon moisture content and size of the sample used. When clay lumps sample used are same in their size distribution, the higher the moisture content of clay lumps samples used, the more rapidly the diffusion of Ca ions occurs, the stable and homogeneous structure being formed at earlier curing periods.
3. The recoverable creep of the soil-cement made using a soil composed of approximately 80 percent sand seems responsible not only for "delayed elasticity" of the skeleton parts, but also for the absorption of moisture from atmosphere. However, almost of the recoverable creep in the soil-cement with much silt may be due only to "absorption of moisture".
4. The energy loss due to anelasticity in soil-cement mixtures decreases, as their moisture content decreases.
5. A considerably great volume fraction of clay pockets in clay lumps-cement mixtures plays a signifi-

cant part in reducing their creep viscosity, though their skeleton phase is so rigid as to compete with that of granular soil-cement.

Shrinkage cracking in soil-cement pavements is recognized as a serious problem. The prevention against shrinkage cracking will lead to a more extensive use of soil-cement. In general, shrinkage cracking of a material depends greatly upon its shrinkage characteristics and mechanical properties. In CHAPTER IV, an effect of clay pockets on the shrinkage characteristics is discussed. Furthermore, two attempts are made to estimate shrinkage stresses in soil-cement, since shrinkage stresses should be determined better to understand shrinkage cracking behavior. Several new findings are drawn as described in the following.

1. The moisture content of clay lumps samples may greatly affect the ultimate shrinkage of the soil-cement mixtures. That is, the shrinkage of soil-cement is found greatly to depend upon the shrinkage characteristics and volume fraction of clay pockets included in it.
2. The diffusivity coefficient of shrinkage (k) in sandy soil-cement mixtures is about 3 to 5 times as large as that in concrete; the surface factor (f) about 1.5 to 2.5 time as large.
3. The sandy soil-cement mixtures become more susceptible to shrinkage cracking, as the amount of cement added increases.
4. It may be considered that increasing silt fractions in soils used decrease the compressive strength of soil-cement for a given cement content. Therefore, in practice, in order to produce a soil-cement developing a given compressive strength, the use of the soil with less silt fraction is desired for reducing shrinkage cracking of soil-cement. However, when soils including comparatively much silt fraction are used, even an addition of a great amount of cement does not make the mixture susceptible to cracking.
5. In order to reduce shrinkage cracking, the original soil material should be prepared so as to produce the soil-cement with homogeneous structure. In this respect, clay pockets are a deleterious element in reducing shrinkage cracking of soil-cement.
6. The value of η_3 (see Fig. 5.23) as well as $E_1 S_\infty$ may be a significant factor for reducing shrinkage cracking.